DEVELOPMENT OF ROBUST CONNECTION MODELS FOR STEEL AND COMPOSITE STRUCTURES IN FIRE

By

Shuyuan Lin

A Thesis Submitted in Partial Fulfilment of the Requirements for the Degree of Doctor of Philosophy

Department of Mechanical, Aerospace and Civil Engineering
College of Engineering, Design and Physical Sciences
Brunel University

October 2014

DECLARATION

The work in this thesis is based upon the research carried out at the Department of Mechanical, Aerospace and Civil Engineering, Brunel University. Except where specific reference has been made to the work of others, this thesis is the result of my own work. No part of this thesis has been submitted elsewhere for any other degree or qualification.

Shuyuan Lin

ACKNOWLEDGEMENTS

I would like to express my sincere gratitude and appreciation to my supervisors Dr Zhaohui Huang and Professor Mizi Fan for their guidance, support, encouragement and patience throughout the completion of this research. It would have been more difficult without their helpful advice and devoted time. The financial support provided by Brunel University is gratefully acknowledged.

I would like to express my gratitude to my parents for their love, trust, support and patience. I also want to extend my appreciation and gratitude to all members of my family and my friends for their support and continuous encouragement.

ABSTRACT

Structural engineers and architects have a responsibility for incorporating fire safety into their building designs in order to minimize loss of life and property. To meet this requirement, extensive research has been carried out, aimed at obtaining better understanding of the performance of steel and composite structures under fire conditions. Recent research indicates that the robustness of steel connections is vitally important to the fire resistance of steel-framed composite buildings. The development of effective connection models is a key issue in this research field. This PhD research is focused on the development of robust connection elements, for modelling steel connections at elevated temperatures.

In this work, a robust simplified two-node connection element has been developed, for modelling the behaviour of the bolted end-plate connections between steel beam and column at elevated temperatures. The proposed numerical procedure is based on the model proposed by Huang (2011), incorporating additional developments to more precisely determine the tension, compression, and bending moment capacities of end-plate connections in fire. The proper failure criteria are proposed to calculate the tension capacity for each individual bolt row. In this new model, the connection failure due to bending, axial tension, compression and shear are considered. The influence of the axial force of the connected beam on the connection is also taken into account. This new model has the advantages of both the simple and component-based models. A total of 22 tests are used to validate the model. From these validations, it is evident that this new connection model has ability to accurately predict the behaviour of the end-plate connection at elevated temperatures, and can be used to represent the end-plate connections in supporting performance-based fire resistance design of steel-framed composite buildings.

For modelling the behaviour of partial end-plate connections between steel beams and columns under fire conditions, a simplified robust 2-node connection element has also been developed. The rotational response of a partial end-plate connection at elevated temperatures comprises of two stages. These stages are due to the shift of the compression centre of the connection from the end of end-plate, to the centre of the beam bottom flange at large rotation. The model proposed in this research accounts for these two stage behaviours, representing the partial end-plate

connection as a 2-node non-linear spring element. Characteristics of the spring, such as stiffness, tension, compression, shear strengths and bending moment resistance, are determined based on a component-based approach. This model therefore retains the advantages of both the simple and component-based models. Compared to normal component-based models, this simplified model has very good numerical stability under static solver condition, and is computationally efficient. Fourteen tests are used to validate the model, showing that the model is capable of accurately predicting the behaviour of partial end-plate connections under fire conditions. A series of numerical studies has been conducted on a 2D steel frame, subjected to ISO834 Fire and Natural Fire, in order to investigate the influences of the connections on the behaviour of steel structures. It is clear that the model can be used to represent the partial end-plate connections in performance-based fire resistance design of steel-framed composite buildings.

According to full-scale fire tests, tensile membrane action within the concrete floor slabs plays an important role in affecting the fire resistance of composite buildings. It is well known that the development of tensile membrane actions relies on the vertical support along the edges of the slab panel. However, there is at present a lack of research into how vertical supports influence the tensile membrane actions of the slab. In this thesis, the performance of a generic three dimensional 45m x 45m composite floor subjected to ISO834 Fire and Natural Fire are investigated. Different vertical support conditions and three steel meshes are applied, in order to assess the impact of vertical supports on tensile membrane action of floor slabs. Unlike other existing large scale modelling which assumed that the connections behave as pinned or rigid for simplicity, the two robust 2-node connection element models described above are used to model the semi-rigid behaviour of end-plate and partial end-plate connections within the fire compartment. The impact of connections on the 3D behaviour of composite floors is taken into consideration. The load-transfer mechanisms of a composite floor, when connections fail due to axial tension, vertical shear and bending are investigated. Based on the results obtained, some design recommendations are proposed for enhancing the fire resistance of composite buildings.

LIST OF CONTENTS

LIST OF FIGURES

LIST OF TABLES

NOTATIONS

The following symbols are used in this thesis:

A_c cross-section area

A_s tensile stress area of the bolt

A_{VC} shear area of the column

b_c width of column

b_p width of end-plate

$d_{c,c}$ depth of the column web between the root radii

d bolt diameter

d_0 diameter of bolt hole

E_{bw} Young's modulus of beam web

E_{bf} Young's modulus of beam flange

E_b Young's module of bolt

E_{cw} Young's modulus of column web

E_{cf} Young's modulus of column flange

E_p Young's modulus of end-plate

f_{by} yield strength of the bolt

f_{bu} ultimate tensile strength of the bolt

$f_{y,b}$ yield strength of the beam

$f_{yf,c}$ yield strength of the column flange

$f_{yw,c}$ yield strength of the column web

$f_{u,b}$ ultimate tensile strength of the beam

$f_{u,c}$ ultimate tensile strength of the column

$f_{u,p}$ ultimate tensile strength of the end-plate

h_b depth of the beam

h_c depth of the column cross-section

k max width of tension bolts across comers

L_b bolt length

t_{fb} thickness of beam flange

t_{fc} thickness of column flange

t_{wb} thickness of beam web

t_{wc} thickness of column web

t_p thickness of end-plate

r_c column fillet radius

w_b bolt gauge between the centrelines

$W_{el,y}$ elastic modulus of the beam section

Chapter 1

Introduction

1.1 Structural fire engineering

Historically, concern with fire safety has tended to follow the occurrence of collapse related events. The devastating consequence of fire would lead to loss of life and huge economic loss. In recognition of the danger of fire, noticeable progress has been made in the implementation of fire safety into the current building regulations. As documented in the Approved Document B, the objectives of ensuring fire safety in buildings are: maintaining the structural stability for a reasonable period under fire conditions, restricting the growth and spread of fire, and provision of safe means of evacuation of the occupants and the rescue operation of the firefighters (ODPM, 2000). To achieve these objectives, active and passive fire protection systems can be applied. Active fire protection systems control the fire by some actions taken by person or automatic device such as alarm systems, smoke control systems and sprinklers, while passive fire protection systems control the fire by systems built into the structure (Buchanan, 2001). From the structural point of view, fire safety of buildings deals with the passive fire protection problem, in terms of designing the structure to maintain its stability during a reasonable period, and inhibiting the spread of fire. Structural fire engineering involves understanding the fire behaviour, heat transfer and structural responses. Up to now, progress has been made in the discipline of structural fire engineering by adopting different design guidance and approaches to predict the structural performance during a fire, such as a simple prescriptive approach, and a performance-based approach. This field is also fuelled by the research studies carried out on full-scale structural fire tests.

For steel structures, the most common way to provide adequate fire protection is to cover all exposed steel members with fire protection materials. However, the approach of covering all the exposed steel members is conservative and expensive. Conventional fire protection can cost up to 30% of the total cost of the multi-storey steel frame (Lawson, 2001). More recent studies indicate that this figure seems to be reduced to 10%-15% of the total construction costs (Chen, 2012). To reduce the cost,

it is more rational to design the structure to withstand fire, without providing full fire protection to all exposed areas of steel members. The development of realistic and reliable design procedures – based on actual structural fire performance – can be helpful to improve cost-effectiveness and reduce construction time.

1.1.1 Fire curves used in structural fire engineering design

To obtain an accurate prediction of structural fire performance, it is essential to understand the development of fire. The occurrence of fire closely depends on the ignition source, sufficient combustible material and oxygen. As illustrated in Figure 1.1, the development of a real fire (or a natural fire) in a compartment contains two stages: the pre-flashover and post-flashover stages.

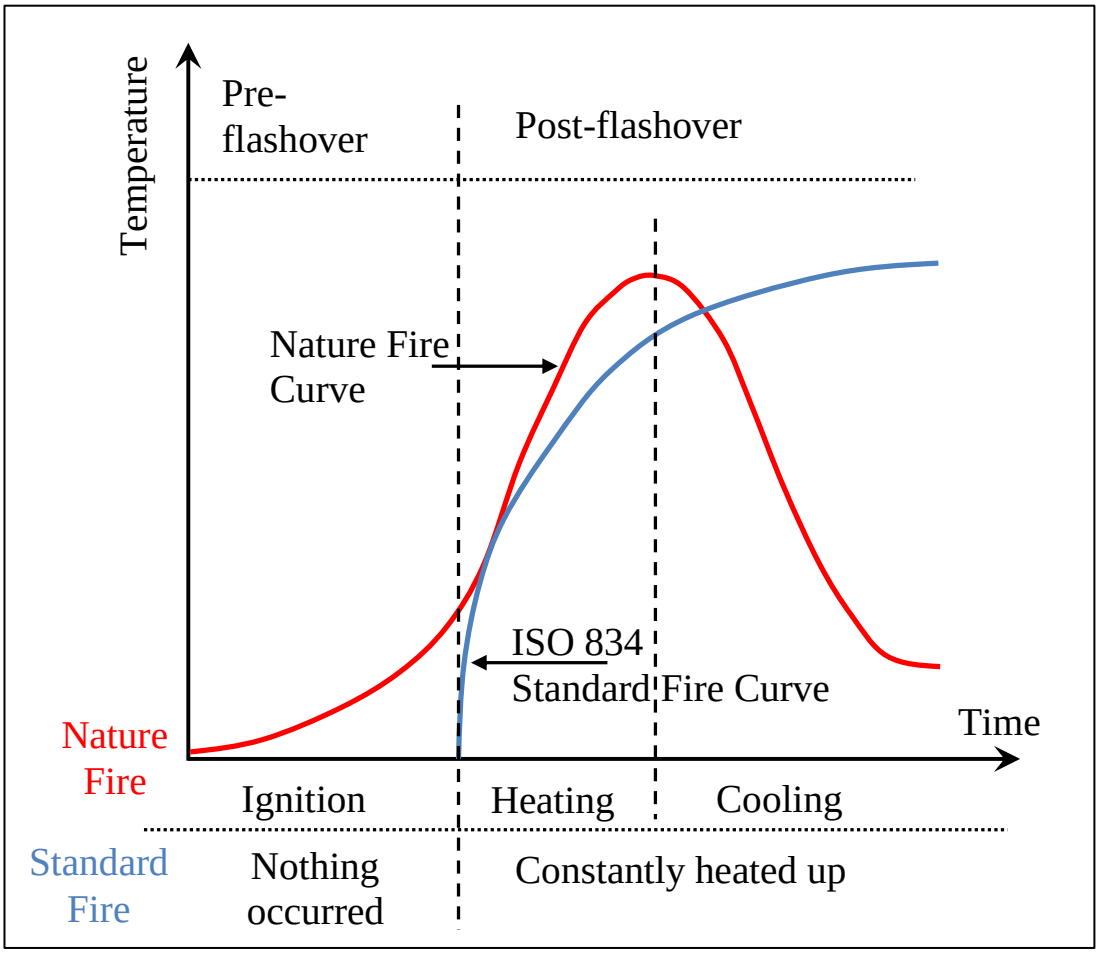

Figure 1.1 Real fire development and ISO 834 Standard fire curve

In the pre-flashover stage, the fire starts as the combustible materials get ignited. For most common material, the ignition temperature is found to be approximately 300°C (Leston-Jones, 1997a). In the ignition phase, the combustion is localised to small areas near ignition source inside the compartment, and the average temperature of compartment is low. Active fire protection measures can be applied to control and prevent the further growth of fire, in the form of automatic sprinkler systems, fire extinguishers and fire detection devices for example. The fire will be well established locally and continue to grow, as long as fuel and oxygen are sufficient. Ventilation conditions in the compartment also have a significant influence in controlling the growing rate of the fire. If a door is opened or windows break, it would change the fire growth situation dramatically. The transition from a localised fire to a fully developed fire is named 'flashover'. The occurrence of flashover is generally sudden, with the flames reaching the ceiling and spreading out to available combustible surface within the compartment. After flashover, active fire protection measures have very little impact in controlling and extinguishing the fire. The main concern for fire brigades is preventing the fire spreading to adjacent floors of the same building or other buildings (Buchanan, 2001). The risk of structural collapse is high, unless sufficient fire protection and fire resistance to the structural members was provided in building design. After flashover, the fire is considered to be fully developed, growing at a steady-state rate. The maximum temperature inside the compartment is often in excess of 1000°C, depending on the ventilation conditions, fire load, and available fuel. At this latter stage, the strength and stability of structural members are largely jeopardised by exposure to fire, possibly leading to the loss of structural integrity or progressive collapse. The fire continues to burn, entering the decay phase after reaching the maximum temperature. The gas temperature decreases as the combustion rate of fuel decreases. In the cooling phase, large tensile contraction forces are generated in the steel beams because of thermal contraction behaviour. These produced forces are likely to result in the tensile failure of connections, which may lead to further local failure within the compartment, and progressive collapse of the whole structure. Towards the end of post-flashover stage, the fire finally dies out from a lack of combustible material or oxygen.

The empirical derivation of a fire curve closely depends on the compartment size, the ventilation condition, the available combustible material, the fire load, and the material of surrounding surfaces. A parametric temperature-time curve is documented in Eurocode EN 1991-1-2 (CEN, 2002) to provide an estimation of the real fire curve. The gas temperature θ_g inside the compartment during heating stage can be determined using the following formula:

$$\theta_g = 20 + 1325\left(1 - 0.324e^{-0.2t^*} - 0.204e^{-1.7t^*} - 0.472e^{-19t^*}\right) \tag{1.1}$$

where,

$$t^* = t \cdot \Gamma \tag{1.2}$$

t is the time.

$$\Gamma = \frac{(O/b)^2}{(0.04/1160)^2} \tag{1.3}$$

b is the thermal absorptivity depending on the density ρ, the specific heat c and the thermal conductivity λ of the boundary of enclosure:

$$b = \sqrt{(\rho c \lambda)} \tag{1.4}$$

O is the opening factor, expressed as:

$$O = \frac{A_V \sqrt{h_{eq}}}{A_t} \tag{1.5}$$

A_V is the total area of vertical openings on the walls. h_{eq} is the weighted average of window heights on all walls. A_t is the total area of enclosure, including openings. The Equation (1.1) would approximate the standard temperature-time curve in the case when $\Gamma = 1$.

The calculation of temperature-time curve for cooling stage given in EN 1991-1-2 is defined as below:

$$\theta_g = \begin{cases} \theta_{\max} - 625\left(t^* - t^*_{\max} \cdot x\right) & t^*_{\max} \le 0.5 \\ \theta_{\max} - 250\left(3 - t^*_{\max}\right)\left(t^* - t^*_{\max} \cdot x\right) & 0.5 < t^*_{\max} < 2 \\ \theta_{\max} - 250\left(t^* - t^*_{\max} \cdot x\right) & t^*_{\max} \ge 2 \end{cases} \tag{1.6}$$

$\theta_{\max}$ is the maximum temperature during the heating stage when $t^* = t^*_{\max}$.

$x = 1.0$ if $t_{\max} > t_{\lim}$; when $t_{\max} = t_{\lim}$, $x = t_{\lim} \cdot \Gamma / t^*_{\max}$.

$$t_{\max} = \max\left[\frac{0.2\times10^{-3}\times q_{t,d}}{O};\quad t_{\lim}\right] \tag{1.7}$$

$$t^{*}_{\max} = t_{\max}\times\Gamma \tag{1.8}$$

where $q_{t,d}$ is the design fire load density related to the surface area A_t; $t_{\lim}$ is the time for maximum gas temperature in case of fuel controlled fire. In the case of slow fire growth rate, $t_{\lim} = 25\min$; in the case of medium fire growth rate, $t_{\lim} = 20\min$ and in the case of fast fire growth rate, $t_{\lim} = 15\min$ (CEN, 2002).

It can be clearly seen that simulating the real fire curve is complex and difficult. Therefore, for convenience, a standard fire curve is adopted to represent the fire using the standard temperature-time relationship. The standard fire curve is defined in accordance with International Standard ISO 834 (ISO834, 1975), independent with the compartment characteristics. As depicted in Figure 1.1, the standard fire curve starts from flashover and does not take account for the pre-flashover phrase and the cooling phrase. The determination of standard fire curve can be given as:

$$\theta_g = 20 + 345\log_{10}(8t+1) \tag{1.9}$$

where θ_g is the gas temperature in the fire compartment (℃), and t is the time (minutes).

The standard fire curve is normally applied for standard fire furnace tests, to provide a common basis comparison between different fire tests. It also serves as a way to evaluate the resistances of structural members subjected to fire. However, the standard fire curve cannot provide a realistic representation of structural behaviour under real fire condition, as it ignores differences in the compartment characteristics and the structural effects during the cooling phrase.

1.1.2 Structural fire engineering design

The most common and conventional way to ensure adequate fire resistance for steel structures, is to cover the exposed steel members using the fire protection materials with a prescribed thickness. A wide range of insulating materials is available to provide sufficient fire protection for structures (such as concrete, sprays, boards and intumescent coatings). In the UK, guidance for the application of fire protection

materials is published and referred to as the 'Yellow Book' (ASFP, 2004). The Yellow Book prescribes the thickness of various fire protection materials for specified periods of fire resistance. Comprehensive design tables are presented in the Yellow Book for designers to look up and specify the thickness – based on the selected steel section size, shape and requested fire resistance. The thickness is selected based on the condition that the temperature of steel does not exceed 550 ℃ for columns and 620 ℃, for beams supporting concrete floors for a given fire resistance period tested in a standard furnace (Bailey, 2007). These maximum temperatures are based on the assumptions that the steel member is fully stressed at ambient temperature, behaved in isolation, and was heated uniformly. These assumptions are not realistic. The Yellow Book design approach is therefore *conservative*, ignoring actual structural behaviour under fire conditions.

The publication of BS 5950 Part 8 provides an alternative approach to designing-in fire resistance by calculation; it is still based on the evaluation of structural performance in the standard fire test (BSI, 2003). It is recognised here that the failure of structure is not only affected by temperature, but also by load level, support conditions, and thermal gradient along the member. This code presents the limiting temperature as a function of load ratio, in order to determine the thickness of fire protection. The load ratio is expressed as the load at the fire limit state, to the load capacity at the ambient temperature. The code also provides another moment capacity method to calculate the fire resistance, which is not widely used as knowledge of the temperature of the beam is required (Lennon et al., 2007). The design methods of composite beams, columns and composite slabs are also given in this code.

In the European Union, a set of documents were developed by the European Commission and member states for determining the actions, and for calculating the stability of building constructions. These are known as the Eurocodes. The Eurocodes provide the framework for calculating the fire resistance for structures (EN 1991-1-2 (CEN, 2002), EN 1993-1-2 (CEN, 2005b), EN 1993-1-8 (CEN, 2005c) and EN 1994-1-2 (CEN, 2005d)). The fire resistance is expressed in terms of three failure criteria: which are the ability to maintain sufficient strength in the required duration, the ability to limit the increase of temperature across separating elements, and the ability to maintain structural integrity against penetration of hot gases

(Purkiss and Li, 2013). These three failure criteria can be identified as the *load-bearing capacity*, *insulation* and *integrity* of the building, respectively.

The prescriptive approach in these building codes focuses solely on the fire resistance, and results in simple deemed-to-satisfy provisions such as thickness of fire protection materials. The derivation of fire resistance relates to the duration for which the structural elements can withstand a standard fire exposure test without losing their load bearing and fire separating function. However, the standard fire test has some limitations, as it is not consistent with the characteristics of a real fire, and only isolated structural members are tested at a load corresponding to the maximum permissible stress of the tested member (Parkinson and Kodur, 2007). Besides, the prescriptive approach constrains flexibility and is unable to adequately cover new innovations in design, and the construction technologies (Kirby, 1986). In recognition of these drawbacks, a more rational performance-based approach has been introduced and adopted in many countries for fire-resistance design. The performance-based approach provides more flexibility in design and it takes the real behaviour of structure under fire into consideration. In recent years, the performance-based approach have been slowly incorporated into a growing number of national and international building codes and standards (Bukowski and Babrauskas, 1994; Beck, 1997; Wang, 2002; Guo, 2005; Hertz, 2005; Buchanan, 2008; Lo et al., 2008; Bailey, 2009; Franssen et al., 2009; Tavares, 2009).

The application of performance-based approach can be simplified into a three-step procedure: estimating the fire behaviour, estimating the temperature distribution through the structure, and analysing the structural response at high temperature (Lennon et al., 2007). The issue prior to estimating the fire behaviour is to determine whether the fire remains localised, or is fully developed. Different fire models are then selected to derive the fire prediction, such as the standard fire curve or the parametric fire curve. Once the temperatures within the compartment are estimated, the temperature distribution within the structure can then be defined, in order to assess the structural response to the fire. The behaviour of structure is designed at the fire limit state, in which different partial safety factors for load are applied, and the strength and stiffness of structural members are reduced according to the temperature through the cross-section (Bailey, 2007).

1.2 Fire resistance of steel-framed composite buildings

In the composite structure, the concrete profiled deck floor slab acts compositely with the steel beams, providing higher load-carrying capacity. At present, the steel framed composite structures account for more than 50% of new office construction in the UK (Lawson, 2001).

The accidental fire cases in steel-framed composite buildings in 1990, such as the Broadgate fire in London and the Churchill Plaza Building fire in Basingstoke (Newman et al., 2006), have indicated that the design of buildings was over-conservative. The performance of real building subjected to fire was different from that assumed in the standard fire test on isolated members. The restraint of thermal expansion from surrounding structure has a significant influence on the performance of beams within the structure (Li and Guo, 2008). When the composite structure is subjected to fire, the interaction between the structural members and the redistribution of loads within the structure have an important impact, in maintaining the stability of the structure.

1.2.1 Full scale fire tests on composite structures

In order to obtain a better understanding of the behaviour of real buildings under fire conditions, full-scale fire tests have been conducted. One of the landmark experimental programs was the real fire tests on a full-scale eight story composite steel-framed building, at the Building Research Establishment (BRE)'s large building test facility at Cardington (Swinden Technology Centre, 1999). The building tested had a floor footprint of 21m x 45m and a total height of 33m, consisting of three bays by five bays. A total of seven fire tests were conducted on various floors. The sizes and locations of these seven fire tests are given in Figure 1.2.

Test 1 investigated the behaviour of a single internal restrained secondary beam and the surrounding floor slabs in an edge bay. Test 2 studied the performance of a place frame including four columns and three primary beams. Test 3 investigated the performance of a complete floor system, focusing on the effects of membrane action of the composite floor. Test 4 aimed to study the behaviour of a complete floor system, with the internal boundaries using steel stud partition walls. Test 5 was concerned with a large compartment which extended over the full width of the

building (with a size of 21m x 18m). Test 6 was carried out on a corner compartment using a fire load of real office furniture such as computers and filing cabinets. Test 7 (Wald et al., 2006) was conducted in a side-compartment, focusing on the behaviour of steel connections and the effects of tensile membrane action.

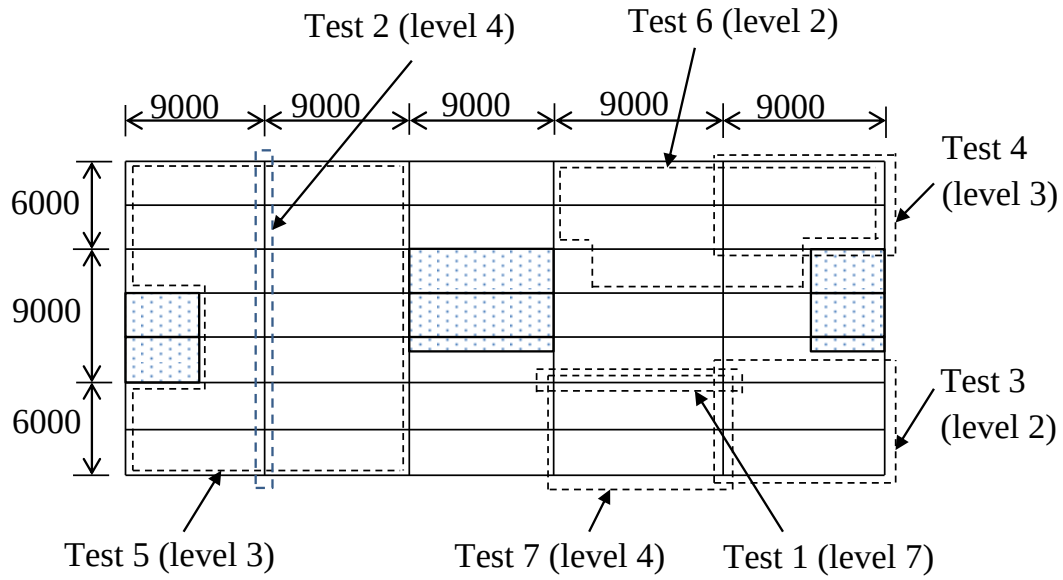

Figure 1.2 Floor plan and locations of the Cardington fire Tests

In all the fire tests conducted at the Cardington test building, the steel beams within the fire compartments were deliberately left unprotected. These tests made it clear that unprotected steel members can have significantly *greater* fire resistance within real multi-storey buildings, than when tested as isolated members. This appeared to be due to an interaction between the heated members within the fire compartment, the concrete floor slabs and the connected steel frame structure. Most significantly, in none of the seven tests was there any indication of run-away failure, which is the eventual outcome of all isolated member tests in which temperatures are progressively increased. This is particularly remarkable, when it is considered that in some cases unprotected steel beam temperatures reached over 1000 ^{0}C, at which point the steel strength has reduced by over 95%. In all tests, the maximum deflections exceeded span/30 and in some cases were greater than span/20. Considerable effort has subsequently been devoted to investigating the reasons for this behaviour, and analytical studies have shown that tensile membrane action in the concrete floor slabs may have played an important role, especially when deflections had become very large.

A furnace fire test was carried out as part of the EU-Commission-funded project on Fire Resistance Assessment of Partially Protected Composite Floors (FRACOF). The aim of this test was to investigate the performance of composite floors under standard fire condition, and to enlarge the application of the design concept based on membrane action (Vassart and Zhao, 2011). The test was carried out on a single bay with a size of 8.7m x 6.7m, composing of four columns, two primary beams and four secondary beams. The test was conducted by exposing the entire bay to the standard ISO 834 fire for 120 minutes. Test results showed that the structure performed very well during the fire exposure. The tensile membrane action of the floor was illustrated by measuring the lateral displacement at the edge of the floor, indicating activation of the membrane action during the test to maintain the stability of the whole floor (Vassart and Zhao, 2011). It was concluded from the test results that the reinforcing steel mesh should be properly overlapped in the composite slab, in order to active membrane action and to ensure the continuity of load transfer.

A full-scale natural fire test on a composite floor slab supported with long-span cellular beams was conducted at the University of Ulster (Nadjai et al., 2011). This test was carried out to investigate the applicability of the membrane action mechanism when the unprotected secondary beams are cellular steel beams. The tested floor size was 15m x 9m, with a height of 3m. All the columns and the perimeter beams were fire protected. The experimental test results indicated that the application of cellular beams does not affect the development of membrane action within the floor slabs.

1.2.2 Computer modelling of composite structures under fire conditions

Due to the high costs and complexities of conducting full-scale fire tests, it was necessary to develop numerical models to simulate the structural behaviour of full frame under fire conditions. With the rapid progress in computing power and modelling techniques, larger and more complex models can be developed. The experimental data obtained from the available full-scale fire tests can then serve as a validation database for the proposed numerical models and simulations.

A specialized finite element program VULCAN (Huang et al. (1999a, 1999b, 2000, 2002, 2003a, 2003b, 2004, 2009); Huang, 2011) has been developed at University of Sheffield, in the United Kingdom. VULCAN is capable of predicting the response

of composite steel-framed structures at elevated temperatures, and has been extensively validated against different tests (including all seven of the Cardington fire tests). In this program, a composite steel-framed building is modelled as an assembly of finite beam-column, connection, slab and shear connector elements. It is assumed that the nodes of these different types of element are defined in a common reference plane that is assumed to coincide with the mid-surface of the concrete slab element, whose location is fixed throughout the analysis.

Another special finite element program SAFIR (Franssen et al., 1995; Franssen, 2005) has been developed at the University of Liège, Belgium. This program can be applied for thermal and structural analysis of steel, concrete and composite structures under fire conditions. 2D and 3D solid elements are included in the program, as well as the shell and beam elements (Franssen, 2005). The program has also been validated against available fire tests, such as two-way reinforced concrete and composite slabs, and the full scale steel frame fire test at Cardington (Lim et al., 2004; Franssen et al., 1995).

Gillie et al. (2001) developed a finite element model to analyse the Cardington Test 1 using FEAST. The program FEAST is a specialist program developed at the University of Edinburgh. The thermal expansion, non-linear thermal gradients, material and geometrical nonlinearity are all taken into consideration in this program. Elghazouli et al. (2000) developed a numerical model to simulate the behaviour of the Cardington Test 3 using the nonlinear finite element software ADAPTIC. ADAPTIC is a special program developed at Imperial College. The analysis demonstrated that the fire protected edge beams provide high axial restraint to the heated floor slab. The thermal expansion resulted in a considerable proportion of the vertical deflection of the floor slabs.

Wang (2000) analysed the structural behaviour of the Cardington Test 5 using a specialist finite element program FIREFRAME. Some tentative conclusions were derived, according to the analysis that the structural members considered as non-loadbearing at ambient temperature may significantly benefit the fire resistance of primary load-bearing members. Large sagging bending moments may generate within a hot beam during the cooling stage, but it was not clear whether this may lead to the failure of beams when cooled down. The numerical procedure

considering the membrane action of the floor slabs should be included to improve the analysis.

In all the Cardington tests, the edge beams were either protected from fire, or had cooler temperatures compared to the internal beams. Therefore, a question is raised concerning the influence of fully heated edge beams on the fire performance of the composite structure. Lamont et al. (2007) carried out a study to investigate the behaviour of composite steel-framed structures, under a natural fire with protected edge beams and with unprotected edge beams. The numerical analysis was conducted using the finite element program FEAST. The analytical results indicated that the slab spanned in two directions when the edge beams were fire protected, developing tensile membrane action. The slab spanned only in one direction when the edge beams were unprotected, which was similar to the catenary action of the beam. The columns displaced inwards towards the end of the fire when the edge beams were fire unprotected, indicating the possibility of runaway collapse. It was also concluded that protecting edge beams from fire would improve the fire resistance of the structure.

Scullion et al. (2012) developed a three-dimensional finite element model using the software package TNO-DIANA Version 9.4, for analysis of the performance of unprotected Elliptical Hollow Section (EHS) steel columns, under the hydrocarbon fire curve. This model was calibrated against 12 experiments, comprising of six unrestrained and six axially restrained EHS columns of two different slenderness. Kodur et al. (2013) conducted a numerical study to evaluate the behaviour of composite beam-slab assemblies under fire conditions, using the finite element software ANSYS. Different shear connection types were modelled in this study, including the welded-bolted shear tab connection and the double-angle connection. The proposed finite element model was validated against three beam-slab assemblies tested by Wellman et al. (2011). These investigation results showed that the developed finite element model can predict the behaviour of beam-slab assemblies with satisfactory accuracy. The analysis demonstrated that the composite action between the beam and slab can improve the overall fire performance, which was achieved by transferring the loads from the fire weakened beams to other adjacent girders.

1.3 Current research of steel connections in fire

Over recent years, there has been growing interest to understand the behaviour of different structural elements in a fire, both in isolation and as a part of the whole building (Burgess et al., 2012a). The steel connections are normally applied to assemble the structural elements together in a steel frame. Observations from the collapse of World Trade Centre buildings (FEMA, 2002a, 2002b), and the full-scale fire tests at Cardington (Newman et al., 2006), have indicated that connections are the vulnerable structural components under fire conditions. The failure of connections may result in the collapse of the connected beams, and further buckling of the columns, which would lead to the progressive collapse of the floor slabs (Burgess, 2012b). Therefore, connections play an important role in maintaining the integrity of the structure. The observations from Cardington fire tests have shown that the steel framed composite structures can survive better than the responses suggested by traditional tests on isolated members. This is largely due to the interactions between the structural members. When subjected to fire, the connection forces are significantly different from those designed at ambient temperature. In the early and intermediate stages of a fire, the connections are subjected to compression due to the restrained thermal expansion of the connected beams. In the later stage of a fire, the forces change to tension because of the catenary action of the connected beams. These complex loading conditions are difficult to produce through experiments on isolated structural members. Only full-scale fire testing can provide data for the complex interactions between structural members. However, conducting large-scale fire testing has many limitations, including the extremely high costs, the time consuming nature of the work, and the constraints imposed by the experimental facility (Chen, 2012). Therefore, it is increasingly necessary to develop software models which are capable of predicting the behaviour of structures under fire conditions with sufficient accuracy. Developing effective connection models is one of the key issues.

Nowadays, there is pressing need to investigate the behaviour of steel connections in fire, and its influence on the whole behaviour of the steel framed structures. Various experimental tests have been conducted on different types of connections in isolation at elevated temperatures (Lawson, 1990; Leston-Jones, 1997a; Al-Jabri, 1999; Spyrou, 2002; Lou and Li, 2006; Hu, 2009a; Yu et al., (2009a, 2009b, 2011)).

Analytical studies have been explored on the behaviour of connections in fire. Different types of numerical models have been developed. In general, three main approaches are adopted for modelling the performance of connections at elevated temperatures:

(1) Using curve-fitting equations to represent the moment-rotation characteristics of the connection (Leston-Jones et al., 1997b; Al-Jabri, 1999; Abolmaali et al., 2005);

(2) Applying detail finite element analysis to simulate the non-linear 3D response of the connection (Liu, 1996; Qian et al., 2009);

(3) Using component-based models to predict the behaviour of the connection (Simões da Silva et al., 2001; Block et al., 2007; Ramli-Sulong et al., 2010).

The first approach is the simplest one. However, these curve-fitting equations can only be used for the connections that possess similar geometrical and mechanical properties to those investigated experimentally. The second approach can be adopted by using general commercial software, such as ABAQUS or ANSYS. This approach is however computationally expensive, especially for modelling large-scale complex global structures or sub-structures. The component-based models (also known as spring-stiffness models) have been widely applied to simulate the behaviour of beam-to-column connections under fire conditions. However, one significant problem for using component-based model is that under a static solver condition, if one of the component springs within the connection fails, then the numerical illness may be generated within the stiffness matrix of connection element. Those illnesses may initiate numerical singularity for whole structures analysed, and the analysis will stop. However, one component spring failure within the connection doesn't mean the failure of the whole connection. Using dynamic solvers can overcome this problem, but it can significantly reduce the computational efficiency of the model. More detail literature review on the behaviour of steel connections at elevated temperatures will be given in Chapter 2.

1.4 Aim and objectives of the research

The primary objective of this PhD research was to develop robust simplified two-node connection element models, which can be used to predict the performance of

bolted end-plate and partial end-plate connections at elevated temperatures. Compared to normal component-based models, the most significant of the current model is that the proposed simplified model has very good numerical stability under static solver condition. The model also retains the advantages of both the simple and component-based models. The connection models developed are incorporated into computer program VULCAN, for investigating the influence of the connections on the 3D structural behaviour of composite buildings under fire conditions.

In this thesis, a robust 2-node connection element has been developed for modelling the bolted end-plate connection between steel beam and column at elevated temperatures (see Chapter 3). The developments are based on the main framework of two-node connection element proposed by Huang (2011), in which the end-plate connection has been represented as a two-node nonlinear spring element. Therefore, the developed model has the advantages of the simple connection model. However, in this research a component-based approach is adopted, to determine the characteristic of the nonlinear spring connection element. These characteristics include rotational stiffness, bending, tension and compression, vertical shear resistances. Hence, the mode also keeps the advantages of component-based models. Some works done by Spyrou et al. (2004a) and Block et al. (2007) have been incoporated into the proposed model, with the new developments of robust displacement failure criteria for three failure modes of T-stubs. The new model developed has the capability to more precisely determinate the tension, compression and bending capacities of end-plate connection at elevated temperatures. Also the connection failure due to bending, axial tension and compression are taken into account in the current model. The developed connection element considers the influence of axial tensile force of the connected beam, on the bending moment resistance of the connection. The developed model has very good numerical stability under a static solver condition. This is very important for larger scale 3D modelling of steel-framed composite buildings under fire conditions.

In order to validate this new connection element, a total of 22 experimental tests were used, including tests with and without applying axial force at both ambient and elevated temperatures, and two tests on a beam-to-column sub-frame subjected to natural fire. Good agreement between the model predictions and the experimental data was achieved. This shows that the developed connection model is able to

accurately model the behaviour of the end-plate connections in fire. The study also indicated that the influence of temperature on the behaviour of the connections is significant. The model developed in this research can therefore be used to represent end-plate connections for performance-based fire resistance design of steel-framed composite buildings.

A simplified robust two-node connection element has also been developed for modelling the behaviour of partial end-plate connections between steel beams and columns under fire conditions (see Chapter 4). In this connection element, the two stage rotational responses of partial end-plate connections are also considered. Component-based approaches are adopted here, to precisely determinate the stiffness, tension, compression and bending capacities of the partial end-plate connection under fire conditions. This new model considers the connection failures, due to bending, axial tension or compression, and vertical shear. The current model is based on the two-node connection element framework of end-plate connection, with further developments for modelling partial end-plate connections at elevated temperatures. Therefore, the new model has the advantages of both the simple and component-based models. Also the current connection element is computationally efficient, with excellent numerical stability under a static solver condition.

A total of fourteen tests were used to validate this second model. The validations demonstrated that the proposed model can predict the two stage rotational characteristics of partial end-plate connections with reasonable accuracy. Therefore, the model presented in this thesis can be used for analysing the behaviour of partial end-plate connections in real performance-based fire resistance design of steel framed composite buildings.

In order to investigate the influences of the connections on the behaviour of steel structures, a series of numerical studies were also conducted on a 2D steel frame subjected to ISO834 Fire and a typical Natural Fire. The analyses indicated that the tensile failure of the connection is more likely to happen within the buildings during the cooling stage of a real fire. From these numerical studies, it is evident that the current fire resistance design of steel-framed composite structures, in which the connections are treated as pinned without considering the failures of axial tension, is *unconservative*, especially in the cooling stages of a fire.

The two connection models developed in this research are implemented into the nonlinear finite element program VULCAN for 3D modelling of the structural behaviour of steel-framed composite buildings in fire. A series of comprehensive parametric studies have been conducted on a generic three dimensional 45m x 45m composite floor subjected to ISO834 Fire and Natural Fire, to investigate the influences of the connections on the performances of composite building in fire (see Chapter 5). A series of numerical analyses have also been conducted, to quantitatively assess the impacts of vertical supports on tensile membrane action within the composite floor slabs. These investigations show that at high temperatures, the strength and stiffness of steel beams reduce rapidly. The loads above the fire compartment are largely carried by the concrete slabs. Therefore, the influence of steel reinforcement on the behaviour of composite floor slabs becomes more significant. The study shows the load-transfer mechanisms of the composite floor, when the connections fail due to axial tension, vertical shear and bending. Based on the analyses, the partial end-plate connections, which connect protected secondary beams to columns, would fail due to the transferred loads from the intermediate unprotected secondary beams. The research indicates that the larger deformation of protected secondary beams, which results from the larger loads transferred from unprotected secondary beams to the protected secondary beams, reduces the vertical supports on the slab panel. Hence, the floor slab panels would deform less double curvature which causes significant reduction of the tensile membrane action within the floor slabs. Therefore, in real performance-based fire resistance design of steel framed composite buildings, in order to maximise the benefit of tensile membrane action, the influence of connections need to be considered carefully. The designers should design adequate strength and stiffness into protected secondary beams and connections.

1.5 Layout of this thesis

The thesis consists of six chapters. The remaining chapters are outlined as follows:

Chapter 2 gives a comprehensive literature review on the state-of-art of the behaviour of steel connections at elevated temperatures. First the classification of steel connections and the deterioration of steel material properties with increasing temperatures are presented. Then a literature review on the performance of

connections at elevated temperatures and the development of numerical models for connections is followed. Finally a brief introduction of the finite element software VULCAN is made.

Chapter 3 presents the developments of a robust 2-node connection element for modelling the bolted flush and extended end-plate connection between steel beam and column under fire conditions. First, the derivation of stiffness matrix and the moment-rotation characteristics of the connection element are described. Then the numerical procedures for determining the tension, compression, shear and bending capacities of the end-plate connection are developed. Finally, the validations of the current developed model against 22 tests at ambient and elevated temperatures are conducted.

Chapter 4 describes the development of a simplified robust 2-node connection element for modelling the behaviour of partial end-plate connections at elevated temperatures. In this chapter, the construction of element stiffness matrix for partial end-plate connection is presented first. Then the details of determination of tension, compression, shear and bending capacities of new connection element are given. Following with the validations of the proposed model using the fourteen partial end-plate connections tested at both ambient and elevated temperatures. Finally a series of comprehensive numerical studies has been conducted on a 2D steel frame to investigate the influences of the connections on the behaviour of steel structures.

Chapter 5 presents the details of an investigation carried out on the performance of a generic three dimensional 45m x 45m composite floor subjected to ISO834 Fire and Natural Fire. The two robust connection elements developed in Chapters 3 and 4 are incorporated into the software VULCAN, for modelling the semi-rigid behaviour of end-plate and partial end-plate connections within the composite floor. A series of numerical studies are then conducted, to investigate the influences of the connections on the fire resistance of the composite buildings under different fires. Also, the influence of the deformation of protected secondary beams on the tensile membrane action within the floor slab panels are analysed in detail. The load-transfer mechanisms of composite floor, when connections fail due to axial tension or vertical shear, are also discussed. Finally proposed design recommendations for enhancing the fire resistance of composite buildings are presented.

Chapter 6 summarises, and concludes the research work reported in this thesis. Some recommendations are also proposed for future research.

1.6 Publications generated from this thesis

1.6.1 Journal publications

Three original research articles have been produced in this PhD project for publication in peer reviewed journals. Details are as follows:

(1) **Lin, S.**, Huang, Z. and Fan, M., 'Analysis of end-plate connections at elevated temperatures', *Steel and Composite Structures*, 15(1), 2013, pp. 81-101.

(2) **Lin**, **S.**, Huang, Z. and Fan, M., 'Modelling partial end-plate connections under fire conditions', *Journal of Constructional Steel Research*, 99, 2014, pp.18-34.

(3) **Lin, S.,** Huang, Z. and Fan, M., 'Performance of composite buildings under fire conditions', *Fire Safety Journal,* (under review).

1.6.2 International conferences

Two international conference presentations have been given:

(1) **Lin, S.**, Huang, Z. and Fan, M., 'Modelling of end-plate connections in fire', Proceedings of International Conference on Design Fabrication and Economy of Metal Structures, Miskolc, Hungary, April 24-26, 2013, pp. 321-326.

(2) **Lin, S.**, Huang, Z. and Fan, M., 'A simplified model for modelling flexible end-plate connections in fire', Proceedings of International Conference: Applications of Structural Fire Engineering, Prague, Czech Republic, April 19-20, 2013, pp.166-172.

Chapter 2

Literature Review on the Behaviour of Steel Connections in Fire

Steel connections provide strong links between the structural members. The connections play important role in maintaining the integrity and stability of the whole structure under fire conditions. Failure of these connections may lead to the progressive collapse of the entire building. The importance of connections in fire was highlighted in the introductory chapter. This chapter will review the commonly used steel connections, and the previous research work investigating the performance of connections at elevated temperatures.

2.1 Introduction

A structural steel frame is an assembly of many universal beams and columns. These individual steel elements are linked together by means of joints, to transfer loads within the structural frame. These joints can be classified in terms of locations such as those shown in Figure 2.1.

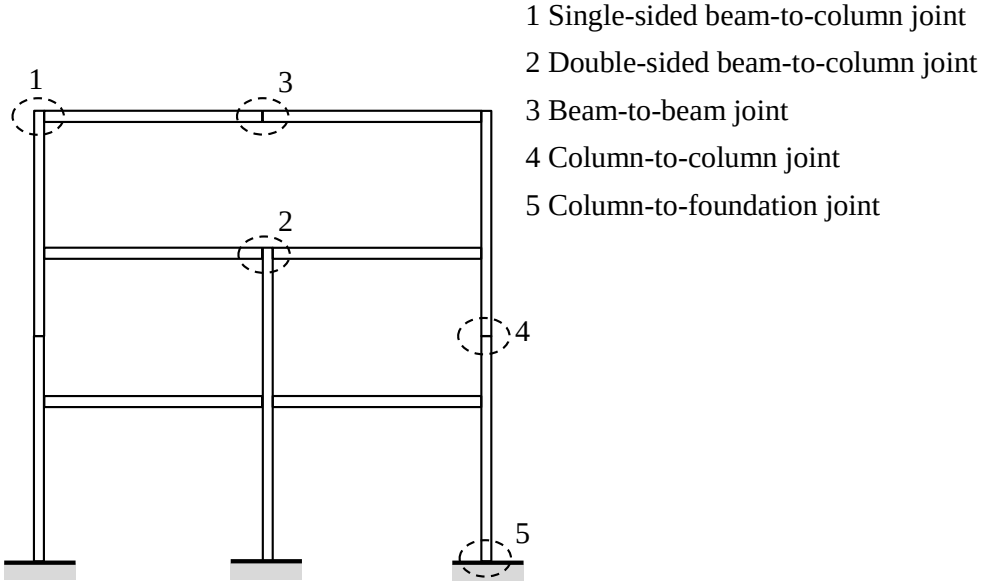

Figure 2.1 Different types of joints in steel frame

According to Eurocode 3 Part 1.8 (CEN, 2005c), the term 'joint' refers to the zone within which two or more members are interconnected, while 'connection' is defined

as the location where two or more members are mechanically fastened, as exemplified in Figure 2.2.

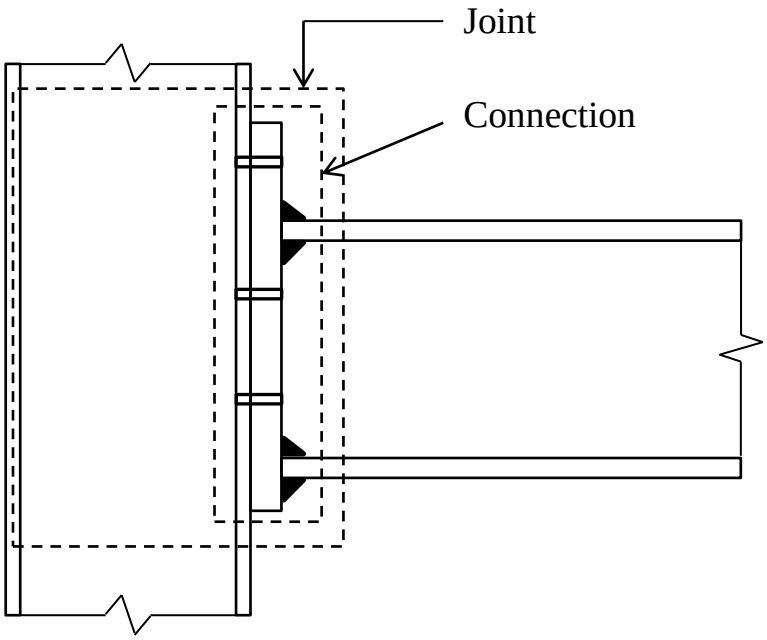

Figure 2.2 Definition of joint and connection

According to the documentation of Joints in Steel Construction-Simple Connections (SCI, 2011), the commonly used steel connections in UK steel construction for beam-to-beam connections and beam-to-column connections are partial end-plate connections, flush end-plate connections, extended end-plate connections and fin-plate connections. The configurations of these four types of connections are given in Figure 2.3.

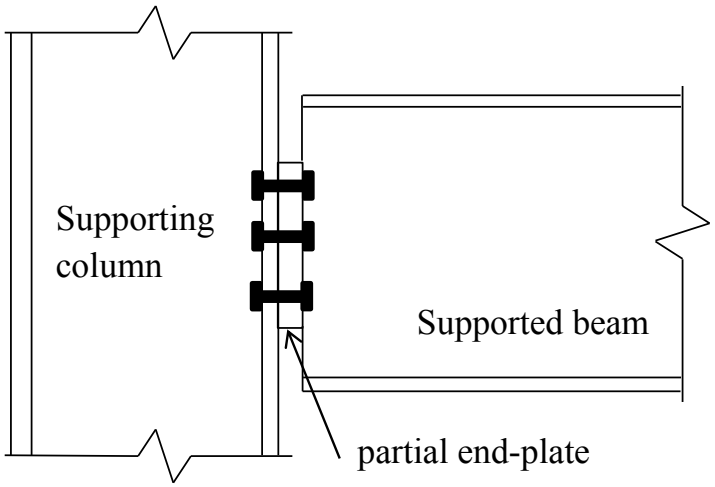

(a) Partial end-plate connection

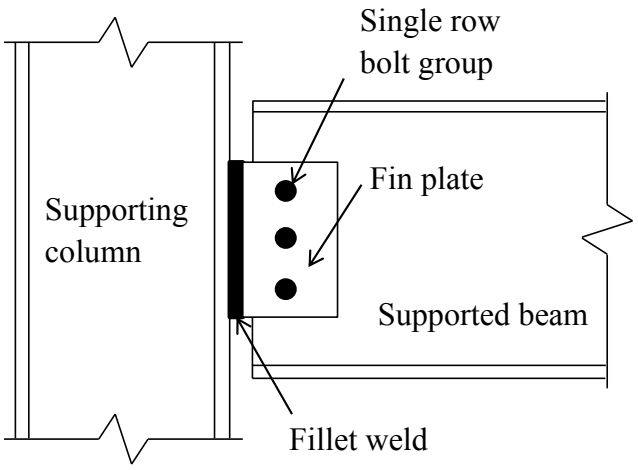

(b) Fin-plate connection

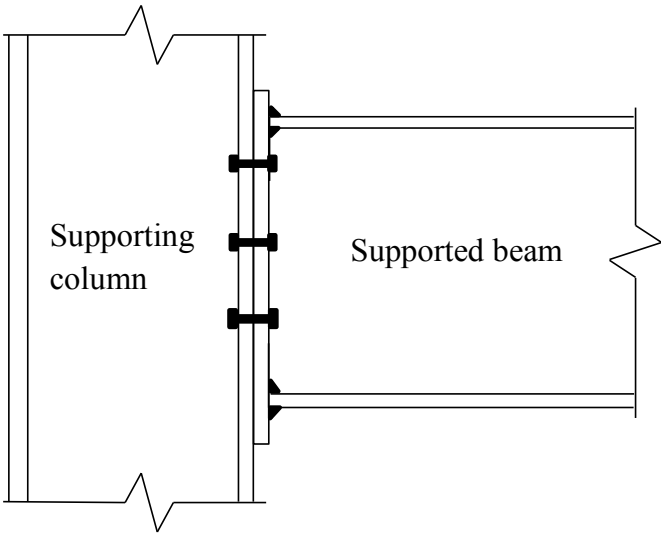

(c) Flush end-plate connection

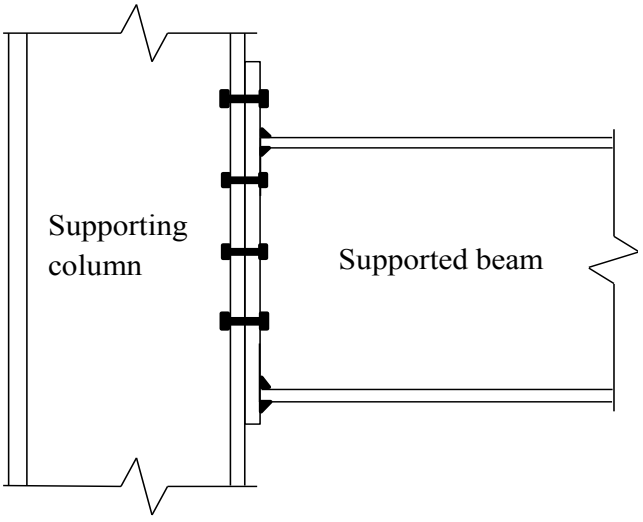

(d) Extended end-plate connection

Figure 2.3 Configurations of commonly used connections

Based on classic structural analysis, the partial end-plate connection and fin-plate connection are simple connections incapable of transmitting significant moments between connected members, while flush end-plate connection and extended end-plate connection are moment connections designed to resist the bending moment and shear forces. Compared to simple connections, the moment connections are more expensive to fabricate.

2.2 Classification of steel connections

2.2.1 Classification based on stiffness

The behaviour of connections is traditionally represented by the moment-rotation relationship. The rotational stiffness of a connection is defined as the initial slope of the moment-rotation curve. In conventional analysis and design, the rotational behaviour of a connection is assumed to be either 'pinned' or 'rigid'. For a pinned connection, the rotational stiffness is regarded as zero. It is incapable of transferring any moment between the beam and the column, as no rotational continuity exists between connected members. For a rigid connection, the rotational stiffness is considered to be infinite. Full beam-end moment is transferred to the column, as there is no relative rotation existed between the beam and the column. However, in reality, the actual rotational behaviour of connections is recognised as being intermediate between these two extremes, where some relative rotations existing between the beam and the column, and some moment transferring within the structures. This kind of behaviour is characterised as 'semi-rigid'. The boundaries to classify different stiffness are documented in Eurocode 3 Part 1.8 (CEN, 2005c) as shown in Figure 2.4.

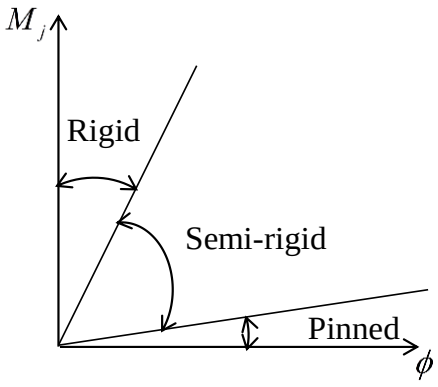

Rigid: $S_{j,\text{int}} \geq k_b EI_{beam} / L_{beam}$

where $k_b = 8$ for braced frames

$k_b = 25$ for other frames

Pinned: $S_{j,\text{int}} \leq 0.5EI_{beam} / L_{beam}$

where I_{beam} is the second moment of area of a beam and L_{beam} is the span of a beam

Figure 2.4 Stiffness classifications of connections in Eurocode 3 Part 1.8 (CEN, 2005c)

2.2.2 Classification based on strength

The connections can be classified as full strength, partial strength and nominally pinned by comparing the design moment resistance of connection to the boundary conditions defined in Eurocode 3 Part 1.8. For a full strength connection, its design moment resistance is larger than or equal to the plastic moment resistance of the connected member. On the other hand, for a partial strength connection, its design moment resistance is less than that of the connected member. If the design moment resistance of connection is lower than 25% of the connected member, the connection can be classified as 'pinned'.

2.3 Steel material properties at elevated temperatures

All common building materials weaken with increasing temperature. For steel, its strength reduces when the temperature exceeds 300 ^{0}C, and decreases approximately at a linear rate up to 800 ^{0}C (Bailey, 1995). At 800 ^{0}C, only 11% of the original strength at ambient temperature remains, reducing to 6% at 900^{0}C (Burgess, 2002). To obtain a clear understanding of the performance of steel structures under fire conditions, it is necessary to investigate the impact of elevated temperatures on the mechanical and thermal properties of steel. The mechanical properties of steel can be expressed in terms of stress-strain characteristics. Generally, there are two test methods to determine the stress-strain relationship of steel at elevated temperatures: the steady-state test, and the transient test. The steady-state test method is conducted by applying strain to a specimen at a steady rate, while keeping the specimen under a constant temperature. Therefore, the obtained stress-strain curve is appropriated for the given constant temperature. In a transient test, the specimen is subjected to a constant load while heated with pre-determined increasing temperatures. Both testing methods were compared by Kirby and Preston (1988). Small scale tensile tests were conducted on grades 43A and 50B steel, utilising two test methods to determine the mechanical properties of steel over a temperature range of 20^{0}C to 900^{0}C. The test results demonstrated that steady-state tests result in higher strength than transient tests. However, a transient test method more realistically represents the actual stress-strain characteristics of steel structural members under fire conditions. The stress-strain characteristics obtained from these tests have been adopted in Eurocode 3 Part 1.2 (CEN, 2005b).

Strength reduction factors are documented in Eurocode 3 Part 1.2 (CEN 2005b), to describe the degradation of steel strength at elevated temperatures. The definition of strength reduction factors can be expressed as the residual strength at a given temperature, relative to the yield strength at ambient temperature. Figure 2.5 demonstrates the reduction factors for yield strength, elastic modulus and proportional limit of steel provided in Eurocode 3 Part 1.2 (CEN 2005b).

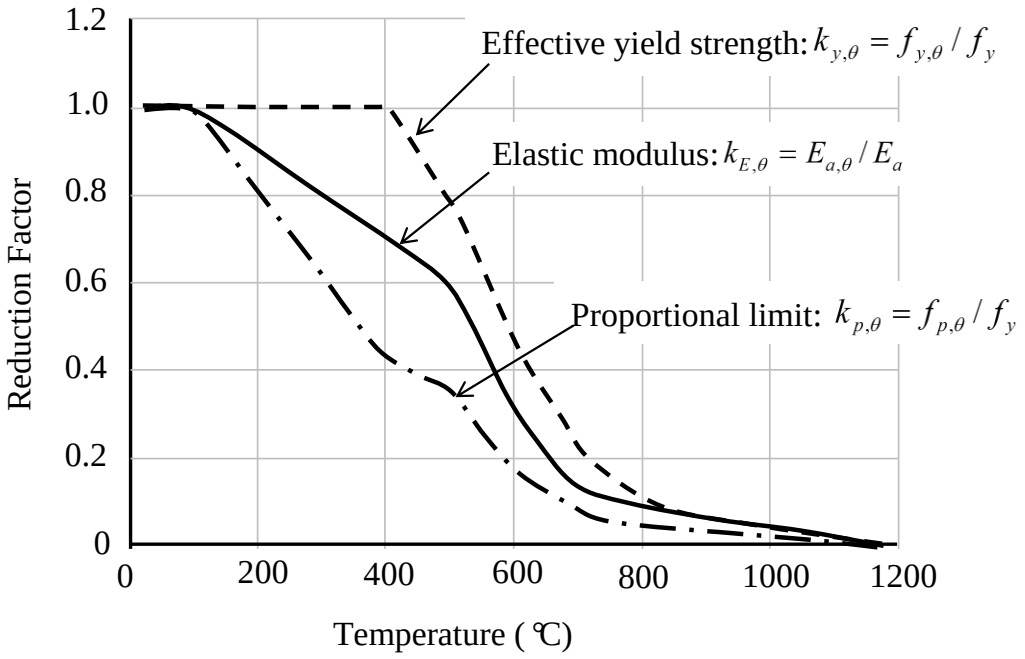

Figure 2.5 Reduction factors for carbon steel according to Eurocode 3 Part 1.2(CEN, 2005b)

At elevated temperatures, the thermal properties of steel need to be taken into consideration (such as thermal expansion, thermal conductivity and specific heat of steel). In Eurocode 3 Part 1.2 (CEN, 2005b), the thermal elongation of steel is defined using a tri-linear curve relates to temperature, as shown in Figure 2.6. It can be noticed that the thermal elongation increases linearly up to around 750 ^{0}C. The material then undergoes a phase-change in crystal structure, and a marked change in the expansion characteristics occurs, as the steel absorbs energy and adopts a denser internal structure (Lawson and Newman, 1996).

Thermal conductivity of steel is defined as the heat flow rate per unit area for a unit temperature gradient. In Eurocode 3 Part 1.2 (CEN, 2005b), thermal conductivity of steel is expressed as a function of the temperature (see Figure 2.7). It can be seen that the thermal conductivity of steel reduces with temperature, in a nearly linear fashion.

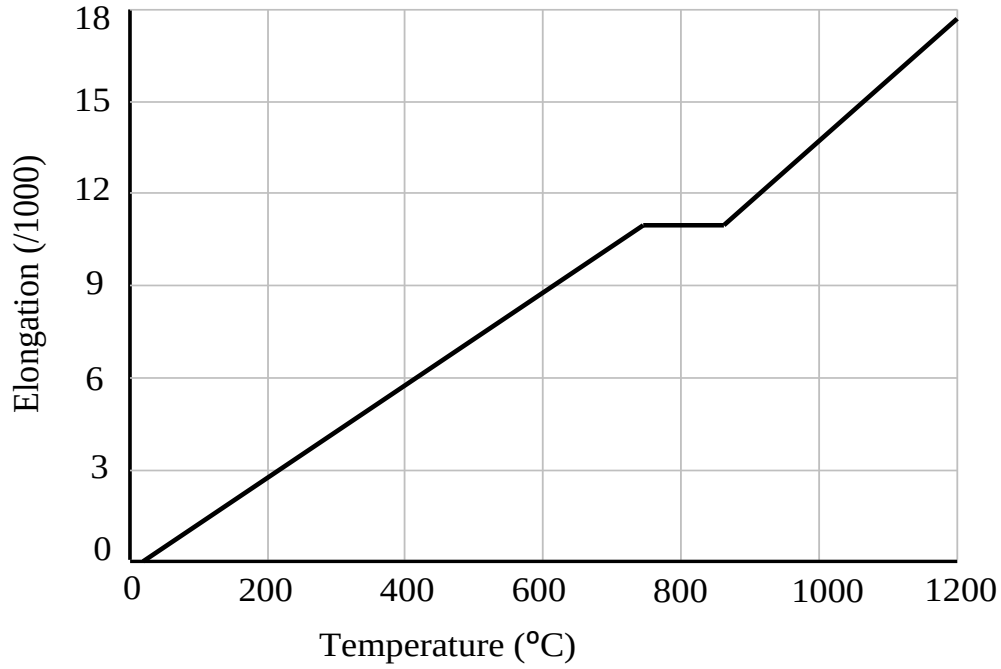

Figure 2.6 Thermal elongations of carbon steel according to Eurocode 3 Part 1.2(CEN, 2005b)

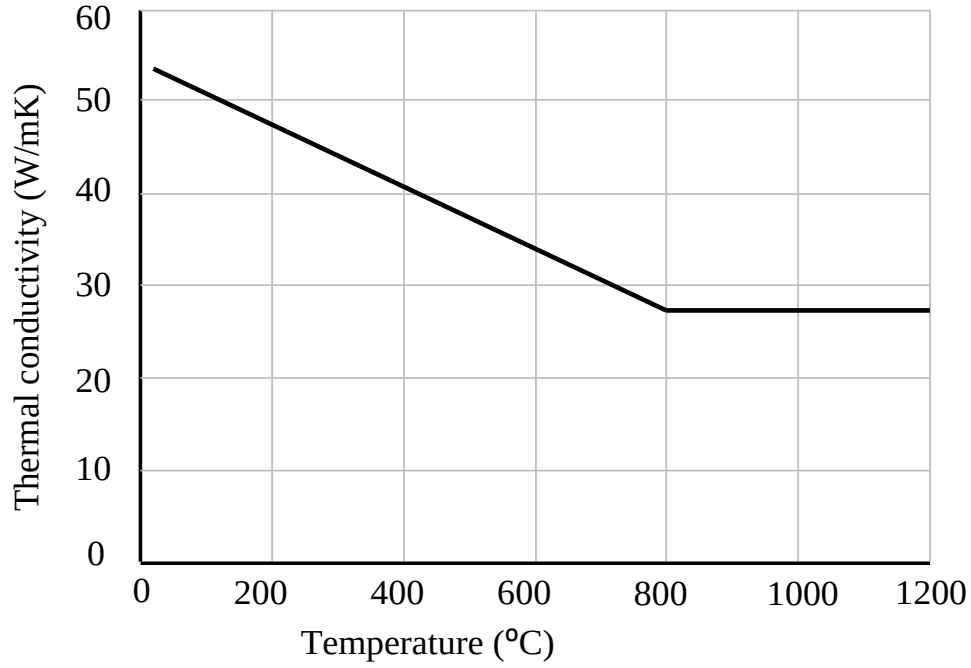

Figure 2.7 Thermal conductivity of carbon steel according to Eurocode 3 Part 1.2(CEN, 2005b)

The specific heat of steel is the amount of heat stored in a unit mass of steel, for 1^{0}C rise in temperature. Eurocode 3 Part 1.2 (CEN, 2005b) specifies the specific heat of steel as a function of temperature, as illustrated in Figure 2.8. It can be observed that the specific heat of steel increases rapidly at around 750^{0}C. The spike results from the phase change occurring in steel, in which the atom structure transits from a face centred cubic to a body centred cubic structure. Considerable heat is absorbed, leading to the appearance of the spike shown in Figure 2.8 (Kodur et al., 2010).

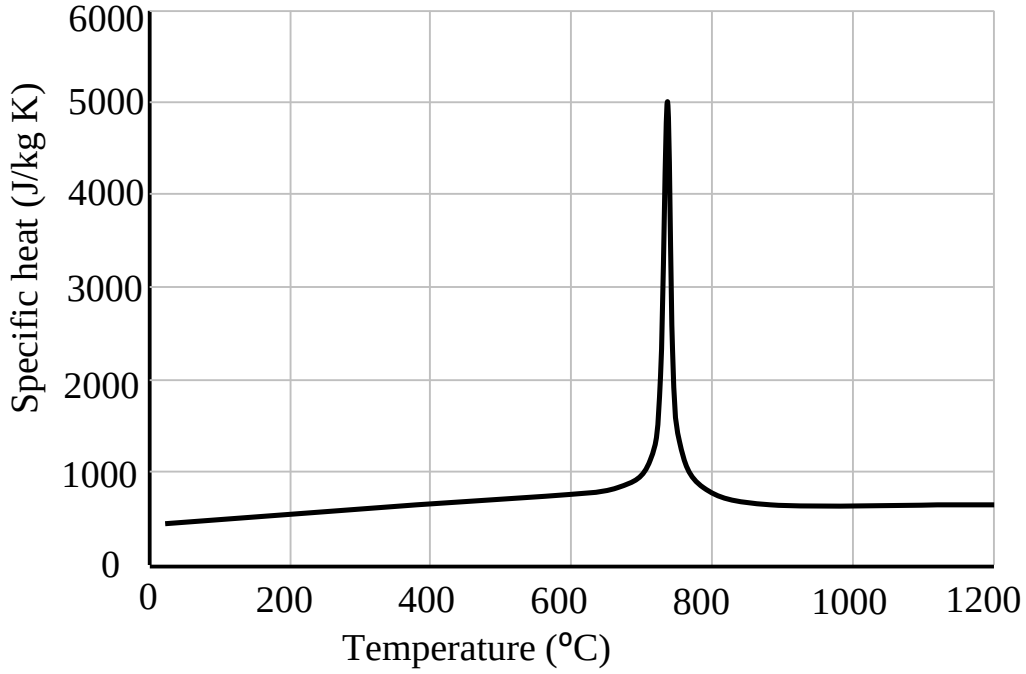

Figure 2.8 Specific heat of carbon steel according to Eurocode 3 Part 1.2(CEN, 2005b)

2.4 Performance of connections at elevated temperatures

In the last two decades, significant progress has been made on understanding the behaviour of steel-framed composite buildings under fire conditions. Current research indicates that the robustness of steel connections is vitally important to the fire resistance of composite buildings. In recent years, an increasing number of investigations on the behaviour of steel connections have been conducted by different researchers.

Eight beam-to-column connections tests subjected to standard fire were conducted by Lawson (1990), in order to measure the moment capacity of beam-to-column connections. Among these eight tests, five of them were carried out on non-

composite beams, two on composite beams, and one on a shelf angle floor beam. In total, three different connections were adopted in this programme, including extended end-plate connection, flush end-plate connection, and double-sided web cleat connection. The time-rotation characteristics of connections at elevated temperatures were established for the first time. The benefit of structural continuity under fire conditions was also analysed in this programme. These experimental results demonstrate that failure of connecting bolts and welds did not take place, *despite* being under considerably larger rotations than at ambient temperature.

The standard fire resistance tests conducted by Lawson did not provide sufficient information to describe the full moment-rotation characteristics of connections at elevated temperatures, however. In 1997, eleven tests were carried out by Leston-Jones (1997a), on bare-steel and composite flush end-plate connections at ambient and elevated temperatures. The experimental results indicate that both the stiffness and moment capacity of connection reduced when temperature increases. A significant downturn in capacity of connection was noticed, when the temperature ranges from 500^0C to 600^0C. Based on these test results, the moment-rotation curves of flush end-plate connection across a range of temperatures have been derived, which can represent the full response of flush end-plate connections under fire conditions.

In Leston-Jones's work, the range of section size and the type of connection was limited. Only small section sizes were taken into consideration. Al-Jabri (1999) extended the scope of the experiments to investigate the influence of parameters, such as member size, connection type, thickness of end-plate and different failure mechanisms. Eleven transient tests were carried out using bare-steel flush end-plate and partial end-plate connections in total. According to the experimental results, a family of moment-rotation curves was established for each connection at elevated temperatures. Two series of tests were additionally performed, on composite partial end-plate connections at both ambient and elevated temperatures. By comparing the moment-rotation characteristics for both bare-steel and composite connections at ambient temperature, it is observed that composite action may attribute to a significant improvement of moment capacity of connection, at low levels of rotation.

Spyrou (2002) carried out a series of experiments on the tension and compression zone of steel connections at elevated temperatures. A total of 45 tests were

conducted on the T-stub assemblies, which have been traditionally applied to represent the components within tension zone. Based on the experimental observations, three failure mechanisms of T-stub assemblies have been summarised. For the compression zone, 29 tests were conducted on column web with various geometrical properties, at ambient and elevated temperatures. However, the influence of axial restraint induced by surrounding cooler structures under fire conditions was not taken into consideration in this study.

A follow up to Spyrou's work was carried out by Block (2006). The work was conducted on column web with different axial compressive load ratios at elevated temperatures. The load ratio is defined as the ratio of the load applied at fire limit state, to the load-carrying capacity at ambient temperature. In fire cases, transverse compressive force is induced by the restraint of surrounding structures due to thermal expansion. In this study, a number of force-displacement characteristics of column web (considering the effect of axial compressive force at elevated temperatures) were derived, providing validation data for numerical studies.

Four transient tests on extended end-plate connections at elevated temperatures were conducted by Wang et al. (2007). The impact of rib stiffener, and depth of end-plate on the fire resistance capacity of extended end-plate connections was investigated in this work. Their experimental results show that both the rib stiffener, and depth of end-plate have some influence on the critical temperature of extended end-plate connections.

Later on, the performances of six extended end-plate connections at elevated temperatures were tested by Qian et al. (2008). Among this study, three tests were conducted by applying three different axial compressive load ratios to the specimens, while keeping the specimens under 700°C. These axial compressive load ratios were adopted to analyse the influence of thermal restraint on the connection while under a constant temperature. Another three tests were carried out on the extended end-plate connections, using a steady-state heating method without applying thermal restraint. According to the experimental results, the moment-rotation-temperature characteristics of extended end-plate connection can be obtained. It is noticeable that the axial restraint force can have a significant impact on the moment capacity of connections at elevated temperatures.

A research programme was conducted jointly by the University of Sheffield and the University Manchester, aimed at investigating the robustness of commonly used connections at elevated temperatures. In total, three kinds of simple connections and moment connections were tested under fire conditions. These were partial end-plate connections, fin-plate connections, web cleat connections and flush end-plate connections. The Sheffield group focused on the performance of isolated connections while the Manchester group investigated the behaviour of structural sub-frames.

Hu et al. (2008) studied the behaviour of partial end-plate connections and conducted a total of 12 tests at ambient and elevated temperatures. The specimens were subjected to different combinations of vertical shear, axial tension and moment. The two stage rotational behaviour of partial end-plate connections were captured at ambient temperature, with the beam bottom flange coming into contact with the column flange after sufficient rotation. The experimental tests showed that the failure of partial end-plate connections were due to the rupture of the end-plate close to the toe of weld.

The 14 tests conducted on fin-plate connections were presented by Yu et al. (2009a). The specimens were subjected to different combinations of tying force and shear force. Besides, three levels of elevated temperatures were applied during the experiments. The influence of bolt grade was also analysed. The experimental results indicated that at elevated temperatures, the failure of fin-plate connections was controlled by bolt shear. The application of strong bolts would significantly improve the resistance of the connections.

Another 14 tests on web cleat connections in fire were carried out by Yu et al. (2009b). Different combination of tying force and shear force were applied to the specimens. The tests results indicated that the combination load does not have a significant influence in the failure mode of web cleat connections. The failure mode of the connections changed with the elevated temperatures. Two main failure mechanisms at high temperatures were observed from these experiments, which were the fracture of the web cleat close to the heel, and the shear failure of the bolts connecting the cleats to the beam web.

The 15 tests on flush end-plate connections at ambient and elevated temperatures were conducted by Yu et al. (2011), aiming to investigate the behaviour of connections when subjected to large tying force and rotations. The specimens were heated to the specified temperature and then loaded until failure occurred. Different combinations of shear and tying forces were adopted in this experiment. It is observed from the experimental results that the failure mode of flush end-plate connection largely relies on the steel temperature, instead of the ratio of tying force to shear force. When the temperature is low, failure mode is determined by the behaviour of the end-plate. While at high temperature, failure is governed by the performance of the bolts.

Daryan and Yahyai (2009) carried out 12 tests on two types of bolted angle, beam-to-column connections, in order to investigate the fire resistance of these connections. One of the tested connection types was the top-seat angle connection, while another one was top-seat angle connection with two additional web angles. The influence of angle thickness, and the usage of additional web angle on the fire resistance of connection were investigated. The experimental results indicated that increasing the thickness of angles would improve the fire resistance of connections. However, using additional web angles does not significantly increase the whole fire resistance of a connection at elevated temperatures, which was due to the premature tension failure of bolts.

It has been noticed that the scale-down experiments on isolated members are insufficient to truly represent the real behaviour of frame structures under fire conditions, due to the lack of structural interaction between components within the structures (Armer and Moore, 1994). During a fire, the performances of beams are associated with the restraint to thermal expansion, due to the interaction between the fire-affected members and the adjacent cooler structures. Liu et al. (2002) carried out 25 tests on sub-frames subjected to ISO 834 standard fire, in order to investigate the influence of axial and rotational restraint on steel beams under fire conditions. These tests were conducted by placing a 2 *m* long beam between two 3 *m* high columns, forming a shape as 'rugby goal post'. Two different types of connections were used in this work: double web-cleats and flush end-plate connections. Three different load ratios and three degrees of horizontal restraint were applied. The experimental results demonstrated that flush end-plate connection can transfer higher

bending moment to column compared to web cleat connections. The catenary action was more visible with the flush end-plate connections, than web cleat connections.

Seven full-scale fire tests were conducted on an eight-storey composite steel-framed building at BRE Cardington Laboratories (Swinden Technology Centre, 1999; Simões da Silva et al., 2005). The tests provided unique and valuable response data regarding the behaviour of a real structure under real fire conditions. The building was designed and constructed as a typical commercial office building, which has eight storeys (33m) and is five bays wide (45m) by three bays deep (21m). Among the seven full-scale fire tests, the seventh test was conducted to investigate the performance of steel-concrete composite frame subjected to natural fire. This test focused particularly on the behaviour of connections, the corresponding distribution of internal forces, and the temperature development within the various structural elements (Wald et al., 2006). In this test, the columns, external joints and edge beams were protected from fire. The partial end-plate connections were adopted for the beam-to-column connections, while the fin-plate connections were applied for the beam-to-beam connections. Both connections were designed to transmit the vertical shear forces. The main failure mechanisms of the connections observed from the experiments were the fracture of the end-plate along the welds, and the elongation of the bolt holes in beam webs as part of the fin-plate connections. These failure mechanisms indicated that considerable horizontal tensile forces were generated within the steel beams, and that the robustness of connections has a significant impact in maintaining structural integrity.

2.5 Development of numerical models for connections

For the past few decades, considerable effort has been concentrated on developing numerical models to represent the behaviour of connections at ambient and elevated temperatures. In general, available analytical models can be classified into three main categories: empirical models; finite element models; and component-based models. In the following sections, the advantages and limitations of these three approaches are discussed in turn.

2.5.1 Empirical models

In empirical models, curve-fitting equations are generated from experimental test data to represent the moment-rotation characteristics of the connections. Parameters within the mathematical expressions are frequently related to the geometrical properties of connections. An early attempt to use the curve-fitting model to describe the moment-rotation-temperature characteristics of connections was made by El-Rimawi et al. (1997). Their model extended the work by Ramberg and Osgood (1943), which developed a polynomial equation to express the stress-strain relationship of metallic material. The modified Ramberg-Osgood equation is given as follows in Equation 2.1:

$$\phi = \frac{M}{A} + 0.01 \times \left(\frac{M}{B} \right)^n \tag{2.1}$$

where ϕ and M are the rotation and moment of connection, respectively. A, B and n are temperature-dependent parameters determining the stiffness, strength and the curve sharpness, respectively. This revised Ramberg-Osgood expression was then adapted by Leston-Jones (1997a) and Al-Jabri (1999) to model their elevated-temperature test data for semi-rigid connections.

Using curve-fitting model can provide accurate numerical results. However, the main disadvantage is that the model is limited to the connections which are similar to those previously investigated experimentally. It would be time consuming and expensive, to perform the tests on the vast number of connection configurations used in practice. Besides, under fire conditions, axial forces are generated due to thermal expansion of the heated beam. It is not suitable to adopt a curve-fitting model, unless all different combinations of moment, axial force and temperatures are tested, which is practically infeasible.

2.5.2 Finite element models

In finite element models, the connections are modelled as an assembly of 3D shell, brick, and contact elements of finite size. The geometric and material nonlinearities of the connections are taken into account using finite element methods. It provides more detailed insight into the behaviour of connections than laboratory-based

investigation. Up to now, finite element method has become a prevalent technique, and a number of finite element models have been proposed by various researchers.

The first attempt to apply the finite element method to describe the performance of connections at elevated temperatures was conducted by Liu (1996). The connections were discretized into flanges and webs of steel I-sections, end-plates and stiffeners by means of eight-node flat-shell quadrilateral elements. A beam element was applied to simulate the behaviour of bolts and the contact between the end-plate and column flange. Their model was validated against two tests conducted by Lawson (1990) on extended end-plate connections. A satisfactory agreement was observed from the comparison results. Later, this model was improved to predict the moment-rotation-temperature characteristics of bare steel and composite connections (Liu, 1999). The concrete slabs were modelled using 3D brick elements. A total of eight sets of fire tests on different types of bare steel and composite beam-to-column connections conducted by previous researchers have been used to validate the proposed model. The numerical prediction obtained from the model corresponded well with the test results.

Spyrou (2002) developed a finite element model to simulate the behaviour of tension components, in the form of T-stubs at elevated temperature, using the commercial software ANSYS. A quarter of the T-stub was modelled by taking advantage of its symmetrical arrangement. For components within the compression zone, the performance of column web was also analysed using a finite element method. The results demonstrated that using three-dimensional analyses is more accurate than the 2D modelling. A close correlation was observed from the 3D analyses compared to the experimental results.

Al-Jabri et al. (2006) established the moment-rotation characteristics of bare-steel flush end-plate connections at elevated temperatures using the commercial software ABAQUS. Only one quarter of the connection was modelled by taking advantage of the symmetric geometry. Three-dimensional brick elements were applied to represent the connection components. The contact between the connected components and the friction between the contact surfaces were all modelled. The finite element results show good agreement with the experimental results.

Sarraj et al. (2007a) developed a finite element model to analyse the behaviour of fin-plate connections under fire condition using ABAQUS software. The friction between the contact surfaces was taken into consideration, by adopting the contact elements at the bolt-hole interface and the surface between the web of the beam and the fin-plate. The fin-plate connection was modelled as an assembly of a series of lap joints. Eight-node hexahedral brick elements were applied to model the beam, fin-plate and bolts. A close agreement was observed from the comparison, between the finite element results and the experimental data.

Dai et al. (2010) proposed a simulation methodology, using three-dimensional solid elements to model the beam, column, and connection components (using the commercial software ABAQUS). The proposed model has been validated against ten fire tests on restrained steel beam-column assemblies. The tests were conducted covering five different types of connections: fin-plate, partial end-plate, web cleat, flush end-plate and extended end-plate. Good agreements were obtained between the ABAQUS simulations and experimental results.

Selamet and Garlock (2014) analysed the behaviour of shear connections in a subassembly under a natural fire, using three-dimensional finite element models. Three types of shear connections were investigated: the single plate, the single angle and the double angle connections. The simulation results indicate that during the heating phase of the fire, different types of shear connections do not have a significant influence on the whole behaviour of the subassembly. However, the connections behave differently during the cooling phase because of the generated large tensile forces.

From the overview presented above, it is obvious that finite element model is capable of providing a detailed and accurate representation of the performance of connections under fire conditions. The finite element model takes into account the complex interaction between the components within the connections, the material, and the geometrical nonlinearities. It is cheaper and easier to perform various loading conditions and different geometries of connections. However, compared to component-based model, finite element modelling is time consuming and computationally expensive. It is difficult to scale-up finite element method for the investigation of complex global structures or sub-structures.

2.5.3 Component-based models

In recent years, component-based models (also known as spring-stiffness models) have been widely adopted to simulate the behaviour of beam-to-column connections under fire conditions (Shi et al., 1996; Simões da Silva et al., 2001; Block et al., 2007; Yu et al., 2009c; Ramli-Sulong et al., 2010; Huang, 2011; Taib, 2012). In comparison with the curve-fitting model and finite element model, component-based modelling is cost-effective and computationally efficient. The component-based method has been standardized in Eurocode 3 Part 1.8 (CEN, 2005c).

In component-based models, the connection is represented as an assembly of a series of springs. Each spring, regarded as an individual basic component, has its own strength and stiffness characteristics in tension, compression, or shear. The application of the component-based method requires the following three steps (Jaspart, 2000):

(1) Identification of the active components within the connections;

(2) Evaluation of the stiffness and resistance characteristics for each basic component;

(3) Combination of all the basic components to evaluate the overall stiffness and resistance characteristics of whole connection.

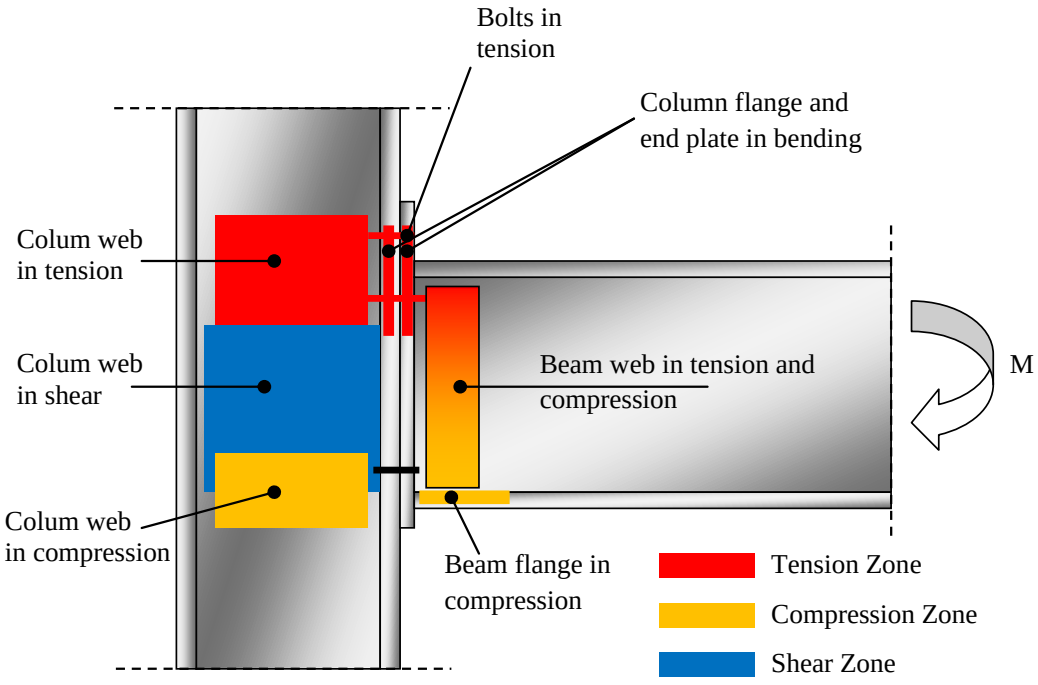

Figure 2.9 Components within a bolted extended end-plate connection

As exemplified in Figure 2.9, a bolted extended end-plate connection subjected to pure bending moment is categorized into three zones (tension, shear and compression). Each zone is divided into a series of basic components, such as column web in tension, bolts in tension, column flange and end-plate in bending, beam web in tension and compression, column web in compression, beam flange in compression, and column web in shear. The overall behaviour of the bolted extended end-plate connection can be represented by as an assembly of these basic components.

One of the early attempts to apply component-based model was made by Wales and Rossow (1983). They analysed the performance of double angle connections, subjected to bending moment and axial force. The connection was simplified as two rigid bars, joined by nonlinear springs which simulated the angle segments and bolts. The force-deformation characteristic of spring was determined using a tri-linear curve. The derived moment rotation relationship of each connection agreed well with experimental test data.

Tschemmernegg and Humer (1988) conducted a series of tests on extended end-plate connections, and modelled the behaviour of connections using three nonlinear springs. The springs were adopted to describe the deformation, due to the load transmitted by the beam flanges and the shear deformation. The overall deformation of the connection was obtained as the sum of deformation of these springs. And the load carrying capacity of the whole connection was determined by its weakest spring. The prediction results of the model corresponded well with the test results.

Shi et al. (1996) proposed an analytical procedure to model the behaviour of flush and extended end-plate connections, which is independent of any empirical coefficients calibrated from test data. T-stub assembly was adopted to represent the components within tension zone. The overall deformation was calculated as the combination of deformation of components in the tension, compression and shear zone. Good approximations were obtained when validated against test data.

Later, Leston-Jones (1997a) applied the component based method to his tests on bare steel and composite flush end-plate connections at elevated temperatures. The validation results show good agreements with experimental data. Al-Jabri (1999) extended the work of Leston-Jones to model the performance of partial end-plate

connections at elevated temperatures. Due to a lack of experimental data, only the rotational behaviour before beam bottom flange comes into contact with column flange was modelled. A component-based model was proposed by Simões da Silva et al. (2001) to predict the behaviour of flush end-plate connections at elevated temperatures. The model was validated against the fire tests conducted on flush end-plate connections by Al-Jabri (1999). Spyrou et al. (2004a, 2004b) developed a component-based model to investigate the behaviour of component within the tension and compression zones of flush end-plate connection at ambient and elevated temperatures. In this model, the inclusion of prying effects, and compatibility of bolts' and end-plates' deformations were taken into consideration. Ramli-Sulong (2005) utilized the component based method to depict the behaviour of a number of typical connections at elevated temperatures, including flush and extended end-plate connections; top, seat and web angle connections; and also fin-plate connections. Good agreements were achieved when validated against test data. Block et al. (2007) focused on the compression zone of end-plate connection, and an analytical model was produced to consider the effects of axial loads in the column. Hu et al. (2009b) proposed a component-based model to describe the performance of partial end-plate connections at ambient and elevated temperatures. They simulated the complete rotational behaviour of partial end-plate connections, including the behaviour of connections after the beam bottom flange made contact with the column flange. A component-based model was developed by Yu et al. (2009c) to describe the behaviour of web cleat connections in fire. This model was validated against test results, and good correlation was achieved. Taib (2012) developed a component-based model focusing on the behaviour of fin-plate connections under fire conditions. The comparison of the model with existing test data show that the model can provide a reasonable prediction of fire performance of fin-plate connections.

In the conventional way of applying a component-based method, the force-displacement of individual basic component within the connection needs to be defined after identification. The accuracy of the derived moment-rotation characteristics of connection largely depends on the quality of force-displacement relationship of each component. One significant problem for using component-based model is that under a static solver condition, if one of the springs within the connection fails, then the numerical illness may be generated within the stiffness

matrix of connection element. Those illnesses may initiate numerical singularity for the whole structures analysed, and the analysis will stop. However, one spring failure within the connection doesn't mean the failure of the whole connection. In order to overcome this problem dynamic solvers are needed. It is well known that using dynamic solver can significantly reduce the computational efficiency of the model.

Huang (2011) proposed a robust 2-node connection element, for modelling flush and extended end-plate connections between steel beam and column under fire conditions. In this model the connection is represented as a 2-node non-linear spring element, and the characteristics of the spring (such as stiffness, tension, compression, shear strengths and bending moment resistance) are determined based on a component-based approach. This model has good numerical stability under a static solver condition, and also retains the advantages of both the simple and component-based models. The validation results illustrate that the model corresponded well with the test results.

2.6 Introduction to the finite element software VULCAN

The finite element software VULCAN is a specialized fire-dedicated program, which is capable of simulating the three dimensional performance of composite and steel-framed buildings under fire conditions. VULCAN was developed at the University of Sheffield, since the 1990s. The program was originally based on the finite element program INSTAF (El-Zanaty et al. (1983)), to simulate the performance of two dimensional steel frames at ambient temperatures. Geometric and material nonlinearities were taken into consideration. This program was extended by Saab (1990) to incorporate the stress-strain relationships at elevated temperatures, and then modified by Najjar (1994) to investigate the three dimensional response of steel frames under fire conditions. Bailey (1995) initially incorporated the spring element into the program to represent the behaviour of semi-rigid connections at elevated temperatures. The bending-moment characteristics of connections under fire conditions were depicted.

VULCAN was then developed significantly further – by Huang et al. (1999a, 1999b, 2000, 2002, 2003a, 2003b, 2004, 2009) and Huang (2011) – for three-dimensional modelling of composite steel-framed structures under fire conditions. In this

program a composite steel-framed building is modelled as an assembly of finite beam-column, connection, slab, and shear connector elements. It is assumed that the nodes of these different types of element are defined under a common reference plane, assumed to coincide with the mid-surface of the concrete slab element (whose location is fixed throughout the analysis). The beam-columns are modelled using 3-node line elements (Huang et al., 2009). The cross-section of each beam element is divided into a number of segments, to allow the variation of temperature, stress, and strain and material properties within the cross-section of the beam element. Both geometric and material nonlinearities are included. The composite floor slabs are represented using 9-noded nonlinear layered slab elements, in which the membrane action of the floor slabs is considered (Huang et al., 2003a, 2003b). The slab elements are divided into a number of plain concrete and reinforcing steel layers. The temperature and material properties for each layer can be specified independently. An effective stiffness model was developed to model the ribbed nature of typical composite slabs (Huang et al., 2000). A simplified two-node connection element has been developed for modelling end-plate connection at elevated temperatures (Huang, 2011). VULCAN has been extensively validated against available experimental results at each step of its developments. At present, the program has been employed for structural fire engineering designs of composite buildings for a number of commercial projects. The program VULCAN therefore provides a solid foundation for the research conducted in this PhD project.

2.7 Conclusions

In this chapter a comprehensive literature review on the behaviour of connections at elevated temperatures has been conducted. It is clear that the robustness of steel connections is a key factor to influence the fire resistance of steel-framed composite buildings. Hence, for performance-based structural fire engineering design of composite structures, more robust connection elements need to be developed for 3D global modelling of composite buildings in fire. The connection element models should have the advantages of both the simple and component-based models, with very good numerical stability under static solver condition, and should be computationally efficient.

In the following Chapters 3 and 4, two robust simplified two-node connection elements are developed for modelling the behaviour of the bolted end-plate, and partial end-plate connections between steel beam and column at elevated temperatures. The proposed numerical procedures are based on the main frame work proposed by Huang (2011), with new developments to more precisely determine the tension, compression, and bending moment capacities of connections during fire.

It is observed from the sub-frame and full-scale frame tests that the steel framed composite structures can provide a significantly greater fire resistance than suggested by conventional tests on isolated steel members. This is largely due to the continuity and interaction between the steel members within the structures. Therefore, it is necessary to investigate the influence of connections on the whole structures when subjected to fire. Unlike other existing large scale 3D modelling of composite structures, which assumed that the connections behave as pinned or rigid for simplicity, these two connection elements presented in Chapters 3 and 4 are incoporated into the program VULCAN to model the semi-rigid behaviour of end-plate and partial end-plate connections for large scale global 3D simulation of composite building under fire conditions (see Chapter 5). The impact of connections on the 3D behaviour of composite structures can thus be assessed in detail. The load-transfer mechanisms of composite floor when connections fail due to axial tension, vertical shear and bending are also investigated in this thesis.

Chapter 3

Modelling of End-plate Connections in Fire

3.1 Introduction

In the last two decades, significant progress has been made on the understanding of steel-framed composite buildings under fire conditions. Current research indicates that the robustness of steel connections is vitally important to the fire resistance of composite buildings. The flush end-plate and extended end-plate connections are popular, and commonly applied for steel framed structures in the UK. The form of flush end-plate connection is a full depth plate welded to the beam flanges and web, then bolted to the column flange. Both the flush and extended end-plate connections can be classified as moment connections, which are required to resist bending moment and shear forces in the design process.

In recent years, an increasing number of investigations on the behaviour of steel connections have been conducted by different researchers. For example, Lawson (1990) carried out a series of experiments to test the behaviour of steel joints at elevated temperatures. Different types of connections were adopted, including flush and extended end-plate connections. Leston-Jones (1997a) conducted the experiments on flush end-plate connections in fire, followed by eight tests on flush end-plate connections with different geometrical and material properties conducted by Al-Jabri et al. (2005). Wang et al. (2007) conducted four transient fire tests on extended end-plate connections, using the standard ISO 834 fire curve. Most recently, Yu et al. (2011) conducted 12 tests on end-plate connections at both ambient and elevated temperatures. Gao et al. (2013) carried out six transient fire tests on flush end-plate connections to investigate the performance of end-plate connection subjected to a combination of shear and tension forces at elevated temperatures.

Structural engineers commonly believe that for performance-based structural fire engineering design the behaviour of steel connections should be simulated through 3D structural global modelling. In recent years, various numerical models have been developed by different researchers. Abolmaali et al. (2005) derived a three-

dimensional finite element model to simulate the moment-rotation characteristics of flush end-plate connections with one bolt row below tension and compression flanges, using the commercial software package ANSYS. The analysis data obtained from the nonlinear finite element model was then curve fitted for the simple Ramberg-Osgood and Three-Parameter Power model to determine the parameters which define the equations. Al-Jabri et al. (2006) developed a finite element model to analyse the performance of flush end-plate connections at elevated temperature, using the finite element software ABAQUS. The moment-rotation characteristics of the connections were established. Wang et al. (2007) developed a component-based model to predict the behaviour of extended end-plate connections under fire conditions. The influence of rib stiffener, and thickness of end-plate on the fire resistance of the connection was also investigated. Block et al. (2007) proposed a component-based model to study the performance of end-plate connections in fire. The force-displacement characteristic of each individual component was defined. This model was incorporated into the non-linear finite element program VULCAN. The behaviour of flush end-plate and extended end-plate connections within the restrained steel beam-column assemblies were established by Dai et al. (2010) using ABAQUS. Gao et al. (2013) used ABAQUS to derive a nonlinear finite element model to predict the fire resistance of flush end-plate connections, considering the interaction mechanism of tension and shear forces on each individual bolt row.

As reviewed in Chapter 2, the component-based modelling approach is now becoming popular for modelling the responses of connections subject to fire attack. The basic idea is to separate the connection into a series of springs. Each spring, regarded as an individual basic component, has its own strength and stiffness characteristics in tension, compression or shear. The overall behaviour of the connection can be then represented by the combination of these springs. However, the major shortcoming of the component-based model is that under a static solver the analysis may terminate due to numerical singularity, if one component of the connection fails. In fact, one single component failure within the connection does not mean that the whole connection will fail. In order to overcome this problem a dynamic solver is needed to perform the analysis, which significantly reduces the computational efficiency of the approach.

Recently, Huang (2011) has developed a robust 2-node connection element for modelling the bolted end-plate connection between steel beam and column at elevated temperatures. The model represents the connection as a 2-node nonlinear spring. The characteristics of the spring, such as stiffness; the resistances of tension, compression and shear; bending moment resistance, are calculated based on the individual components of the connections. In Huang's model the characteristic of each component is determined by using the formulas proposed in Eurocode 3 Part 1.8 (CEN, 2005c; this reference is represented as EN 1993-1-8 in the rest of this thesis), and extended specifically for modelling fire by considering material properties as temperature dependent. This model has been found to be on the conservative side compared with test results. However, Huang's model combines the advantages of both the simplified and component-based models.

In this chapter, the developments of a robust two-node connection element, for modelling end-plate connection at elevated temperatures, are presented. The model is based on the framework of Huang's connection model (Huang, 2011). A number of new sub-models are developed for predicting the tension capacity of each individual bolt row and compression resistances of end-plate connections. These sub-models are based on a component-based approach with robust deformation criteria for a T-stub. For modelling the behaviour of a T-stub, the three failure modes of a T-stub have been taken into account. These new developments are all incorporated into Huang's 2-node end-plate connection framework (Huang, 2011). Through this integration, the new two-node connection element developed in this research also retains the advantages of both the simplified and component-based models.

3.2 Development of element stiffness matrix

As mentioned above, the proposed connection element is based on a modification of the two-node connection element developed by Huang (2011). In the original model, the connection is regarded as a two-node element which has no physical length (see Figure 3.1). Each node has six degrees of freedom: three translational degrees of freedom u, v, w, and three rotational degrees of freedom $\theta_x, \theta_y, \theta_z$; where *x, y, z* are local coordinates of steel beam element in which *x* is the direction of longitudinal axis of the beam element. Hence, the relationship between the nodal force increment

vector $\mathbf{\Delta F}$ and the nodal displacement increment vector $\mathbf{\Delta u}$ can be described using a stiffness matrix $\mathbf{K}$, as shown below:

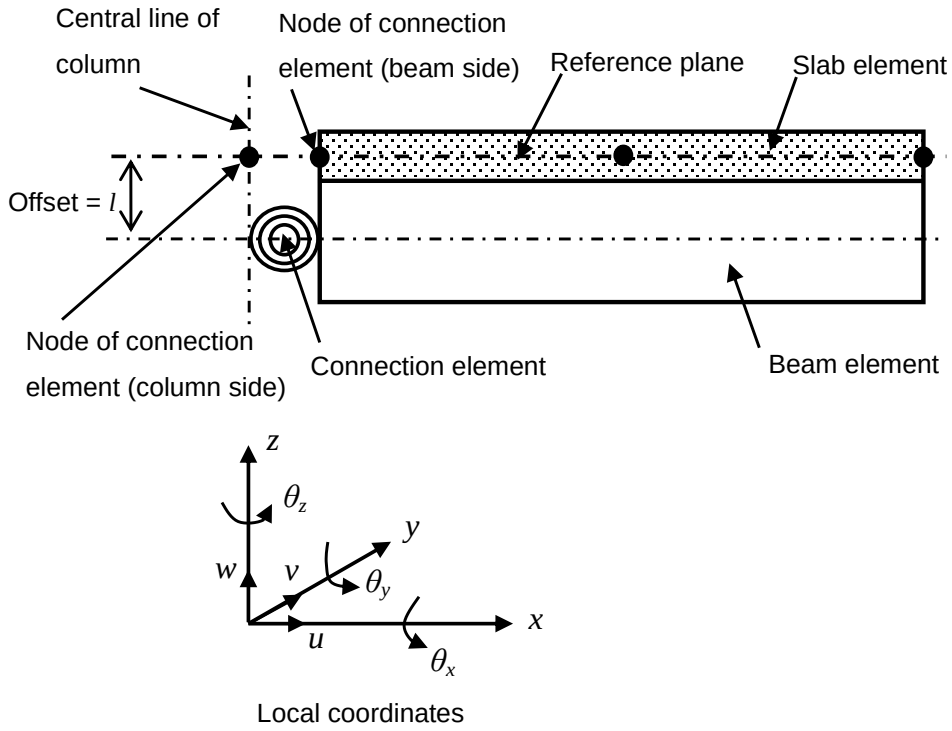

Figure 3.1 Two-node connection element

$$\begin{Bmatrix} \Delta F_{x,1} \\ \Delta F_{y,1} \\ \Delta F_{z,1} \\ \Delta M_{x,1} \\ \Delta M_{y,1} \\ \Delta M_{z,1} \\ \Delta F_{x,2} \\ \Delta F_{y,2} \\ \Delta F_{z,2} \\ \Delta M_{x,2} \\ \Delta M_{y,2} \\ \Delta M_{z,2} \end{Bmatrix} = \begin{bmatrix} k_{11} & 0 & 0 & 0 & -k_{11}\ell & 0 & -k_{11} & 0 & 0 & 0 & k_{11}\ell & 0 \\ 0 & k_{22} & 0 & 0 & 0 & 0 & 0 & -k_{22} & 0 & 0 & 0 & 0 \\ 0 & 0 & k_{33} & 0 & 0 & 0 & 0 & 0 & -k_{33} & 0 & 0 & 0 \\ 0 & 0 & 0 & k_{44} & 0 & 0 & 0 & 0 & 0 & -k_{44} & 0 & 0 \\ -k_{11}\ell & 0 & 0 & 0 & (k_{55}+k_{11}\ell^2) & 0 & k_{11}\ell & 0 & 0 & 0 & -(k_{55}+k_{11}\ell^2) & 0 \\ 0 & 0 & 0 & 0 & 0 & k_{66} & 0 & 0 & 0 & 0 & 0 & -k_{66} \\ -k_{11} & 0 & 0 & 0 & k_{11}\ell & 0 & k_{11} & 0 & 0 & 0 & -k_{11}\ell & 0 \\ 0 & -k_{22} & 0 & 0 & 0 & 0 & 0 & k_{22} & 0 & 0 & 0 & 0 \\ 0 & 0 & -k_{33} & 0 & 0 & 0 & 0 & 0 & k_{33} & 0 & 0 & 0 \\ 0 & 0 & 0 & -k_{44} & 0 & 0 & 0 & 0 & 0 & k_{44} & 0 & 0 \\ k_{11}\ell & 0 & 0 & 0 & -(k_{55}+k_{11}\ell^2) & 0 & -k_{11}\ell & 0 & 0 & 0 & (k_{55}+k_{11}\ell^2) & 0 \\ 0 & 0 & 0 & 0 & 0 & -k_{66} & 0 & 0 & 0 & 0 & 0 & k_{66} \end{bmatrix} \begin{Bmatrix} \Delta u_1 \\ \Delta v_1 \\ \Delta w_1 \\ \Delta \theta_{x,1} \\ \Delta \theta_{y,1} \\ \Delta \theta_{z,1} \\ \Delta u_2 \\ \Delta v_2 \\ \Delta w_2 \\ \Delta \theta_{x,2} \\ \Delta \theta_{y,2} \\ \Delta \theta_{z,2} \end{Bmatrix} \quad (3.1)$$

where ℓ is the offset between the reference plane and position of the connection element, as shown in Figure 3.1.

In Equation (3.1), six stiffness coefficients need to be determined in the stiffness matrix. These are the axial stiffness coefficient k_{11} , vertical shear stiffness

coefficient k_{33}, rotational stiffness coefficient k_{55}, and stiffness coefficients related to the out-of-plane degrees of freedom k_{22}, k_{44} and k_{66}. In this model, only the in-plane behaviour of connection referenced to local coordinates is taken into account. The out-of-plane degrees of freedom referenced to local coordinates (see Figure 3.1) are considered to be rigid. Therefore, the values of the stiffness coefficients k_{22}, k_{44} and k_{66} are assumed to be much larger ($10^9\, kN/mm$). As for the axial stiffness coefficient k_{11} and the vertical stiffness coefficient k_{33}, it is assumed that the initial value of these two coefficients are $10^9\, kN/mm$ before the failure. When the axial tensile force of the connection is greater than the tension resistance of the connection, the connection fails by tension. At this stage, the axial stiffness coefficient k_{11} reduces to zero. However, if the connection fails due to compression, it is assumed that the axial stiffness coefficient k_{11} still has large magnitude. The same principle can be adopted for the vertical stiffness coefficient k_{33}. If the vertical shear force exceeds the vertical shear resistance of the connection, the connection then fails by shear. At this stage, the vertical stiffness coefficient k_{33} decreases to zero. The rotational stiffness coefficient k_{55} is defined based on the moment-rotation curve described in the following sections.

3.3 Moment-rotation characteristic of connection element

The model developed in this chapter, for the calculation of rotational stiffness coefficient k_{55}, is mainly based on the ambient temperature formulations proposed in EN 1993-1-8; the model is extended to account for fire conditions by considering all material properties as temperature dependent. Details of the bolted end-plate connection between the steel column and beam are shown in Figure 3.2.

As mentioned before, only the local in-plane behaviour of the connection element is considered. Hence, one of the main objectives of this research is to develop a numerical procedure for determining the bending moment characteristic of the end-plate connection in fire. The moment-rotation characteristic of the connection element is represented as a tri-linear curve as shown in Figure 3.3 (broken line O-A-

B-C). In this figure, $S_{j,\text{int}}$ is the initial rotational stiffness of the connection, and $M_{j,Rd}$ is the moment resistance of the connection.

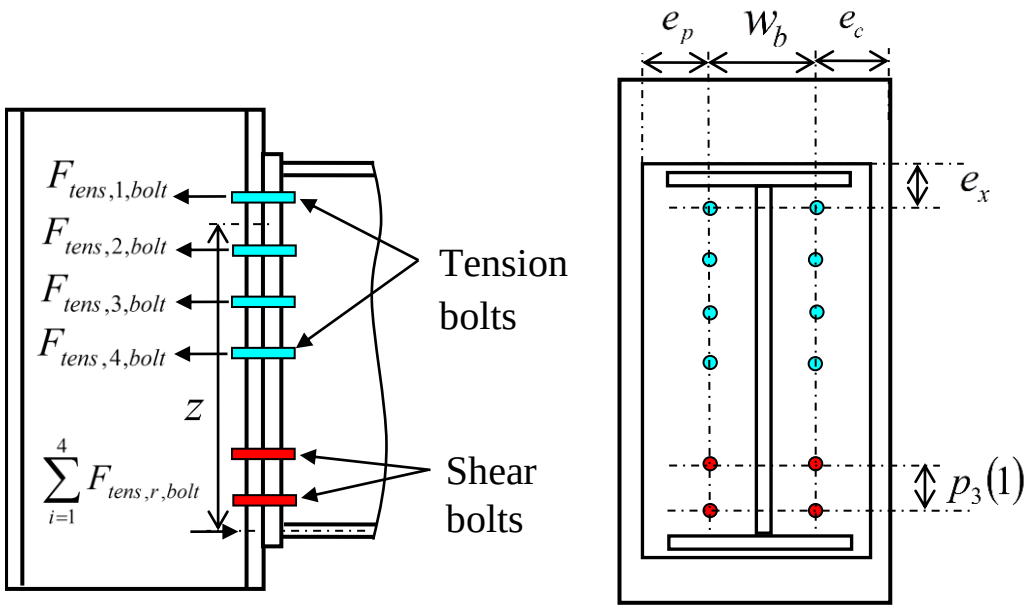

(a) flush end-plate connection

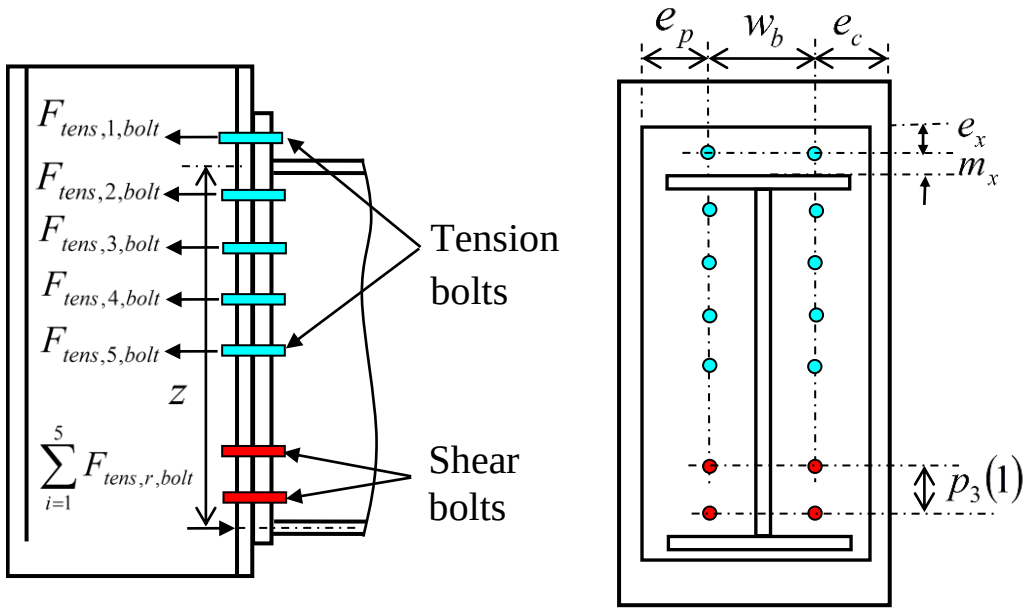

(b) Extended end-plate connection

Figure 3.2 Configuration of bolted end-plate connection

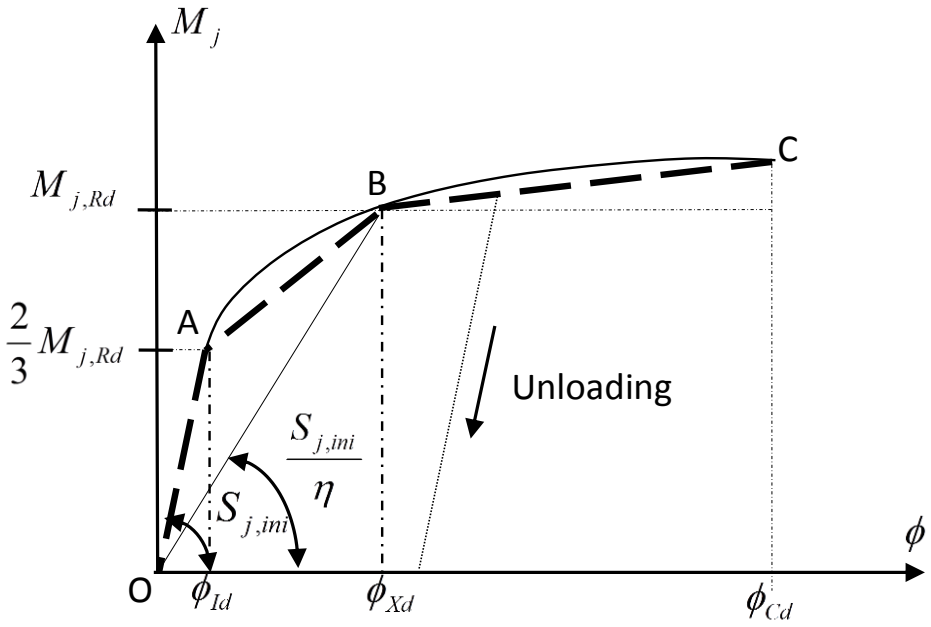

Figure 3.3 Tri-linear moment-rotation characteristic used for the connection element

In this tri-linear representation of moment-rotation characteristics, ϕ_{Xd} is the rotation when the moment applied to the connection first reaches the moment resistance of the connection $M_{j,Rd}$. ϕ_{Cd} is the maximum rotation of the design moment-rotation characteristic of the connection. These rotations can be calculated as follows:

$$\phi_{Id} = \frac{2M_{j,Rd}}{3S_{j,\text{int}}} \tag{3.2}$$

$$\phi_{Xd} = \frac{M_{j,Rd}}{\frac{S_{j,\text{int}}}{\eta}} \tag{3.3}$$

where η is the stiffness modification coefficient, $S_{j,\text{int}}$ is the initial rotational stiffness. For bolted end-plate beam-to-column connections, its value is assumed to be $\eta = 2$ according to EN 1993-1-8.

As explained above, the rotational stiffness coefficient k_{55} within the stiffness matrix is derived based on the moment-rotation curve. The moment-rotation characteristic of end-plate connection can be expressed as:

For line OA ($\phi \le \phi_{Id}$):

$$M_j = k_{55}\phi = S_{j,\text{int}}\phi \tag{3.4}$$

where $k_{55} = S_{j,\text{int}}$.

For line AB ($\phi_{Id} < \phi \le \phi_{Xd}$):

$$M_j = k_{55}(\phi - \phi_{Id}) + \frac{2}{3}M_{j,Rd} \tag{3.5}$$

where $k_{55} = \dfrac{M_{j,Rd}}{3(\phi_{Xd} - \phi_{Id})}$.

For line BC ($\phi_{Xd} < \phi \le \phi_{Cd}$):

$$M_j = k_{55}(\phi - \phi_{Xd}) + M_{j,Rd} \tag{3.6}$$

where $k_{55} = 0.065\, S_{j,\text{int}}$.

The moment-rotation curve of the connection is defined for each temperature level. At elevated temperatures, the moment resistance of the connection $M_{j,Rd}$ and the initial rotational stiffness $S_{j,\text{int}}$ change with the temperatures.

3.3.1 Initial rotational stiffness of the connection, $S_{j,\text{int}}$

As documented in EN 1993-1-8, the initial rotational stiffness is derived according to the stiffness of basic component within the connection. For flush and extended end-plate connection, the initial rotational stiffness can be obtained as:

$$S_{j,\text{int}} = \frac{Ez^2}{\mu\sum_i \frac{1}{k_i}} \tag{3.7}$$

where $\mu = 1$, z is the lever arm, k_i is the stiffness coefficient of the basic component within the connection, E is the average Young's module of the connection; E can be calculated as:

$$E = \frac{E_{cw} + E_{cf} + E_{bw} + E_{bf} + E_p}{5} \tag{3.8}$$

where E_{cw}, E_{cf}, E_{bw}, E_{bf} and E_p are the Young's modulus of column web, column flange, beam web, beam flange and end-plate, respectively.

If there is only one bolt row in tension, the initial rotational stiffness can be represented as:

$$S_{j,\text{int}} = \frac{Ez^2}{\mu\left(\frac{1}{k_1}+\frac{1}{k_2}+\frac{1}{k_3}+\frac{1}{k_4}+\frac{1}{k_5}+\frac{1}{k_{10}}\right)} \tag{3.9}$$

Otherwise, the initial rotational stiffness is derived as:

$$S_{j,\text{int}} = \frac{Ez^2}{\mu\left(\frac{1}{k_1}+\frac{1}{k_2}+\frac{1}{k_{eq}}\right)} \tag{3.10}$$

The stiffness coefficients k_i for the related basic components are calculated according to EN 1993-1-8. The details of numerical derivation are described in the following sections.

3.3.2 Stiffness coefficients for basic components

3.3.2.1 The column web in shear (k_1)

For an unstiffened single-side joint, or a double-sided joint in which the beam depths are similar, the stiffness coefficient for column web in shear can be determined as:

$$k_1 = \frac{0.38 A_{VC}}{\beta z} \tag{3.11}$$

A_{VC} is the shear area of the column, for rolled I and H sections, it can be given as Eurocode 3 Part 1.1(CEN, 2005a):

$$A_{VC} = A_c - 2b_c t_{fc} + (t_{wc} + 2r_c)t_{fc} \text{ But not less than } \eta(h_c - 2t_{fc})t_{wc} \tag{3.12}$$

where A_c is the cross-section area, b_c is the width of column, t_{fc} is the thickness of column flange, t_{wc} is the thickness of column web, h_c is the depth of the column cross-section, r_c is the column fillet radius and $\eta = 1.2$ is recommended for steel grades up to S460 (Eurocode 3 Part 1.5, CEN, 2006).

β is the transformation parameter, its value is approximated to be 1.0 for single-sided connection while 2.0 for double-sided connection. z is the lever arm. If there is only one bolt row in tension within the bolted end-plate connection, z is taken as

the distance from the centre of compression to the bolt row in tension. For a bolted end-plate connection which has two or more bolt rows in tension, z is defined as the distance from the centre of compression to a point midway between the farthest two bolt rows in tension. The centre of compression is located in line with the mid-thickness of the compression flange (see Figure 3.3).

3.3.2.2 The column web in compression (k_2)

The stiffness coefficient for column web in compression is given as:

$$k_2 = \frac{0.7 b_{eff,c,wc} t_{wc}}{d_{c,c}} \tag{3.13}$$

where $d_{c,c}$ is the depth of the column web between the root radii.

For bolted end-plate connection, the effective width of column web in compression $b_{eff,c,wc}$ can be given as:

$$b_{eff,c,wc} = t_{fb} + 2\sqrt{2}a_p + 5(t_{fc} + s) + s_p \tag{3.14}$$

where t_{fb} is the thickness of beam flange. For a rolled I or H section column, $s = r_c$, $s_p = \sqrt{2}t_p$, $a_p = 0.55t_p$ where t_p is the thickness of end-plate.

3.3.2.3 The column web in tension (k_3)

The stiffness coefficient for column web in tension is determined as:

$$k_3 = \frac{0.7 b_{eff,t,wc} t_{wc}}{d_{c,c}} \tag{3.15}$$

where $b_{eff,t,wc}$ is the effective width of column web in tension. As provided in EN 1993-1-8, the value of $b_{eff,t,wc}$ varies according to the position of bolt row (see Table 3.1).

The definition of e_c and e_x are demonstrated in Figure 3.2. For a rolled I section column, as illustrated in Figure 3.4, $m_{1,c}$ can be derived as:

$$m_{1,c} = 0.5(w_b - 0.8 \times 2r_c - t_{wc}) = 0.5(w_b - 1.6r_c - t_{wc}) \tag{3.16}$$

where w_b is the bolt gauge between the centrelines, as shown in Figure 3.2.

Table 3.1 Effective lengths for a column flange

Bolt-row location	Effective width for column flange
Inner bolt-row	Smallest of $2\pi m_{1,c}$ $4m_{1,c}+1.25e_c$
End bolt-row	Smallest of $2\pi m_{1,c}$ $\pi m_{1,c}+2e_x$ $4m_{1,c}+1.25e_c$ $2m_{1,c}+0.625e_c+e_x$

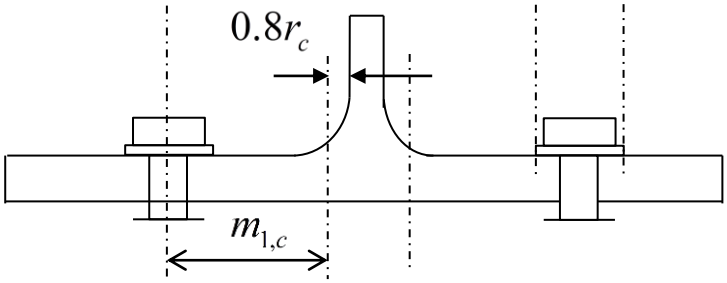

Figure 3.4 Definition of $m_{1,c}$

3.3.2.4 The column flange in bending (k_4)

The stiffness coefficient for the column flange in bending can be calculated as:

$$k_4 = \frac{0.9 b_{eff,t,fc} t_{fc}^3}{m_{1,c}^3} \tag{3.17}$$

The effective width $b_{eff,t,fc}$ is calculated as same as $b_{eff,t,wc}$, which can determined according to Table 3.1.

3.3.2.5 The end-plate in bending (k_5)

The stiffness coefficient for end-plate in bending can be derived as:

$$k_5 = \frac{0.9 b_{eff,p} t_p^3}{m_p^3} \tag{3.18}$$

The value of the effective width $b_{eff,p}$ varies based on the position of bolt-row, given as below in Table 3.2 according to EN 1993-1-8.

Table 3.2 Effective width for an endplate

Bolt-row location	Effective width for T-stub flange
Bolt-row outside tension flange of beam	Smallest of $2\pi m_x$ $\pi m_x + w_b$ $\pi m_x + 2e_p$ $4m_x + 1.25e_x$ $e_p + 2m_x + 0.625e_x$ $0.5b_p$ $0.5w_b + 2m_x + 0.625e_x$
First bolt-row below tension flange of beam	Smallest of $2\pi m_{1,p}$ $\alpha m_{1,p}$
Other inner bolt-row and other end bolt-row	$2\pi m_{1,p}$ $4m_{1,p} + 1.25e_p$

In this table, b_p is the width of end-plate. The determination of e_p is illustrated in Figure 3.2. The coefficient α can be determined based on the Figure 6.11 of EN 1993-1-8. For a bolt row located in the extended part of an extended endplate, m_p in Equation (3.18) is defined to be equal to m_x shown in Figure 3.2. For a bolt-row not located within the extension of end-plate, $m_p = m_{1,p}$.

$m_{1,p}$ can be defined according to EN 1993-1-8 as:

$$m_{1,p} = 0.5(w_b - 0.8 \times 2\sqrt{2} a_p - t_{wb}) \tag{3.19}$$

where t_{wb} is the thickness of beam web.

3.3.2.6 The bolts in tension (k_{10})

The stiffness coefficient for bolts in tension can be determined as:

$$k_{10} = \frac{1.6 A_s}{L_b} \tag{3.20}$$

where A_s is the tensile stress area of the bolt. L_b is the bolt length, which is considered to be equal to the total thickness of material and washers, plus half of the height of the bolt head and half of the height of the nut.

3.3.2.7 The equivalent stiffness coefficient (k_{eq})

For an end-plate connection with two or more bolt rows in tension, a single equivalent stiffness coefficient k_{eq} is applied to represent the stiffness coefficient of basic components related to all of these bolt rows in tension. This can be determined from the following expression:

$$k_{eq} = \frac{\sum_r k_{eff,r} h_r}{z_{eq}} \tag{3.21}$$

where h_r is the distance between bolt row r and the centre of compression. z_{eq} is the equivalent lever arm, given as:

$$z_{eq} = \frac{\sum_r k_{eff,r} h_r^2}{\sum_r k_{eff,r} h_r} \tag{3.22}$$

$k_{eff,r}$ is the effective stiffness coefficient for bolt row r taken into account. Its value is determined by considering the stiffness coefficients $k_{i,r}$ representing basic components relative to bolt row r. $k_{eff,r}$ can be calculated as:

$$k_{eff,r} = \frac{1}{\sum_i \frac{1}{k_{i,r}}} \tag{3.23}$$

As given in EN 1993-1-8, for end-plate connection, $k_{eff,r}$ is defined based on the stiffness coefficients for the column web in tension, the column flange in bending, the end-plate in bending and the bolts in tension. Therefore, for bolt row r, $k_{eff,r}$ can be expressed as:

$$k_{eff,r} = \frac{1}{\frac{1}{k_{3,r}} + \frac{1}{k_{4,r}} + \frac{1}{k_{5,r}} + \frac{1}{k_{10,r}}} \tag{3.24}$$

3.4 The tension resistance of the connection

In the proposed model, the numerical procedure for determining the tension resistance of the end-plate connection is based on the component-based method. The main components in the bolted end-plate connection can be represented using equivalent T-stubs, as shown in Figure 3.5, which have been traditionally applied to represent the components in the tension zone. Therefore, the end-plate connection can be regarded as an assembly of the column flange T-stub and the end-plate T-stub.

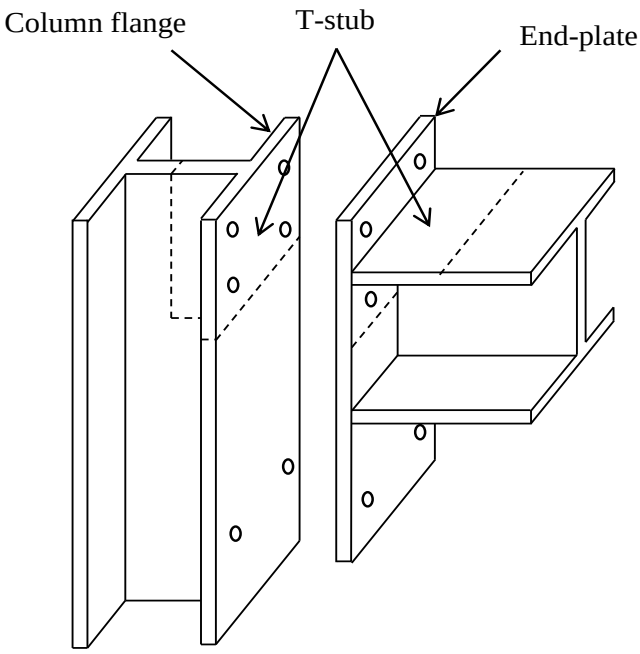

Figure 3.5 T-stubs configuration of end-plate connection

Previous research indicates three different failure modes for a T-stub assembly, depending on the ratio between the resistance of the flange and the resistance of bolts. The three failure models are shown in Figure 3.6. It can be seen that in *Failure*

Mode I, a first plastic hinge is formed at the flange-to-web intersection, this is then followed by the yielding and fracture of the bolts. In *Failure Mode II*, the T-stub flange suffers complete yielding, which has a first plastic hinge occurring in the middle and a second plastic hinge forming in the bolt line. In *Failure Mode III*, however, the T-stub flange remains elastic but fails due to the fracture of the bolts. These three failure mechanisms should therefore be considered in the proposed model.

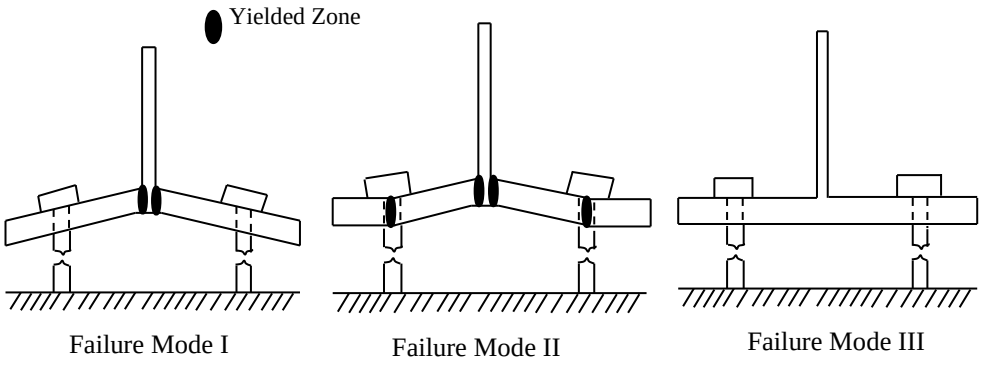

Figure 3.6 Three failure mechanisms of a T-stub

A simplified analytical model has been developed by Spyrou et al. (2004a) to calculate the tension resistance of individual T-stub. The model is derived from elastic beam theory, and a multi-linear representation is used to describe the relationship between tension resistance of the T-stub and the deformation of the T-stub and bolts. However, the failure criterion hasn't been developed in his model, so the model cannot be directly adapted to calculate the tension capacity of the connection. Hence, in this research based on Spyrou's model, three proper displacement failure criteria are proposed for the three failure modes of a T-stub, to capture its tension resistance at elevated temperatures. In the current model (in this thesis), the resistances of tension and bending of the connection are calculated based on the tension capacity of the T-stub of each bolt row.

In order to obtain the tension resistance of a T-stub assembly, the T-stub assembly is assumed to be simple supported. The tension force acting on the T-stub assembly F is assumed to be a concentrated load locating at the mid-length. The prying force Q needs to be taken into consideration when analysing the behaviour of the T-stub in tension. The prying force is generated because of the tension force of the T-stub,

and the reaction of the bolts between the contact surfaces of the end-plate and the column flange. It is assumed that the prying force acts at the beam edge, with the same direction as the tension force of the T-stub. The bolt force (wk) can be assumed to be distributed uniformly over a finite length, as illustrated in Figure 3.7.

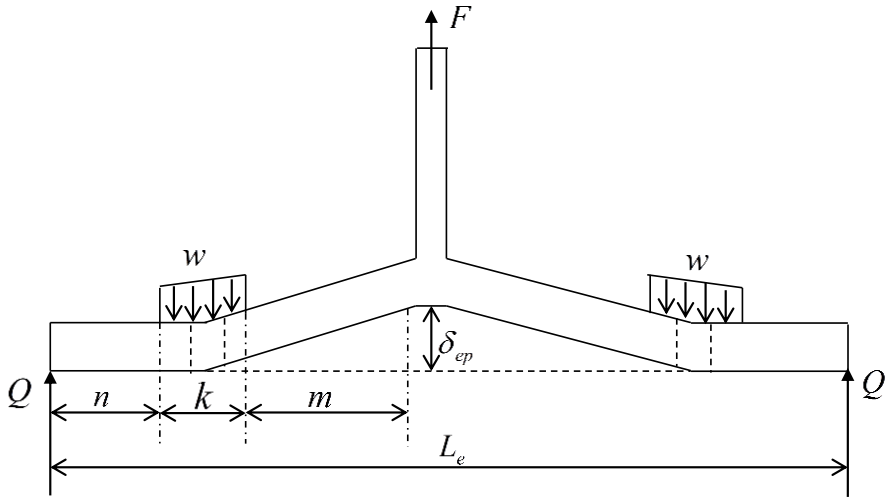

Figure 3.7 Forces on a T-stub assembly

The deflection of the T-stub at the bolt line $(n+k/2)$ can be calculated based on the classical beam theory. In order to express the bolt force relating to the tension force of the T-stub, it is assumed that the deflection of the T-stub at the bolt line is equal to the bolt elongation. Therefore, the bolt force can be determined as:

$$wk = \rho F \tag{3.25}$$

$$\rho = \frac{\dfrac{1}{EI}\left[\dfrac{(n+\frac{k}{2})L_e^{\,2}}{16} - \dfrac{(n+\frac{k}{2})^3}{12}\right]}{\dfrac{L_b}{E_b A_s} - \dfrac{1}{EI}\left[\dfrac{(n+\frac{k}{2})^3}{6} + \dfrac{k^2(n+\frac{k}{2})}{24} + \dfrac{(n+\frac{k}{2})(m+\frac{k}{2})^2}{2} - \dfrac{(n+\frac{k}{2})L_e^{\,2}}{8} - \dfrac{k^3}{384}\right]} \tag{3.26}$$

where k is the max width of tension bolts across comers, E_b is the Young's Modulus of the bolt, $I = L_{eff} t_f^3 / 12$. L_{eff} is the effective width, which is obtained as dispersion at 45° starting from the washer edge of bolt and finishing at $0.8r_c$ or $0.8a_p\sqrt{2}$ from the face of the web (Faella et al., 1998). For column flange T-stub, E is the Young's Modulus of column flange while for end-plate T-stub, E is the

Young's Modulus of end-plate. The same rule applies for the parameter t_f in Equation (3.26).

As demonstrated in Figure 3.8, the effective width can be calculated as follows:

$$L_{eff} = k + 2(m + \frac{k}{2}) \tag{3.27}$$

$$m = \begin{Bmatrix} \frac{w_b - t_{wb} - k}{2} - 0.8r_c & \text{for Column } T-stub \\ \frac{w_b - t_{wb} - k}{2} - 0.8a_p\sqrt{2} & \text{for Endplate } T-stub \end{Bmatrix} \tag{3.28}$$

A multi-linear curve is applied to represent the relationship between the tension resistance and the deformation of the T-stub. The numerical derivation procedure of the force-displacement characteristics of the T-stub assembly under three failure mechanisms are described in the following sections.

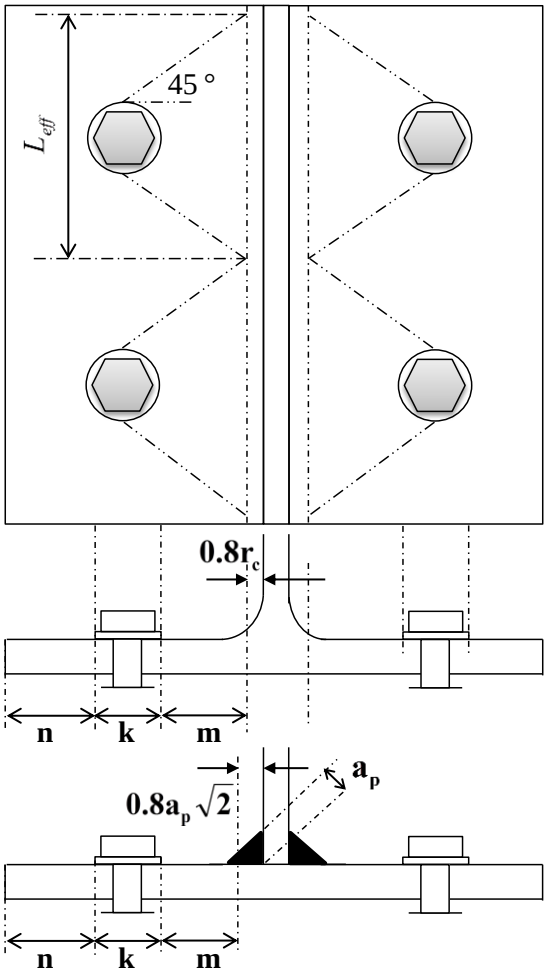

Figure 3.8 Column flange and end-plate T-stub assembly

3.4.1 Failure Mode I

In Failure Mode I, bolts start to yield after the formation of the first plastic hinge, and then fracture before further yielding of the T-stub (as shown in Figure 3.6). In this case, a tri-linear curve is employed, to determine the relationship between the tension force and the displacement of the T-stub as shown in Figure 3.9. In order to define the tri-linear curve, three points ($\delta^I_{cl,pl}, F^I_{cl,pl}$), ($\delta^I_{bl,pl}$, $F^I_{bl,pl}$) and (δ^I_{final}, F^I_{final}) need to be defined. The magnitudes of these six parameters are dependent on the geometric and material properties of the T-stub considered. At point A, $F^I_{cl,pl}$ and $\delta^I_{cl,pl}$ are the force and displacement at the T-stub flange respectively, when the first plastic hinge forms at the flange-to-web intersection (see Figure 3.6).

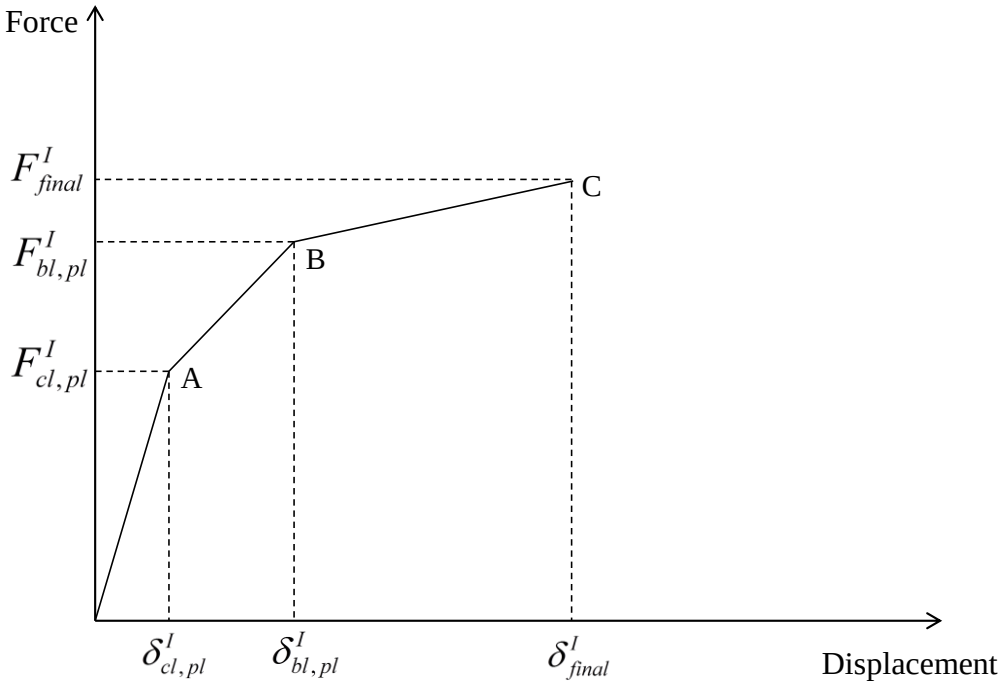

Figure 3.9 Tri-linear force-displacement characteristic for Failure Mode I

The formation of the first plastic hinge is due to the excess of the maximum bending moment of the T-stub compared to the plastic moment resistance M_p given by:

$$M_p = \frac{L_{eff} t_f^2 f_y}{4} \tag{3.29}$$

For column flange T-stub, f_y is the yield strength of column while for end-plate T-stub f_y is the yield strength of end-plate.

Therefore, the tension force of T-stub when the first plastic hinge occurs can be obtained according to the beam bending theory, as given in Equation (3.30).

$$F_{cl,pl}^{I} = \frac{M_p}{\frac{n+m+k}{2} - \rho\left(n+\frac{k}{2}\right)} \tag{3.30}$$

The deformation of the T-stub can be calculated as:

$$\delta_{cl,pl}^{I} = \frac{F_{cl,pl}^{I}}{EI}\left(\frac{L_e^{\,3}}{48} - \rho\left(\frac{L_e^{\,3}}{24} + \frac{(m+\frac{k}{2})^3}{6} - \frac{(m+\frac{k}{2})^2 L_e}{4} - \frac{k^2(n+\frac{k}{2})}{24}\right)\right) \tag{3.31}$$

At point B, $F_{bl,pl}^{I}$ and $\delta_{bl,pl}^{I}$ are the T-stub force and corresponding displacement, when bolts start to yield after the formation of the first plastic hinge. At this stage, part of the T-stub still remains elastic. By applying the same analysis theory, the tension force of the T-stub at this stage can be calculated as:

$$F_{bl,pl}^{I} = \frac{2M_p + 2A_s f_{by}\left(n+\frac{k}{2}\right)}{n+m+k} \tag{3.32}$$

where f_{by} is the yield strength of the bolt.

The deformation of the T-stub $\delta_{bl,pl}^{I}$ could be determined as a linear function relating to the T-stub force $F_{bl,pl}^{I}$, given as:

$$\delta_{bl,pl}^{I} = \frac{\frac{F_{bl,pl}^{I}}{2}(n+k+m) - M_p}{\left(n+\frac{k}{2}\right)EI} \times \left(\frac{(n+k+m)^3}{6} - \frac{(m+\frac{k}{2})^3}{6}\right) - \frac{F_{bl,pl}^{I}}{12EI}(n+k+m)^3 + \frac{A(n+k+m)}{EI} + \frac{B}{EI} \tag{3.33}$$

where

$$A=\frac{\frac{F_{bl,pl}^{I}}{2}(n+k+m)-M_{p}}{(n+\frac{k}{2})}\times\left[\frac{k^{3}}{384(n+\frac{k}{2})}-\frac{(n+\frac{k}{2})^{2}}{6}-\frac{k^{2}}{24}\right]+\frac{F_{bl,pl}^{I}}{12}(n+\frac{k}{2})^{2}+$$
$$+\frac{EI}{n+\frac{k}{2}}\times\frac{\rho F_{cl,pl}^{I}L_{b}}{E_{b}A_{s}}+\frac{EIL_{b}}{E_{b}A_{s}(n+\frac{k}{2})}\times\left(\frac{\frac{F_{bl,pl}^{I}}{2}(n+k+m)-M_{p}}{(n+\frac{k}{2})}-\rho F_{cl,pl}^{I}\right) \quad (3.34)$$

$$B=\frac{\frac{F_{bl,pl}^{I}}{2}(n+k+m)-M_{p}}{(n+\frac{k}{2})}\times\frac{k^{2}(n+\frac{k}{2})}{24} \quad (3.35)$$

After the yielding of bolts, the increment of T-stub force is all taken by the bolts until they fracture. Therefore, at point C F_{final}^{I} is the ultimate tension resistance of the T-stub when bolts fracture, and δ_{final}^{I} is the corresponding total deformation of the T-stub. The values of these two parameters are given by the following formulae:

$$F_{final}^{I}=F_{bl,pl}^{I}+2\left(A_{s}f_{bu}-A_{s}f_{by}\right) \quad (3.36)$$

$$\delta_{final}^{I}=\delta_{bl,pl}^{I}+\frac{2\left(A_{s}f_{bu}-A_{s}f_{by}\right)}{EI}\left[\frac{(m+\frac{k}{4})^{2}(m+\frac{k}{2})}{8}-\frac{(m+\frac{k}{4})^{3}}{24}+\frac{k^{3}}{1536}+\frac{EIL_{b}}{0.02E_{b}A_{s}}\right] \quad (3.37)$$

where f_{bu} is the ultimate tensile strength of the bolt.

3.4.2 Failure Mode II

The main difference between Failure Mode II and Failure Mode I is that in Failure Mode II, after the formation of the first plastic hinge, instead of bolts starting to yield, a second plastic hinge forms at the bolt axis (see Figure 3.6). Multi-linear curves are used to represent the relationship between the tension force and the displacement of the T-stub. Again, the value of these eight parameters is depended on the geometric and material properties of the T-stub considered.

As shown in Figure 3.10, there are four points ($\delta_{cl,pl}^{II}, F_{cl,pl}^{II}$), ($\delta_{bl,pl}^{II}$, $F_{bl,pl}^{II}$), ($\delta_{fl,pl}^{II}$, $F_{fl,pl}^{II}$) and (δ_{final}^{II}, F_{final}^{II}) which need to be defined. At point A, $F_{cl,pl}^{II}$ and $\delta_{cl,pl}^{II}$ are the force and displacement of T-stub respectively when first plastic hinge forms, which can be calculated as same as given in Equations (3.30) and (3.31), respectively. At

point B, $F^{II}{}_{bl,pl}$ and $\delta^{II}{}_{bl,pl}$ are the force and displacement when a second plastic hinge appears at the bolt line. In this case, the tension force of the T-stub can be given by:

$$F_{bl,pl}^{II} = \frac{2M_p\left(2n+\frac{7}{8}k\right)}{mn+\frac{3kn}{8}+\frac{3km}{8}+\frac{k^2}{8}} \tag{3.38}$$

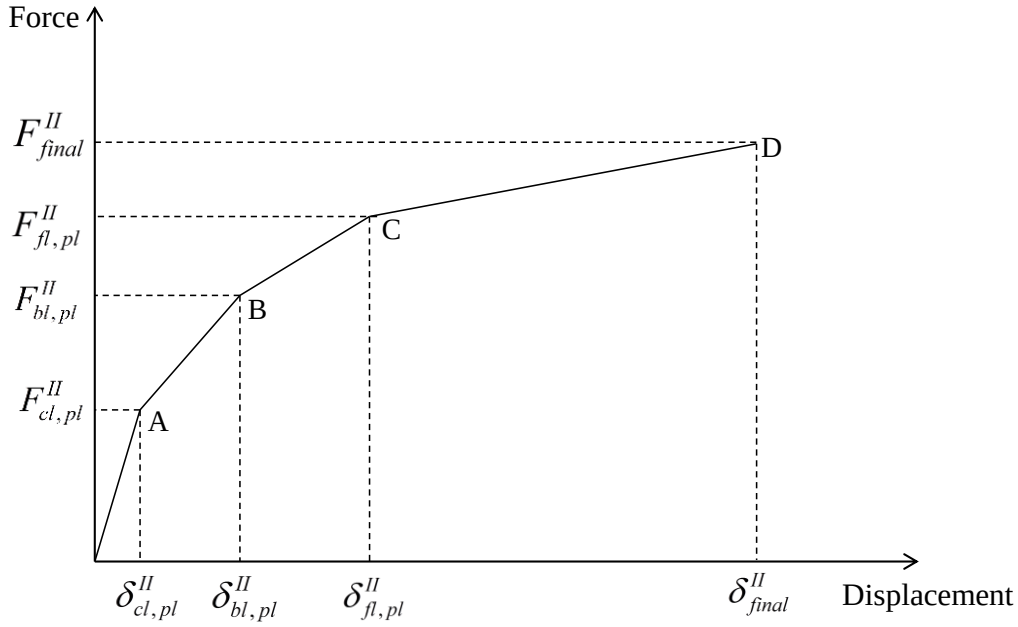

Figure 3.10 Multi-linear force-displacement characteristic for Failure Mode II

The deflection of the T-stub at this stage can be determined as:

$$\delta_{bl,pl}^{II} = \delta_{cl,pl}^{II} + \frac{\Delta Q}{EI}\left[\frac{(n+k+m)^3}{6}\right] - \frac{\Delta(wk)}{EI}\frac{(m+\frac{k}{2})^3}{6} + \frac{C(n+k+m)}{EI} + \frac{D}{EI} \tag{3.39}$$

where

$$\Delta Q = \frac{\left(F_{bl,pl}^{II} - F_{cl,pl}^{II}\right)}{2}\left(\frac{m+\frac{k}{2}}{n+\frac{k}{2}}\right) \tag{3.40}$$

$$\Delta(wk) = \frac{\left(F_{bl,pl}^{II} - F_{cl,pl}^{II}\right)}{2}\left(\frac{m+\frac{k}{2}}{n+\frac{k}{2}}+1\right) \tag{3.41}$$

$$C = \Delta(wk)\left(\frac{k^3}{384(n+\frac{k}{2})} - \frac{k^2}{24} + \frac{EIL_b}{E_b A_s (n+\frac{k}{2})}\right) - \frac{\Delta Q(n+\frac{k}{2})^2}{6} \tag{3.42}$$

$$D = \Delta(wk)\left(\frac{k^2(n+\frac{k}{2})}{24}\right) \tag{3.43}$$

After the formation of the two plastic hinges in the T-stub, the bolts start to yield. The force and deflection of the T-stub at this stage (point C in Figure 3.10) are given below in Equations (3.44) and (3.45):

$$F_{fl,pl}^{II} = F_{bl,pl}^{II} + 2\left(A_s f_{by} - \left(\rho F_{cl,pl}^{II} + \frac{\left(F_{bl,pl}^{II} - F_{cl,pl}^{II}\right)}{2}\left(\frac{m+\frac{k}{2}}{n+\frac{k}{2}} + 1\right)\right)\right) \tag{3.44}$$

$$\delta_{fl,pl}^{II} = \delta_{bl,pl}^{II} + \frac{2\left(A_s f_{by} - (wk)_{bl,pl}^{II}\right)}{0.015EI}\left(\frac{(m+\frac{k}{4})^2(m+\frac{k}{2})}{8} - \frac{(m+\frac{k}{4})^3}{24} + \frac{k^3}{1536} + \frac{0.015EIL_b}{2E_b A_s}\right) \tag{3.45}$$

$$(wk)_{bl,pl}^{II} = \rho F_{cl,pl}^{II} + \frac{\left(F_{bl,pl}^{II} - F_{cl,pl}^{II}\right)}{2}\left(\frac{m+\frac{k}{2}}{n+\frac{k}{2}} + 1\right) \tag{3.46}$$

The bolts finally fracture after the yielding. The force and deformation of the T-stub when the bolts fracture (point D in Figure 3.10) are derived as:

$$F_{final}^{II} = F_{fl,pl}^{II} + 2\left(A_s f_{bu} - A_s f_{by}\right) \tag{3.47}$$

$$\delta_{final}^{II} = \delta_{fl,pl}^{II} + \frac{2\left(A_s f_{bu} - A_s f_{by}\right)}{0.015EI}\left(\frac{(m+\frac{k}{4})^2(m+\frac{k}{2})}{8} - \frac{(m+\frac{k}{4})^3}{24} + \frac{k^3}{1536} + \frac{0.015\,EIL_b}{0.02\,E_b A_s}\right) \tag{3.48}$$

3.4.3 Failure Mode III

Unlike the previous two failure modes, in Failure Mode III, the T-stub flange remains elastic, and it is the yielding of the bolts, and fractures that cause the failure. As shown in Figure 3.11, a bilinear curve is adopted to represent the force-displacement relationship of the T-stub.

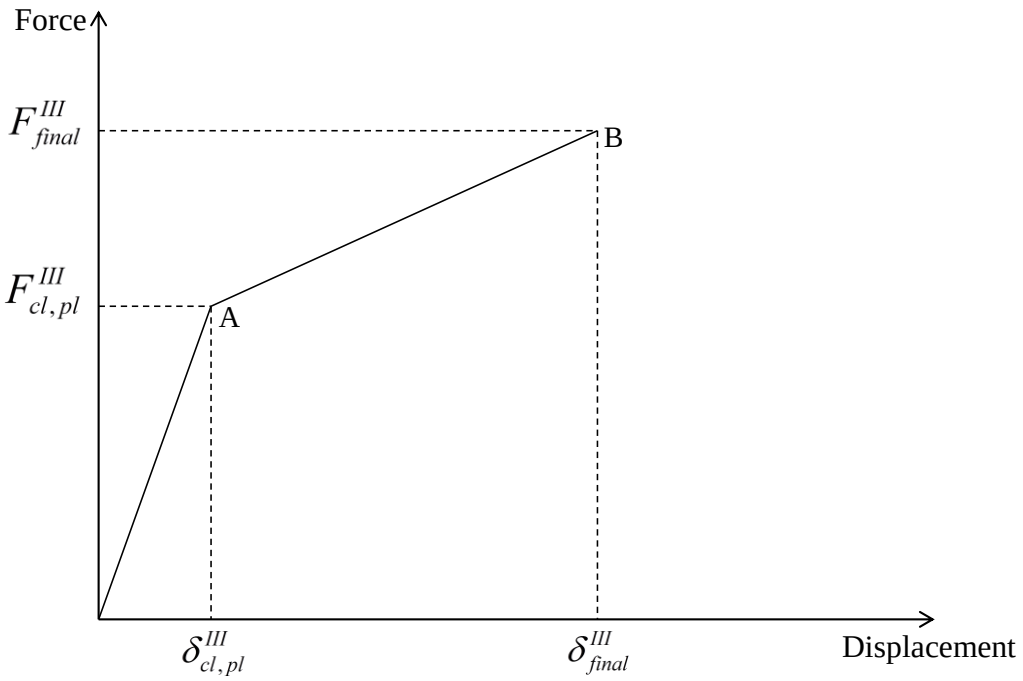

Figure 3.11 Bi-linear force-displacement characteristic for Failure Mode III

There are two points ($\delta_{cl,pl}^{III}, F_{cl,pl}^{III}$) and ($\delta_{final}^{III}$, F_{final}^{III}) which need to be defined. The force and deformation of the T-stub when bolts yielding (point A in Figure 3.11) are given below:

$$F_{cl,pl}^{III} = \frac{2A_s f_{by}}{\rho} \tag{3.49}$$

$$\delta_{cl,pl}^{III} = \frac{F_{cl,pl}^{III} L_e^{\,3}}{48EI} - \frac{\rho F_{cl,pl}^{III}}{EI}\left[\frac{L_e^{\,3}}{24} + \frac{(m+\frac{k}{2})^3}{6} - \frac{(m+\frac{k}{2})^2 L_e}{4} - \frac{k^2(n+\frac{k}{2})}{24}\right] \tag{3.50}$$

The total T-stub force and deflection when the bolts fracture can be determined as:

$$F_{final}^{III} = F_{cl,pl}^{III} + 2\left(A_s f_{bu} - A_s f_{by}\right) \tag{3.51}$$

$$\delta_{final}^{III} = \delta_{cl,pl}^{III} + \frac{2\left(A_s f_{bu} - A_s f_{by}\right)}{EI}\left[\frac{(m+\frac{k}{4})^2(m+\frac{k}{2})}{8} - \frac{(m+\frac{k}{4})^3}{24} + \frac{k^3}{1536} + \frac{EIL_b}{0.02E_bA_s}\right] \tag{3.52}$$

3.4.4 Displacement failure criteria for three failure modes

In Spyrou's model (Spyrou et al., 2004a), it is assumed that bolt fracture is the ultimate failure mode for all three failure modes. However, it is noticed that the tension resistance obtained from experimental test results are lower than the tension

force of the T-stub when bolts fracture. Therefore, it is necessary to propose reasonable failure criteria to predict the tension resistance of the T-stub. In the experimental studies conducted by Spyrou et al. (2004a), the performances of a total of 45 T-stub specimens with different geometrical and mechanical properties were investigated at ambient and elevated temperatures. The 45 tests were divided into three phases, with twelve tests in Phase A, eight tests in Phase B and twenty-five tests in Phase C. The force-displacement characteristics of these specimens in the three phases were analysed using the equations illustrated above. The prediction results were compared to the experimental test data. According to these comparison results, three displacement criteria are proposed for the different failure mechanisms of the T-stub. For Failure Mode I, the displacement criterion $\delta_{cri,1}$ is defined to be $7mm$; For Failure Mode II, the displacement criterion $\delta_{cri,2}$ is identified to be $15mm$; For Failure Mode III, the displacement criterion $\delta_{cri,3}$ is determined to be $3mm$. The developed displacement criteria are then used to predict the tension resistances of 45 tested T-stubs, where good agreement with the test results was achieved. Here, six of the validation results are presented. The dotted line in Figures 3.12 to 3.17 represents the tension resistance capacities determined by the current model with the proposed displacement failure criteria. In the test AA, the T-stub arrangement was different from the configuration in the real connection. One of the T-stubs was rotated by $90°$ relative to the other, keeping the orientations of the two T-stubs in the same direction. Two identical T-stubs (UB 305x165x40) were connected using Grade 8.8 M20 bolts. The experimental result shows that the T-stub fails due to complete yielding (Failure Mode II) in this test. Figure 3.12 displays the comparison results for the test AA at the temperature of 570℃. It is evident that a reasonable agreement is achieved.

In the test AC, different bolts were used, which was High Strength Friction Grip-HSFG M16 bolts. The same failure mode as the test AA was observed from the test. The comparison result of the test AC at temperature of 360℃ is shown in Figure 3.13. It can be seen that the prediction corresponds well with the test results.

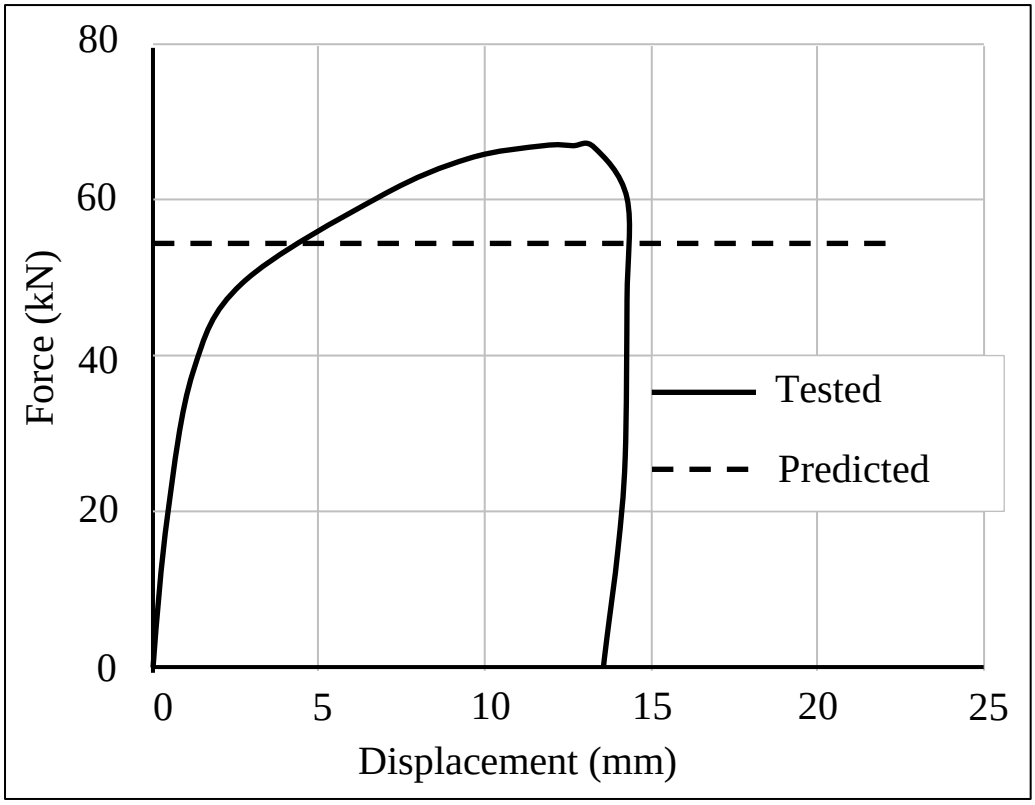

Figure 3.12 Tension capacity predicted with applied displacement criteria (Test AA, 570 ℃, Spyrou et al., 2004a)

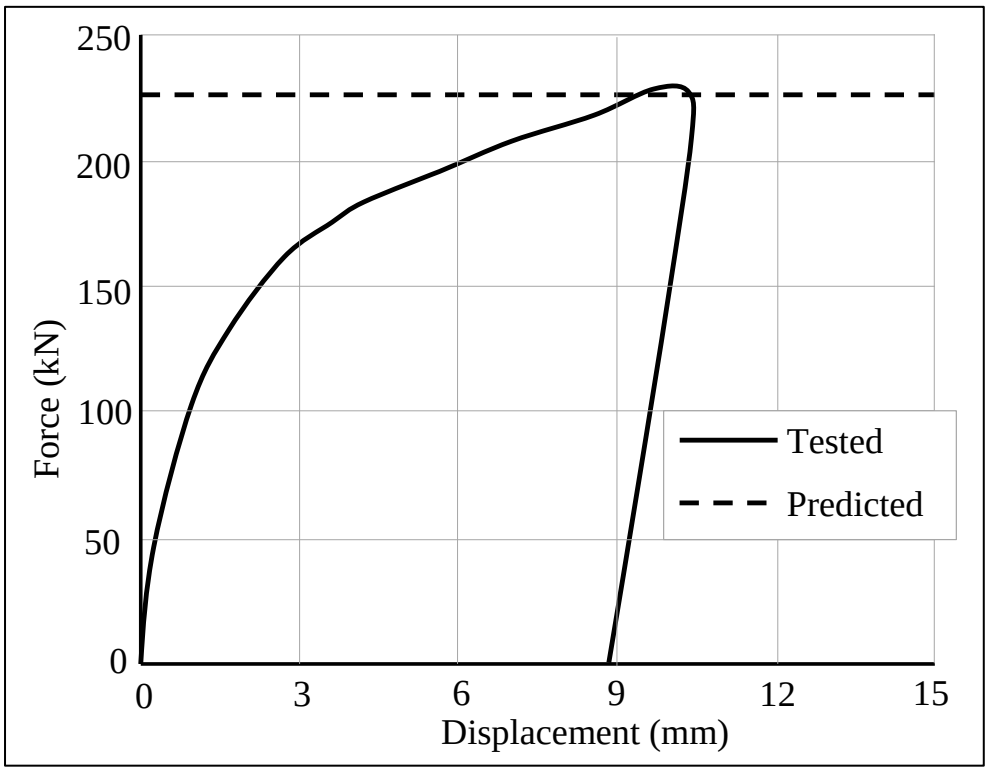

Figure 3.13 Tension capacity predicted with applied displacement criteria (Test AC, 360 ℃, Spyrou et al., 2004a)

In the Phase B, the configuration of T-stubs is the same as in the real beam-to-column connections. In the test BA, a 200x200x20 mm end-plate was bolted to a UC 203x203x52 column using HSFG M20 bolts. The experimental data indicates that the T-stub specimens fail due to fracture of bolts with yielding of T-stub flange (Failure Mode I). Figures 3.14 and 3.15 demonstrate the comparison results for the test BA with the test temperatures of 505℃ and 610℃, respectively. It can be noticed that the correlation between the predicted and tested tension resistances is satisfactory.

In the Phase C, the T-stub arrangement was the same as in the Phase B but different geometrical properties. The 200x200x20 mm end-plate was bolted to a UC 203x203x60 column using Grade 8.8 M20 bolts. The experimental results show that the failure models of the majorities of the specimens in the Phase C tests were Failure Mode I and II. Figures 3.16 and 3.17 illustrate the comparison results for test CA with the test temperatures of 660℃ and 730℃, respectively. The predicted tension resistance agree well with the test results.

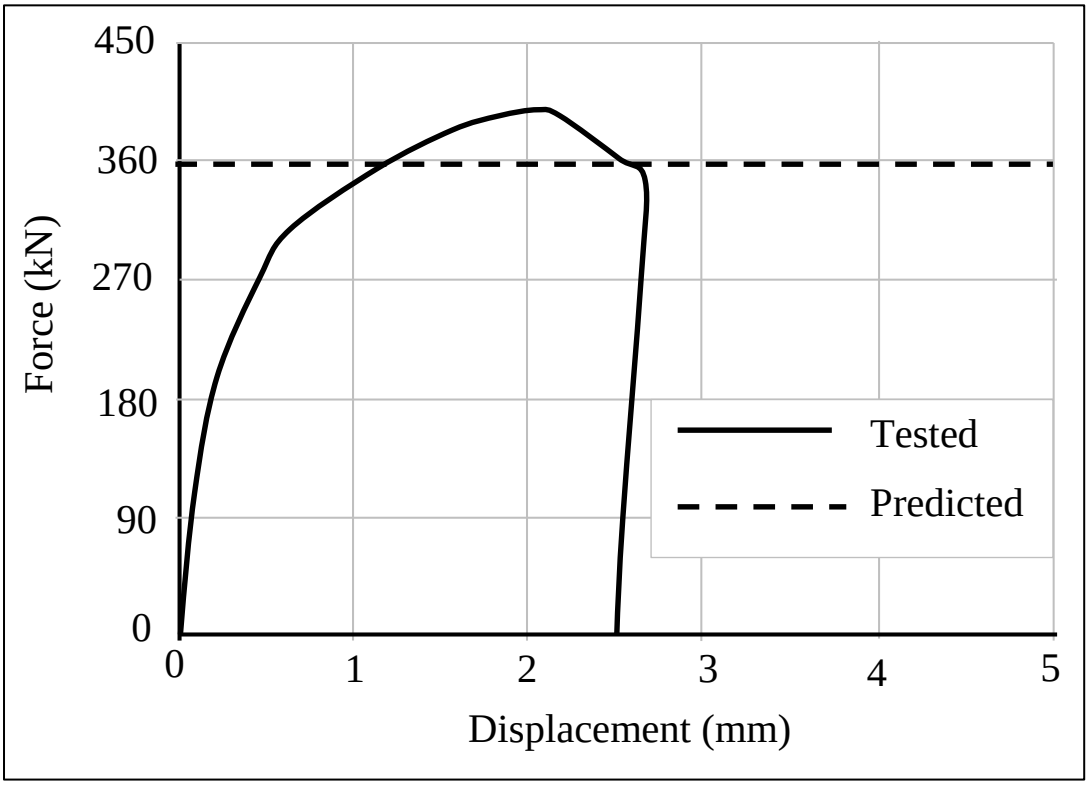

Figure 3.14 Tension capacity predicted with applied displacement criteria (Test BA, 505℃, Spyrou et al., 2004a)

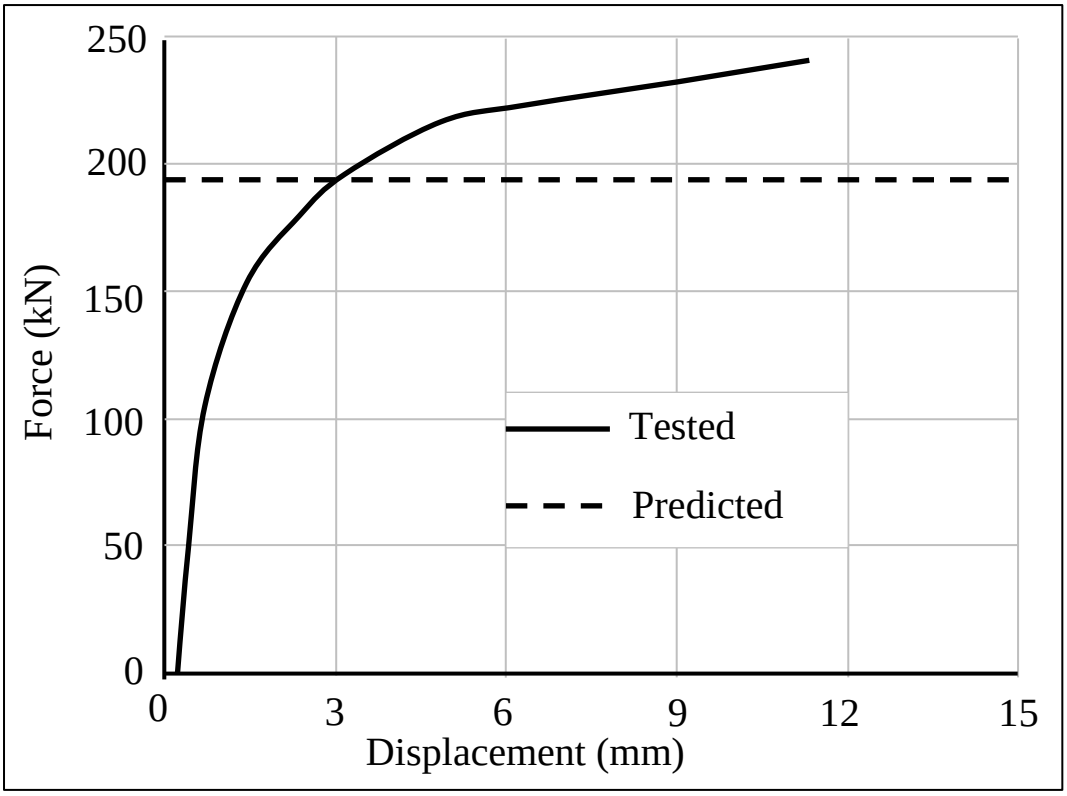

Figure 3.15 Tension capacity predicted with applied displacement criteria (Test BA, 610 ℃, Spyrou et al., 2004a)

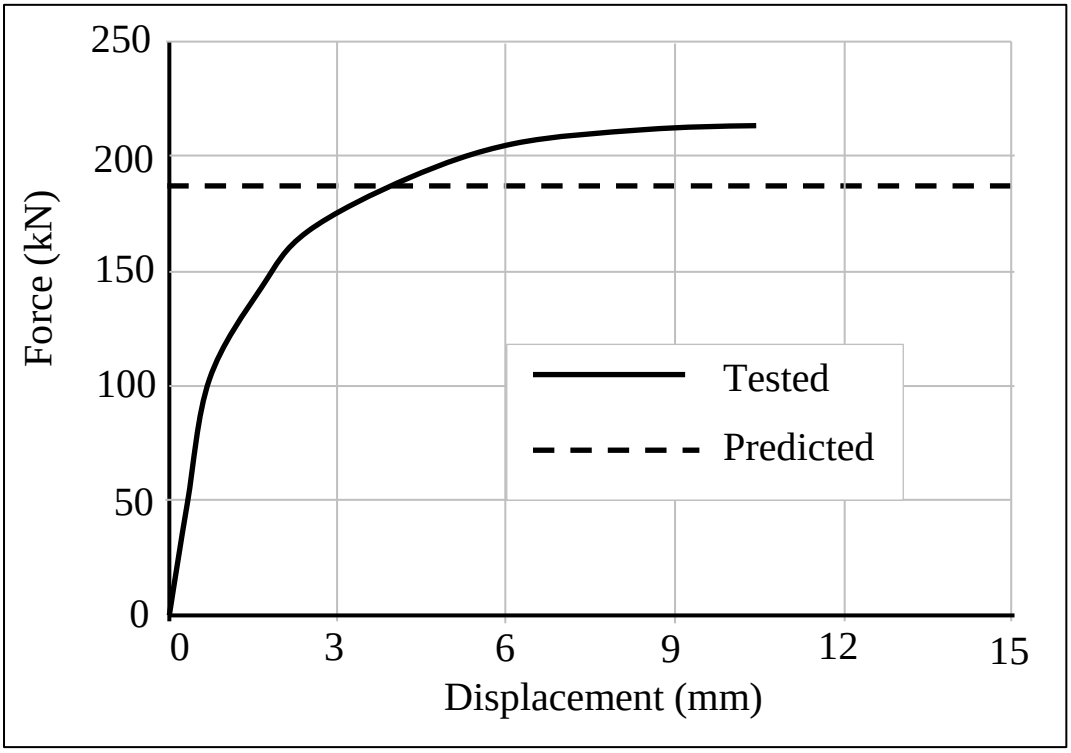

Figure 3.16 Tension capacity predicted with applied displacement criteria (Test CA, 660 ℃, Spyrou et al., 2004a)

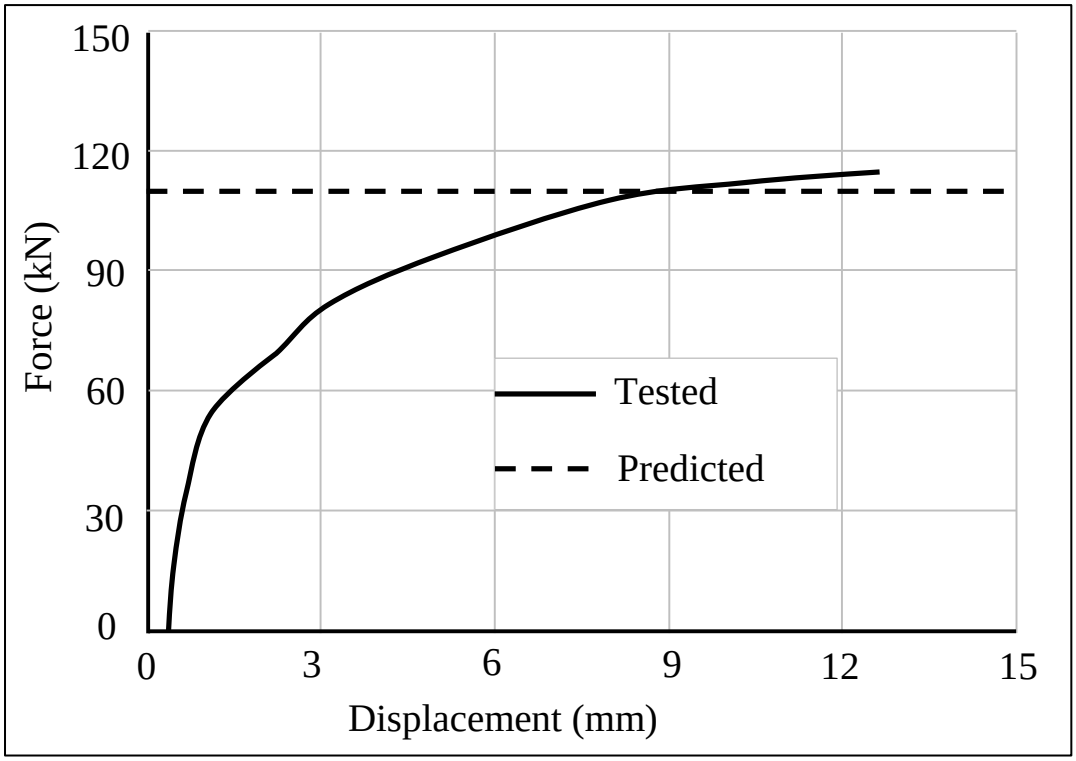

Figure 3.17 Tension capacity predicted with applied displacement criteria (Test CA, 730℃, Spyrou et al., 2004a)

Using the proposed displacement failure criteria for the three failure modes of T-stub, the final tension resistance of T-stub can be determined based on the position of the displacement criteria within the multi-linear force-displacement curves, as shown in Figures 3.9 to 3.11. For Failure Mode I, the tension resistance of T-stub $F_{t,1}$ is given as:

$$F_{t,1}=\begin{cases} F_{cl,pl}^{I} & 0<\delta_{cri,1}\le\delta_{cl,pl}^{I} \\ F_{cl,pl}^{I}+\left(F_{bl,pl}^{I}-F_{cl,pl}^{I}\right)\left(\delta_{cri,1}-\delta_{cl,pl}^{I}\right)/\left(\delta_{bl,pl}^{I}-\delta_{cl,pl}^{I}\right) & \delta_{cl,pl}^{I}<\delta_{cri,1}\le\delta_{bl,pl}^{I} \\ F_{bl,pl}^{I}+\left(F_{final}^{I}-F_{bl,pl}^{I}\right)\left(\delta_{cri,1}-\delta_{bl,pl}^{I}\right)/\left(\delta_{final}^{I}-\delta_{bl,pl}^{I}\right) & \delta_{bl,pl}^{I}<\delta_{cri,1}\le\delta_{final}^{I} \\ F_{final}^{I} & \delta_{cri,1}>\delta_{final}^{I} \end{cases} \quad (3.53)$$

where $\delta_{cri,1}$ is the displacement failure criterion of Failure Mode I.

For Failure Mode II, the tension resistance of T-stub $F_{t,2}$ is calculated as:

$$F_{t,2}=\begin{cases} F_{cl,pl}^{II} & 0<\delta_{cri,2}\le\delta_{cl,pl}^{II} \\ F_{cl,pl}^{II}+\left(F_{bl,pl}^{II}-F_{cl,pl}^{II}\right)\left(\delta_{cri,2}-\delta_{cl,pl}^{II}\right)/\left(\delta_{bl,pl}^{II}-\delta_{cl,pl}^{II}\right) & \delta_{cl,pl}^{II}<\delta_{cri,2}\le\delta_{bl,pl}^{II} \\ F_{bl,pl}^{II}+\left(F_{fl,pl}^{II}-F_{bl,pl}^{II}\right)\left(\delta_{cri,2}-\delta_{bl,pl}^{II}\right)/\left(\delta_{fl,pl}^{II}-\delta_{bl,pl}^{II}\right) & \delta_{bl,pl}^{II}<\delta_{cri,2}\le\delta_{fl,pl}^{II} \\ F_{fl,pl}^{II}+\left(F_{final}^{II}-F_{fl,pl}^{II}\right)\left(\delta_{cri,2}-\delta_{fl,pl}^{II}\right)/\left(\delta_{final}^{II}-\delta_{fl,pl}^{II}\right) & \delta_{fl,pl}^{II}<\delta_{cri,2}\le\delta_{final}^{II} \\ F_{final}^{II} & \delta_{cri,2}>\delta_{final}^{II} \end{cases} \quad (3.54)$$

where $\delta_{cri,2}$ is the displacement failure criterion of Failure Mode II.

For Failure Mode III, the ultimate tension resistance of the T-stub $F_{t,3}$ is determined as:

$$F_{t,3}=\begin{cases} F_{cl,pl}^{III} & 0<\delta_{cri,3}\le\delta_{cl,pl}^{III} \\ F_{cl,pl}^{III}+\left(F_{final}^{III}-F_{cl,pl}^{III}\right)\left(\delta_{cri,3}-\delta_{cl,pl}^{III}\right)/\left(\delta_{final}^{III}-\delta_{cl,pl}^{III}\right) & \delta_{cl,pl}^{III}<\delta_{cri,3}\le\delta_{final}^{III} \\ F_{final}^{III} & \delta_{cri,3}>\delta_{final}^{III} \end{cases} \quad (3.55)$$

where $\delta_{cri,3}$ is the displacement failure criterion of Failure Mode III.

3.4.5 Tension resistance of the connection

In this connection element model, the whole connection is considered as a combination of a column T-stub and an end-plate T-stub. Therefore, for each failure mode, the tension resistance is taken as the smaller value of two T-stub resistances. The final tension resistance of a single bolt row is determined as the minimum value of tension resistances of three failure modes. Hence, the final tension resistance of a single bolt row $F_{tens,r,bolt}$ can be calculated as:

$$F_{tens,r,bolt}=\min(F_{t,1,fc};F_{t,1,ep};F_{t,2,fc};F_{t,2,ep};F_{t,3,fc};F_{t,3,ep}) \quad (3.56)$$

where $F_{t,1,fc}$, $F_{t,2,fc}$ and $F_{t,3,fc}$ are the tension resistances of the column T-stub for Failure Mode I, Failure Mode II and Failure Mode III, respectively; $F_{t,1,ep}$, $F_{t,2,ep}$ and $F_{t,3,ep}$ are the tension resistances of the end-plate T-stub for Failure Mode I, Failure Mode II and Failure Mode III. The tension resistances of column T-stub and end-plate T-stub for three failure modes are determined by using Equations (3.53)-(3.55).

Hence, the tension resistance of the connection F_{tens} is given as follows,

$$F_{tens} = \sum_{r=1}^{N} F_{tens,r,bolt} \tag{3.57}$$

where N is the total number of bolt rows in tension.

3.5 The compression resistance of the connection

In the current model, the numerical procedure for determining compression resistance of the end-plate connection is based on the component-based method. The main components within the compression zone of end-plate connection are the column web in compression, and the beam flange and web in compression.

3.5.1 Column web in compression

Generally, the failure form of the column sections with stocky webs is governed by the yielding of the web and formation of a plastic hinge mechanism in the flange (Spyrou, 2002). For column sections with slender webs, the failure is dominated by the plastic or inelastic buckling of the web. If the column web is very slender, the occurrence of buckling might be early than the stress underneath the load reaching the yield stress, leading to the failure of elastic buckling or web crippling (Block, 2006). For column web with practical column sections, the most likely failure form is local buckling and web crushing (Qian, 2007).

An analytical model was proposed by Roberts and Rockey (1979) to predict the resistance of plate girders subjected to concentrated load in the plane of the web. The plastic hinges in the flange and the formation of yield lines were considered in this model. Later this model was modified by Lagerqvist and Johansson (1996) to consider part of the column web, when calculating the plastic moment resistance of the flange. Based on this revised model, Block (2006) extended the model to the elevated temperature conditions and also considered the influence of axial load as well.

The compression resistance of the column web $F_{c,cw}$ in the current model is based on the simplified model proposed by Block et al. (2007), as expressed below:

$$F_{c,cw} = \frac{f_{yw,c} t_{wc} \chi_F l_y}{\gamma_{M1}} \tag{3.58}$$

where γ_{M1}=1.0, $f_{yw,c}$ is the yield strength of the column web. l_y is the yielded length of the web, calculated as:

$$l_y = c + 2t_{fc}\left(1+\sqrt{\frac{f_{yf,c}b_c}{f_{yw,c}t_{wc}}+0.02\left(\frac{d_{c,c}}{t_{fc}}\right)^2}\right) \tag{3.59}$$

where $d_{c,c}$ is the depth of the column web between the root radii, $f_{yf,c}$ is the yield strength of the column flange, c is the load width calculated by using a dispersion angle of 45 °in the end-plate.

χ_F is a stability reduction factor related to the slenderness factor λ_F, given as:

$$\chi = 0.06 + \frac{0.47}{\lambda_F} \le 1.0 \tag{3.60}$$

The slenderness factor λ_F is determined in the classical way as the square root of the yield resistance over the elastic buckling resistance of the web, shown as:

$$\lambda_F = \sqrt{\frac{F_y}{F_{cr}}} = \sqrt{\frac{l_y t_{wc} f_{yw,c}}{F_{cr}}} \tag{3.61}$$

The elastic buckling resistance of the web F_{cr} is obtained according to the classical elastic buckling theory, given as:

$$F_{cr} = k_F \frac{\pi^2 E_{cw}}{12(1-\upsilon^2)}\frac{t_{wc}^3}{d_{c,c}} \tag{3.62}$$

where $\upsilon = 0.3$, k_F is the buckling coefficient.

The buckling coefficient k_F is derived according to a series of numerical parametric study conducted by Lagerqvist and Johansson (1996), as shown in the following expression:

$$k_F = 3.5 + 2\left(\frac{d_{c,c}}{a}\right)^2 \text{ for opposite loads i.e. in an internal connection} \tag{3.63}$$

$$k_F = 6 + 2\left(\frac{d_{c,c}}{a}\right)^2 \text{ for a single load i.e. in an external connection} \tag{3.64}$$

where a is the distance between web stiffeners. For the unstiffened column web, a is assumed to be infinite. Therefore, the value of k_F would be 3.5 and 6, respectively.

3.5.2 Beam flange and web in compression

The resistance of beam flange and the adjacent compression zone within beam web can be determined as follows according to EN 1993-1-8:

$$F_{c,bf} = \frac{M_{c,Rd}}{h_b - t_{fb}} \tag{3.65}$$

where h_b is the depth of the beam, $M_{c,Rd}$ is the design moment resistance of the beam cross-section.

As documented in Eurocode 3 Part 1.1 (CEN, 2005a), the design moment resistance of the beam cross-section can be determined as:

$$M_{c,Rd} = \frac{W_{el,y} f_{y,b}}{\gamma_{M0}} \tag{3.66}$$

where $W_{el,y}$ is the elastic modulus of the beam section, $f_{y,b}$ is the yield strength of the beam, γ_{M0}= 1.0 .

The contribution of the beam web to the design compression resistance should be limited to 20%, if the height of the beam including the haunch exceeds 600mm (EN 1993-1-8).

3.5.3 Compression resistance of the connection

The compression resistance of the whole connection F_{comp} is taken as the smaller value of the resistance of column web $F_{c,cw}$ and the resistance of beam flange and web $F_{c,bf}$, that is

$$F_{comp} = \min\left(F_{c,cw}; F_{c,bf}\right) \tag{3.67}$$

In this model, it is required that the tension and compression resistances need to reach equilibrium. The first condition that the effective tension resistance has to satisfy is:

$$F_{et,Ed} \le F_{comp} \tag{3.68}$$

$$F_{et,Ed} = \sum_{r=1}^{N} F_{tens,r,bolt} \tag{3.69}$$

If the effective design tension resistance exceeds the compression resistance, the force redistribution is taken into consideration. It is conducted by reducing the force from the tension bolt row with the largest bolt row number (see Figure 3.2). The redistribution is adopted in tension bolt rows until the condition stated below is satisfied:

$$F_{et,Ed} = \sum_{r=1}^{N} F_{tens,r,bolt} = F_{comp} \tag{3.70}$$

3.6 Components within the shear zone of the connection

There are three basic components within the shear zone of the connection: the bolts bearing in column flange, the bolts bearing in end-plate and the bolts in shear. As documented in EN 1993-1-8, the shear resistance of one bolt can be calculated as:

$$F_{v,Rd} = \frac{\alpha_V f_{bu} A_s}{\gamma_{M2}} \tag{3.71}$$

where $\gamma_{M2} = 1.25$. For classes 4.6, 5.6 and 8.8 bolts, $\alpha_V = 0.6$; for classes 4.8, 5.8, 6.8 and 10.9 bolts, $\alpha_V = 0.5$.

The bearing resistance of bolts on column flange is obtained as:

$$F_{b,cf,Rd} = \frac{k_{1,c}\alpha_{b,c} f_{u,c} d\, t_{fc}}{\gamma_{M2}} \tag{3.72}$$

where d is the bolt diameter. $f_{u,c}$ is the ultimate tensile strength of the column. The other coefficients are given as follows:

$$k_{1,c} = \min\left(\left(2.8\frac{e_c}{d_0} - 1.7\right); \left(1.4\frac{w_b}{d_0} - 1.7\right); 2.5\right) \tag{3.73}$$

$$\alpha_{b,c} = \min\left(\alpha_{d,c};\ \frac{f_{bu}}{f_{u,c}};\ 1.0\right) \tag{3.74}$$

$$\alpha_{d,c} = \min\left(\frac{e_x}{3d_0};\ \left(\frac{p_3}{3d_0} - 0.25\right)\right) \tag{3.75}$$

where d_0 is the diameter of bolt hole, p_3 is the spacing between centre of shear bolt rows (see Figure 3.2).

The bearing resistance of bolts on end-plate can be calculated as:

$$F_{b,ep,Rd} = \frac{k_{1,p}\alpha_{b,p} f_{u,p} d\, t_p}{\gamma_{M2}} \tag{3.76}$$

where $f_{u,p}$ is the ultimate tensile strength of endplate.

$$k_{1,p} = \min\left(\left(2.8\frac{e_p}{d_0} - 1.7\right); \left(1.4\frac{w_b}{d_0} - 1.7\right); 2.5\right) \tag{3.77}$$

$$\alpha_{b,p} = \min\left(\alpha_{d,p};\ \frac{f_{bu}}{f_{u,p}};\ 1.0\right) \tag{3.78}$$

$$\alpha_{d,p} = \min\left(\frac{e_x}{3d_0};\ \left(\frac{p_3}{3d_0} - 0.25\right)\right) \tag{3.79}$$

For one shear bolt row, the design shear resistance is taken as the smallest among the three basic components, given as:

$$V_{b,r,Rd} = \min\left(F_{v,Rd};\ F_{b,cf,Rd};\ F_{b,ep,Rd}\right) \tag{3.80}$$

The total vertical shear resistance of the connection is defined as the summation of the resistance of shear bolt rows.

3.7 The bending moment resistance of the connection

The moment resistance $M_{j,Rd}$ of a bolted end-plate connection can be calculated as:

$$M_{j,Rd} = \sum_r h_r F_{tens,r,bolt} \tag{3.81}$$

where $F_{tens,r,bolt}$ is effective tension resistance of bolt-row *r*, h_r is distance from bolt-row *r* to the centre of compression, *r* is bolt-row number (see Figure 3.2).

The method given above for determining the moment resistance of a connection $M_{j,Rd}$ does not take into account any coexisting axial force $N_{j,Ed}$ in the connected beam. In order to consider the influence of axial force on the moment resistance of a connection $M'_{j,Rd}$ a simply model proposed by Huang (2011) is adopted in this research. The moment resistance of connection considering the influence of axial force can be expressed as:

$$M'_{j,Rd} = \left(1.0 - \left(\frac{N_{j,Ed}}{F_{j,Rd}}\right)^{B}\right) M_{j,Rd} \tag{3.82}$$

where $F_{j,Rd}$ is the axial resistance of the connection, $N_{j,Ed}$ is the co-existing axial force in the connected beam.

The degree of influence of axial force on the bending moment resistance of connection is determined by B, which can be calculated as:

$$B = \frac{f_{y,T}}{f_{y,20}} \tag{3.83}$$

$f_{y,T}$ and $f_{y,20}$ are yield strength of steel at elevated temperatures and ambient temperatures respectively. It can be noted that B is less than 1.0, and its value reduces when temperatures increases.

In this developed model, the deterioration of material properties with temperatures is taken into account. Parameters such as the yield strength, ultimate tensile strength and Young's module of steel and bolts are considered to be temperature dependent. Previous studies showed that elevated temperatures have a more significant influence on the degradation of mechanical properties of bolts compared to the end-plate and the section of steel beam or column. However, the research conducted by Hu et al. (2009a) indicated that the majorities of failure models of T-stubs are Mode I and Mode II. The influence of material degradation of the bolt by using different models on the final tension resistance of one bolt row is not very significant. Therefore, for simplicity, it is assumed that the material degradation of bolts at elevated temperatures follows the same law for the beam, column and end-plate. The reduction factors documented in Eurocode 3 Part 1.2 (CEN, 2005b) are adopted in this developed model.

The developed two-node connection element presented here for modelling steel end-plate connection has been incorporated into the computer program VULCAN (Huang et al. (2003a, 2003b); Huang et al. (2009)) for 3D modelling of steel-framed composite buildings under fire conditions. The total loading or temperature rise for which the response of the structure is to be traced is divided into a number of steps. It is assumed that changes in the loads or temperatures occur only at the beginning or end of a step. During any step the external loads and temperatures in the different components of the connection elements are assumed to remain unchanged.

3.8 Validations

The model presented above has been validated using a total of 22 end-plate connection tests. The validation includes 8 tests without the axial force at elevated temperatures, 12 tests subjected to axial force at both ambient and elevated temperatures and 2 fire tests of beam-to-column sub-frame. The geometrical properties, the tested material properties and the measured temperature distribution within the connection are employed as the input data for modelling. Subsequent sections describe the details of the test data and comparison results.

3.8.1 Validations against isolated tests by Leston-Jones

Figure 3.18 presents the arrangement of fire tests conducted by Leston-Jones (1997a). All tests are consisted of a symmetric cruciform arrangement of a single 152x152x23UC column with two cantilever beams (254x102x22UB). The column is 1400 mm high and the beam is 1700 mm long. The tests adopted a 12 mm thick end-plate with six M16-8.8 bolts in 18mm diameter clearance holes. In all cases, the specimens were keeping at a constant load then gradually increased the temperature, which reflected the real situation in building fire. In the testes the temperatures were increased following a linear steel heating rate of 10°C per minute. The beams were restrained horizontally at a distance of 1524 mm from the column centre-line while the loads were applied to the column head. Four different loads were applied to the connection during the tests, which were 5 kNm, 10 kNm, 15 kNm and 20 kNm to Test 1, Test 2, Test 3 and Test 4 respectively.

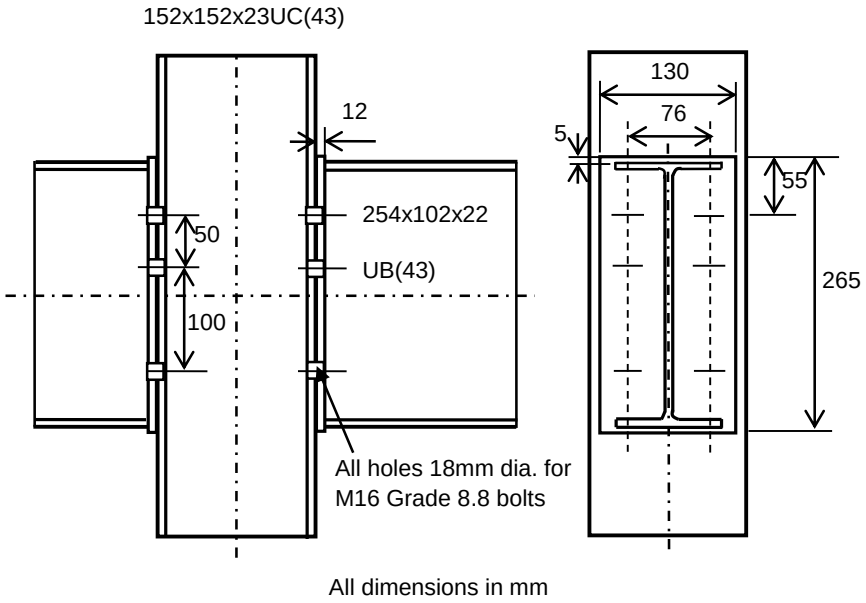

Figure 3.18 Details of test specimens used by Leston-Jones (1997a)

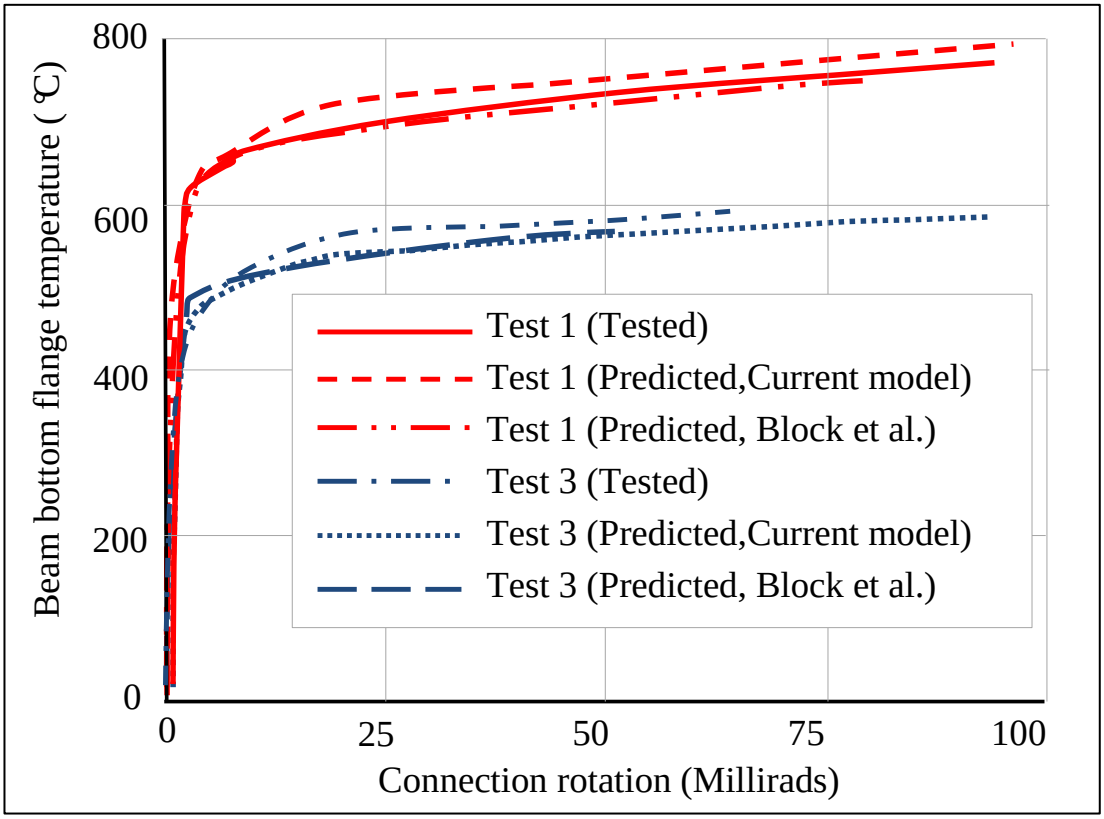

Figure 3.19 Comparison of predicted and measured connection rotations at elevated temperatures for Test 1 and Test 3 (Leston-Jones, 1997a)

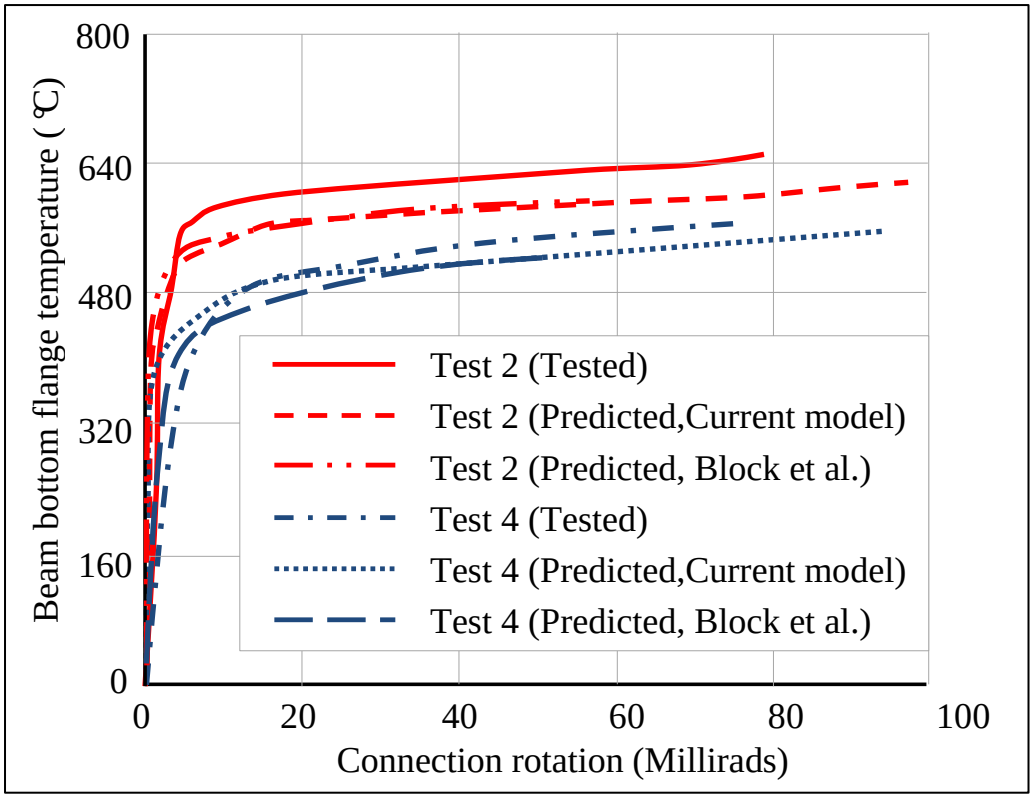

Figure 3.20 Comparison of predicted and measured connection rotations at elevated temperatures for Test 2 and Test 4 (Leston-Jones 1997a)

The comparison results are illustrated in Figures 3.19 and 3.20, together with the predictions by the component model (Block et al., 2007). It is evident that the predictions of the current model agree well with the experimental data and the component model's predictions.

3.8.2 Validations against isolated tests by Al-Jabri

Another four tests without axial force at elevated temperature utilized for validation were conducted by Al-Jabri (1999). The test configuration is given below in Figure 3.21, symmetrically connecting two 356x171x51UB beams to one 254x254x89UC column. The beam within this cruciform arrangement is 1900 mm long and the column is 2700 mm high. The thickness of endplate adopted was 10 mm. Eight M20 Grade 8.8 bolts in 22mm diameter clearance holes were used. All these tests were conducted under a constant load and then the temperature was increased gradually. Loads were applied to the beams at a distance of approximately 1500 mm from the centre line of column. The heating rate for the specimen was 10°C per minute. Four different load levels were applied to the same connection,

which were 27.4k Nm, 54.8 kNm, 82.1 kNm and 110 kNm to Test 1, Test 2, Test 3 and Test 4 respectively.

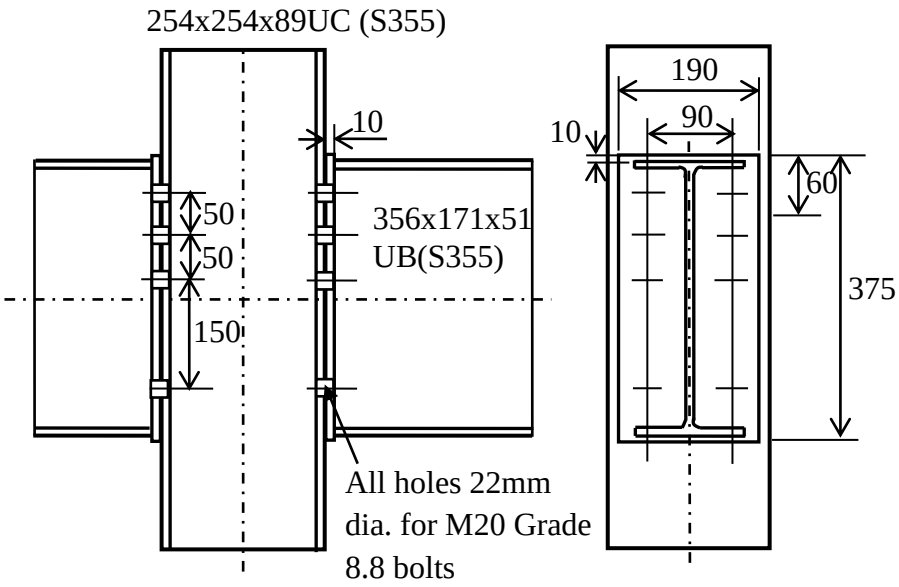

Figure 3.21 Details of test specimens used by Al-Jabri (1999)

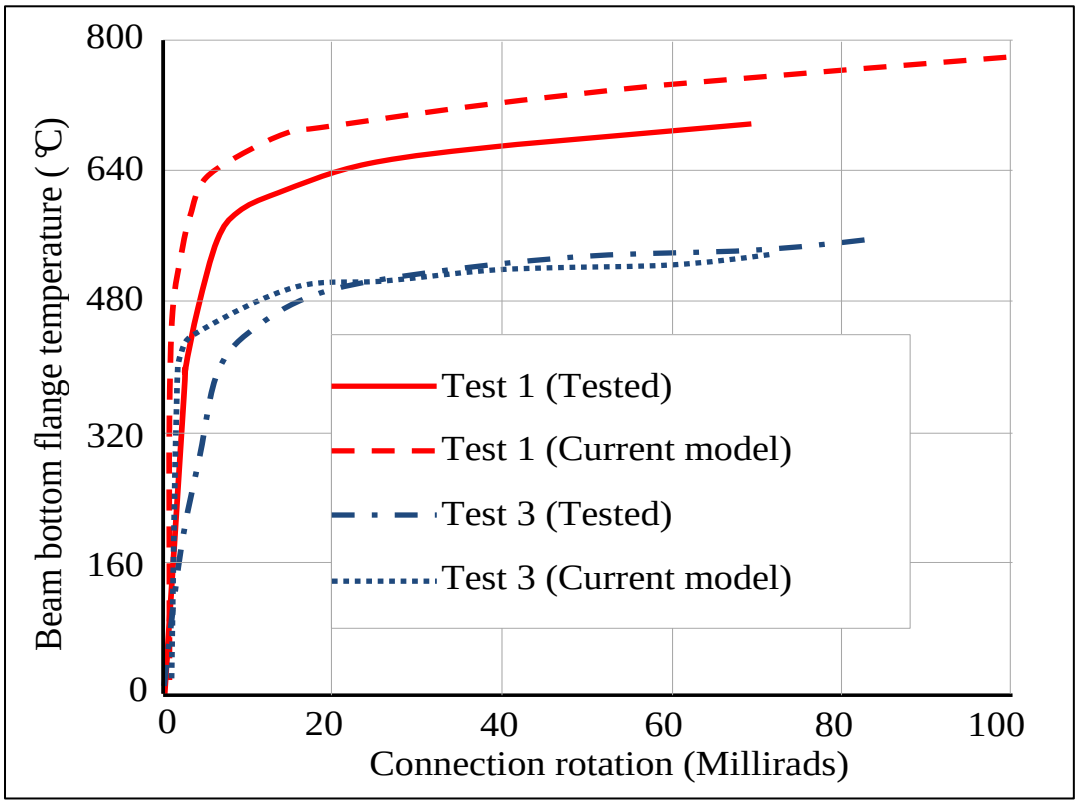

Figure 3.22 Comparison of predicted and measured connection rotations at elevated temperatures for Test 1 and Test 3 (Al-Jabri, 1999)

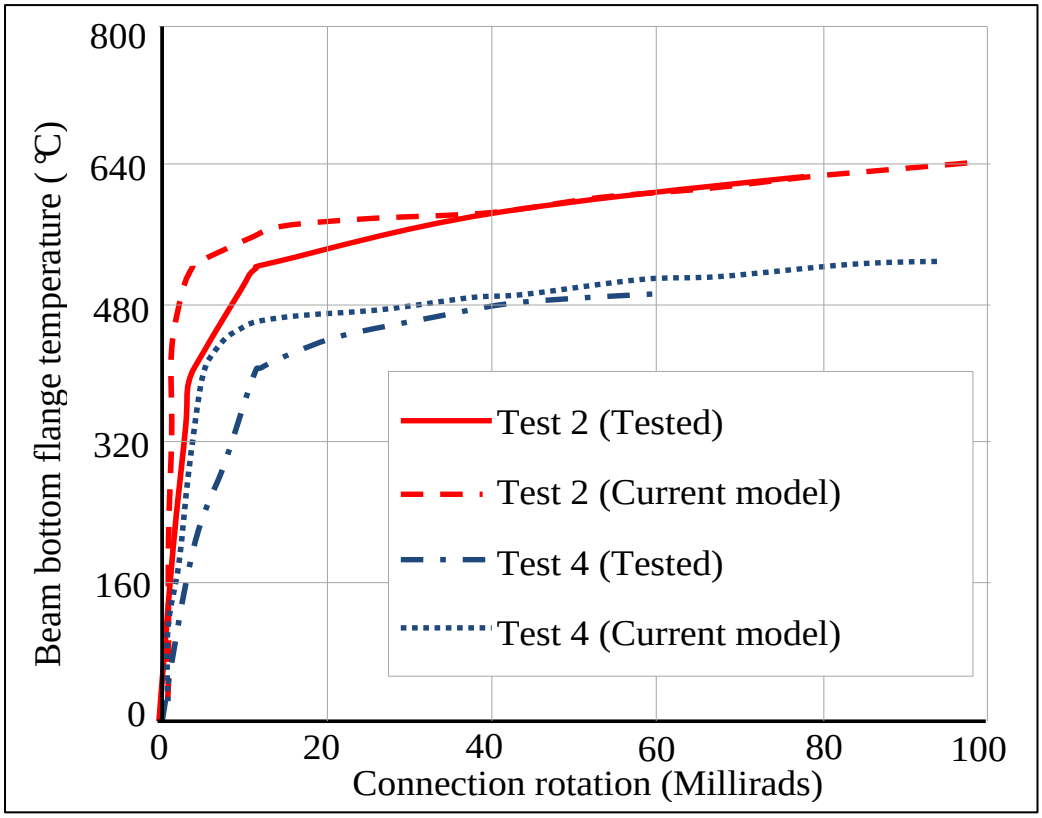

Figure 3.23 Comparison of predicted and measured connection rotations at elevated temperatures for Test 2 and Test 4 (Al-Jabri, 1999)

The comparison results are given in Figures 3.22 and 3.23. It is evident that the proposed analytical model agrees well with the experimental data. These comparison results demonstrate that the new model has the ability to accurately predict the behaviour of connections without axial force at elevated temperatures.

3.8.3 Validations against isolated tests by Yu

For verification of the end-plate connections subjected to both shear and axial forces at ambient and elevated temperatures, the studies conducted by Yu et al. (2009d) are selected. These experimental studies are parts of the joint research programme conducted by the University of Sheffield and the University of Manchester aiming to analyse the tying capacity and ductility of steel connections under fire conditions. A total 12 tests were carried out on flush end-plate connections at ambient and elevated temperatures. The test arrangement is depicted in Figure 3.24.

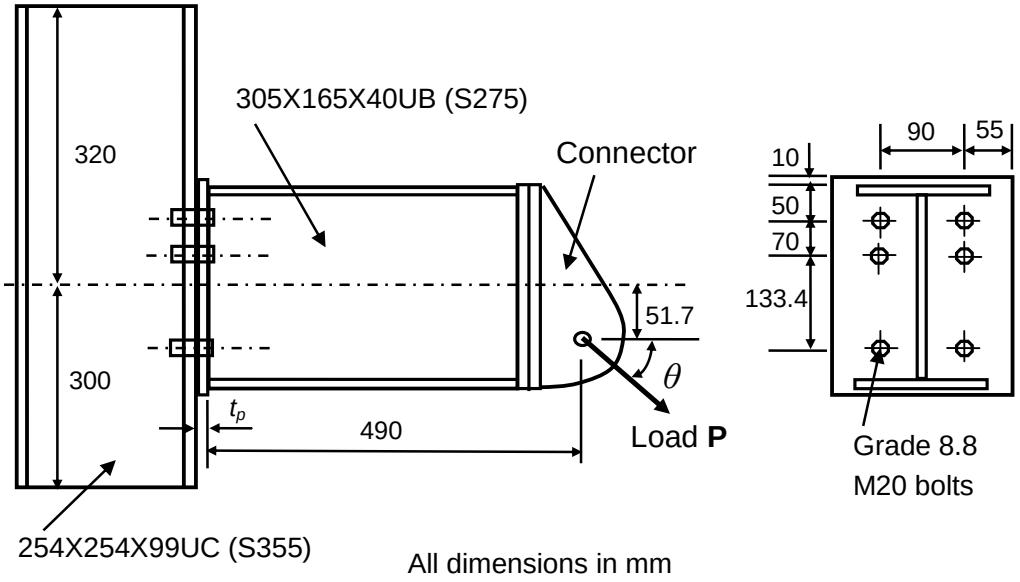

Figure 3.24 Details of test specimens used by Yu et al. (2009d)

The connections are comprised of a 305x165x40UB beam connected to a 254x 254x89UC column with six M20 Grade 8.8 bolts. The arrangement of the bolts is typical of practical design in accordance with current design recommendations in the UK (Yu et al., 2009d). The thickness of end-plate was 10 mm in the eleven tests, except for the test EP_550_35_11-12-07_8 mm, which adopted the end-plate with 8 mm thickness. The tests were conducted by heating the specimen to the specified temperature then increasing the load until failure. The force was applied with inclined angle (θ) to the axis of the connected beam. A total of three angles were employed, θ = 35°, 45°, 55°. These three different angles represent three different combinations of shear and tying forces. Figure 3.25 shows the comparisons between the test results and the predictions of proposed model for these two tests at ambient temperature. The loading angles for these two tests are $\theta = 35°$ and $\theta = 55°$. Figures 3.26 to 3.30 present the comparison results for the rest of 10 tests at elevated temperatures. As shown in the figures, the unloading path is predicted well by the current model, depicting as the straight lines with the slopes equal to initial stiffness of the connections. The descending part of the curves observed from the experimental tests results indicates the unstable failure process of the connection. As shown in the figures, the agreements between the model predictions and test data are satisfactory. The current model can provide a good prediction of the moment-rotation characteristics of end-plate connections subjected to combined vertical shear and axial loading at both ambient and elevated temperatures.

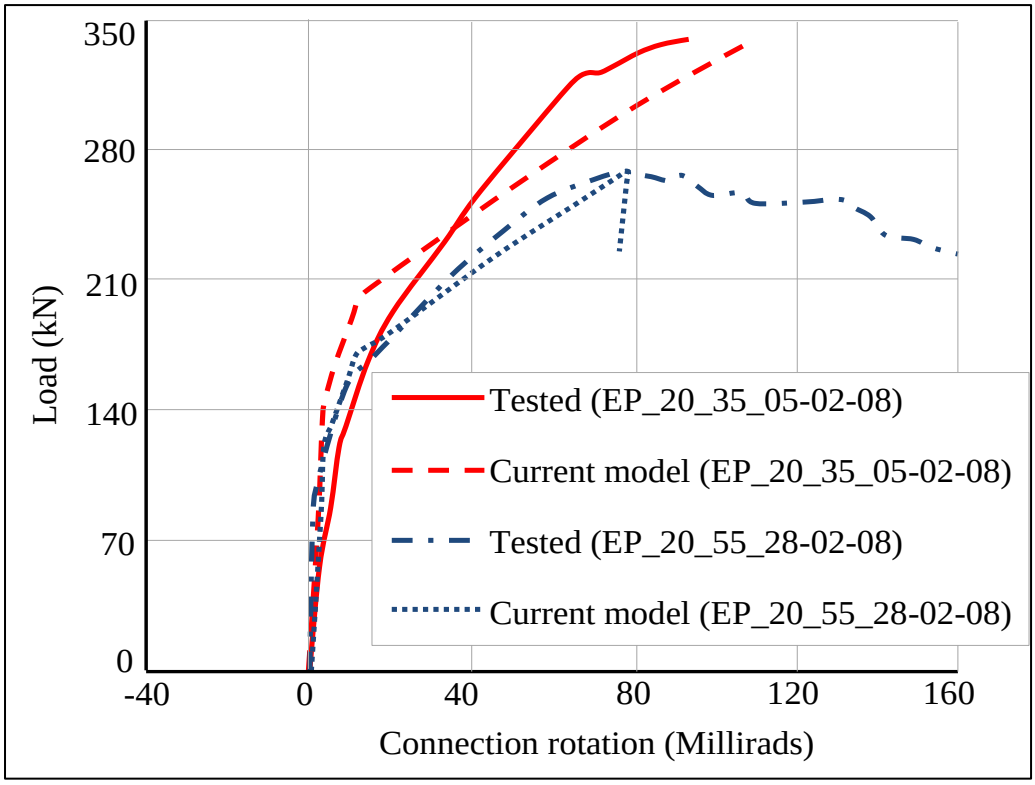

Figure 3.25 Comparison of predicted and measured connection rotations at ambient temperature for Sheffield's tests: EP_20_35_05-02-08 (θ=35°) and EP_20_55_28-02-08 (θ=55°) (Yu et al., 2009d)

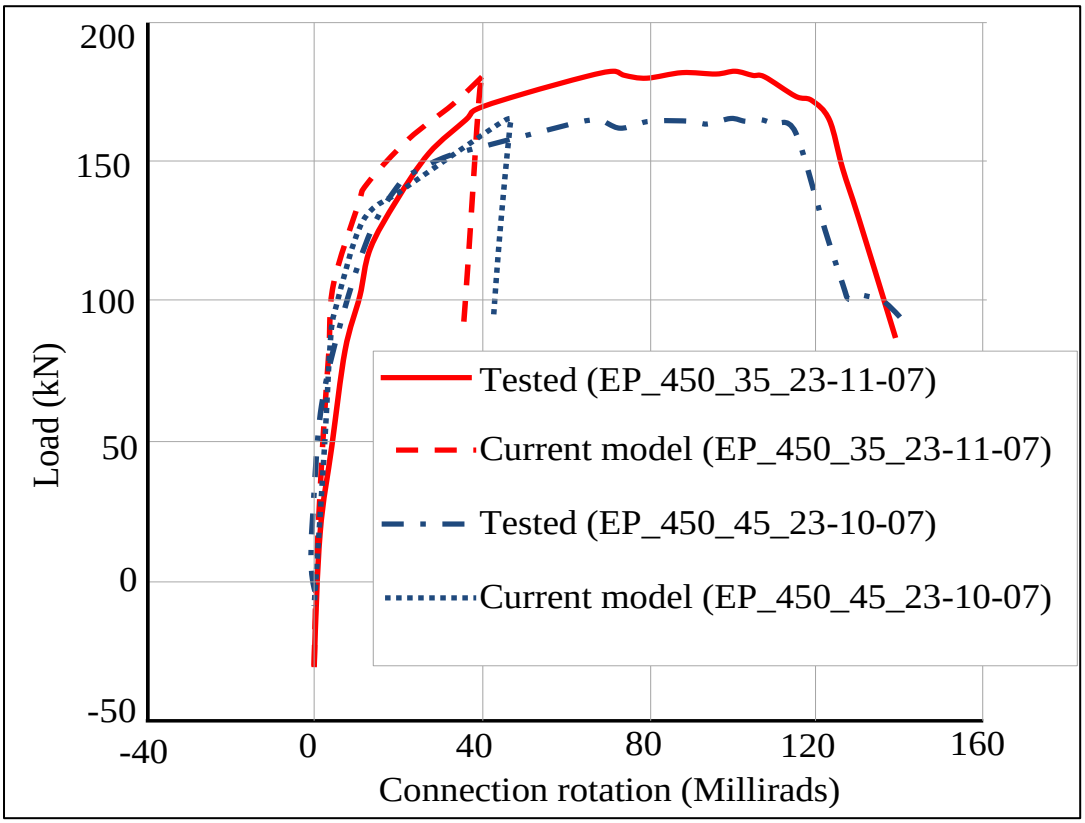

Figure 3.26 Comparison of predicted and measured connection rotations at 450 °C for Sheffield's tests: EP_450_35_23-11-07 (θ=35°) and EP_450_45_23-10-07 (θ=45°) (Yu et al., 2009d)

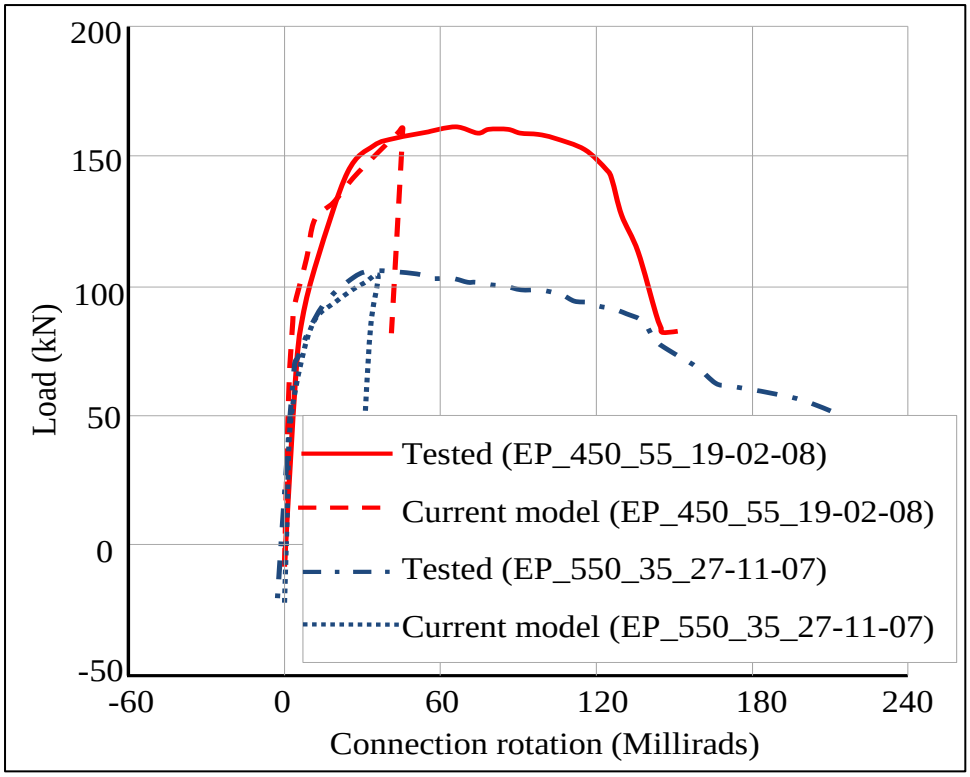

Figure 3.27 Comparison of predicted and measured connection rotations for Sheffield's tests: EP_450_55_19-02-08 (450°C, θ=55°) and EP_550_35_27-11-07 (550°C, θ=35°) (Yu et al., 2009d)

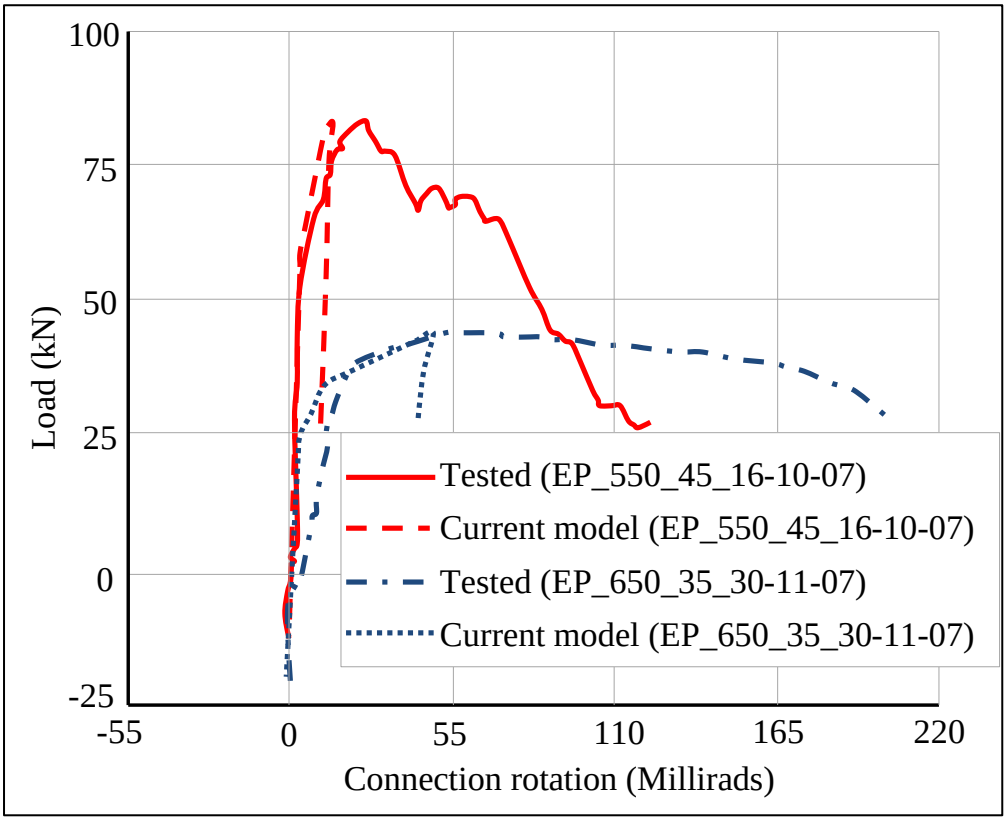

Figure 3.28 Comparison of predicted and measured connection rotations for Sheffield's tests: EP_550_45_16-10-07 (550°C, θ=45°) and EP_650_35_30-11-07 (650°C, θ=35°) (Yu et al., 2009d)

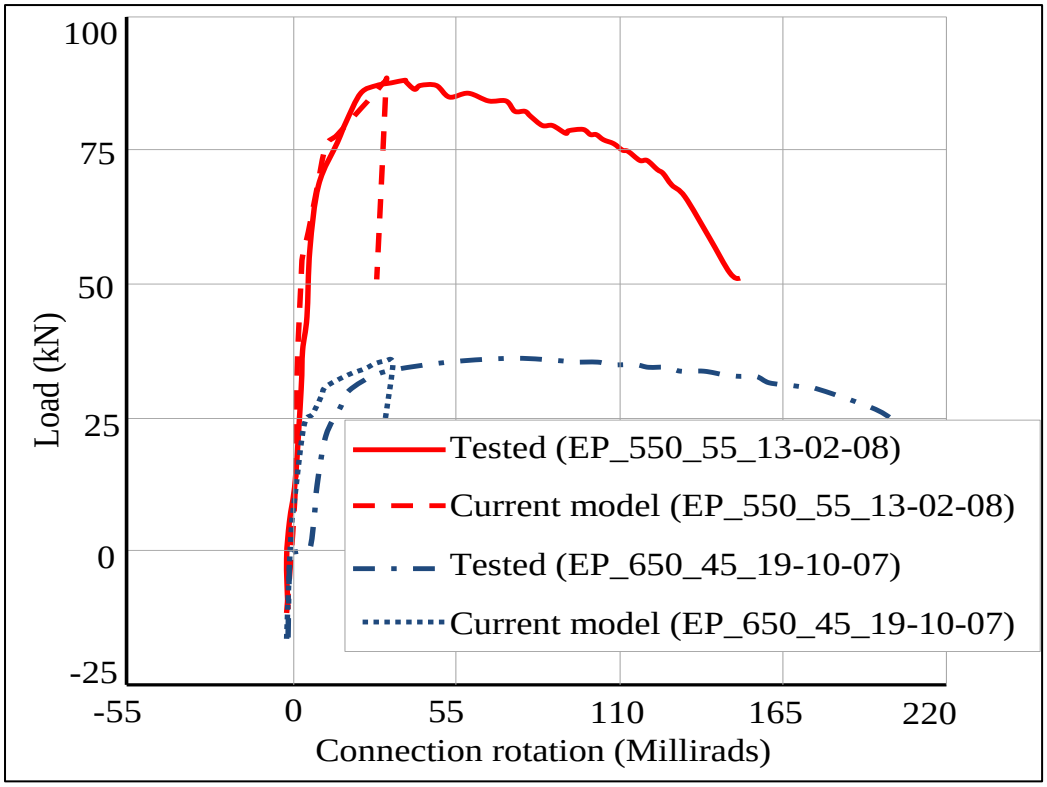

Figure 3.29 Comparison of predicted and measured connection rotations for Sheffield's tests: EP_550_55_13-02-08 (550°C, θ=55°) and EP_650_45_19-10-07 (650 ℃, θ=45°) (Yu et al., 2009d)

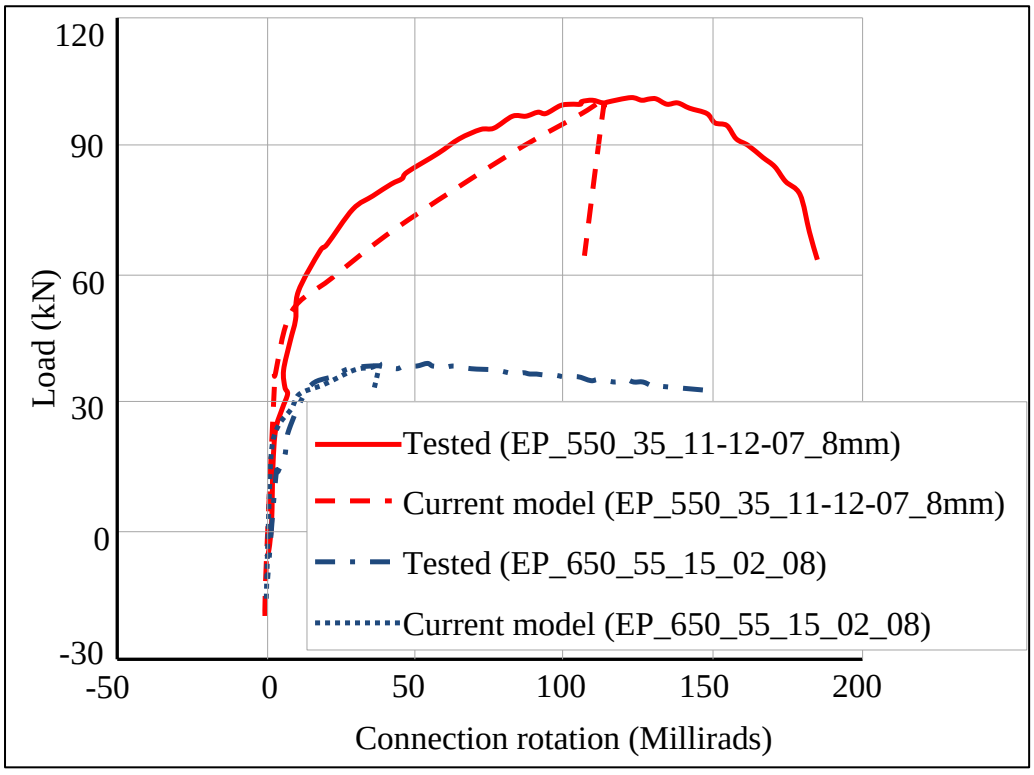

Figure 3.30 Comparison of predicted and measured connection rotations for Sheffield's tests: EP_550_35_11-12-07_8mm (550°C, θ=35°) and EP_650_55_15_02_08 (650°C, θ=55°) (Yu et al., 2009d)

3.8.4 Validations against a sub-frame test

Two fire tests on a beam-to-column sub-frame conducted at the University of Coimbra (Santiago, 2008) are employed to validate the developed model. The tests details are shown in Figure 3.31. This sub-frame is consisted of an unprotected IPE300 cross-section beam with 5.7 m free span connected to two thermally insulated HEA300 cross-section columns. A natural fire was applied to this sub-frame, which including the heating and cooling phases. The behaviour of two connections EJ01 and FJ03 in the tests were investigated. EJ01 is an extended end-plate connection adopting three M20 Grade 8.8 bolts while FJ03 is a flush end-plate connection with two M20 Grade 8.8 bolts. For test EJ01 the maximum beam temperature of 898 ^{0}C was reached at about 50 min then cooled down to about 180 ^{0}C at 150 min. For test FJ03 the maximum beam temperature of 900 ^{0}C was reached at about 40 min and kept almost constant until 50 min then cooled down to about 200 ^{0}C at 150 min. All tested material properties and temperatures of unprotected beam, connections and protected columns were used as input for the modelling.

Figures 3.32 and 3.33 show the comparisons of the predicted and tested rotations for the tests EJ01 and FJ03. It is noted that the predicted rotations are significant lower than tested data. This is due to a lack of details for the tested temperature distributions within the connections. In the modelling the connections' temperatures were assumed as uniform and equalled to average tested temperatures. Therefore, connections' temperatures used in the modelling may significant lower than real tested temperatures within the connections. In order to investigate the influence of temperatures on the behaviour of the connections two tests (EJ01 and FJ03) were modelled again with two different temperature patterns. The first temperature pattern is to increase the connections' temperature by 5% of the original temperatures. The second temperature pattern is to reduce the connections' temperature by 5% of the original temperatures. The predictions by using those two temperature's patterns are also shown in Figures 3.32 and 3.33. It can be clearly seen that the rotations of the connections are very sensitive to the small temperature variations. The predicted axial force acting on the connection EJ01 predicted by current model is shown in Figure 3.34, together with the predictions by Santiago (2008) in which the detail 3D finite element approach was used. It is clear that good

agreement was achieved. Figure 3.35 shows the comparison of tested and predicted axial force acting on the connection FJ03. It can be seen that the predictions of the current model are in very good agreement with the test data.

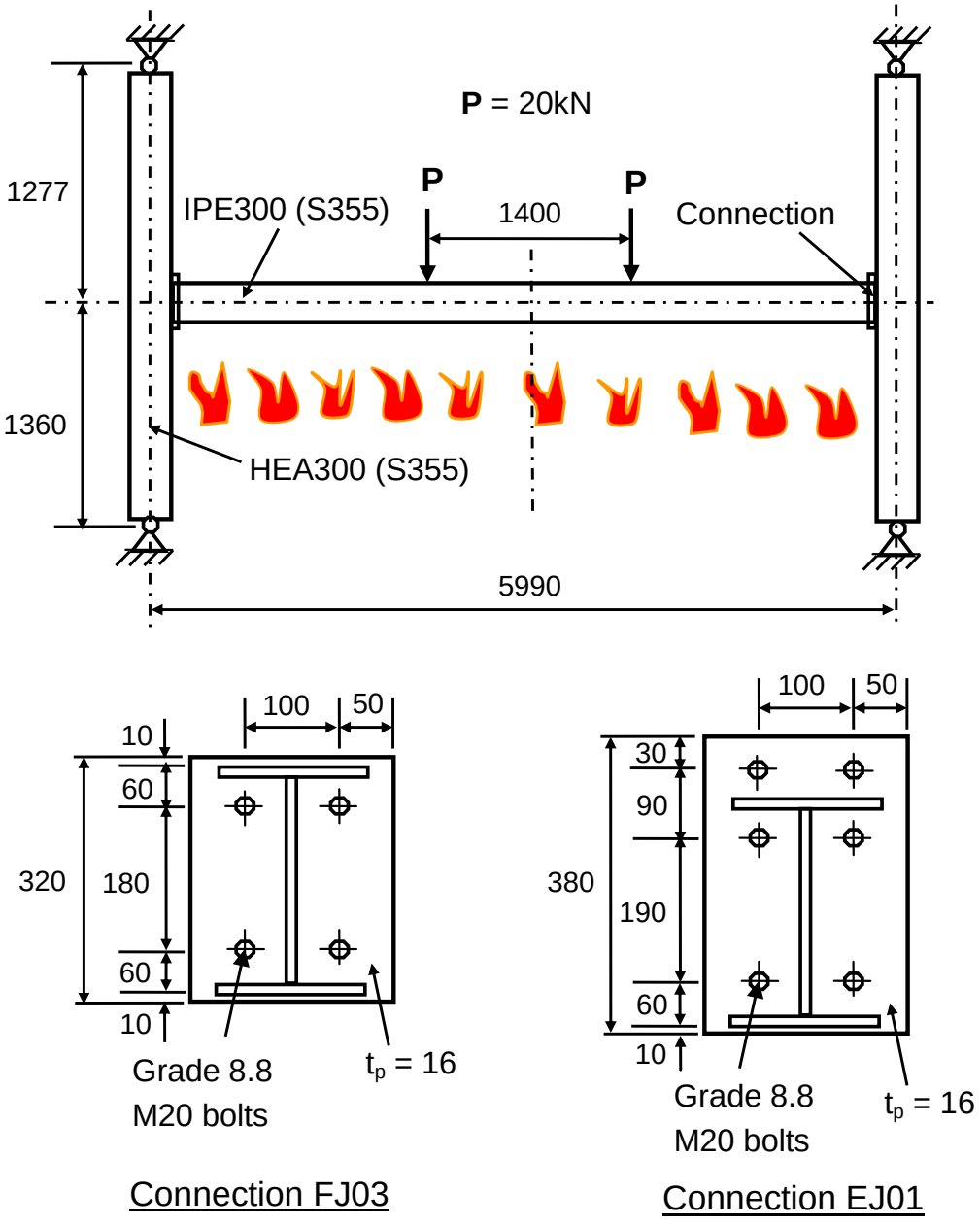

Figure 3.31 Test details of a beam-to-column substructure (Santiago, 2008)

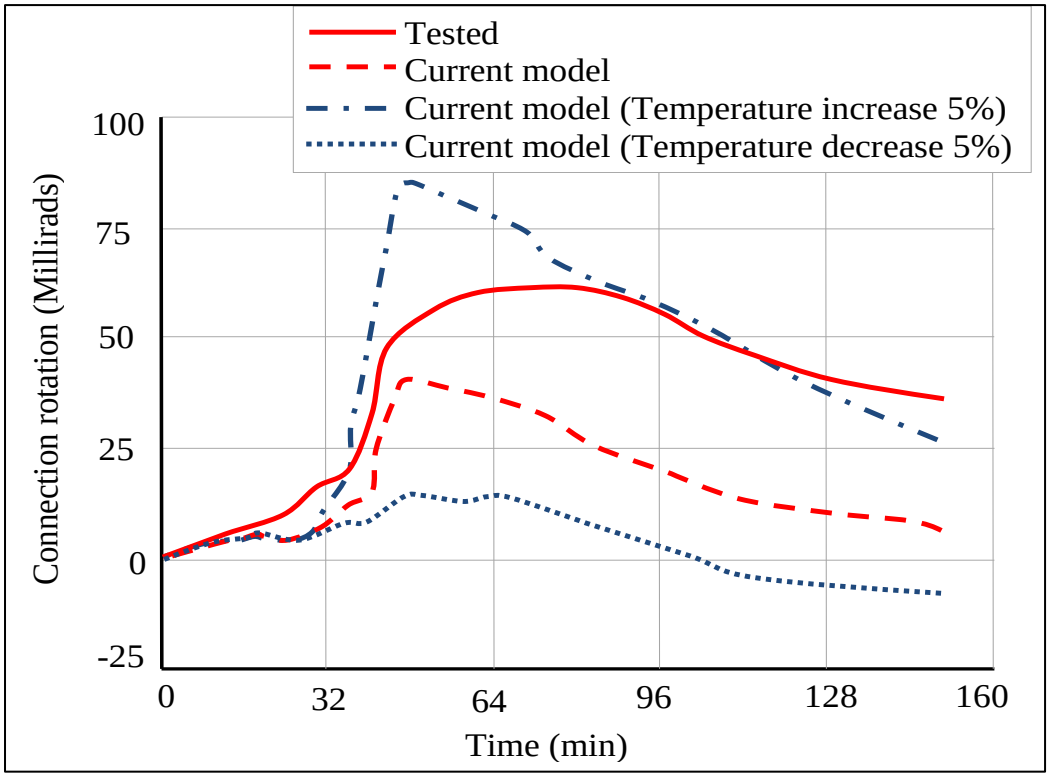

Figure 3.32 Comparison of predicted and measured connection rotations for test EJ01 (Santiago, 2008)

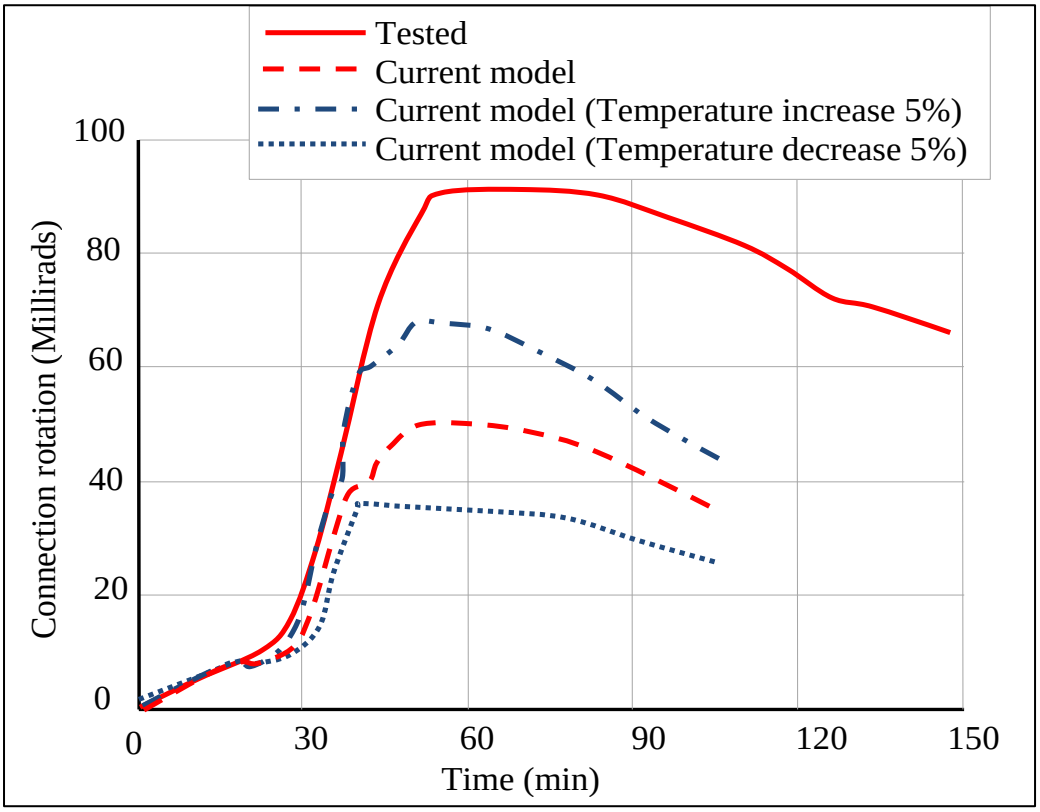

Figure 3.33 Comparison of predicted and measured connection rotations for test FJ03 (Santiago, 2008)

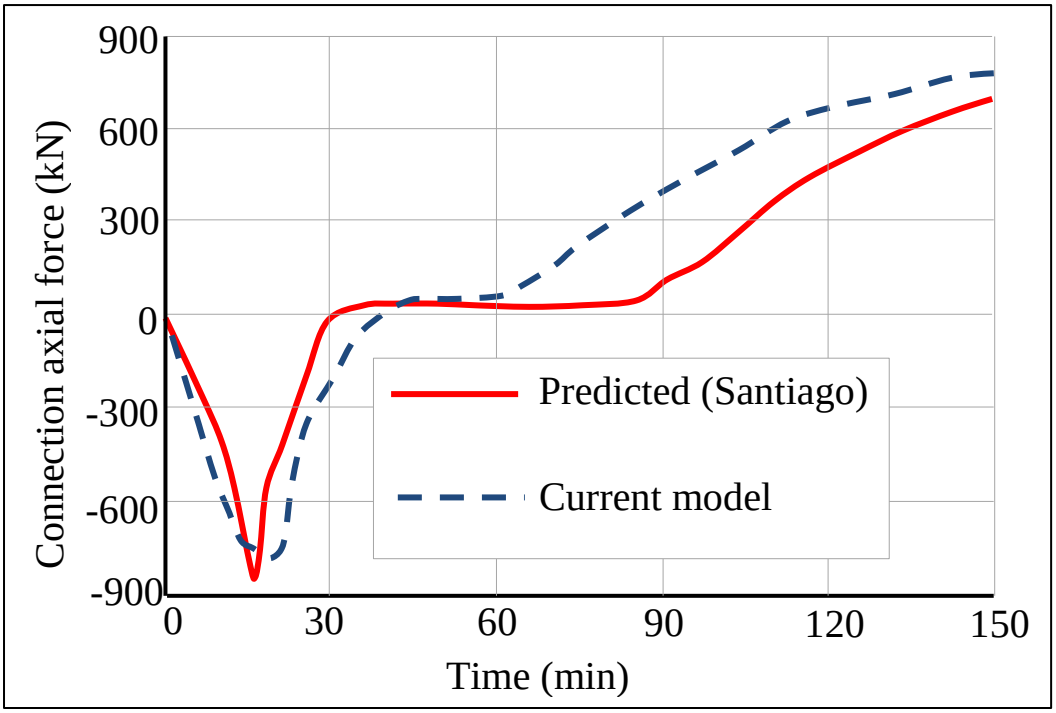

Figure 3.34 Comparison of predicted axial forces at the connection for test EJ01 (Santiago, 2008)

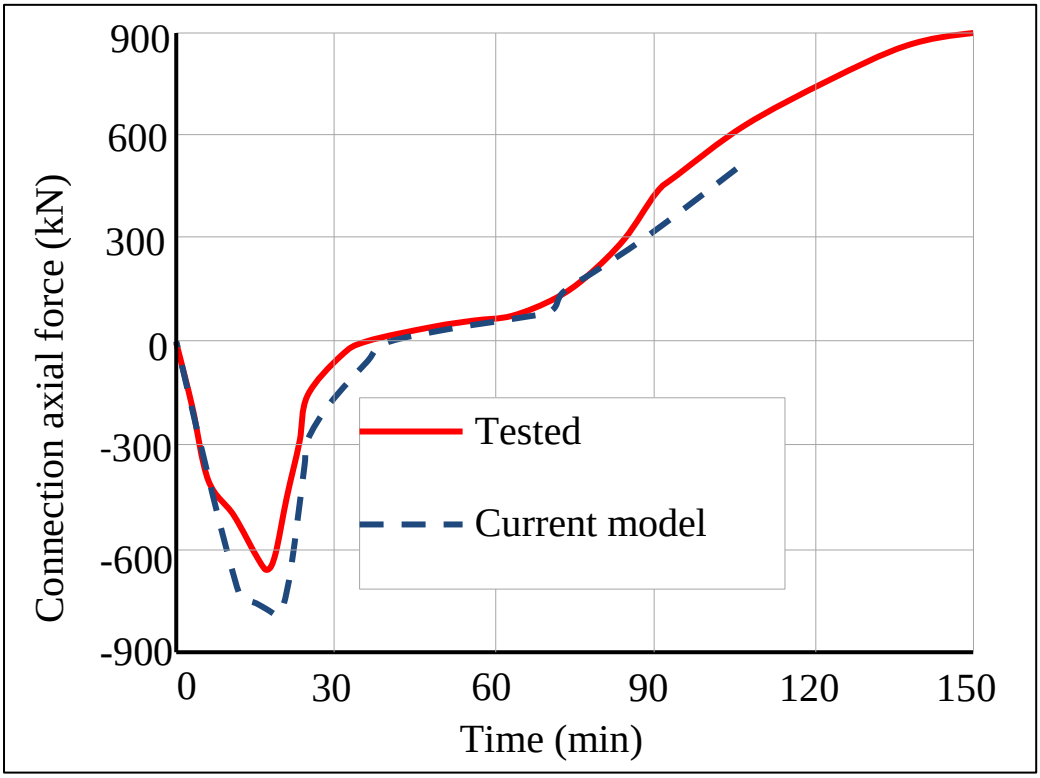

Figure 3.35 Comparison of predicted and measured axial forces at the connection for test FJ03 (Santiago, 2008)

3.9 Conclusions

In this chapter, a robust 2-node connection element has been developed for modelling the bolted end-plate connection between steel beam and column at elevated temperatures. The developments were based on the main framework of two-node connection element proposed by Huang (2011). In the developed model, the end-plate connection has been represented as a two-node nonlinear spring element. The advantages of the simple connection model are therefore retained. However, the characteristic of the nonlinear spring connection element, such as rotational stiffness, bending moment, tension and compression, vertical shear resistances are calculated based on a component model approach. Hence, the model developed also keeps the advantages of component-based models. The proposed model has also incorporated with some works done by Spyrou et al. (2004a) and Block et al. (2007), with the development of robust displacement failure criteria for three failure modes of T-stub. The proposed model has the capability to more precisely determine the tension, compression and bending capacities of end-plate connections under fire conditions. In this model, the connection failure due to bending, axial tension and compression are considered. Also, the influence of axial tensile force of the connected beam on the bending moment resistance of the connection is taken into account. Another very important aspect of the developed model is that the model has very good numerical stability under a static solver condition. This is very beneficial for the developed connection element to be used for larger scale 3D modelling of steel-framed composite buildings in fire.

A total of 22 experimental tests are used to validate the proposed model, including tests with and without applying axial force at both ambient and elevated temperatures, and two tests on a beam-to-column sub-frame subjected to natural fire. The validation results show good agreement between the model predictions and the experimental data. It is obvious that this new connection model has the ability to accurately predict the behaviour of the end-plate connections at elevated temperatures. It is evident that the influence of temperature on the behaviour of the connections is significant. Based on these comprehensive validations, it can be concluded that the developed model can be used to represent the end-plate connections for performance-based fire resistance design of steel-framed composite buildings.

Chapter 4

Modelling of Partial End-plate Connection in Fire

4.1 Introduction

The robustness of structures under fire conditions is a major consideration for structural engineers and architects. To improve the survival time of structures, and minimize the loss of life and property, extensive research has been devoted to the performance of steel-framed composite buildings under fire conditions (Moore and Lennon, 1997; Huang et al., 2004; Foster et al., 2007; Yu et al., 2008; Yu et al., 2010; Wang et al., 2011; Yang and Tan, 2012; Sun et al., 2012). Previous research shows that the behaviour of connections has a significant effect on the fire resistance of composite buildings (Burgess et al., 2012a). For structural fire engineering design, the connections between steel beams and columns are conventionally assumed to be "pinned" or "rigid", according to the rotational stiffness. However, a "semi-rigid" assumption better describes the behaviour of connection in reality (Nethercot et al., 2000). At present, partial end-plate connections, which have higher flexibility and larger rotational capacity, are commonly used in steel-framed composite buildings in the UK. A popular form of this connection consists of a rectangular plate, which is symmetrically welded into the supported beam web, and bolted to the supported column flange. Such partial end-plate connections are of great popularity for their construction efficiency. They are easy to fabricate, can be assembled and erected on site, and have been widely used in the construction of braced multi-storey steel framed buildings in the UK. One of the main characteristics of partial end-plate connection is that its rotational response contains two stages. The beam bottom flange would come into contact with the column flange after the connection rotates sufficiently, denoted as the second stage.

Up to now, the behaviour of partial end-plate connection has been investigated by experimental tests on partial end-plate connections at ambient and elevated temperatures. An experimental study was carried out by Owens and Moore (1992) on the performance of partial end-plate connections. Two different failure modes were observed from the test data, which were the bearing failure of the end-plate, and the fracture of the end-plate closed to the toe of the weld. Al-Jabri et al. (2005)

conducted a series of experimental tests on bare-steel and composite partial end-plate connections under fire conditions. In these experimental studies, only the rotational behaviour of the first stage of partial end-plate connections was performed (until the beam flange comes into contact with the column flange). In 2008, Hu et al. (2008) carried out a series of elevated temperature tests on partial end-plate connections. The dominant failure mechanism observed from the test results was the fracture of the end-plate closed to the toe of the weld. In this study, the second stage behaviour of partial end-plate connection occurred at the ambient temperature tests, while the end-plate ruptured before the beam flange contacted with the column at elevated temperature tests. Ten fire tests on steel sub-frames were conducted by Wang et al. (2011) aiming to investigate the behaviour and robustness of different types of connections in fire. In the study, the failure was defined as physical detachment of one component from another, in order to analyse the contribution of connections to prevent progressive collapse of the steel structures under fire condition. Two of the tests were carried out using partial end-plate connection with different column sections. The experimental results showed that for the larger column size test, the failure modes were the fracture of beam web, and complete detachment from column. For the smaller column section test, the failure model was excessive end-plate deformation.

At present, a number of component-based models have been developed for the analysis of partial end-plate connections at elevated temperatures. Al-Jabri et al., (2005) proposed a component-based model, and validated against the tests of partial end-plate connections at ambient and elevated temperatures (also conducted by them). In this component-based model, only the behaviour of partial end-plate connection at the first stage, before the bottom flange of beam contacts to the column flange, can be simulated. Later on, a component-based model was developed by Hu et al. (2009b), which can predict the two stage behaviours of partial end-plate connections at elevated temperatures. In this model, the connection is regarded as a series of non-linear springs connected together, using a rigid bar at each bolt row position. The performance of the connection is dependent on the force-displacement characteristics of these springs.

As mentioned in Chapter 3, one significant problem for using component-based model is that under a static solver condition, if one of the springs within the

connection fails, then numerical illness may be generated within the stiffness matrix of a connection element. Those illnesses may initiate numerical singularity for the whole structure analysed, and stop the analysis. However, one spring failure within the connection doesn't mean the failure of the whole connection. In order to overcome this problem dynamic solvers are needed (Block et al., 2007). It is well known that using a dynamic solver can significantly reduce the computational efficiency of the model, however.

In this chapter, the developments of a robust two-node connection element for modelling partial end-plate connection under fire conditions are presented. The model is mainly based on the two-node connection element framework described in Chapter 3, with further developments for analysis of partial end-plate connections. Hence, it is expected that the connection element developed in this Chapter should have good numerical stability under a static solver condition, and also retains the advantages of both the simple and component-based models. As mentioned in Chapter 3, in the developed model the connection is represented as a 2-noded non-linear spring element, and the characteristics of the spring (such as stiffness, tension, compression, shear strengths and bending moment resistances) are determined based on a component-based approach. Also, the two stage behaviours of partial end-plate connections will be considered in the model presented here.

4.2 Construction of element stiffness matrix

As mentioned above, the two-node connection element developed in this Chapter is mainly based the developments presented in Chapter 3, with some further developments to model the behaviour of partial end-plate connections at elevated temperatures. As shown in Figure 3.1, in this model the partial end-plate connection is represented as a two-node spring element, which has no physical length. Each node has six degrees of freedom referenced to the local coordinates. The element nodal force increment vector $\mathbf{\Delta F}$, and the element nodal displacement increment vector $\mathbf{\Delta u}$ can be related using Equation (3.1). As represented by Equation (3.1), the stiffness matrix of the two-node connection element $\mathbf{K}$ has a total of six stiffness coefficients need to be defined, which are the axial stiffness coefficient k_{11}, vertical shear stiffness coefficient k_{33}, rotational stiffness coefficient k_{55}, and stiffness

coefficients related to the out-of-plane degrees of freedom k_{22}, k_{44} and k_{66}. In the current developed connection element, the definitions of k_{11}, k_{33}, k_{22}, k_{44} and k_{66} are the same as defined in Chapter 3 for flush and extended end-plate connection element. The main objective of this section is to develop a robust procedure to calculate the rotational stiffness coefficient k_{55} for partial end-plate connection under fire conditions.

4.2.1 Determination of the rotational stiffness coefficient, k_{55}

In the normal component-based model, such as the model developed by Hu et al. (2009b), the rotational stiffness coefficient (k_{55}) is calculated according to the stiffness of a set of springs at each bolt row. The spring stiffness is derived based on the force-displacement characteristics of each spring. In the model presented here, k_{55} is calculated based on the proposed moment-rotation curve. The initial rotational stiffness $S_{j,\mathrm{int}}$ and the moment resistance $M_{j,Rd}$ of the whole connection are two main parameters for the construction of the proposed moment-rotation curve. In this research $S_{j,\mathrm{int}}$ and $M_{j,Rd}$ are determined based on component-based approach. Therefore, $S_{j,\mathrm{int}}$ and $M_{j,Rd}$ are calculated from each component of the connection. The details are discussed in the following sections.

4.2.2 Initial rotational stiffness of the connection, $S_{j,\mathrm{int}}$

The initial rotational stiffness $S_{j,\mathrm{int}}$ of the connection is the slope of the elastic range of the moment-rotation curve. It can be calculated based on the assembled stiffness of the components within the tension zone and compression zone applying the component-based approach (Al-Jabri et al., 2005), that is:

$$S_{j,\mathrm{int}} = \frac{1}{\frac{1}{K_{eqt} z^2} + \frac{1}{K_c z^2}} \tag{4.1}$$

where K_{eqt} and K_c are equivalent tension stiffness and compression stiffness of the connection respectively, and z is the lever arm.

4.2.3 Equivalent tension stiffness, K_{eqt}

As shown in Figure 4.1, when the connection has more than one bolt row in tension, an equivalent stiffness K_{eqt} is used to represent the overall stiffness of the tension bolt rows in the connection. K_{eqt} is derived according to EN 1993-1-8, given as:

$$K_{eqt} = \frac{\sum_{r}(K_{tt,r}h_r)}{z} \tag{4.2}$$

where $K_{tt,r}$ is the tension stiffness of each individual tension bolt row and h_r is the distance between individual bolt row r and the compression centre of the connection.

When the connection has only one bolt row in tension, the lever arm z is the distance between the centre of compression and the tension bolt row. If the connection has more than one tension bolt rows, the lever arm z is taken as the distance from the centre of compression to the equivalent tension bolt row (see Figure 4.1).

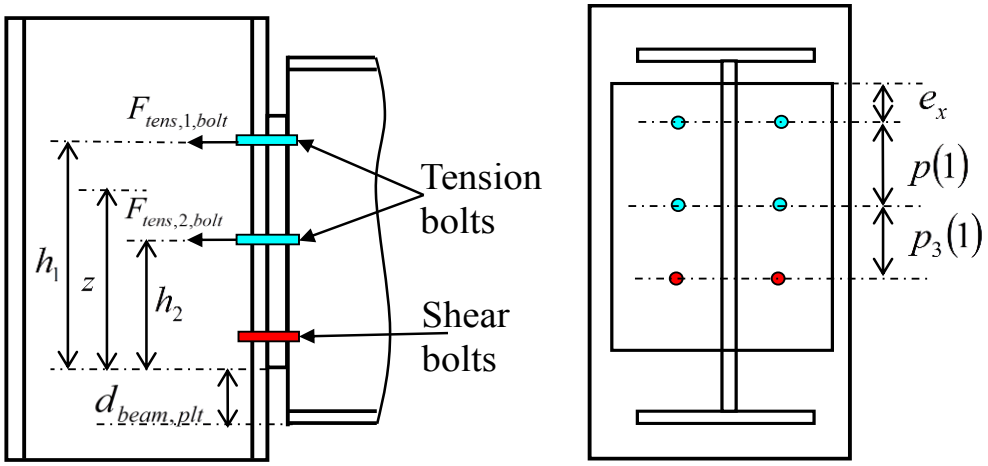

Figure 4.1 Determination of lever arm z

For partial end-plate connection, the centre of compression locates at the bottom end of the end-plate at the beginning. After the connection rotates sufficiently, the bottom flange of beam comes into the contact with the column flange. As a result, the compression centre of the connection moves from the bottom end of the end-plate, to the middle of the beam bottom flange. The change of compression centre leads to an increase of lever arm, as illustrated in Figure 4.2.

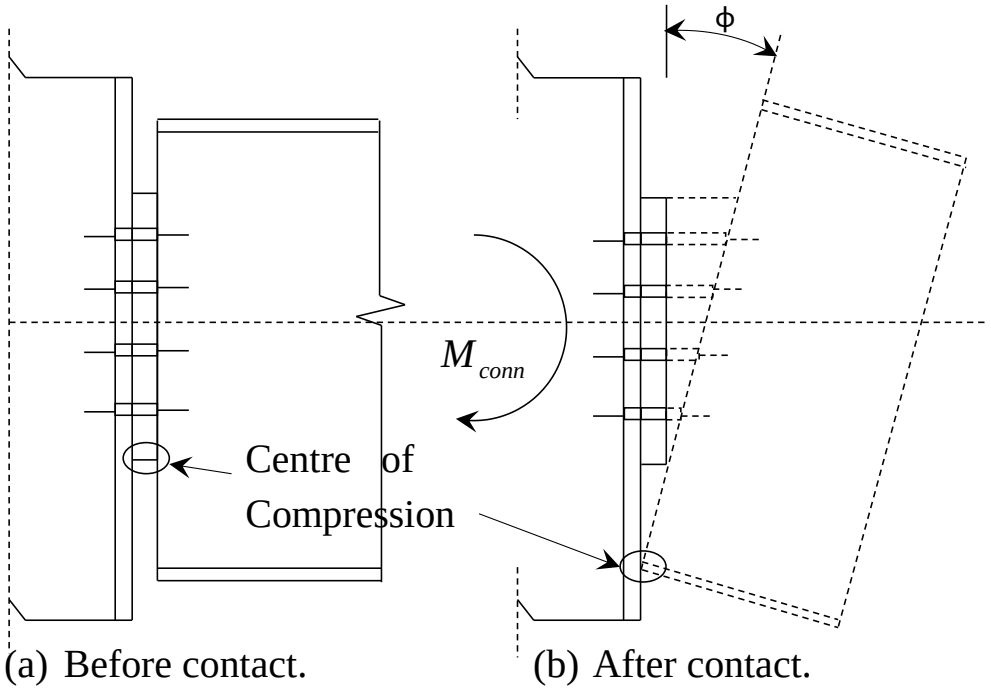

Figure 4.2 Movement of compression centre of a partial end-plate connection

The lever arm z can be calculated using the following expression:

$$z = \frac{\sum_r (K_{tt,r} h_r^2)}{\sum_r (K_{tt,r} h_r)} \tag{4.3}$$

The tension stiffness of each individual tension bolt row $K_{tt,r}$ is derived as a combination of the stiffness of the basic components within the tension zone of connection. For the partial end-plate connection, there are three basic components in the tension zone, which are the bolt, the weld and a T-stub assembly comprising of the end-plate and the beam web. It is assumed that the contributions of column flange and web can be negligible as the partial end-plate connection are designed as simple with limited stiffness compared to the attached column (Hu et al., 2009b). Therefore the tension stiffness of each individual tension bolt row can be expressed as:

$$K_{tt,r} = \frac{1}{\frac{1}{K_{bt}} + \frac{1}{K_{weld}} + \frac{1}{K_{plt}}} \tag{4.4}$$

where K_{bt} is the stiffness of the bolts, K_{weld} is the stiffness of the weld and K_{plt} is the stiffness of the T-stub assembly.

4.2.3.1 Tension stiffness of the bolt, K_{bt}

The stiffness of the bolt K_{bt} can be calculated based on the formula documented in EN 1993-1-8, as given below:

$$K_{bt} = 1.6 \times \frac{A_s E_b}{L_b} \tag{4.5}$$

where A_s is the bolt shaft area; E_b is the Young's module of the bolt; L_b is the bolt length, including the total thickness of the end-plate, column flange and washers, in addition to half of the sum of the height of the bolt head and nut.

4.2.3.2 Tension stiffness of the welds, K_{weld}

The performance of the welds can be represented using the force-deformation relationship. The tension stiffness of the welds relates to the design resistance and the failure deformation of the welds. The design weld resistance per unit length can be obtained according to the expressions given in EN 1993-1-8. The failure deformation of welds is assumed to be 30% of the effective throat thickness. This assumption is derived based on the experimental studies conducted by Kanvinde et al. (2009). In the studies, 24 cruciform weld tests loaded in direct tension were carried out with different root notch lengths, weld sizes and weld classifications. The test results indicate that the root notch length does not have a significant impact on the strength of the welds.

The stiffness coefficient for the weld K_{weld} is calculated as:

$$K_{weld} = \frac{\min(f_{u,b}; f_{u,p})\, d_{weld,r}}{0.3 \times \sqrt{3} \beta_w \gamma_{M2}} \tag{4.6}$$

where $f_{u,b}$ is the ultimate tensile strength of the beam; $f_{u,p}$ is the ultimate tensile strength of the end-plate; $d_{weld,r}$ is the weld length for each individual bolt row r; which r is bolt row number; β_w is the correlation factor for fillet welds, which is taken as 0.85 for S275 steel while 0.9 for S355 steel. If the material strength grades

of the two parts joined are different, the welds are designed using the properties of the material with the lower strength grade (EN 1993-1-8).

4.2.3.3 Tension stiffness of the T-stub assembly, K_{plt}

When load is applied to the connection, the end-plate is pulled away from the column face, generating plastic deformation. Traditionally, a T-stub assembly is used to represent the end-plate, where the flange simulates the end-plate while the stem models the beam web. As shown in Figure 3.6, there are three failure mechanisms for a T-stub assembly depending on the differences in the resistance of the end-plate compared to bolts. For *Failure Mode I*, the bolts yield and fracture after a first plastic hinge forms at the flange-to-web intersection. For *Failure Mode II*, a second plastic hinge forms at the bolt line after the formation of the first plastic hinge, follows by the bolts yielding and fracturing. For *Failure Mode III*, the T-stub fails due to the yielding and fracture of the bolts, while the T-stub flange remains elastic. For a partial end-plate connection, experimental tests conducted by Hu et al. (2009b) indicated that the failure mode of this kind of connection can be mainly classified as *Failure Mode II* – in which the T-stub flange suffers completed yielding. Therefore in the current model, it is assumed that the T-stub assembly fails according to *Failure Mode II*.

As mentioned in Chapter 3, a simplified mathematical model was proposed by Spyrou et al. (2004a) to simulate the force-deformation characteristics of the T-stubs at ambient and elevated temperatures. All three failure mechanisms have been taken into consideration. Hence, for *Failure Mode II*, a piecewise linear curve is used to represent the force-deformation relationship, as shown in Figure 3.10. The detail numerical derivation has been demonstrated in Chapter 3. The tension stiffness of T-stub assembly can be calculated relating to the force and deformation of T-stub when the first plastic hinge forms. Hence, the tension stiffness of the T-stub assembly K_{plt}, which represents the end-plate and the beam web, is expressed as below:

$$K_{plt} = \frac{1}{\frac{L_e^3}{48E_pI} - \frac{\rho}{E_pI}\left(\frac{L_e^3}{24} + \frac{(m+k/2)^3}{6} - \frac{(m+k/2)^2 L_e}{4} - \frac{k^2(n+k/2)}{24}\right)} \tag{4.7}$$

where $I = L_{eff} t_f^3 / 12$; L_{eff} is the effective length of T-stub assembly; t_f, n, k, and m are defined in Figure 3.8; L_e is the width of end-plate; E_p is the Young's module of end-plate; ρ is the ratio of the tension force and the bolt force.

4.2.4 Equivalent compression stiffness, K_c

The compression stiffness of partial end-plate connection is determined by the compression stiffness of column web. A design approach was proposed by Block (2006) to predict the stiffness of column web at elevated temperatures. This approach was derived based on the experimental and numerical investigation conducted by Aribert et al. (2002). The stiffness of column web can be calculated as:

$$K_c = \frac{2}{3} E_{cw} \left(\frac{b_c t_{fc}^3 t_{wc}^2}{b_{eff,c,wc} d_{c,c}} \right)^{0.25} \tag{4.8}$$

where E_{cw} is the Young's module of column web, b_c is the width of column flange, t_{fc} is the thickness of the column flange, t_{wc} is the thickness of column web, $b_{eff,c,wc}$ is the effective length, and $d_{c,c}$ is the distance of column web between the root radii.

The effective length $b_{eff,c,wc}$ is expressed as:

$$b_{eff,c,wc} = t_{fb} + 2\sqrt{2} a_p + 5(t_{fc} + s) + s_p \tag{4.9}$$

where $s = r_c$, $s_p = \sqrt{2} t_p$, $a_p = 0.55 t_p$.

4.2.5 Moment-rotation curve of the connection

As illustrated in Figure 4.2(b), the rotational response of partial end-plate connection is comprised of two stages. In the first stage, the compression centre of the connection is located at the bottom end of the end-plate, where the connection rotates unimpeded. In the second stage, after the connection rotates sufficiently, the bottom flange of beam comes into the contact with the column flange. As a result, the compression centre of the connection moves from the bottom end of the end-plate, to the middle of the beam bottom flange. The change of compression centre leads to an increase of lever arm, and increases the moment resistance of the connection.

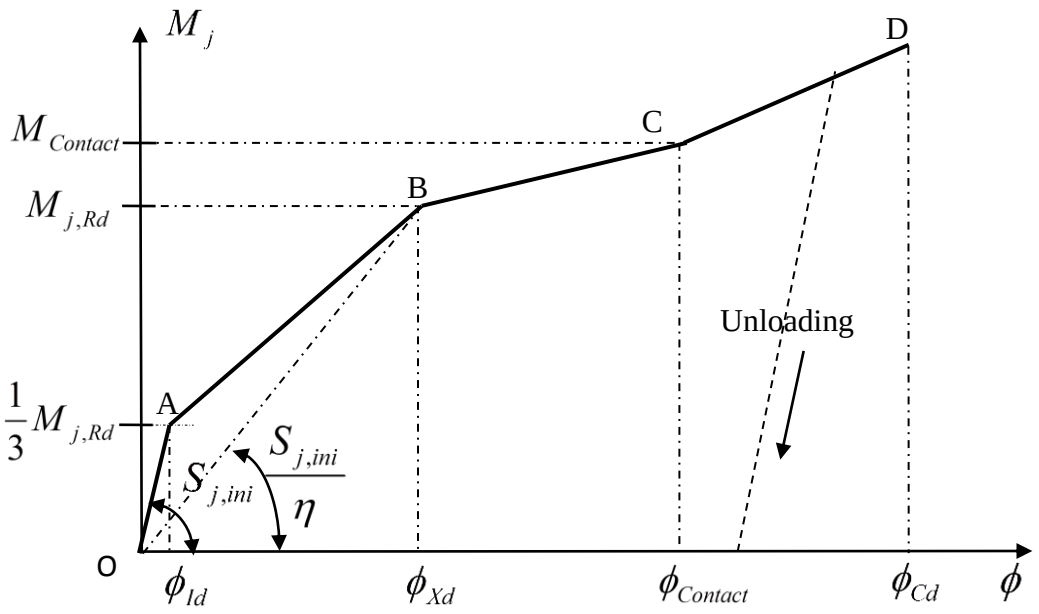

Figure 4.3 Multi-linear moment-rotation characteristic used for the connection element

Such two stage rotational behaviours are taken into account in the model presented here. As demonstrated in Figure 4.3, a multi-linear curve is proposed to describe the bending moment characteristic of the connection. In the figure, $S_{j,\mathrm{int}}$ is the initial stiffness of the connection, $M_{j,Rd}$ is the bending moment resistance of the connection, ϕ_{Xd} is the rotation when the moment of the connection first reaches to $M_{j,Rd}$, $M_{Contact}$ is the moment of the connection when the beam bottom flange comes into the contact with column flange, $\phi_{Contact}$ is the rotation of the connection referenced to $M_{Contact}$, and ϕ_{Cd} is the maximum rotation of the connection.

The proposed formulations to determine the rotations ϕ_{Id}, ϕ_{Xd}, $\phi_{Contact}$ are as follows:

$$\phi_{Id} = \frac{M_{j,Rd}}{3S_{j,\mathrm{int}}} \tag{4.10}$$

$$\phi_{Xd} = \frac{M_{j,Rd}}{\frac{S_{j,\mathrm{int}}}{\eta}} \tag{4.11}$$

$$\phi_{Contact} = \frac{t_p}{0.5h_b - d_{beam,plt}} \tag{4.12}$$

where h_b is the depth of beam, $d_{beam,plt}$ is the distance between the bottom flange of the beam and the end of end-plate. It can be seen that $\phi_{Contact}$ is directly related to the geometry of the partial end-plate and the supported beam. This multi-linear moment-rotation curve is proposed based on the one introduced in EN 1993-1-8 for the moment-rotation characteristic of flush or extended end-plate connection with some modifications. Compared to partial end-plate connection, the behaviour of flush or extended end-plate connection is more rigid. Therefore, in this model, ϕ_{Id} is calculated by proposed Equation (4.10). Also in the current model it is assumed that the stiffness coefficient $\eta = 3$. Compared to the moment-rotation curve of flush or extended end-plate connection proposed in EN 1993-1-8 $\phi_{Id} = 2M_{j,Rd}/(3S_{j,\text{int}})$ and $\eta = 2$.

The proposed multi-linear moment-rotation curve of partial end-plate connection can therefore be represented as (see Figure 4.3):

For line OA ($\phi \le \phi_{Id}$):

$$M_j = k_{55}\phi = S_{j,\text{int}}\phi \tag{4.13}$$

where $k_{55} = S_{j,\text{int}}$.

For line AB ($\phi_{Id} < \phi \le \phi_{Xd}$):

$$M_j = k_{55}(\phi - \phi_{Id}) + \frac{1}{3}M_{j,Rd} \tag{4.14}$$

where $k_{55} = \dfrac{2M_{j,Rd}}{3(\phi_{Xd} - \phi_{Id})}$.

For line BC ($\phi_{Xd} < \phi \le \phi_{Contact}$):

$$M_j = k_{55}(\phi - \phi_{Xd}) + M_{j,Rd} \tag{4.15}$$

where $k_{55} = 0.065\, S_{j,\text{int}}$.

For line CD ($\phi_{Contact} < \phi \le \phi_{Cd}$):

$$M_j = 0.065 \times S_{j,\text{int}} \times (\phi_{Contact} - \phi_{Xd}) + M_{j,Rd} + k_{55}(\phi - \phi_{Contact}) \tag{4.16}$$

where $k_{55} = 0.15 S_{j,\text{int},II}$, $S_{j,\text{int},II}$ is the initial stiffness of the connection for the second stage when the centre of compression switches to the middle of beam bottom flange. If $\phi > \phi_{Cd}$, it is assumed that the connection is broken, that is $M_j = 0$ and $k_{55} = 0$.

The details for calculating the bending moment resistance of the connection $M_{j,Rd}$ will be presented in the following sections.

4.3 Determination of the tension resistance of the connection

As described above, in the tension zone the connection is regarded as the combination of three basic components: the welds, the bolts and a T-stub assembly. The tension resistance of connection is determined by the weakest components within the tension zone.

4.3.1 Tension resistance of the welds, F_{weld}

The tension resistance of the welds is calculated according to the formulae given in EN 1993-1-8, as shown below:

$$F_{weld} = \frac{\min(f_{u,b}; f_{u,p}) a d_{weld,r}}{\sqrt{3}\beta_w \gamma_{M2}} \tag{4.17}$$

where a is the effective throat thickness of a fillet weld, and other parameters in Equation (4.17) are the same as defined in Equation (4.6).

4.3.2 Tension resistance of the bolts, F_{bt}

The tension resistance of the bolt can be expressed as:

$$F_{bt} = N_{bt} A_s f_{by} \tag{4.18}$$

where f_{by} is the yield strength of bolts at a given temperature. N_{bt} is the number of bolts in tension at a given bolt row.

4.3.3 Tension resistance of the T-stub assembly, F_{plt}

As described above, for partial end-plate connection the failure mode of the T-stub assembly is mostly similar to the second failure mode. In the current model the tension resistance of T-stub assembly F_{plt} is therefore calculated according to the

multi-linear force-deformation curve for *Failure Mode II*. It is taken as the tension resistance when the bolts fracture. The derivation procedure is displayed in Chapter 3. Hence, in the current model, the tension resistance of T-stub assembly can be calculated as:

$$F_{plt} = \frac{2M_p\left(2n+\frac{7}{8}k\right)}{mn+\frac{3k\,n}{8}+\frac{3k\,m}{8}+\frac{k^2}{8}} + 2\left(A_s\ f_{by} - A\right) + 2\times\left(A_s\ f_{bu} - A_s\ f_{by}\right) \tag{4.19}$$

$$A = \frac{\rho M_p}{\frac{n+m+k}{2} - \rho\left(n+\frac{k}{2}\right)} + B \tag{4.20}$$

$$B = \frac{\left(\frac{2M_p\left(2n+\frac{7}{8}k\right)}{mn+\frac{3k\,n}{8}+\frac{3k\,m}{8}+\frac{k^2}{8}} - \frac{M_p}{\frac{n+m+k}{2} - \rho\left(n+\frac{k}{2}\right)}\right)}{2} \times \left(\frac{m+\frac{k}{2}}{n+\frac{k}{2}}+1\right) \tag{4.21}$$

4.3.4 Tension resistance of the connection, $F_{t,Rd}$

For each individual bolt row, its tension resistance $F_{tens,r,bolt}$ is taken as the minimum value of the tension resistance of three basic components as follows:

$$F_{tens,r,bolt} = \min(F_{plt}, F_{weld}, F_{bt}) \tag{4.22}$$

The total tension resistance of the connection $F_{t,Rd}$ is obtained as the sum of all the tension bolt rows as:

$$F_{t,Rd} = \sum_{r=1}^{N} F_{tens,r,bolt} \tag{4.23}$$

where N is the total number of the bolt rows in tension.

4.4 The compression resistance of the connection

For the compression zone within the partial end-plate connection, the compression resistance of the connection can be considered as the compression resistance of the column web (Al-Jabri et al., 2005;Hu et al., 2009b). The simplified model developed

by Block et al. (2007) is adopted here to calculate the compression resistance of column web. The details and equations of this approach have been presented in

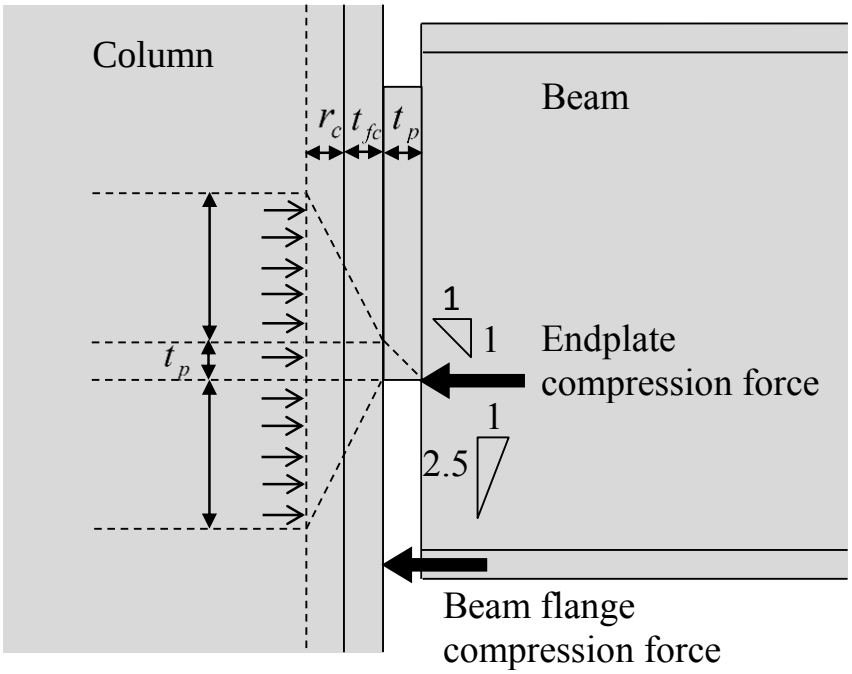

(a) End-plate compression force

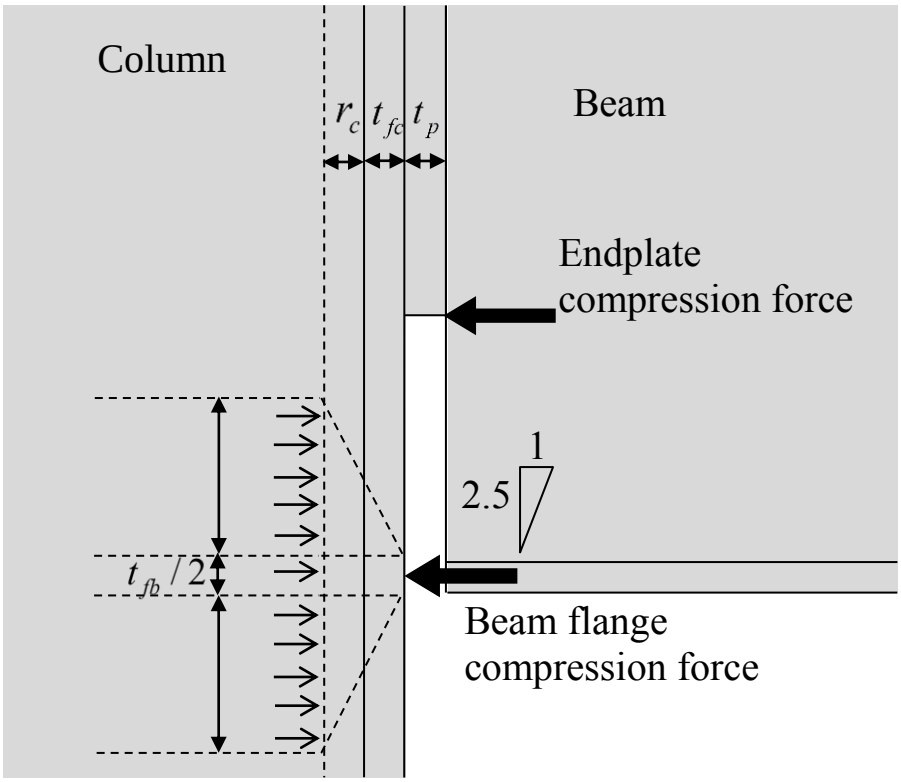

(b) Beam flange compression force

Figure 4.4 Loading cases for compression zone: (a) End-plate compression force (b) Beam flange compression force (Hu, 2009a).

Chapter 3. The only difference is that for partial end-plate connection, the value of load width c changes with the shift of the centre of compression. In the first stage, $c = t_p$, which is calculated using a dispersion angle of 45° in end-plate. After the beam bottom flange comes into contact with column, c is taken as $t_{fb}/2$, assuming half of the beam flange thickness contacts with the column face (Hu et al., 2009b).

The force redistribution is also taken into account here, where the effective tension resistance $F_{t,Ed}$ needs to meet the following criteria:

$$F_{t,Ed} = \sum_{r=1}^{N} F_{tens,r,bolt} \leq F_{c,Rd} \tag{4.24}$$

If the effective tension resistance $F_{t,Ed}$ is larger than the compression resistance $F_{c,Rd}$, the force distribution in the bolt rows should be adopted to make sure that:

$$F_{t,Ed} = \sum_{r=1}^{N} F_{tens,r,bolt} = F_{c,Rd} \tag{4.25}$$

Normally the force will be reduced from the tension bolt row with the largest bolt row number (from the top of the connection).

4.5 The bending moment resistance of the connection

The bending moment resistance of a partial end-plate connection can be expressed as:

$$M_{j,Rd} = \sum_{r} h_r F_{tens,r,bolt} \tag{4.26}$$

where h_r is the distance between individual bolt row r and the centre of compression.

4.6 The vertical shear resistance of the connection

The active components within the shear zone in partial end-plate connection are bolts in shear and plate in bearing. For an individual shear bolt row, the shear resistance $V_{b,r,Rd}$ is calculated as the minimum value of the shear resistance of bolt $F_{v,Rd}$, the bolts in bearing on end-plate $F_{b,ep,Rd}$ and bolts in bearing on column flange $F_{b,cf,Rd}$, as:

$$V_{b,r,Rd} = \min(F_{v,Rd}; F_{b,ep,Rd}; F_{b,cf,Rd}) \tag{4.27}$$

4.6.1 Bolt in shear

The shear resistance of bolt $F_{v,Rd}$ is obtained as:

$$F_{v,Rd} = \frac{\alpha_V f_{ub} A_s}{\gamma_{M2}} \tag{4.28}$$

where $\gamma_{M2} = 1.25$. For classes 4.6, 5.6 and 8.8 bolts, $\alpha_V = 0.6$; for classes 4.8, 5.8, 6.8 and 10.9 bolts, $\alpha_V = 0.5$.

4.6.2 Plate in bearing

The bearing failure of the plates characterises the deformation of the holes, affected by the lateral constraint around the hole. The performance of plate in bearing is investigated by Sarraj (2007b), and an analytical model was proposed based on the investigation results. In the study, the influence of different parameters was analysed, such as end distance, plate thickness and bolt size. The simulation results demonstrated that the bearing strength increases proportional to the plate thickness and bolt size. The bearing strength improves significantly if the end distance increases from $2d_b$ to $3d_b$. However, from this value ($3d_b$), increasing end distance only has very slightly impact on the bearing strength. d_b is the nominal diameter of the bolt.

The shear resistance of bolt in bearing on end-plate $F_{b,ep,Rd}$ can then be expressed as:

$$F_{b,ep,Rd} = \begin{cases} \dfrac{e_x}{d} f_{u,p} d t_p & e_x \le 2d \\ 0.92 \dfrac{e_x}{d} f_{u,p} d t_p & e_x \ge 3d \end{cases} \tag{4.29}$$

where e_x is the distance between the bolt hole and the edge of end-plate.

For the column flange in bearing, the shear resistance can be calculated as:

$$F_{b,cf,Rd} = \begin{cases} \dfrac{p_3}{d} f_{u,p} d t_p & p_3 \le 2d \\ 0.92 \dfrac{p_3}{d} f_{u,p} d t_p & p_3 \ge 3d \end{cases} \tag{4.30}$$

where p_3 is defined in Figure 4.1.

4.6.3 The vertical shear resistance of the connection

The vertical shear resistance of the connection $V_{s,Rd}$ can be then given as:

$$V_{s,Rd} = \sum_{r=1}^{N} V_{b,r,Rd} \tag{4.31}$$

where N is the number of bolts in vertical shear.

In this research, the strength and stiffness of the bolts, end-plate, beam and column reduce at elevated temperatures. The degradation of the connection's material properties, such as yield strength, ultimate strength and Young's modulus, are all considered in the current model. As mentioned in Chapter 3, the influence of material degradation of the bolt by using different models on the final tension resistance of one bolt row is not very significant. For simplicity, it is therefore reasonable to assume that the material degradation of bolts at elevated temperatures is the same, for the beam, column and end-plate. The model specified in Eurocode 3 Part 1.2 (CEN, 2005b) is used.

The two-node connection element developed in this chapter (for modelling partial end-plate connection) has been incorporated into computer program VULCAN (Huang et al. (2003a); Huang et al. (2009)) – for 3D modelling of steel-framed composite buildings under fire conditions.

4.7 Validations

The model presented above has been validated using a total of fourteen partial end-plate connections, tested at both ambient and elevated temperatures by other researchers (Al-Jabri et al., 2005; Hu et al., 2009b). In these validations, the tested ambient temperature material properties, and measured temperature distributions within the connections, were used as input data for the model.

4.7.1 Validation against isolated tests by Hu

A joint research programme has been carried out by two research groups at the University of Manchester and the University of Sheffield, in order to investigate the tying capacity and ductility of different steel connections at ambient and elevated temperatures. Four types of connections were used in this programme, which were flush end-plates, partial end-plates, fin plates and web cleats connections. The

twelve experimental tests on partial end-plate connections conducted by Hu et al. (2009b) were used to validate the model developed in this chapter, including three ambient temperature tests and nine tests at elevated temperatures.

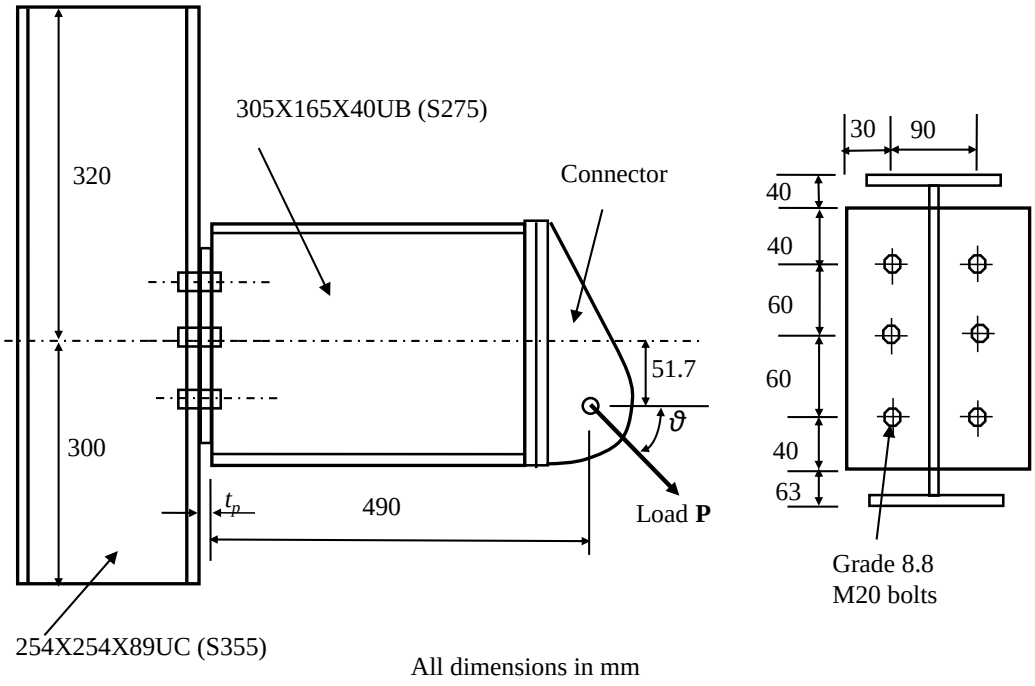

Figure 4.5 Details of test specimens used by Hu et al. (2009b)

Figure 4.5 illustrates the details of the test configurations. The tested connections were comprised of a 305x165x40UB beam, connected to a 254x254x89UC column with six M20 Grade 8.8 bolts in 22mm clearance holes. The thickness of the partial endplate was 10 mm. The steel used for the connection was S275 for the end-plate and beams, and S355 for the column. The yield strengths of the connection materials at ambient temperature were 275 N/mm^2 for S275, 355 N/mm^2 for S355 and 640 N/mm^2 for the 8.8 bolt. The ultimate strengths of the connection materials were: 450 N/mm^2 for S275 steel, 550 N/mm^2 for S355 steel and 800 N/mm^2 for the 8.8 bolt. The Young's modulus was 205000 N/mm^2 for both the steel and the bolts. In the experiments a force, with an inclined angle (θ) to the axis of the connected beam, was applied. Three different inclined angles were employed, where θ =35°, 45° and 55°. These angles represented different combination of vertical shear and axial tension forces. All fire tests were conducted by uniformly heating the specimen to the specified temperature, then gradually increasing load until connection failure.

The experimental results demonstrate that the failure mechanism for most of the partial end-plate connections is fracture of end-plate, close to the toe of the weld.

Figures 4.6 and 4.7 show the comparison results for the three ambient temperature tests. The results of these three tests indicated that the connections have suffered sufficient rotation, which lead to the contact between the beam bottom flange and the column. It can be seen from the figures that the proposed model can reasonably predict the two stage behaviours of the connection. The second stage behaviour of partial end-plate connection in the ambient tests started at about 6 ° rotation, as depicted by the kink in the curve. The discrepancies between the tested results and current model predictions were mainly due to the multi-linear moment-rotation curve used. In fact, the real moment-rotation curve of the connection should be a smooth curve. However, the predictions of the current model agreed reasonably well with the tested results. Figures 4.8 to 4.12 show the comparison results for the nine tests at elevated temperatures, where three different temperatures were employed (at 450 ℃, 550 ℃ and 650 ℃). It can be seen that the rotation capacities reduced compared to the ambient tests.

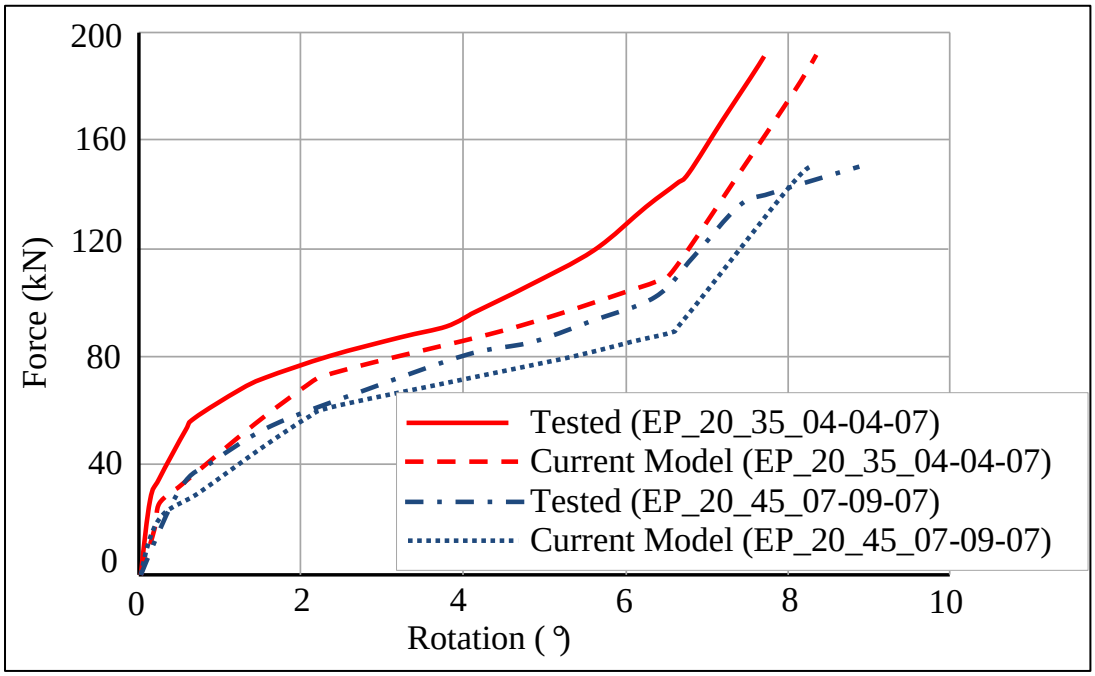

Figure 4.6 Comparison of predicted and measured rotations for tests: EP_20_35_04-04-07(20 ℃, θ=35°) and EP_20_45_07-09-07(20°C, θ=45°) (Hu et al., 2009b)

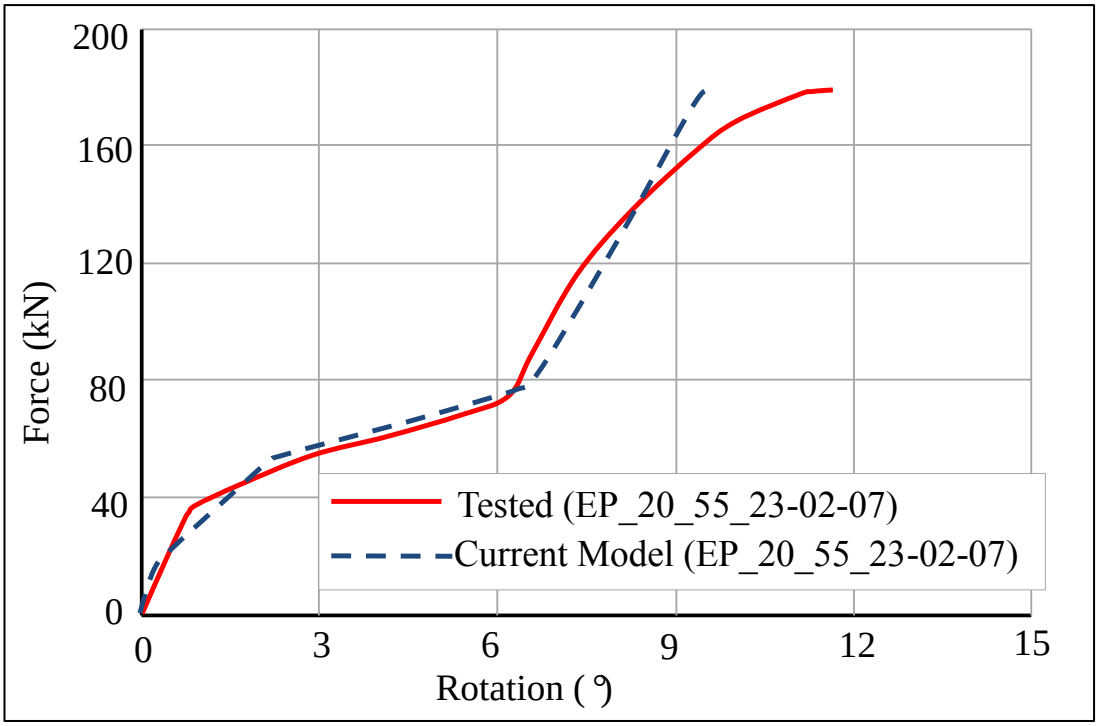

Figure 4.7 Comparison of predicted and measured rotations for tests: EP_20_55_23-02-07(20 ℃, θ=55°) (Hu et al., 2009b)

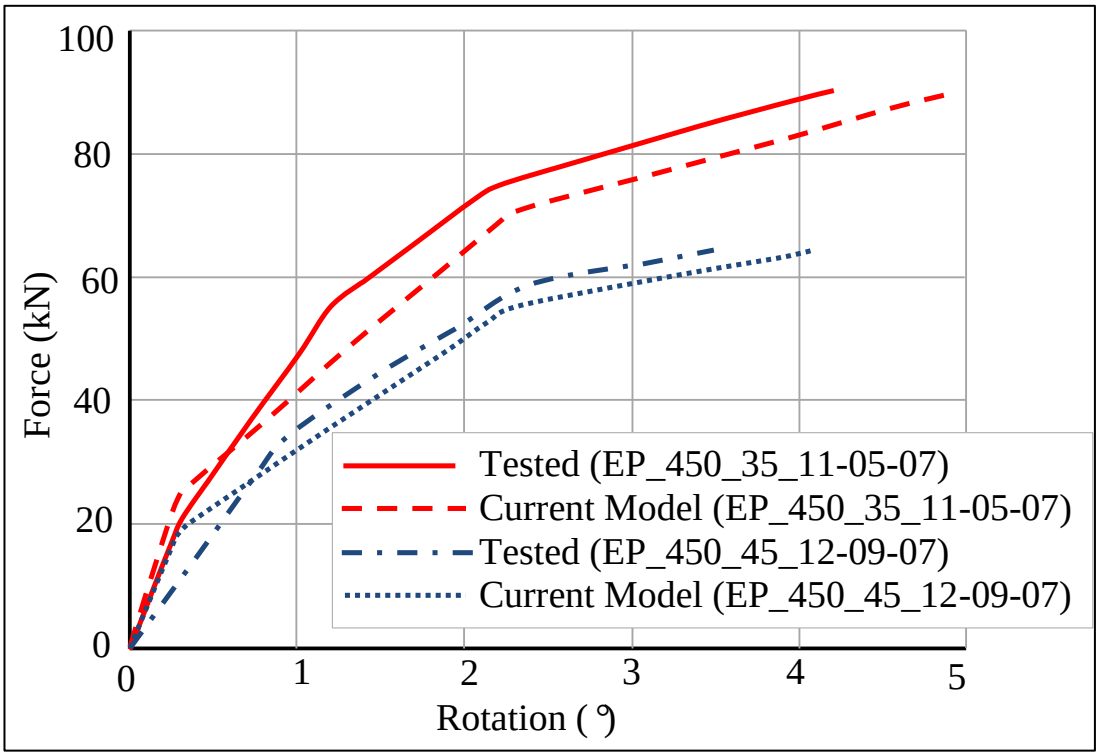

Figure 4.8 Comparison of predicted and measured rotations for tests: EP_ 450_35_11-05-07(450 ℃, θ=35°) and EP_ 450_45_12-09-07 (450°C, θ=45°) (Hu et al., 2009b)

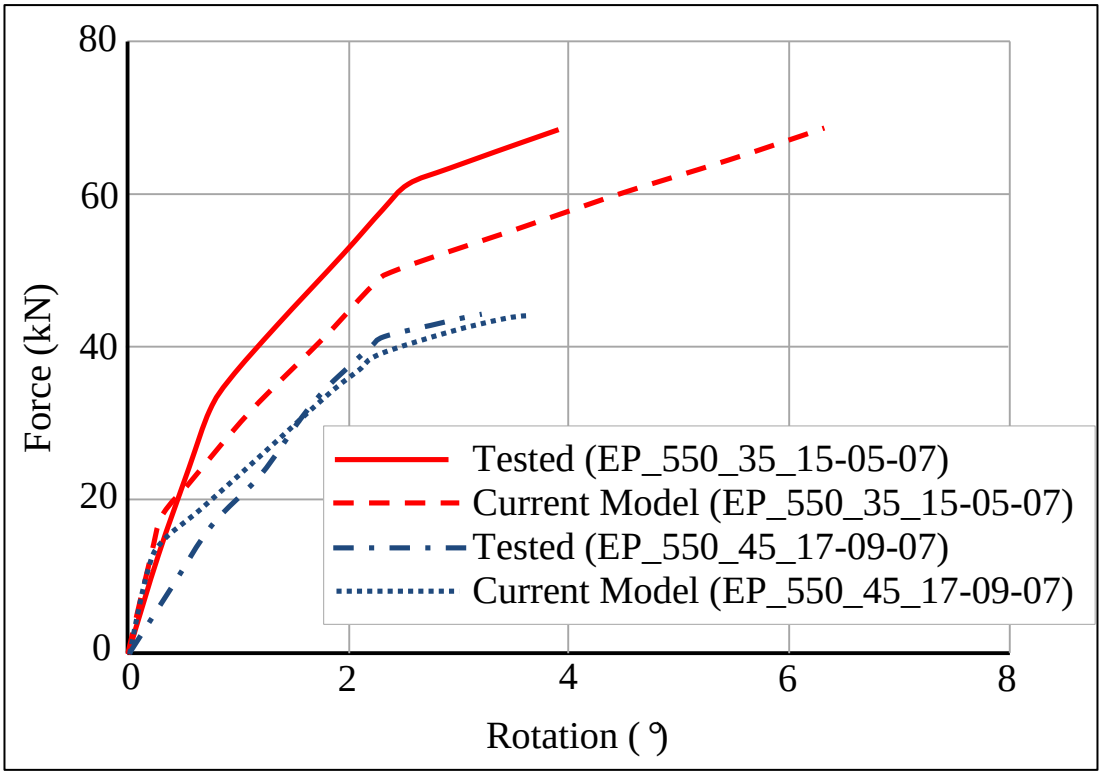

Figure 4.9 Comparison of predicted and measured rotations for tests: EP_ 550_35_15-05-07 (550 ℃, θ=35°) and EP_ 550_45_17-09-07 (550°C, θ=45 °) (Hu et al., 2009b)

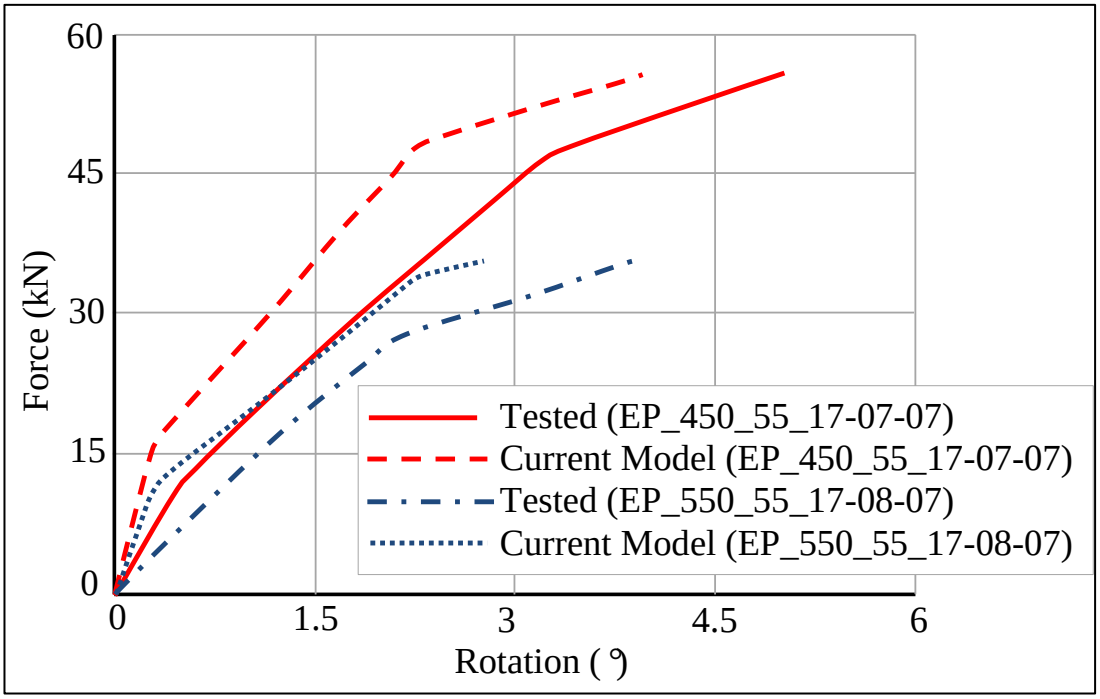

Figure 4.10 Comparison of predicted and measured rotations for tests: EP_450_55_17-07-07 (450°C, θ=55°) and EP_ 550_55_17-08-07 (550°C, θ=55°) (Hu et al., 2009b)

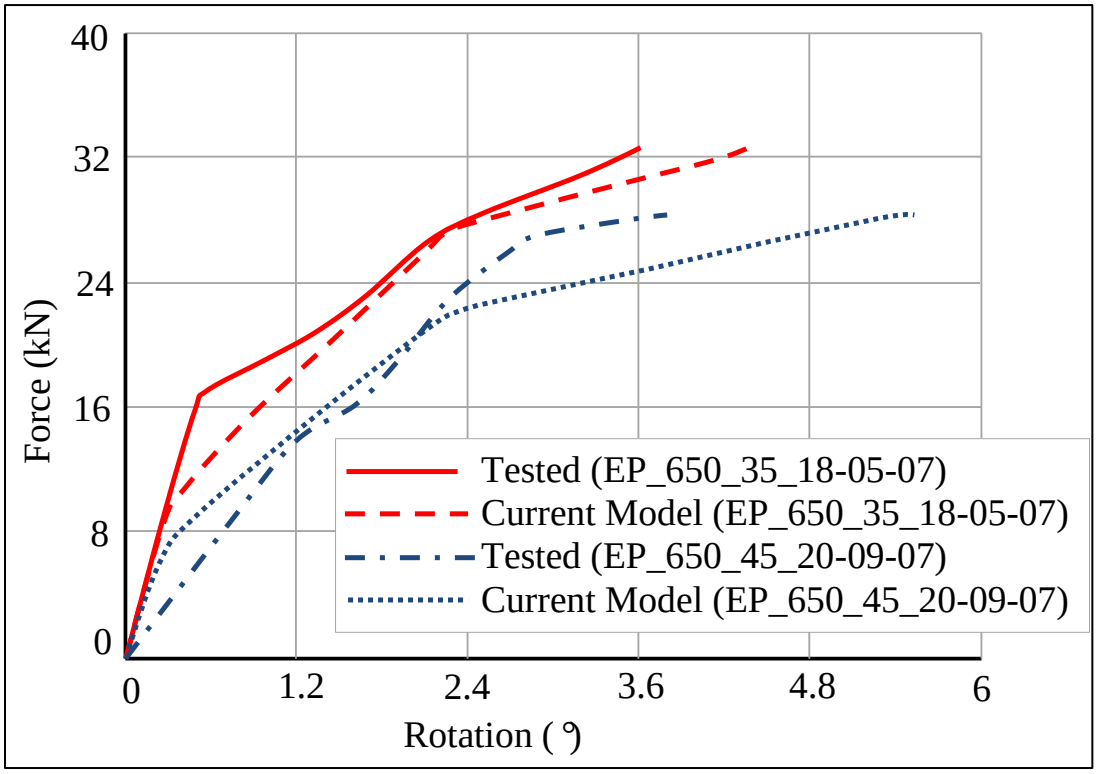

Figure 4.11 Comparison of predicted and measured rotations for tests: EP_ 650_35_18-05-07 (650°C, θ=35 ℃) and EP_ 650_45_20-09-07 (650°C, θ=45°) (Hu et al., 2009b)

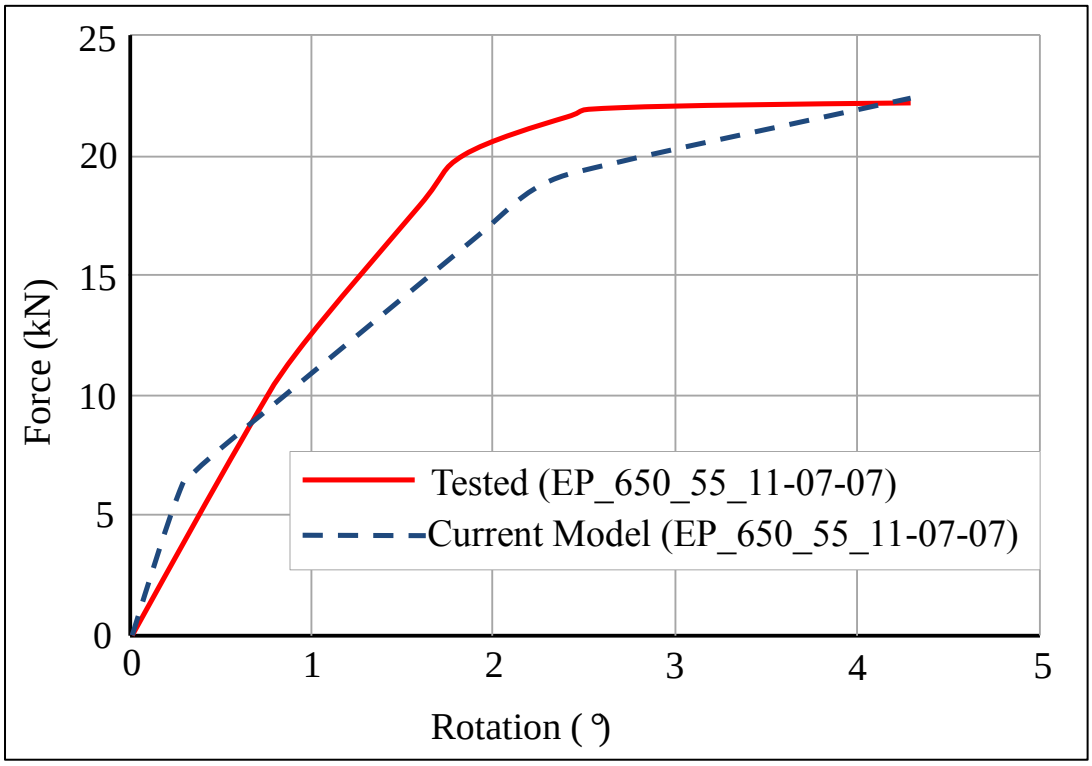

Figure 4.12 Comparison of predicted and measured rotations for tests: EP_650_55_11-07-07 (650°C, θ=55°) (Hu et al., 2009b)

Experimental results from these nine fire tests reached to failure, by bending before the bottom flange of the beam contacted to the column. Hence no two stage behaviours happened for those fire tests. The predicted failure modes of all nine tests were bending failure. The accuracy of the predictions by current model was mainly affected by the proposed multi-linear moment-rotation curve, which is degraded at elevated temperatures. A factor which should also be considered is the uncertainty of the fire tests. From these results, it is evident that overall the predictions of the proposed model agreed reasonably well with the test data.

4.7.2 Validation against isolated tests by Al-Jabri

Two additional tests, conducted by Al-Jabri et al. (2005), were also used to validate the model. The test arrangement is given in Figure 4.13, which is chosen as one of the typical connections used in Cardington full-scale fires building. In the tests a cruciform arrangement was chosen, which was consisted of two 356x171x51UB beam symmetrically connected to a 254x254x89UC column. The beam was 1.9 m long, and the column was 2.7 m high. The thickness of the partial end-plate was 8 mm. Eight M20 Grade 8.8 bolts in 22 mm diameter holes were used in this experiment. The steel used for the connection was Grade 50 for the beam, end-plate and column. The material properties at ambient temperature were: the yield strength = 412 N/mm^2, the ultimate strength = 545 N/mm^2 and the Young's modulus = 195000 N/mm^2. The tests were conducted under a constant load, with increased temperatures. The load was applied to the both beams at a distance of 1500 mm from the column centre-line. The heating rate for the specimen is 10 ℃ per minute. Two different load levels were employed, which were 8.2 kNm and 16.5 kNm. The observation of the tests indicated that only the rotational behaviour for the first stage of the connections (before the bottom flange of beam comes into contact with the column) happened during the tests. The comparison between the predictions of the current model and the tests data is given in Figures 4.14 and 4.15. The experimental data indicates that the rotation of connection was small, before the temperature increased to approximately 500 ℃ in both cases. Beyond 500 ℃, the end-plate deformed excessively, leads to the fracture of the connection. Therefore, the rotation increased significantly after 500 ℃. Again, it can be seen that the predictions of the proposed simplified model are in good agreement with the test data.

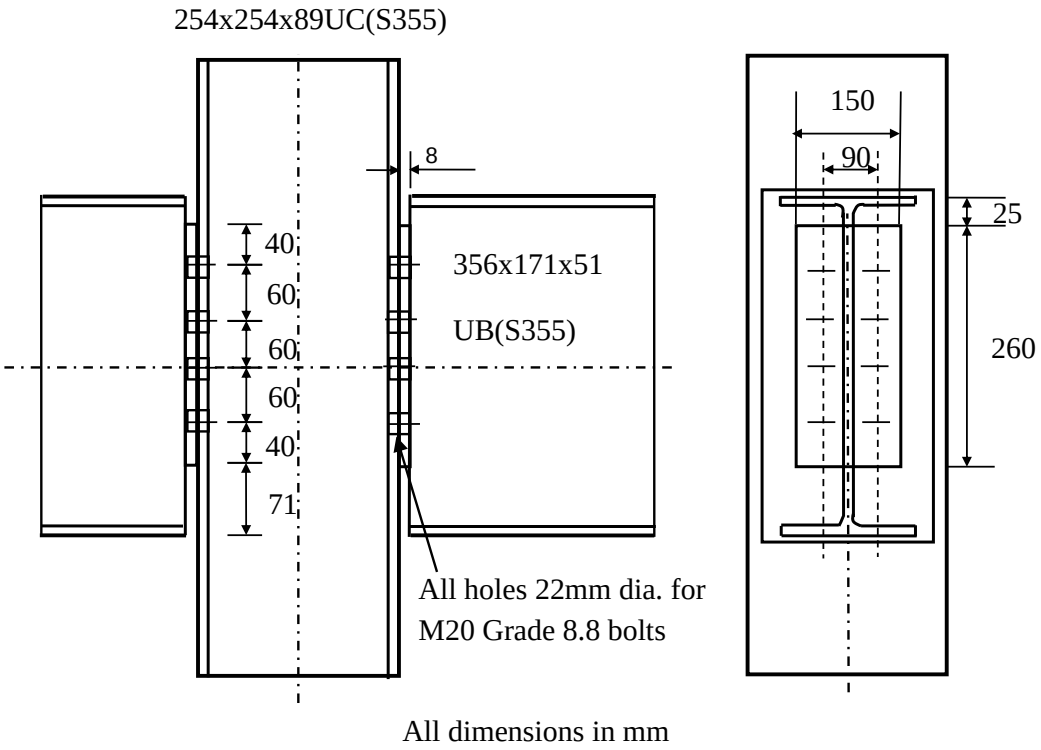

Figure 4.13 Details of test specimens used by Al-Jabri et al. (2005)

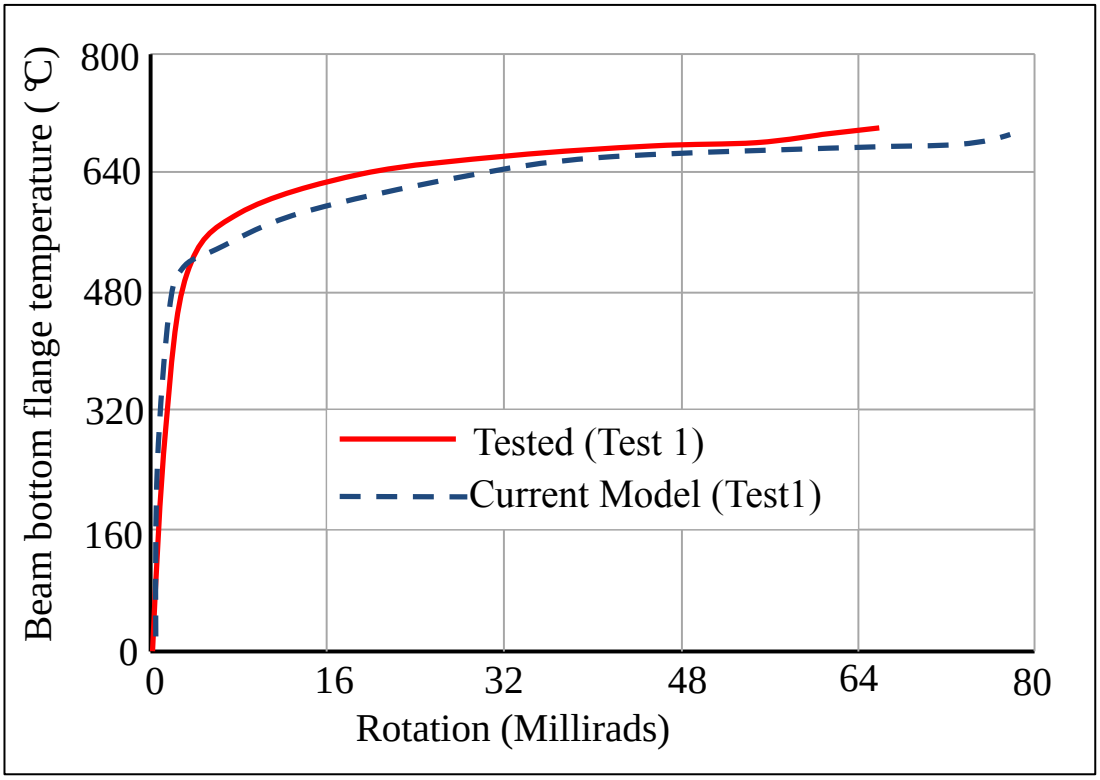

Figure 4.14 Comparison of predicted and measured rotations for Test 1 (Al-Jabri et al., 2005)

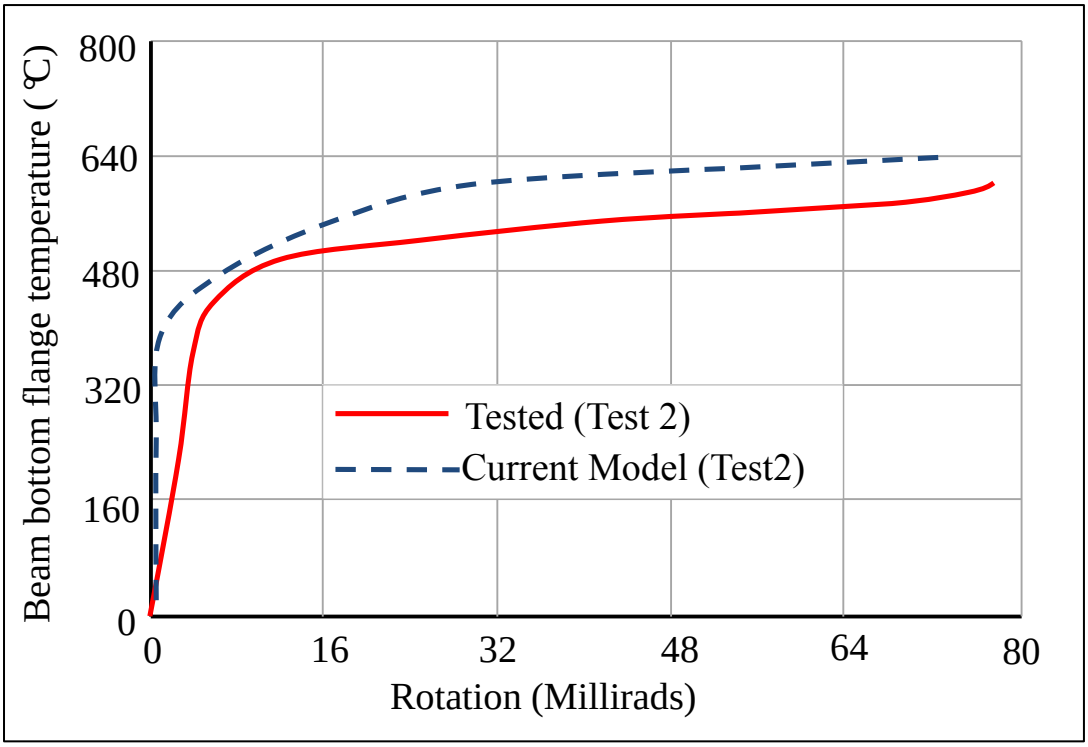

Figure 4.15 Comparison of predicted and measured rotations for Test 2 (Al-Jabri et al., 2005)

The validation using fourteen tests shows that the simplified model presented in this thesis can predict the behaviour of the partial end-plate connections at both ambient and elevated temperatures. The model is computationally very stable and efficient under a static solver condition.

4.8 Numerical studies on a 2D steel frame

In order to investigate the influences of the connections on the behaviour of frame, a series of numerical studies has been conducted on a 2D steel frame under different fire scenarios. The frame was constructed using a 533x210x92 section for the beams and a 305x305x97 section for the columns. The geometry detail of partial end-plate connection used is shown in Figure 4.16, which has a thickness of 12 mm with ten M24 Grade 8.8 bolts. S275 structural steel was used for all sections. In this study, it was assumed that the beams were uniformly loaded to 20kN/m. Within the fire compartment, all beams were unprotected, and the columns protected.

Figure 4.17 shows temperatures of unprotected beams and protected columns under ISO 834 Fire and a typical Natural Fire. The temperature curve for the natural fire presented in Figure 4.17 was calculated based on the assumed compartment size and

type, a typical fire load, and air ventilation condition according to Eurocode 3 Part 1.2 (CEN, 2005b). Based on previous research, it was assumed that the temperatures

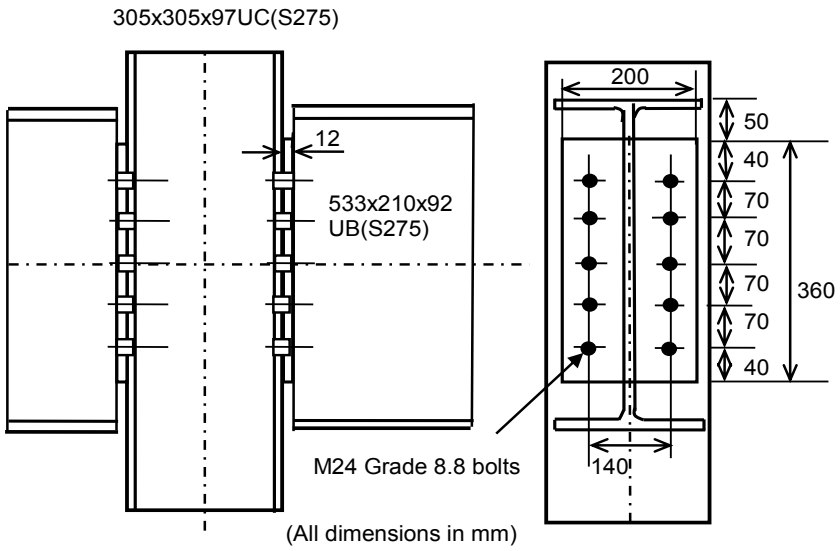

Figure 4.16 Detail for the partial endplate connection used

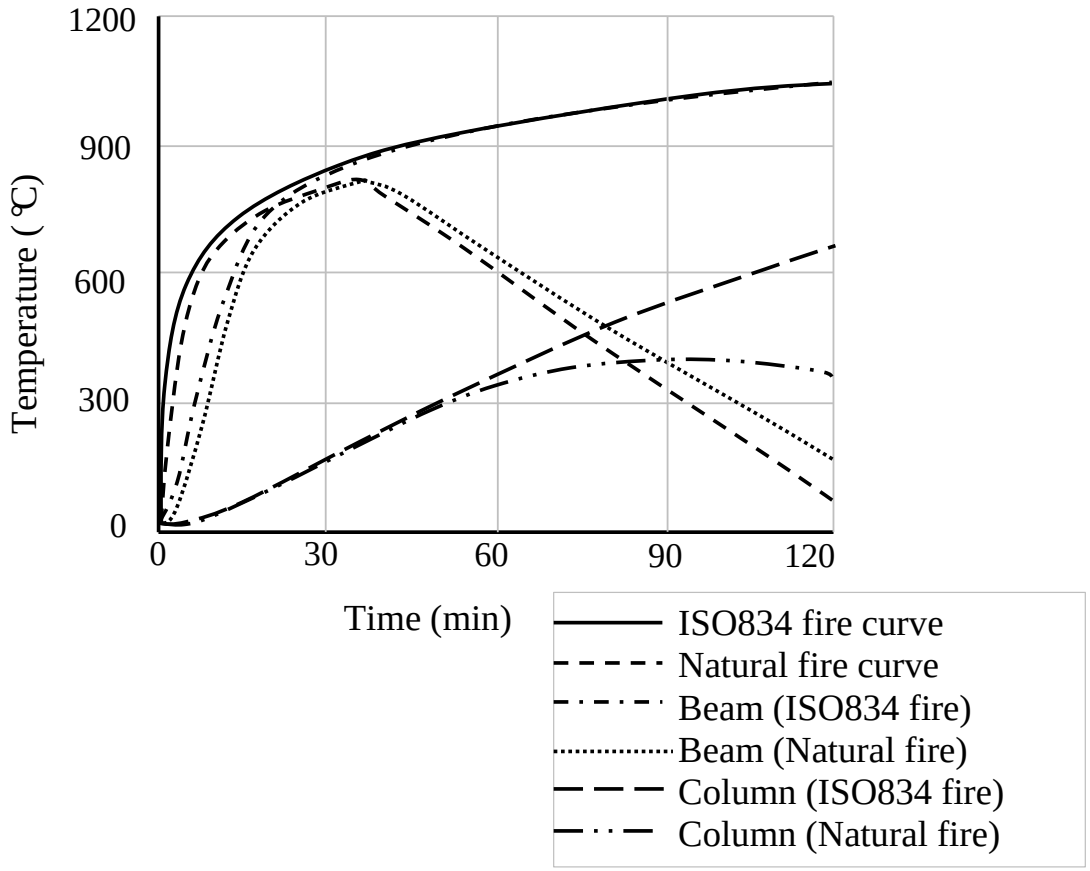

Figure 4.17 Temperatures of unprotected beams and protected columns under ISO834 Fire and Natural Fire

of connections were 75% of the temperatures of heated beams. The beam above the fire was assumed to have a non-uniform temperature distribution along the cross-section. The temperature of beam web was the same as that of the beam's bottom flange. The temperature of beam's top flange was assumed to be 80% of the temperatures of beam bottom flange.

4.8.1 2D steel frame subjected to whole floor fire

Figure 4.18 shows a two dimensional steel frame subjected to whole floor fire. ISO834 Fire and a typical Natural Fire were used to investigate the influences of different types of connections on the frame's behaviour. Three different types of connections (pinned, rigid and partial end-plate connections) were considered. For the pinned connection the failures of axial tension and vertical shear were not considered.

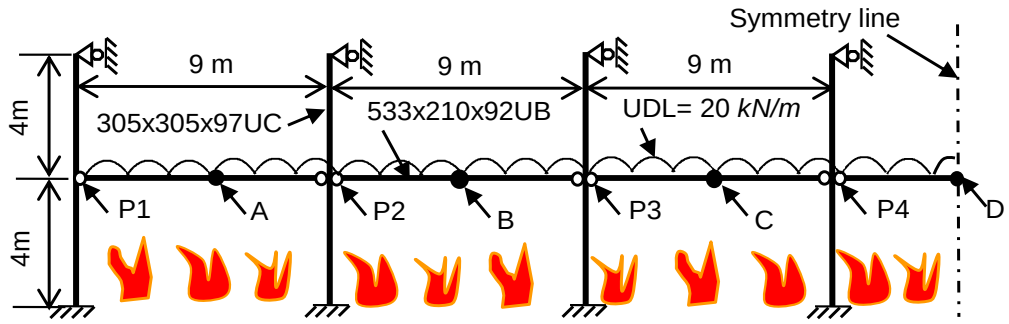

Figure 4.18 Two-dimensional steel frame subjected to whole floor fire

Figures 4.19 and 4.20 demonstrate the deflections of the beams at positions A and D under ISO834 Fire. The axial forces of the connections at positions P1 and P4 under ISO834 Fire are presented in Figures 4.21 and 4.22. For partial end-plate connection case, all connections failed by bending, and the analysis stopped early compared to the other two cases. It is evident that different types of connections significantly influence the deflections of beams. The partial end-plate connection behaved like a semi-rigid connection. However, the connection types have less influence on the maximum axial compressive and tensile forces of the connections. The axial compressive force of the connection increased very quickly at the beginning of the heating, reaching the peak at around 10 min. It then changed from compression to tension, proportionately to the deflection of the connected beams. The axial tensile

forces of the connections at a later stage were due to the large deflections and catenary actions of the connected beams.

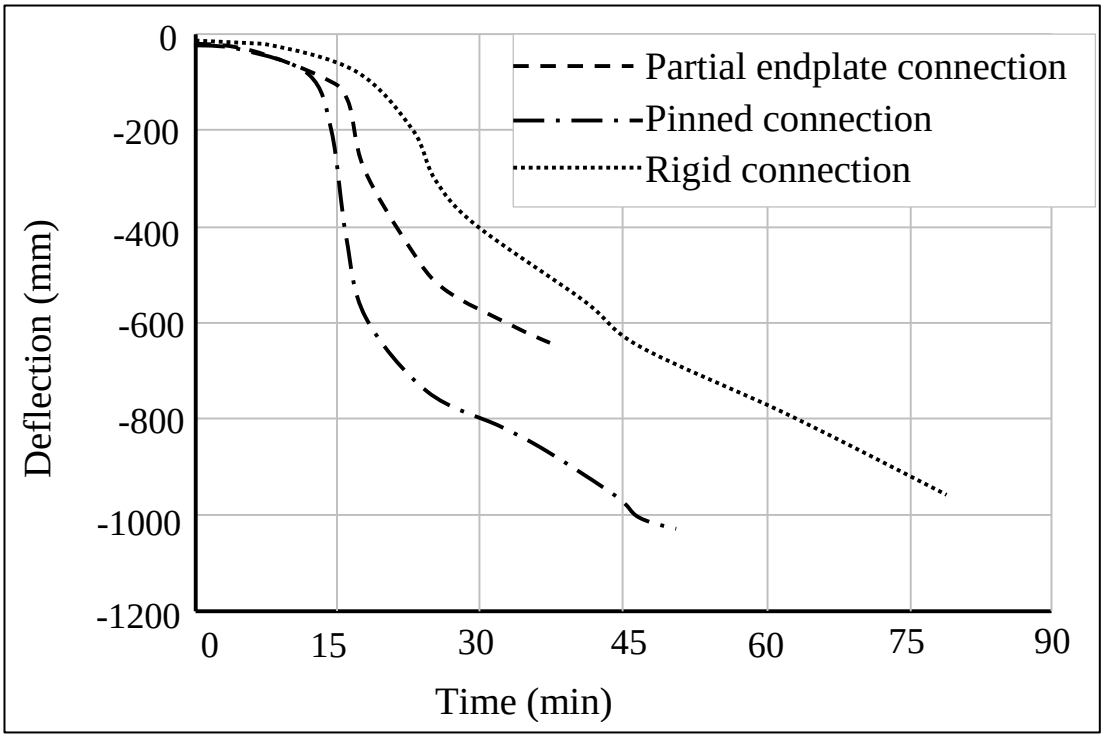

Figure 4.19 Predicted deflections at Position A for different types of connections (whole floor heated-ISO834 Fire)

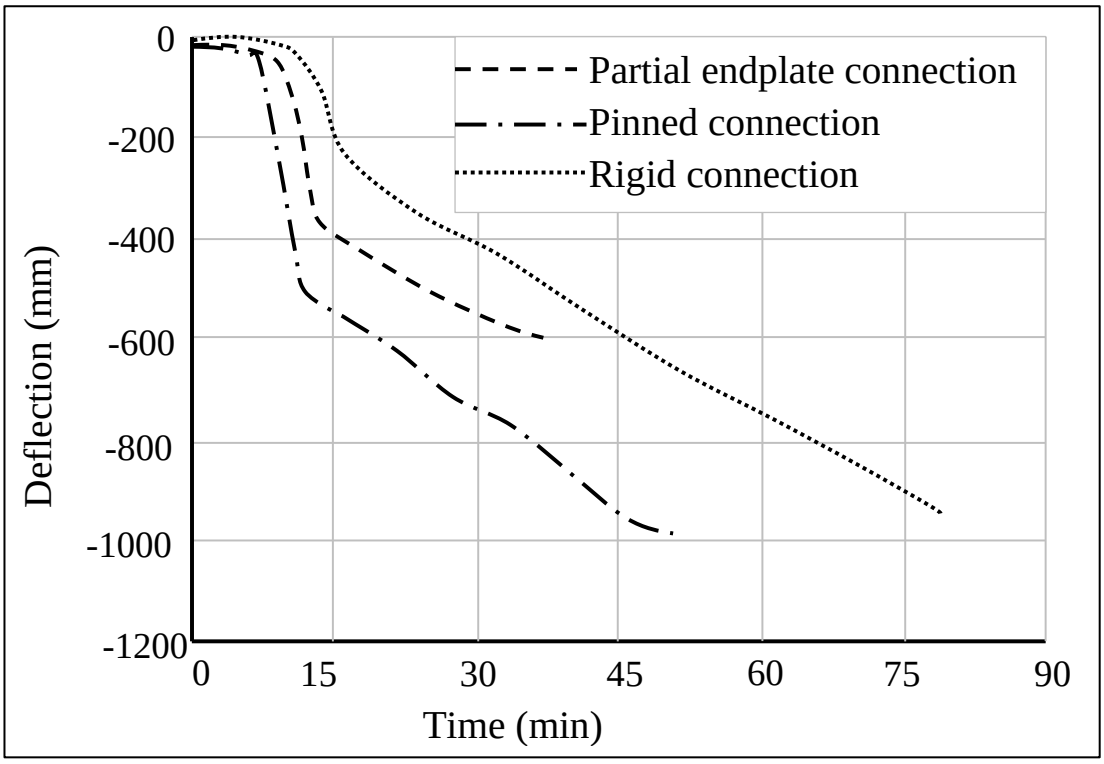

Figure 4.20 Predicted deflections at Position D for different types of connections (whole floor heated-ISO834 Fire)

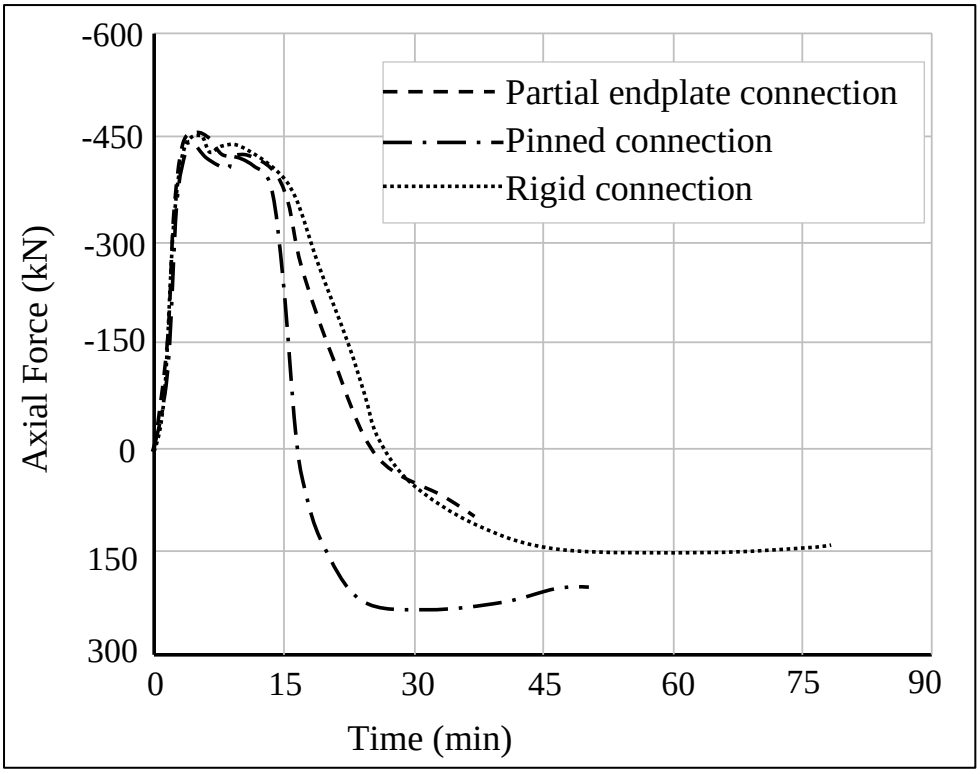

Figure 4.21 Predicted axial forces at Position P1 for different types of connections (whole floor heated-ISO834 Fire)

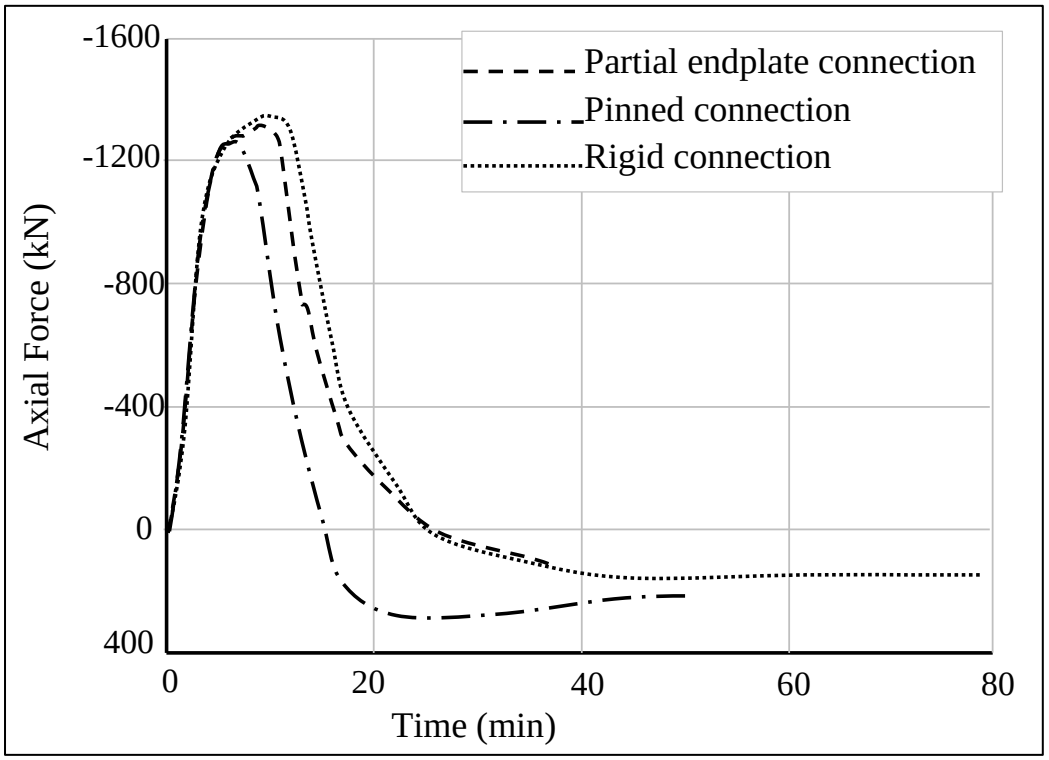

Figure 4.22 Predicted axial forces at Position P4 for different types of connections (whole floor heated-ISO834 Fire)

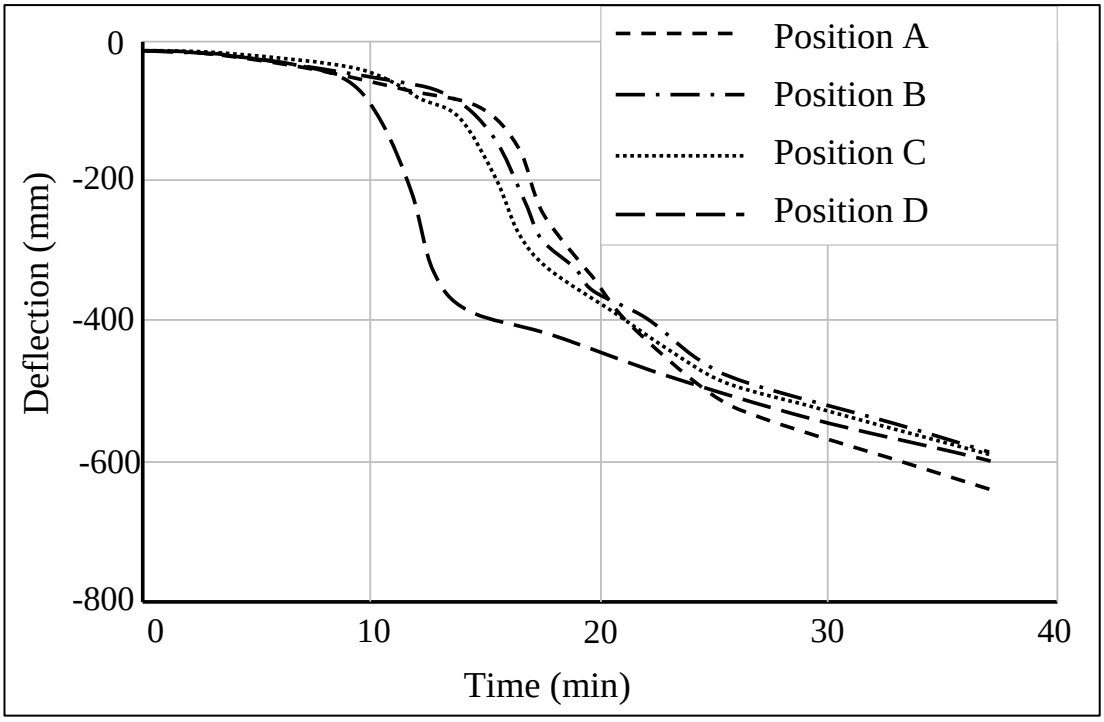

Figure 4.23 Predicted deflections at Positions A, B, C and D for partial endplate connection case (whole floor heated-ISO834 Fire)

For comparison, Figure 4.23 presents the predicted deflections at positions A, B, C and D; Figure 4.24 shows the predicted axial forces at different positions for the partial end-plate connection case under ISO834 Fire. It is obvious that the connected beams were under compression in the early stage of the fire. These compressive forces were produced by restraining thermal expansion of the heated beams. The restraints of the heated beams were mainly provided by the surrounding columns. Therefore, as shown in Figure 4.24, the axial compressive force at Position P4 is nearly three times higher than that at position P1. In the later stage of the fire, with the increasing of temperatures, the stiffness and strength of beams reduced, and the heated beams were under axial tensile forces due to the catenary action resulting from large deflections.

Figures 4.25 and 4.26 show the deflections of the beams at Positions A and D under the Natural Fire. The axial forces of the connections at Positions P1 and P4 under the Natural Fire are demonstrated in Figures 4.27 and 4.28. Again the deflections of the connected beams were significantly affected by using different types of connections under this fire scenario. For the case with partial end-plate connection, as shown in Figure 4.28, the connection at Position P4 failed in tension, at around

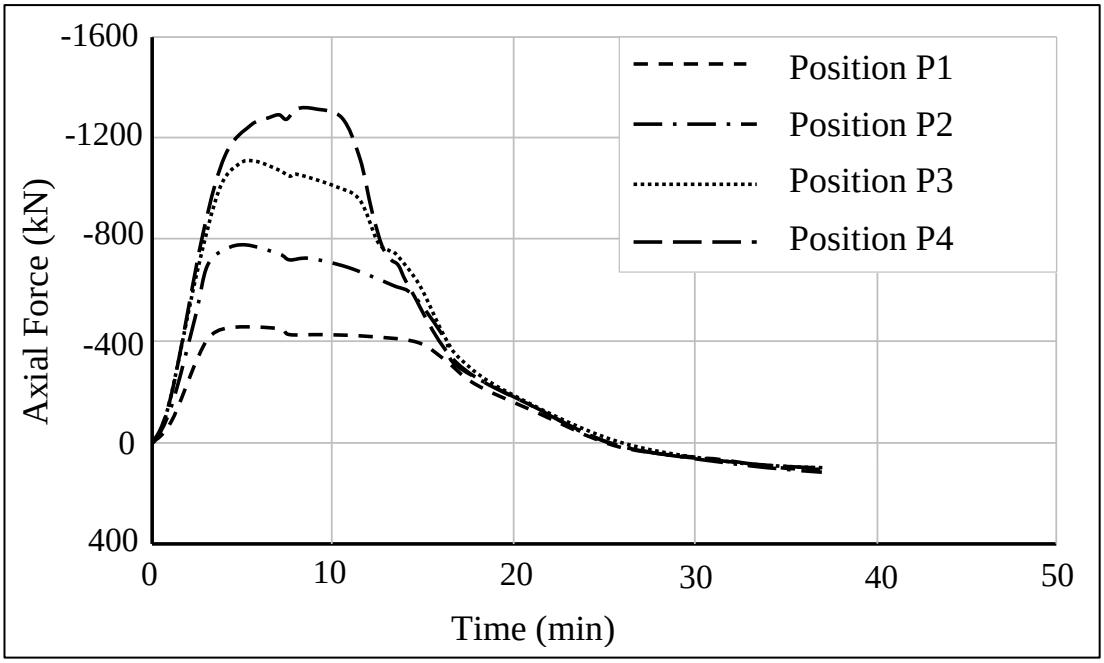

Figure 4.24 Predicted axial forces at different positions for partial endplate connections (whole floor heated-ISO834 Fire)

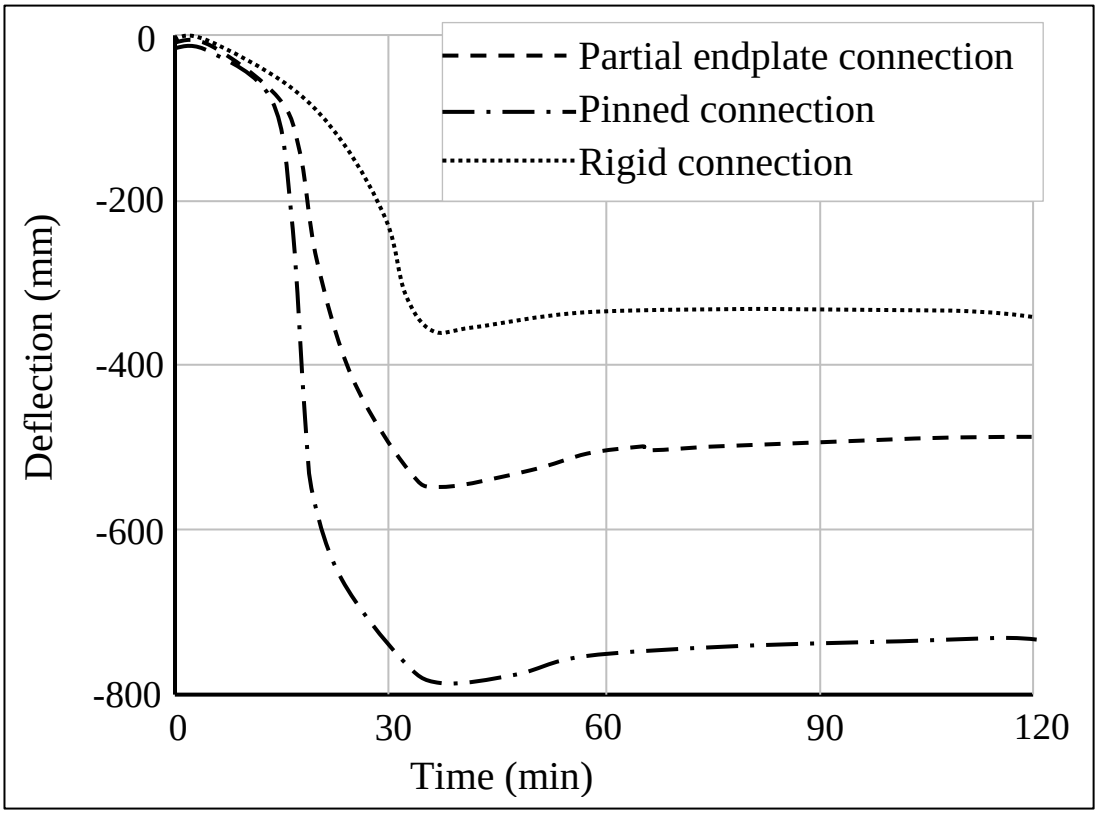

Figure 4.25 Predicted deflections at Position A for different types of connections (whole floor heated-Natural Fire)

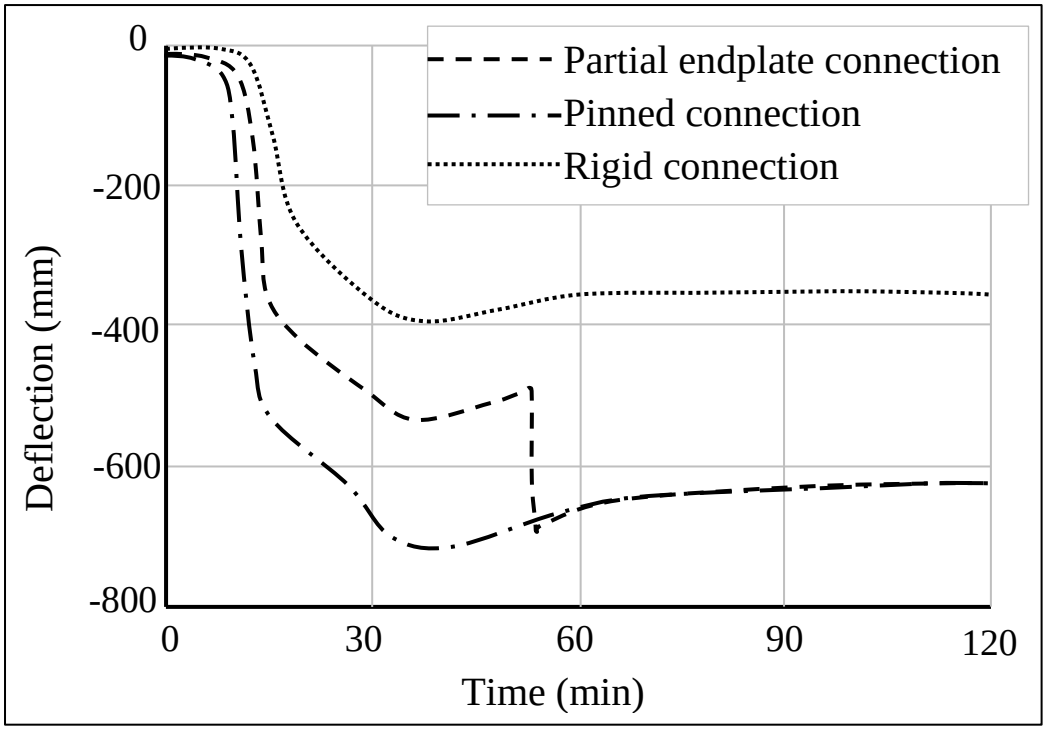

Figure 4.26 Predicted deflections at Position D for different types of connections (whole floor heated-Natural Fire)

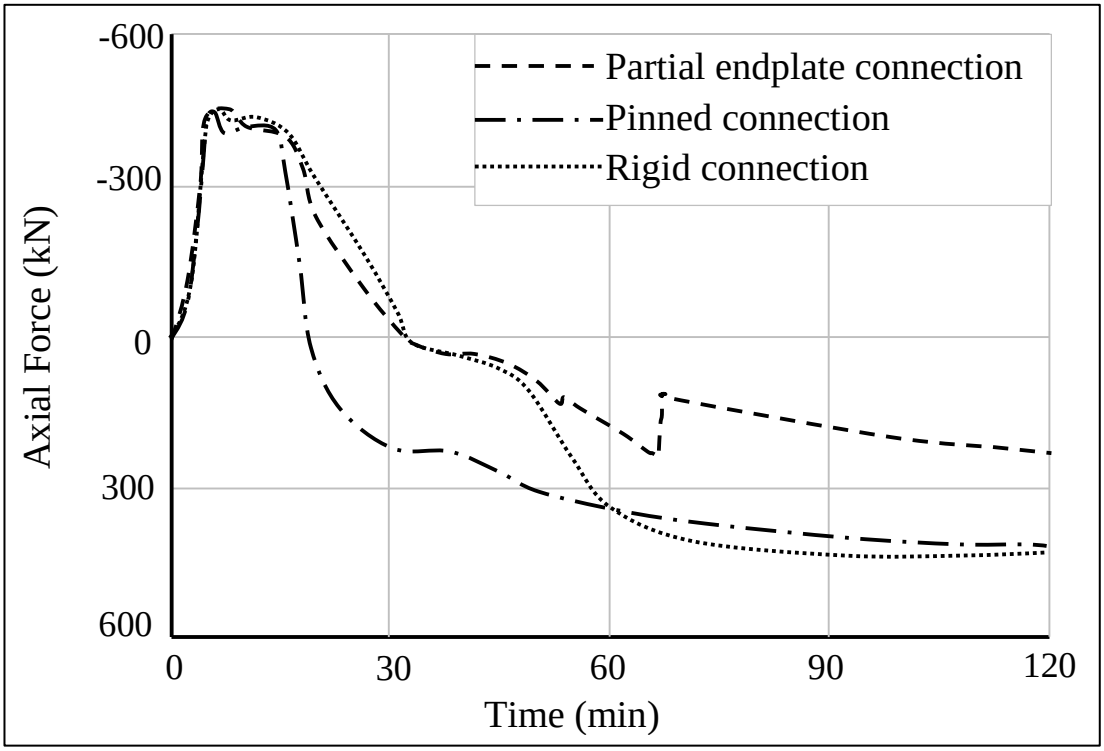

Figure 4.27 Predicted axial forces at Position P1 for different types of connections (whole floor heated-Natural Fire)

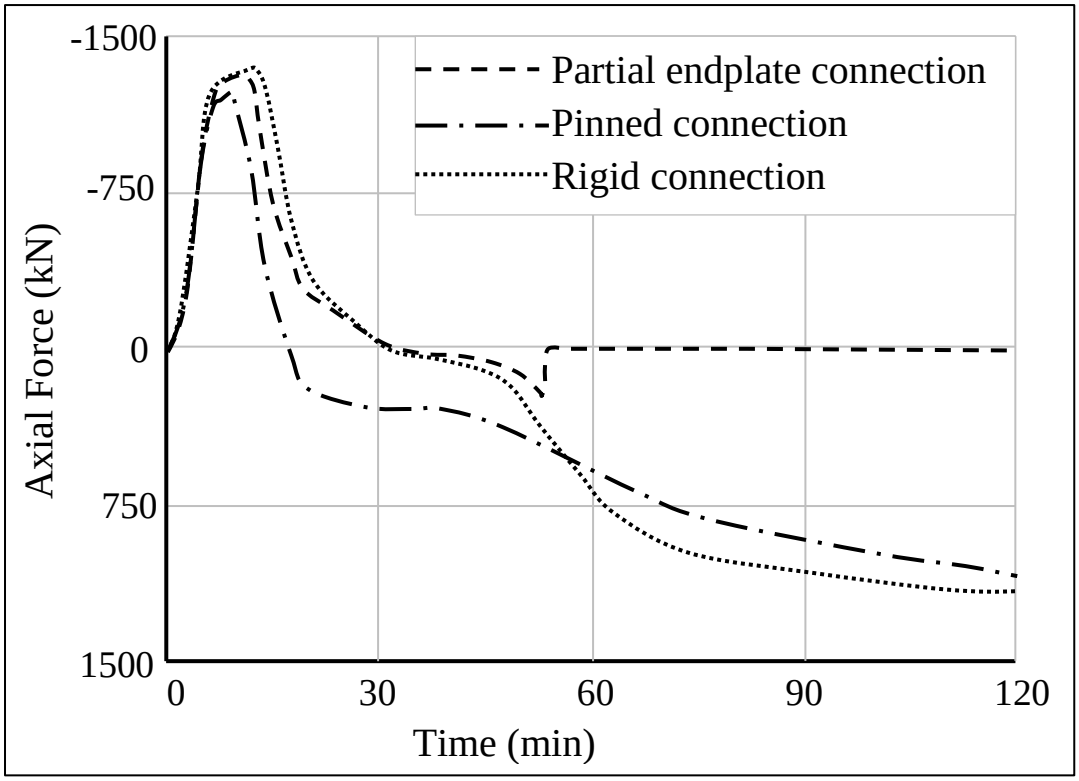

Figure 4.28 Predicted axial forces at Position P4 for different types of connections (whole floor heated-Natural Fire)

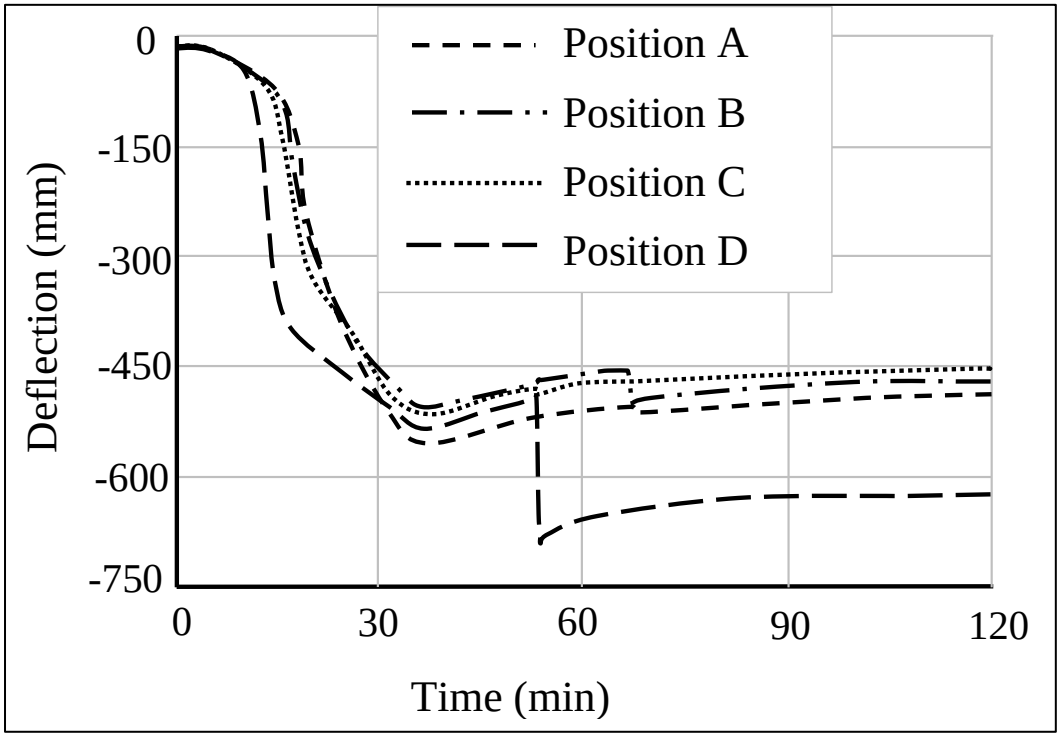

Figure 4.29 Predicted deflections at Positions A, B, C and D for partial end-plate connection case (whole floor heated-Natural Fire)

54 min in which the temperature of the connection was around 523℃. From Figure 4.17, it is clear that the fire was in the cooling stage. Therefore the large axial tensile force of the connection was generated due to the cooling of the connected beam. Figure 4.28 indicates that the axial force of the partial end-plate connection dropped to nearly zero after the connection failed by tension. As shown in Figure 4.26 the deflection at Position D suddenly increased due to the connection tensile failure at Position P4. It is interesting to note that the maximum axial compressive and tensile forces were not significantly affected by using pinned or rigid connections. From this study one can conclude that modelling a connection as pinned, without considering the failures of axial tension is not conservative, especially in the cooling stages of the fire.

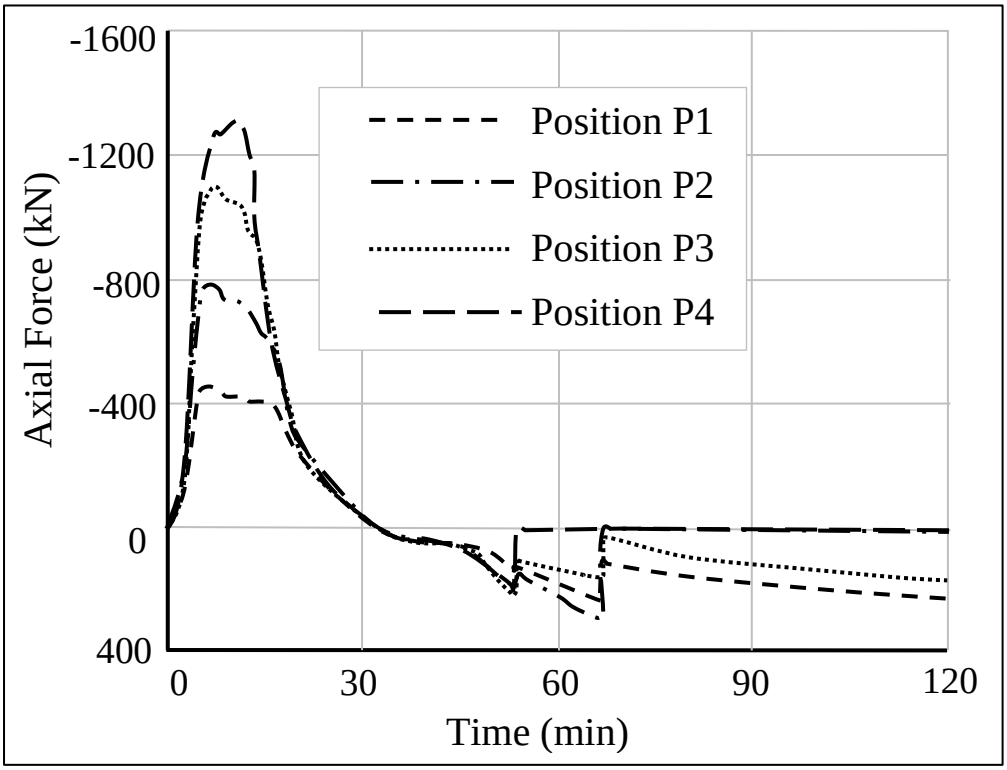

Figure 4.30 Predicted axial forces of partial endplate connections at different positions (whole floor heated-Natural Fire)

For comparison, the predicted deflections and axial forces of the connections at different positions for the partial end-plate connection case under the Natural Fire are presented in Figures 4.29 and 4.30, respectively. These two figures clearly show the failure procedure of the connections at different positions during the fire. It is evident that the tension failure of the connection happened during the cooling phase of the fire. As shown in Figure 4.30, after the connection at position P4 failed due to

tension at about 54 min, the axial forces of the connections at positions P1, P2 and P3 were all reduced. However, at the same time all other connections were reached to plastic moment resistances, and the axial tensile forces were less than the tensile strength of the connections. After the connection at position P4 failed by tension, only one column remained to restrain the connection at position P3. But the connection at position P2 was still restrained by two columns. Hence, when the fire was further cooling down, the connection at position P2 failed by tension at about 65 min, in which the temperature of the connection was reduced to 435℃. The axial tensile forces of the connections at positions P1 and P3 suddenly dropped, due to the failure of the connection at P2. This is the reason why the deflections at positions D and B suddenly dropped at 54 min and 65 min respectively (see Figure 4.29).

4.8.2 Four different compartment fires

As illustrated in Figure 4.31, the performances of four different compartment fires were analysed under ISO834 Fire and the Natural Fire conditions. Partial end-plate connections were used for this study. It was assumed that apart from fire compartment, the temperatures of all other adjacent compartments were at ambient temperature. Figures 4.32 and 4.33 show the predicted deflections at positions A, B, C, and D, for different compartment fires under two fire curves. The predicted axial forces at positions P1, P2, P3 and P4 (for different compartment fires) were presented in Figures 4.34 and 4.35, respectively.

It can be seen that under ISO834 Fire condition similar behaviours were observed compared to a whole floor fire. As shown in Figures 4.33 and 4.35, all connections in compartment Fire 2, Fire 3 and Fire 4 failed due to tension. These results further indicated that larger tensile forces were generated, when beams contracted in the cooling stage of the Natural Fire. As discussed in the previous section, when beams were exposed to a natural fire, the axial tensile forces generated during the cooling phase of the fire and magnitudes were dependent on the position of the heated beams within the structures. These results provide further evidence that the tensile failure of the connection is more likely to happen within buildings during the cooling stages of a real fire.

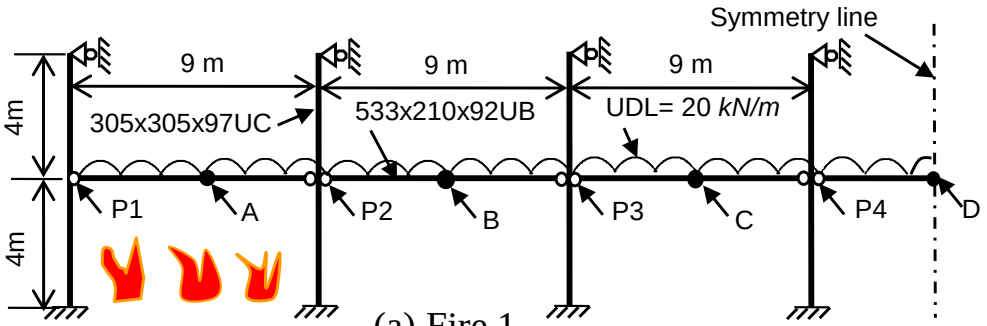

(a) Fire 1

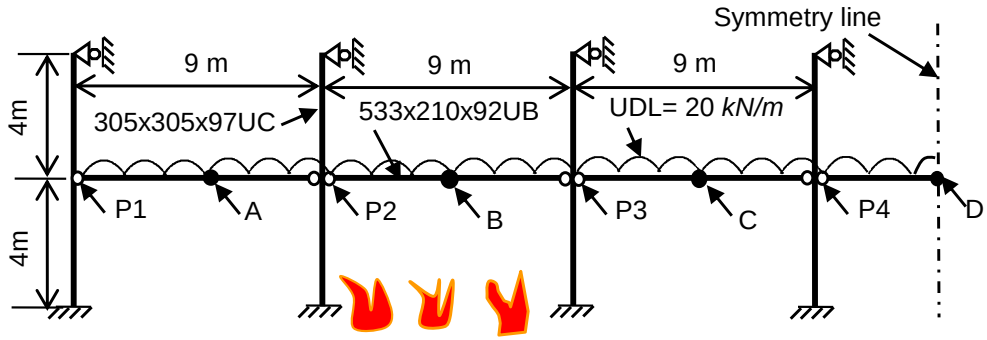

(b) Fire 2

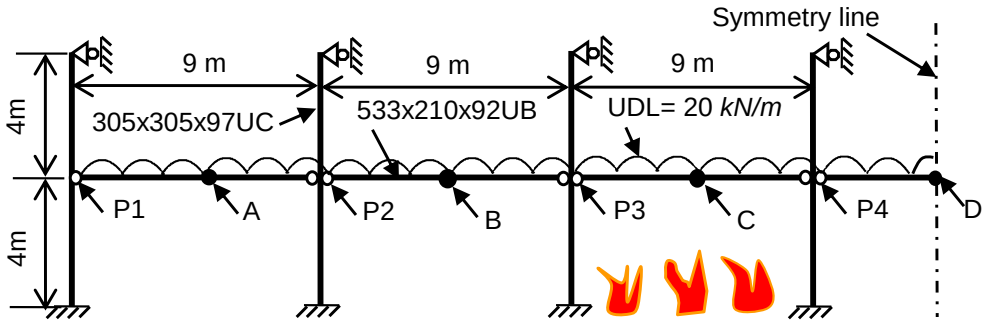

(c) Fire 3

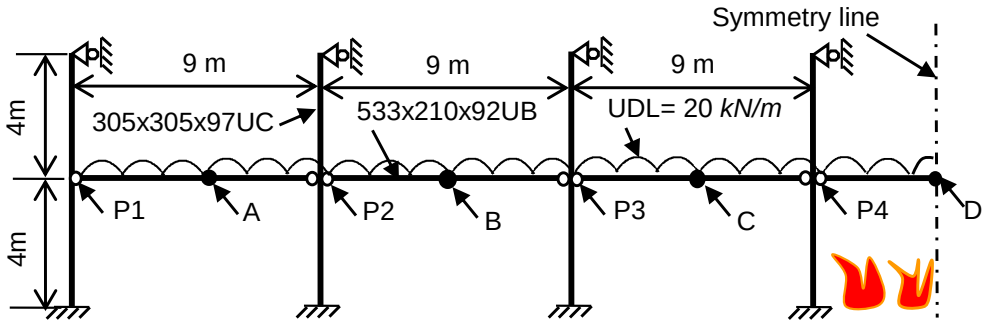

(d) Fire 4

Figure 4.31 Four different compartment fires

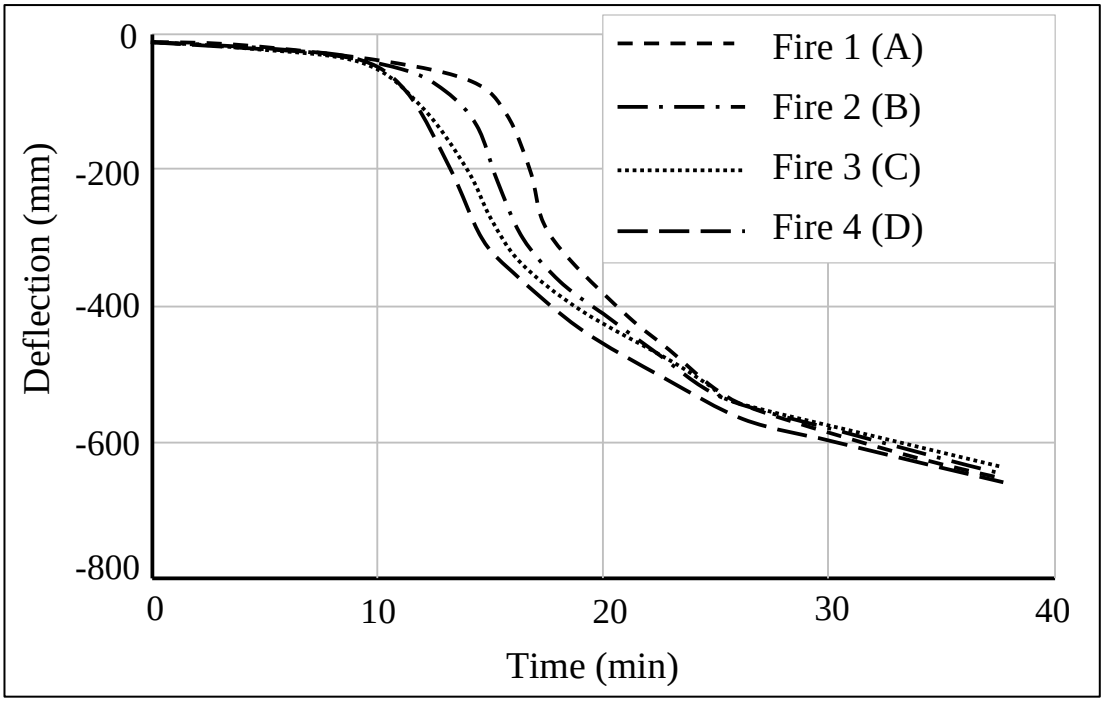

Figure 4.32 Predicted deflections at Positions A, B, C and D for four different compartment fires (ISO834 Fire)

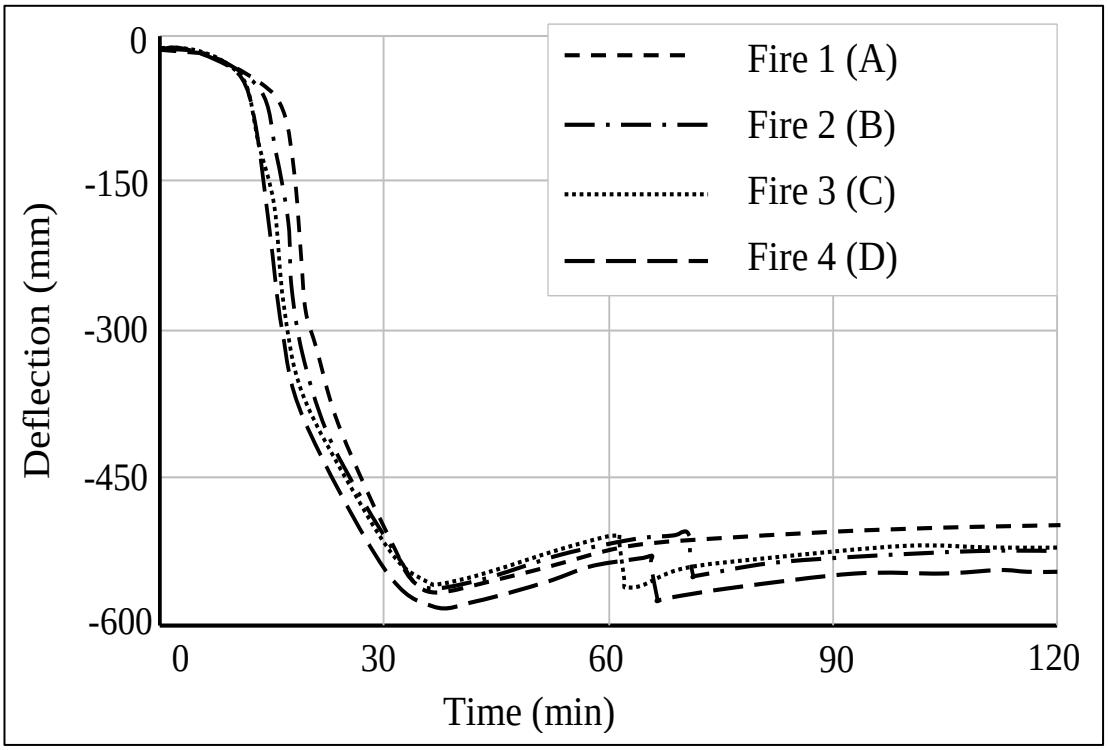

Figure 4.33 Predicted deflections at Positions A, B, C and D for four different compartment fires (Natural Fire)

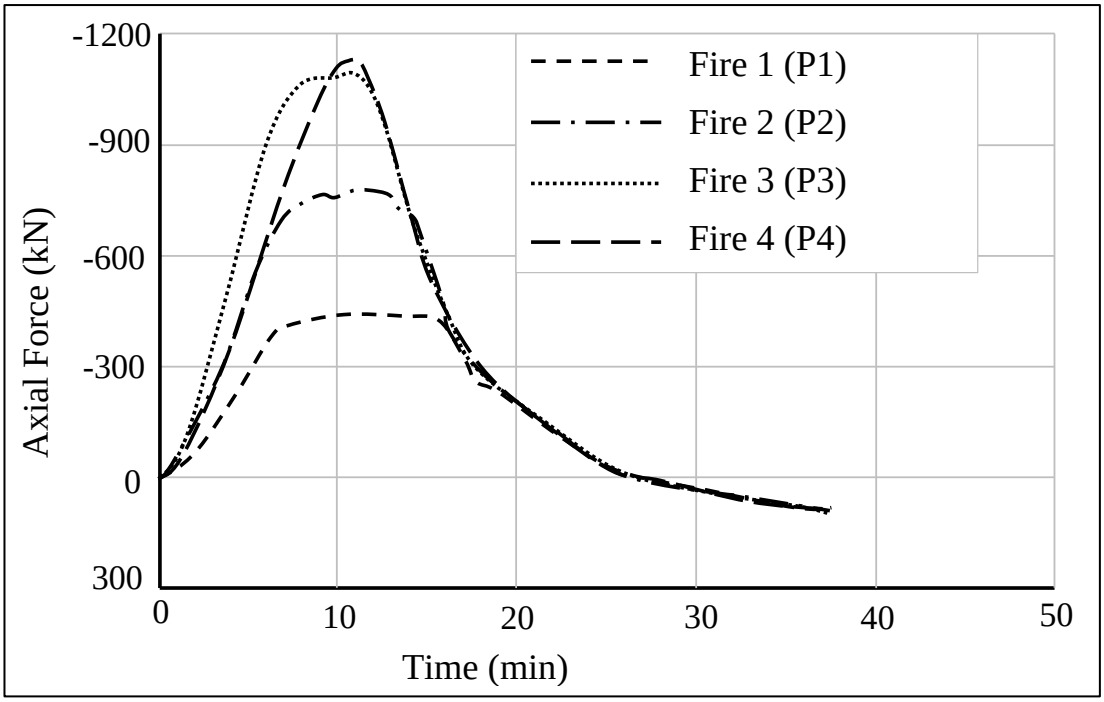

Figure 4.34 Predicted axial forces at Positions P1, P2, P3 and P4 for four different compartment fires (ISO834 Fire)

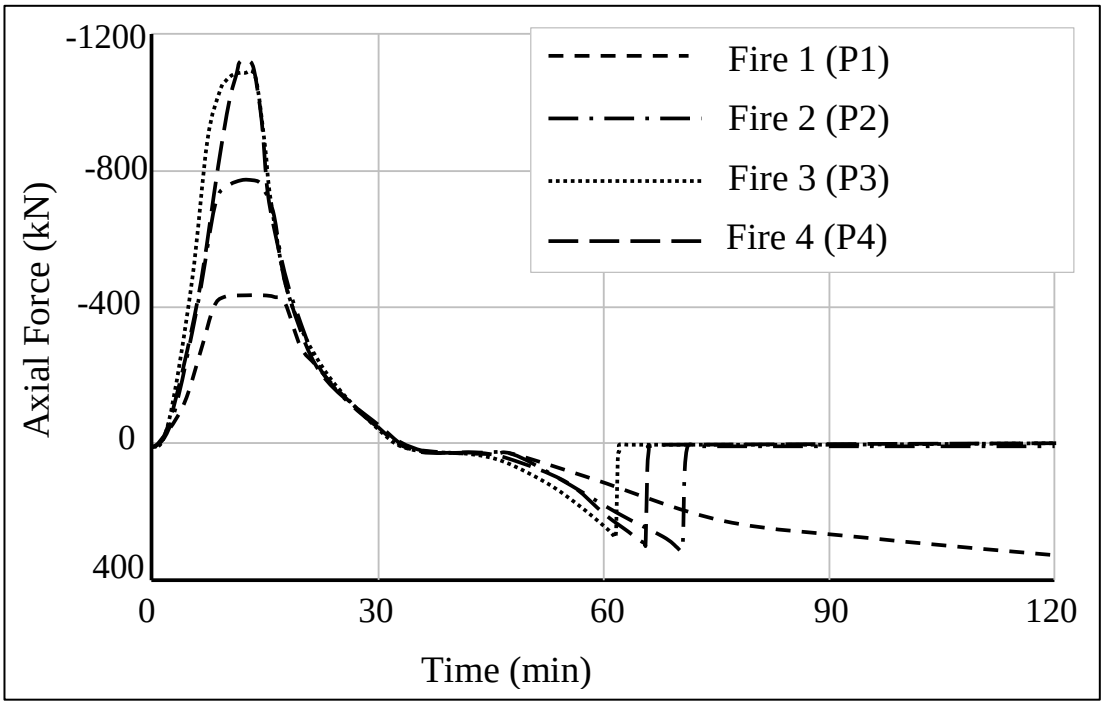

Figure 4.35 Predicted axial forces at Positions P1, P2, P3 and P4 for four different compartment fires (Natural Fire)

4.9 Conclusions

In this chapter, a simplified robust two-node connection element has been developed to model the behaviour of partial end-plate connections between steel beams and columns under fire conditions. The two stage rotational responses of partial end-plate connections are considered, and component-based approaches are employed to precisely determine the stiffness, tension, compression and bending moment capacities of the partial end-plate connection under fire conditions. Connection failures due to bending, axial tension or compression, and vertical shear are also modelled. The current model is based on the two-node connection element framework presented in Chapter 3, with further developments for modelling partial end-plate connections at elevated temperatures. The model retains the advantages of both the simple and component-based models. It is also computationally efficient, with excellent numerical stability under a static solver condition. A total of fourteen tests were used to validate the model, demonstrating that the proposed model can predict the two stage rotational characteristics of partial end-plate connections with reasonable accuracy. Therefore, the model presented in this chapter can be used for analysing the behaviour of partial end-plate connections in real performance-based fire resistance design of steel framed composite buildings.

In order to investigate the influences of the connections on the behaviour of steel structures, a series of numerical studies were also conducted on a 2D steel frame subjected to ISO834 Fire and a typical Natural Fire. The results indicate that the tensile failure of the connection is more likely to happen within the buildings during the cooling stage of a real fire. From these results, one can conclude that modelling a connection as pinned, without considering the failures of axial tension, is unconservative for structural fire engineering design, especially in the cooling stages of a fire.

Chapter 5

Performance of Composite Buildings under Fire Conditions

5.1 Introduction

Significant progress has been made in analysing the performance of steel framed composite buildings under fire conditions over the last decades. The most common and conventional way of retaining the strength and stiffness of steel-framed buildings under fire conditions, is to provide fire protection to all exposed steel members. However, observations from a series of full-scale Cardington fire tests have shown that steel framed composite structures can provide a significantly greater fire resistance than is suggested by standard fire tests on isolated structural members (Bailey et al., 1999). This appeared to be due to an interaction between the heated members within the fire compartment, the concrete floor slabs and the connected steel frame structure. If steel members within the structures loss strength and stiffness rapidly due to high temperatures, alternative load paths would be adopted to transfer load for the remaining part of the structures. Experimental and analytical investigations involving full-scale fire tests indicated that tensile membrane action within the concrete floor slabs plays an important role in enhancing the fire resistance of composite buildings. The load carrying capacity of slab due to tensile membrane action is significantly higher than the slab under pure bending (Wang, 2005). Tensile membrane action can occur when the slabs undergoes large vertical displacements. As shown in Figure 5.1, the induced radial tension in the centre of the slab is balanced by a peripheral ring of compression (Abu, 2009). The occurrence of tensile membrane action mainly relies on the conditions of vertical support maintained around the edges of the slab panel. To utilize the tensile membrane action, the composite floors need to be divided into slab panels, consisting of an array of steel beams. The beams around the perimeter of the slab panels are protected, while the internal secondary beams can be left unprotected.

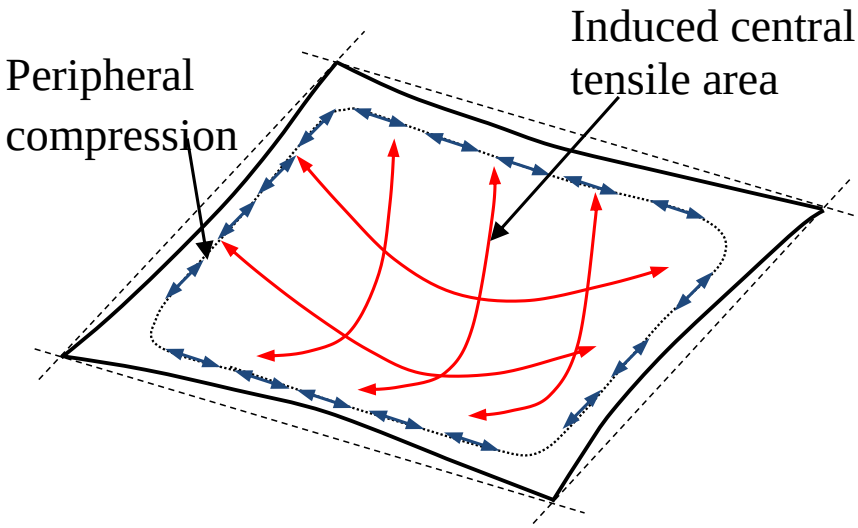

Figure 5.1 Tensile membrane action within floor slabs

Up to now, research has focused on the influence of the tensile membrane actions on the fire resistance of composite floors, with the assumption that the fully vertical supports along the perimeter of the slab panel are provided by protected beams. Different design methods have been developed to simulate the behaviour of composite slab at elevated temperatures incorporating tensile membrane action (Bailey, 2004; Lim et al., 2004; Li et al., 2007; Moss et al., 2008; Zhang and Li, 2010; Jahromi et al., 2013; Dat and Tan, 2013; Abu et al., 2013). However, there is as yet a lack of detail research into the influence of the vertical deflections of protected beams during fire on the tensile membrane actions of the slab panel. For the majority of previous research on modelling composite floor subjected to fire, the beam-to-column and beam-to-beam connections were assumed to behave either as pinned or rigid for simplicity, and the vertical shear and axial tension failures of the connection were not taken into account.

This chapter presents a comprehensive study conducted on a generic three dimensional 45m x 45m composite building, with realistic loading conditions and structural layout, under different fire conditions. A series of analyses has been carried out using different support conditions on slab panels and slab reinforcement details. In this research, it is assumed that the beam-to-column and beam-to-beam connections behave as semi-rigid. The end-plate connections are used to connect primary beams to columns. The partial end-plate connections are adopted to connect secondary beams to columns, and primary beams to secondary beams, respectively.

These two types of the connections are modelled using the simplified connection models developed in Chapters 3 and 4. The proposed two connection models have good numerical stability under a static solver condition, and can be used for large scale modelling of composite buildings in fire. The main objectives of this study are:

- To systematically investigate the impact of the connections for protected beams on the tensile membrane actions of supported floor slabs, in which the failure of the connections due to axial tension, vertical shear or bending is considered.
- To understand the influence of the vertical deflections of protected beams on the tensile membrane action of the floor slabs.
- To analyse the effects of different reinforcement details of the floor slabs on the performance of composite floor under different fire conditions.

5.2 Theoretical background of the software VULCAN

In this study, the finite element software VULCAN (Huang et al. (2003a, 2003b); Huang et al. (2009)) is employed. As briefly introduced in Chapter 2, VULCAN is capable to model the three dimensional performance of composite and steel-framed buildings under fire conditions. The software VULCAN has been developed through long term research, and has been extensively validated against available experimental results. VULCAN has also been used in many real projects for structural fire engineering design. As shown Figure 5.2, in this program the steel-framed composite buildings are modelled as an assembly of finite beam-column, connection and slab elements. It is assumed that the nodes of these different types of element are defined in a common reference plane that is assumed to coincide with the mid-surface of the concrete slab element, whose location is fixed throughout the analysis.

The beam-columns are modelled using 3-noded line elements (Huang et al., 2009). The cross-section of each element is divided into a number of segments to allow the required variation of the distributions of temperature, stress, and strain. Both geometric and material non-linearities are included. The reinforced concrete slabs are represented using 9-noded nonlinear layered elements, in which the membrane action of the floor slabs is considered (Huang et al. (2003a, 2003b)). The slab

elements are divided into a number of plain concrete and reinforcing steel layers. The temperature and material properties for each layer can be specified independently. An effective stiffness model was developed to model the ribbed nature of typical composite slabs (Huang et al., 2000). For modelling composite steel decking concrete floor slabs, a maximum-strain failure criterion is applied for plain concrete layers, and the concrete layers are considered to be orthotropic after the initiation of cracking.

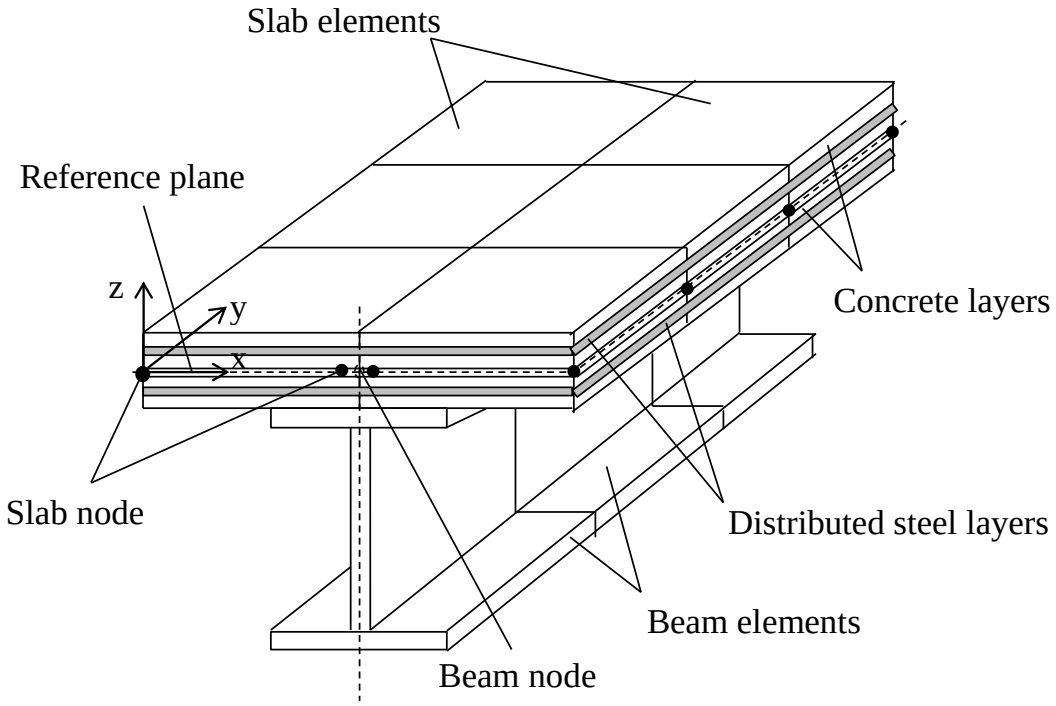

Figure 5.2 Division of composite structures into beam, slab elements

5.2.1 Simplified major-axis connection models

For modelling the behaviour of connections which connect beam to flange of column (major-axis) at elevated temperatures, two simplified connection models are proposed and incorporated into software VULCAN. As described in Chapter 3, a simplified model has been developed to predict the performance of flush and extended end-plate beam-to-column flange (major-axis) connections in fire. The connections failure due to bending, axial tension, compression and vertical shear are all taken into account, as well as the impact of axial tensile force of the connected beam on the connection. Validation results show that the proposed model is capable of predicting the performances of flush and extended end-plate connections under fire conditions with reasonable accuracy.

Another simplified 2-node connection element model for simulating the behaviour of partial end-plate beam-to-column flange (major-axis) connections under fire conditions is presented in Chapter 4. The two stage rotational behaviour of partial end-plate connection is taken into consideration, including the performance of the connections after the beam bottom flange comes into contact with the column flange. Connection failures due to bending, axial tension, compression, and vertical shear are taken into account. The validation results demonstrate that the proposed model is capable to precisely predict the performance of partial end-plate connections between steel beams and column flange at both ambient and elevated temperatures.

5.2.2 Simplified minor-axis partial end-plate connection model

For minor axis connections between steel beam and column web, or secondary beam and the web of primary beams it is generally to assume these connections behave as pinned. In reality however, the great majority of connections behave as semi-rigid. The minor-axis connection behaves differently from the major-axis connection, as the column web resists the tension and compression forces produced from the beam flanges in bending (Neves and Gomes, 1999). Lima et al. (2002) proposed a finite element model to simulate the behaviour of a minor-axis connection consisting of double web angles, a seat angle, or a transverse web stiffener welded to the column web. The initial stiffness of the whole connection was assessed using the component-based method, which requires defining the active basic components within the connection. Compared to the typical major connection component-based model, a new basic component of column web in bending was taken into consideration.

At present, Eurocode 3 only provides guidance for designing connections between a steel beam and column flange. Given that there are no existing code provisions for semi-rigid minor axis partial end-plate connections, a simplified model is proposed here – in accordance with the general principles provided in EN1993-1-8 (CEN, 2005c) for modelling minor-axis partial end-plate connections in fire. The main frame of the 2-node connection element model for partial end-plate beam-to-column flange connections is adopted here, with developments to incorporate the behaviour of a new basic component of the column web in bending into the model. The evaluation of the new component of the column web is given in the following section.

To implement the new component of column web in bending into the simplified partial end-plate connection model developed in Chapter 4, the initial stiffness and resistance of this component should be determined. The initial stiffness of column web component is calculated according to the mechanical model proposed by Lima et al., (2002), regarding the column web as a plate supported at the junction with the flanges and free in the other borders. The initial stiffness can be expressed as:

$$k_{cw,\min or} = \frac{16\, t_{wc}^3 E_{cw}}{L_{cw,\min or}^2} \left(\frac{\alpha + (1-\beta)\tan(35-10\beta)}{(1-\beta)^3 + \frac{10.4(1.5-1.63\beta)t_{wc}^2}{L_{cw,\min or}^2}} \right) \tag{5.1}$$

where E_{cw} is the Young's modulus of column web, t_{wc} is the thickness of column web.

$$L_{cw,\min or} = h_c - 2t_{fc} - 1.5r_c \tag{5.2}$$

$$\alpha = \frac{k}{L_{cw,\min or}} \quad \text{for } 0.05 \le \alpha \le 0.2 \tag{5.3}$$

$$\beta = \frac{w_b + k}{L_{cw,\min or}} \quad \text{for } 0.08 \le \beta \le 0.75 \tag{5.4}$$

h_c is the depth of the column cross-section, t_{fc} is the thickness of column flange, r_c is the column fillet radius, k is the max width of tension bolts across comers, w_b is the bolt gauge between the centrelines.

The tension resistance of column web component is obtained based on SCI P358 (2011), which can be defined as:

$$F_{cw,\min or,tens} = \frac{8M_{pl,Rd,u}}{1-\beta_1}\left(\eta_1 + 1.5(1-\beta_1)^{0.5}(1-\gamma_1)^{0.5}\right) \tag{5.5}$$

$$M_{pl,Rd,u} = \frac{f_{u,c}t_{wc}^2}{4\gamma_{M,u}} \quad \text{with} \quad \gamma_{M,u} = 1.1 \tag{5.6}$$

$$\beta_1 = \frac{w_b}{L_{cw,\min or}} \tag{5.7}$$

$$\gamma_1 = \frac{d_0}{L_{cw,\min or}} \tag{5.8}$$

$$\eta_1 = \begin{cases} \dfrac{p(r) - d_0}{L_{cw,\min or}} & for \quad r = 1 \\ \dfrac{p(r) - 0.5d_0}{L_{cw,\min or}} & for \quad r \neq 1 \end{cases} \tag{5.9}$$

Where $f_{u,c}$ is the ultimate tensile strength of the column, d_0 is the diameter of bolt hole, r is the bolt row number, $p(r)$ is the vertical spacing between tension bolt rows.

The two-node connection element model (major-axis) presented in Chapter 4 has been modified with the new component described above, to produce a new two-node connection element (minor-axis) for modelling the partial end-plate connections between beam to column web, or secondary beam to the web of primary beam in fire. However, due to a lack of experimental tests available on minor-axis partial end-plate connections between steel beam and column web or beam web, the proposed model cannot be validated against test results. Hence, as a qualitative indication, three tests on major-axis partial end-plate connections used in Chapter 4 were modified as minor-axis connections with the same geometry of the connection. The only difference for the modified connection, is that the partial end-plate is connected to the column web not the column flange. These modified connections were simulated using the model described above.

Figures 5.3 to 5.5 show the predictions of the current minor-axis model, together with both the test results (Hu et al., 2009b) and predictions of the major-axis partial end-plate connections presented in Chapter 4. Figure 5.3 shows the comparison results of the ambient temperature test EP_20_45_07-09-07. It is noticed that the minor-axis model developed here is also capable of predicting the second stage rotational behaviour of partial end-plate connection when the beam bottom flange comes into contact with the column web. Figures 5.4 and 5.5 illustrate the comparison results for test EP_ 450_35_11-05-07 at 450 ℃, and test EP_650_55_11-07-07 at 650 ℃, respectively. It is evident that the predicted results generated by minor-axis model are closed to the predictions of major-axis model.

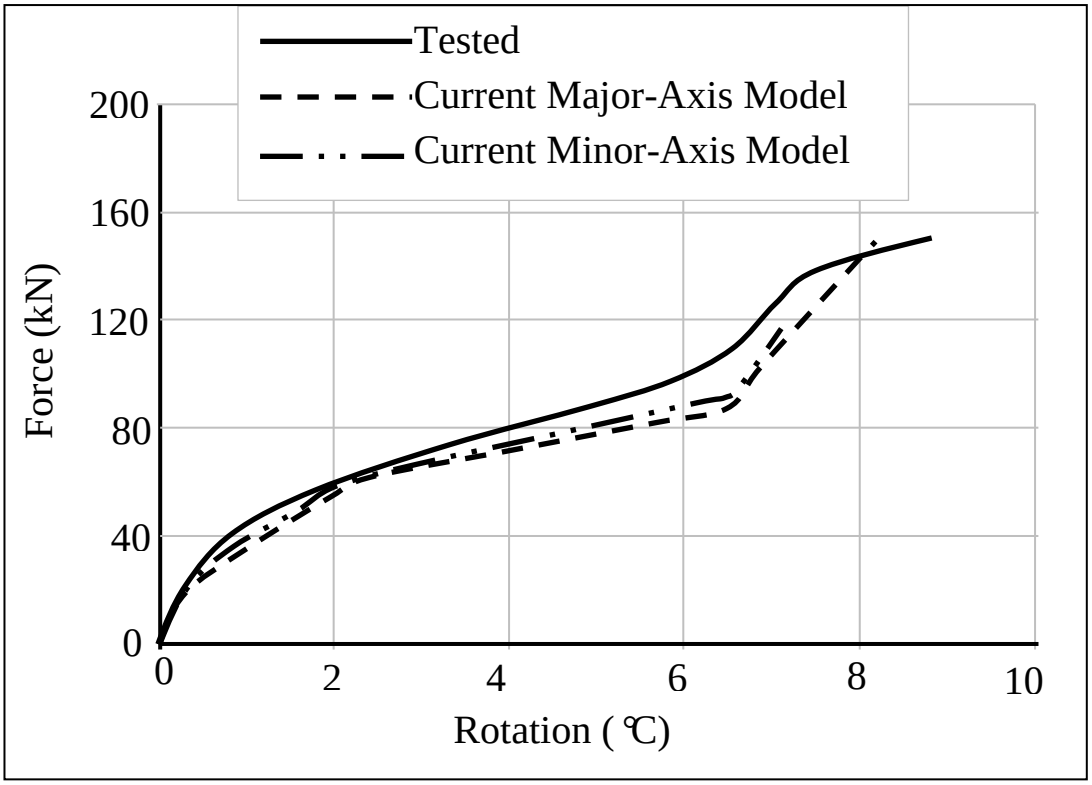

Figure 5.3 Comparison results EP_20_45_07-09-07(20°C, θ=45°) (Hu et al., 2009b)

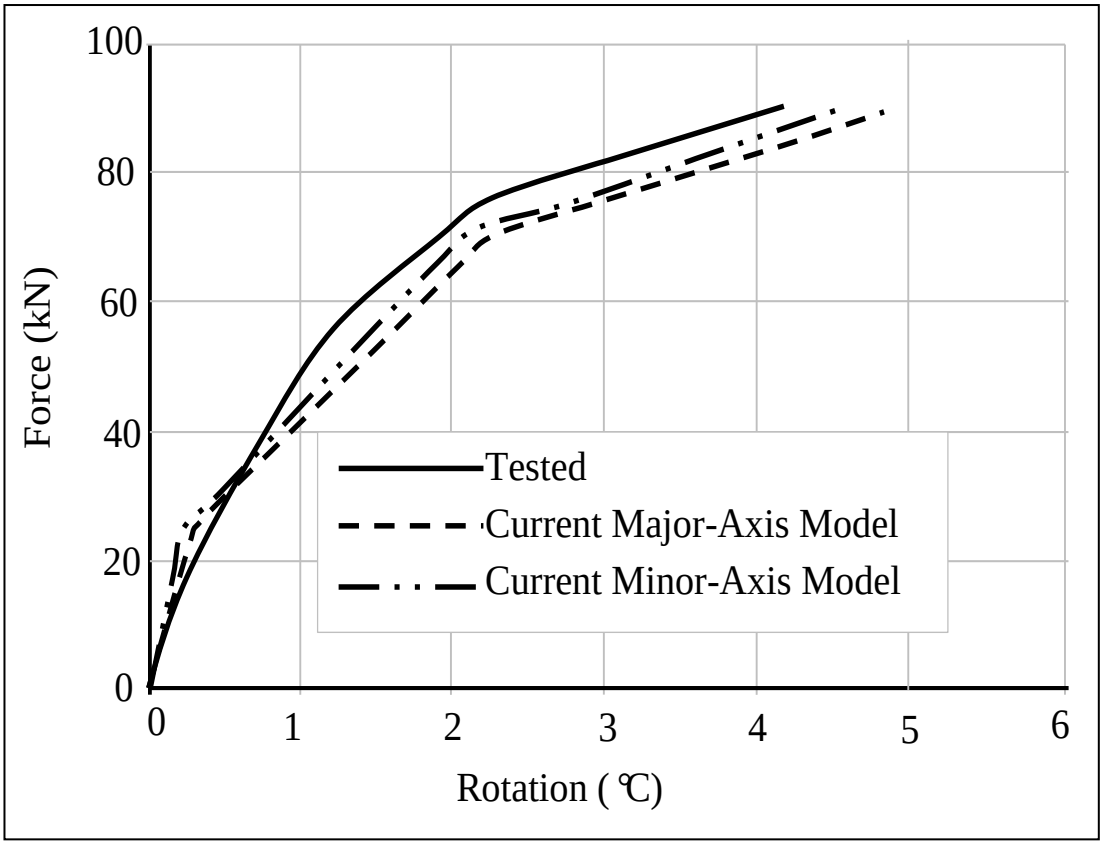

Figure 5.4 Comparison results EP_ 450_35_11-05-07(450°C, θ=35°) (Hu et al., 2009b)

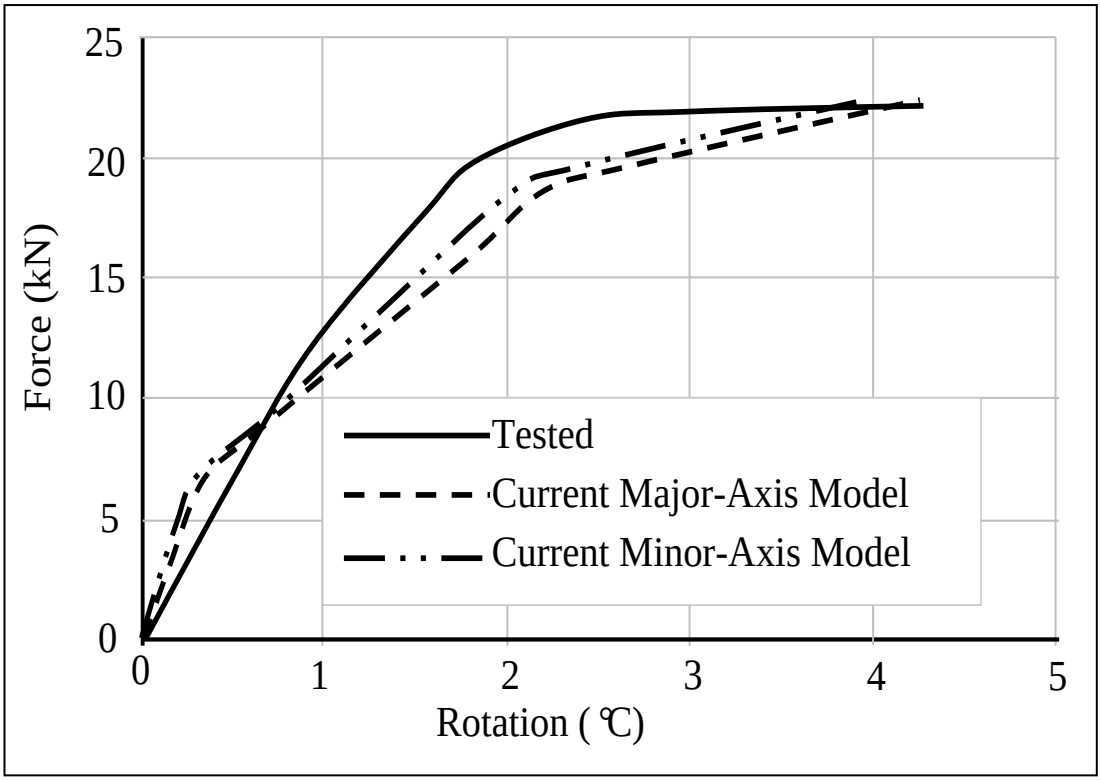

Figure 5.5 Comparison results EP_650_55_11-07-07 (650°C, θ=55°) (Hu et al., 2009b)

This means that the strength and stiffness of minor-axis partial end-plate connections are similar to the major-axis connections with the same geometry. This may be the reasons why current design codes, such as Eurocode 3 only provides guidance for designing major-axis partial end-plate connections between steel beam and column flange. Therefore, in this study it is reasonable to assume that the proposed minor axis partial end-plate connection model can be used to represent the partial end-plate connections between steel beams and column web and beam web, in order to investigate the behaviours of steel framed composite building in fire.

5.3 Analysis of 3D composite frame under different fire conditions

A series of numerical studies have been conducted on a generic three dimensional 45m x 45m composite building, under two typical fire conditions. As shown in Figure 5.6, the floor consists of five 9m x 9m bays in each direction. For steel beam members within the frame, the section of 533x210x92UB was used for the primary beam, while size of 356x127x39UB was adopted for the secondary beam with S355 steel. The column of size 305x305x97UC was applied with a height of 4.5m. The lightweight concrete composite floor had an overall depth of 130 mm, with PMF

CF70 metal decking. It was assumed that the composite frame was designed for an office building, and two hours fire resistance was required. The realistic design load for this building was assumed as follows:

- Self-weight of composite slab: 2.08 kN/m^2
- Self-weight of steel: 0.2 kN/m^2
- Raised floor, services and ceiling: 0.8 kN/m^2
- Partitions: 1.0 kN/m^2
- Imposed load: 2.5 kN/m^2

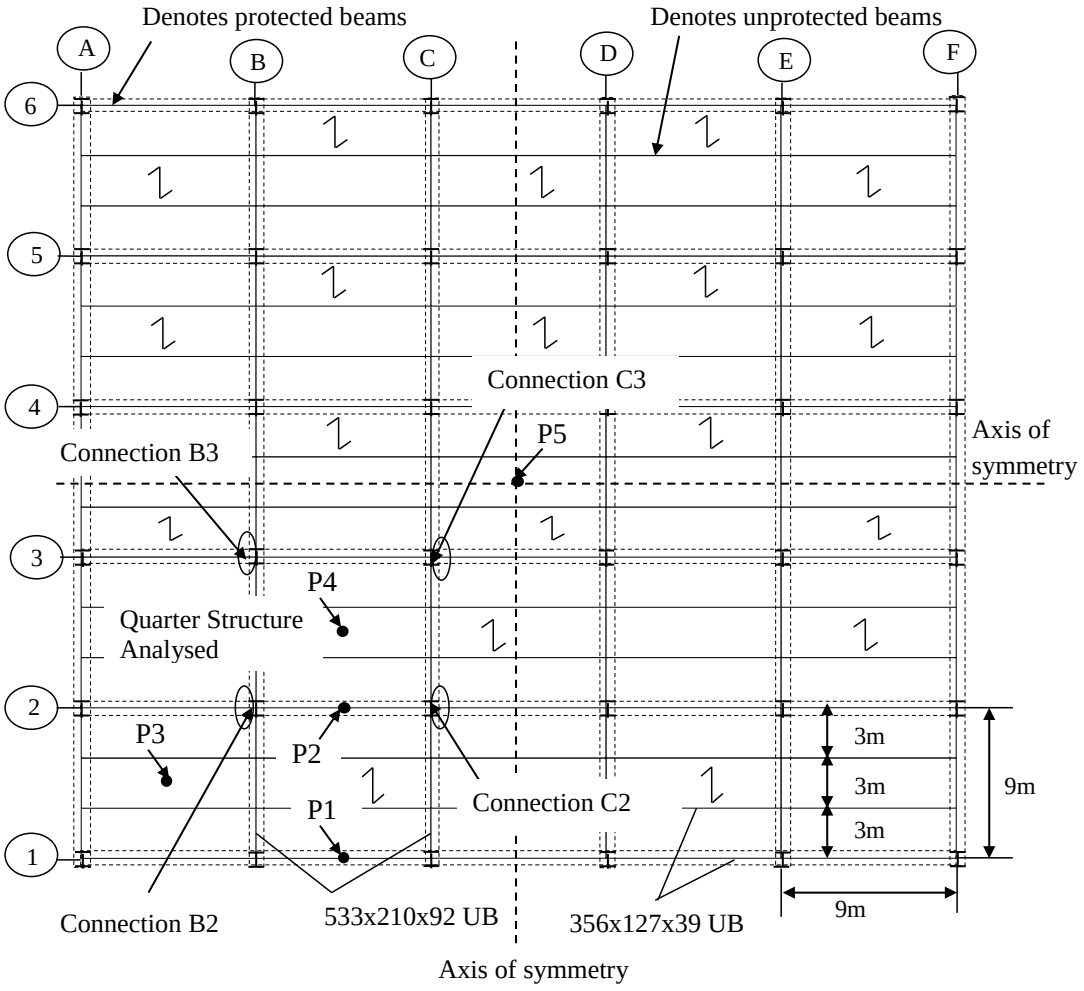

Figure 5.6 Layout of 45m x 45m composite floor

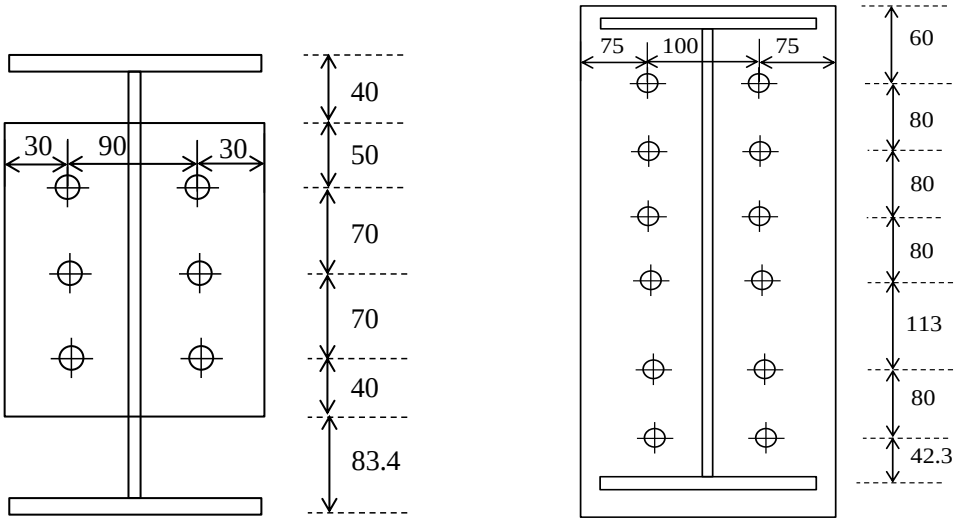

All dimensions in *mm*

Figure 5.7 Configurations of flush endplate and partial endplate connections

At the fire limit state, the total design load is 6.1 kN/m^2, with the applied partial load factors of 1.0 for dead loads, and 0.8 for non-permanent imposed loads. Flush end-plates connections (major-axis) were applied to connect the primary beam-to-column flange. Partial end-plate connections (minor-axis) were used to connect the secondary beams to the columns' web, and secondary beams to the web of primary beams. The configurations of flush end-plate and partial end-plate connections are illustrated in Figure 5.7. For a flush end-plate connection, section of 573x250x25 was used with six M24 Grade 8.8 bolt rows. Among the six bolt rows, four of them were designed to resist axial tensile force, while the rest two bolt rows functioned as shear bolt rows. The vertical shear resistance of the connection at ambient temperature is 542 kN. For a partial end-plate connection, a size of 230x150x10 was applied with three M24 Grade 8.8 bolt rows. Two of these bolt rows were assumed to be tension bolt rows, while the other one was designed to resist vertical shear force. The vertical shear resistance of the connection at ambient temperature is 271 kN. Hence, the load ratio related to vertical shear for secondary beam is 0.3, while for the primary beam it is 0.15.

In this study, two different fire scenarios were adopted: ISO 834 Fire and Natural Fire. The Natural Fire was defined using a parametric temperature-time curve, calculated according to EN 1993-1-2 (CEN, 2005b). The 'office' usage class was assumed. The calculation considered the size of compartment, the given fire load, the assumed air ventilation condition, and the amount of combustibles. It was assumed

that two hours fire resistance was required. All columns, primary beams and secondary beams along the column grid lines were fire protected, and all internal secondary beams were left unprotected.

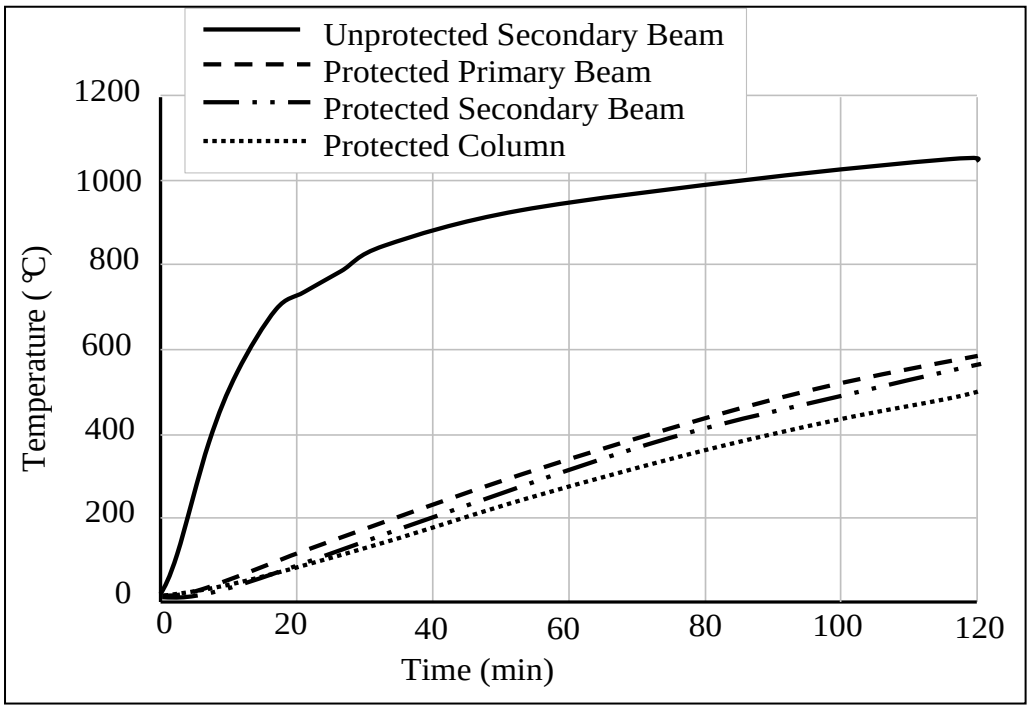

(a)

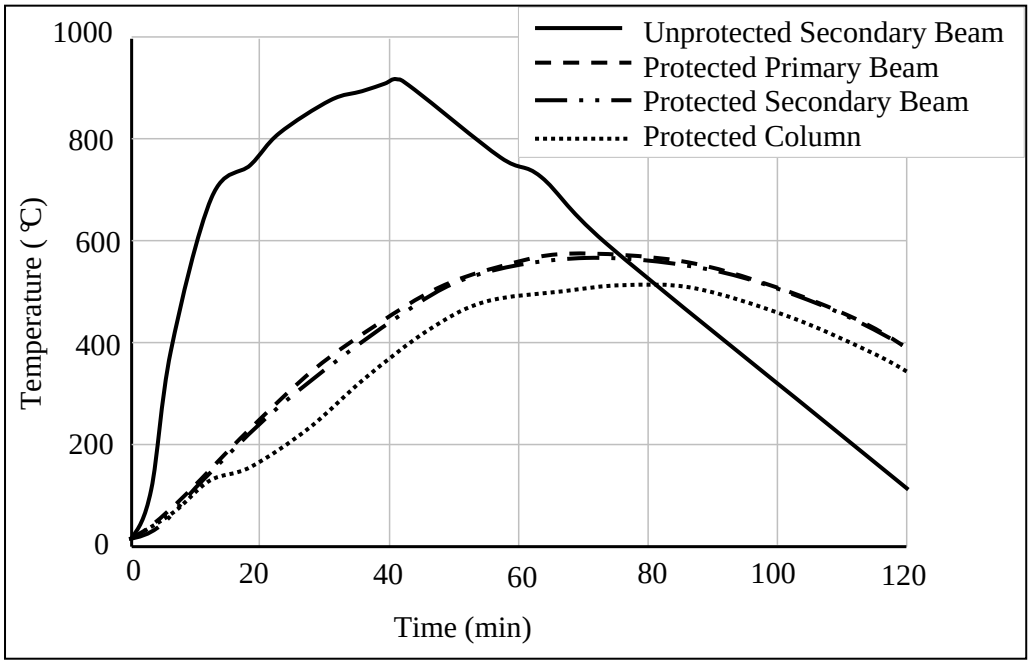

(b)

Figure 5.8 Temperature profiles of columns, unprotected and protected beams: (a) ISO Fire; (b) Natural Fire

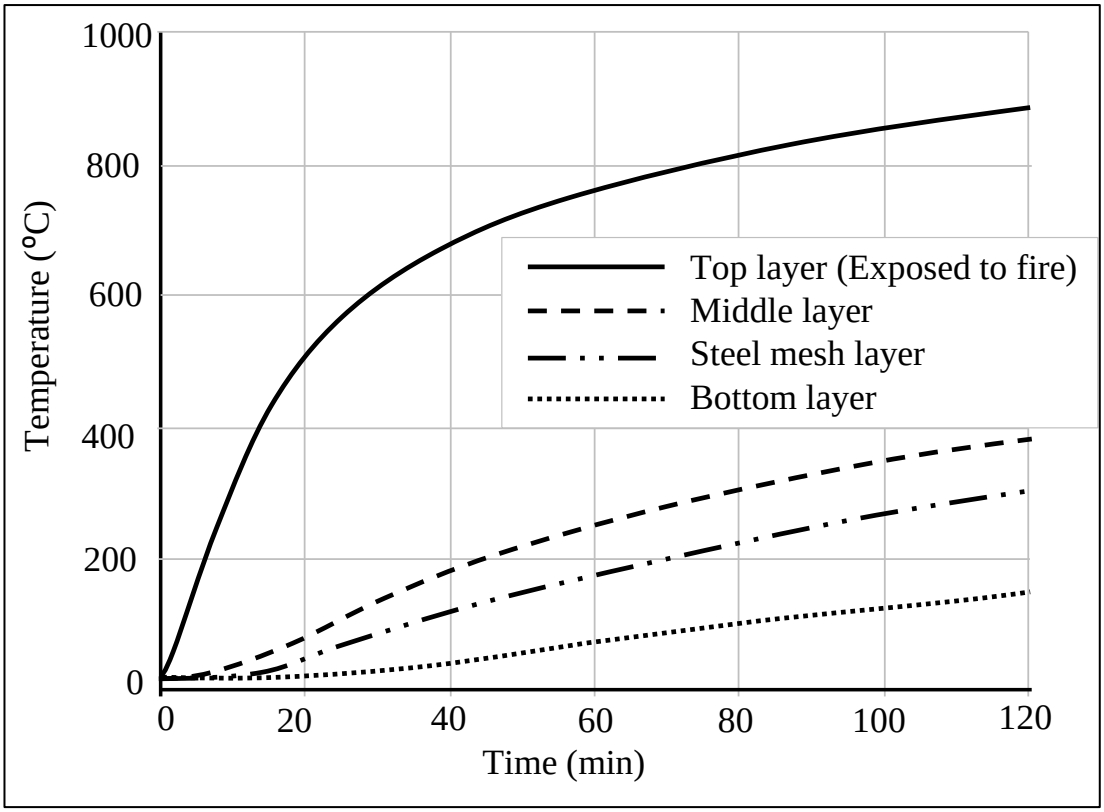

(a)

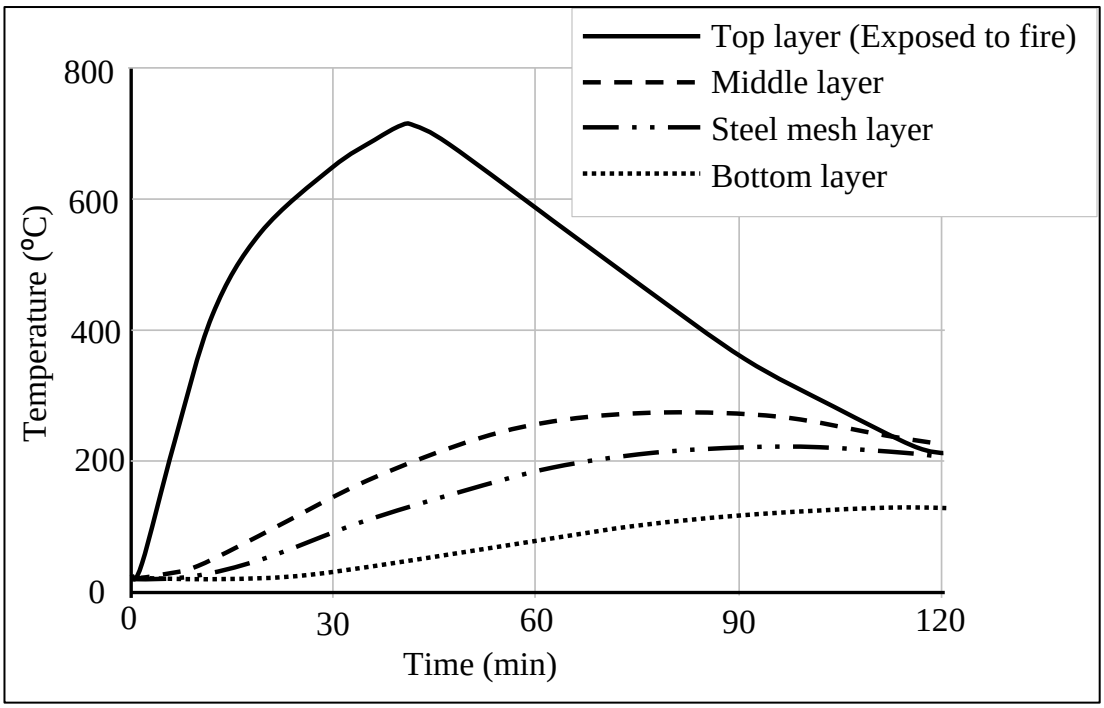

(b)

Figure 5.9 Temperature profiles of top, middle, steel mesh and bottom layer of slabs: (a) ISO Fire; (b) Natural Fire

Figure 5.8 shows the temperatures of unprotected beams, protected beams and columns with time. The maximum temperatures designed for unprotected secondary beams are 1047℃ and 915℃ respectively, under ISO 834 Fire and Natural Fire conditions. During the cooling phases of the Natural Fire scenario, the designed minimum temperature is 114℃. For protected beams and columns, the maximum temperatures are less than 600℃ and 550℃, respectively. The temperatures of connections were assumed to be 80% of the temperatures of the connected beams. As for slabs, the temperatures were calculated along the thickness using a finite element program developed by Huang et al. (1996). The concrete slab was divided into fourteen layers. Each layer had a different uniform temperature distribution. It was assumed that the reinforcement was positioned just above the metal decking. The temperatures of the top, middle, and bottom concrete layers of slab and steel mesh under ISO 834 Fire and Natural Fire are illustrated in Figure 5.9.

In this research, only one quarter of the frame was analysed, in order to save computing time by taking the advantage of symmetry. It was assumed that the whole ground floor of the building was under fire. A total of 15 cases were analysed using different steel meshes (A142, A252 and A393), under two different fire scenarios. In the following sections the reference temperatures for all figures are related to the temperatures of unprotected secondary beams within the fire compartment.

5.3.1 The impact of the connections

The first two cases were analysed using a A142 steel mesh for floor slabs, under ISO 834 Fire and Natural Fire conditions respectively. Figures 5.10 and 5.11 show the predicted vertical shear forces of the partial end-plate connections against temperature and time, for protected secondary beams at the positions B2, C2, B3 and C3 (see Figure 5.6) under ISO Fire and Natural Fire, respectively. These four connections connect the protected secondary beams to columns. It can be clearly seen from the results that all the four connections failed due to vertical shear under two fire scenarios. As can be seen in Figure 5.10, under ISO Fire condition, the vertical shear forces acting on the partial end-plate connections at B2, C2, B3 and C3 ranged from 50 to 60 kN at ambient temperature, which is less than 25% of the vertical shear resistance of the connections used. When temperatures of unprotected secondary beams were higher than 300 ℃, these beams gradually lost their loading

capacity, and the loads on the floor slabs were redistributed from the hot beams to the protected beams. When the unprotected beam temperature reached about 700 ℃, the vertical shear forces acting on the partial end-plate connections at B2 and B3 increased to around 270 kN , exceeding the vertical shear resistance of the connections. Therefore, the connections positioned at B2 and B3 failed by vertical shear. The vertical supports of the protected secondary beams B2-C2 and B3-C3 were lost. When the temperature approached around 850 ℃, the partial endplate connections located at C2 and C3 failed due to the vertical shear. Then the vertical supports of the protected secondary beams C2-D2 and C3-D3 were also lost.

Similar load transfer mechanism can be observed from the results under the Natural Fire condition (see Figure 5.11). When temperatures reached 300 ℃, unprotected secondary beams started to lose strength and stiffness. Then with the increasing of temperature, more loads were redistributed from the unprotected secondary beams to the protected beams. The applied vertical shear forces exceeded the shear resistances of partial end-plate connections located at B2 and B3 when the temperatures were around 600 ℃. After that, the partial end-plate connections positioned at C2 and C3 also failed by vertical shear when temperature was around 750 ℃.

Figures 5.12 and 5.13 show the deflections versus temperatures and times at position P1, P2, P3, and P4 (see Figure 5.6), under ISO 834 Fire and Natural Fire scenarios respectively. As shown in Figure 5.6, the positions of P1 and P2 are located at the mid-span of protected secondary beams, B1-C1 and B2-C2, while P3 and P4 are positioned at the centres of the compartments. It can be observed that the deflections at the mid-span of the protected beams increased significantly, when the temperature of unprotected beams was beyond 800 ℃. Therefore, the vertical support for the floor slab panels, provided by the protected beams, was significantly reduced. As illustrated in the deflection profiles at 1008 ^{0}C (see Figure 5.14), the floor slab panels deformed less double curvature, due to the significant deflections of protected secondary beams. Hence, the tensile membrane actions within the floor slabs were reduced considerably.

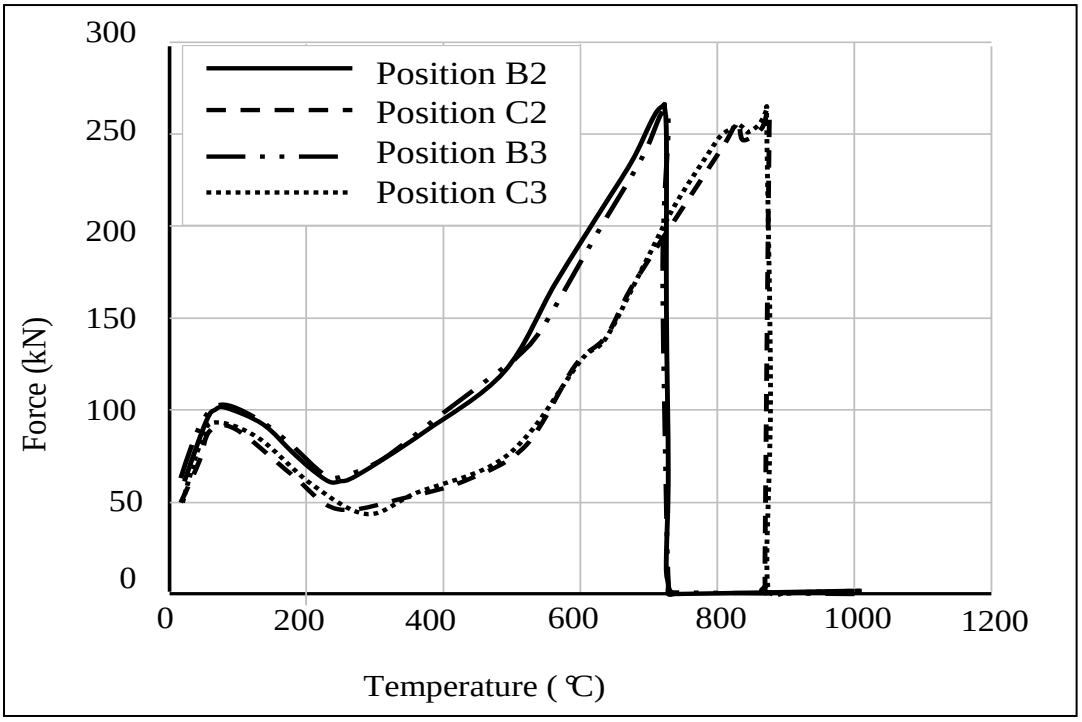

(a)

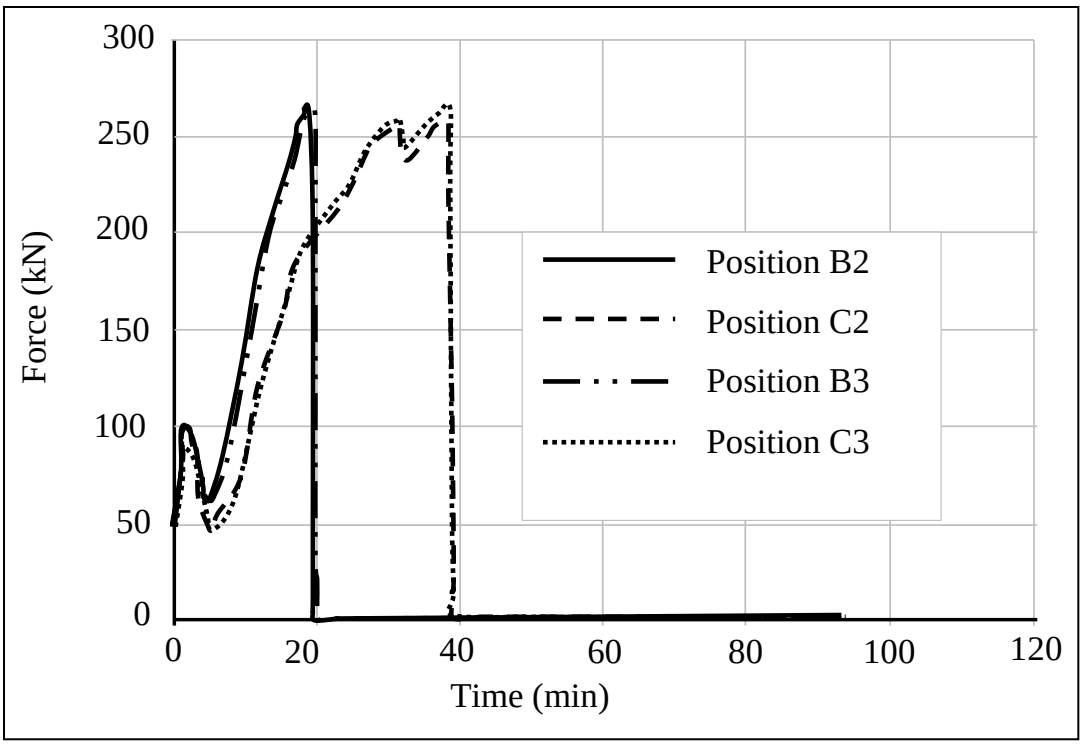

(b)

Figure 5.10 Predicted vertical shear forces of connections at different positions under ISO Fire: (a) connection shear force versus beam temperatures; (b) connection shear force versus time

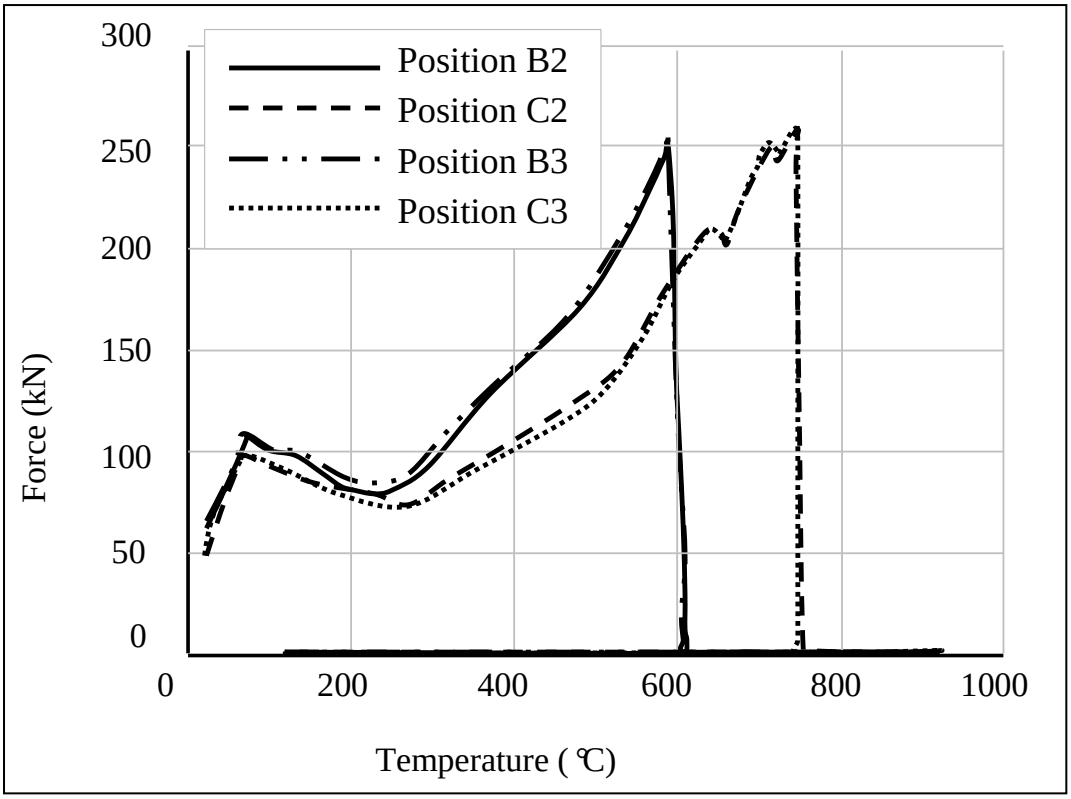

(a)

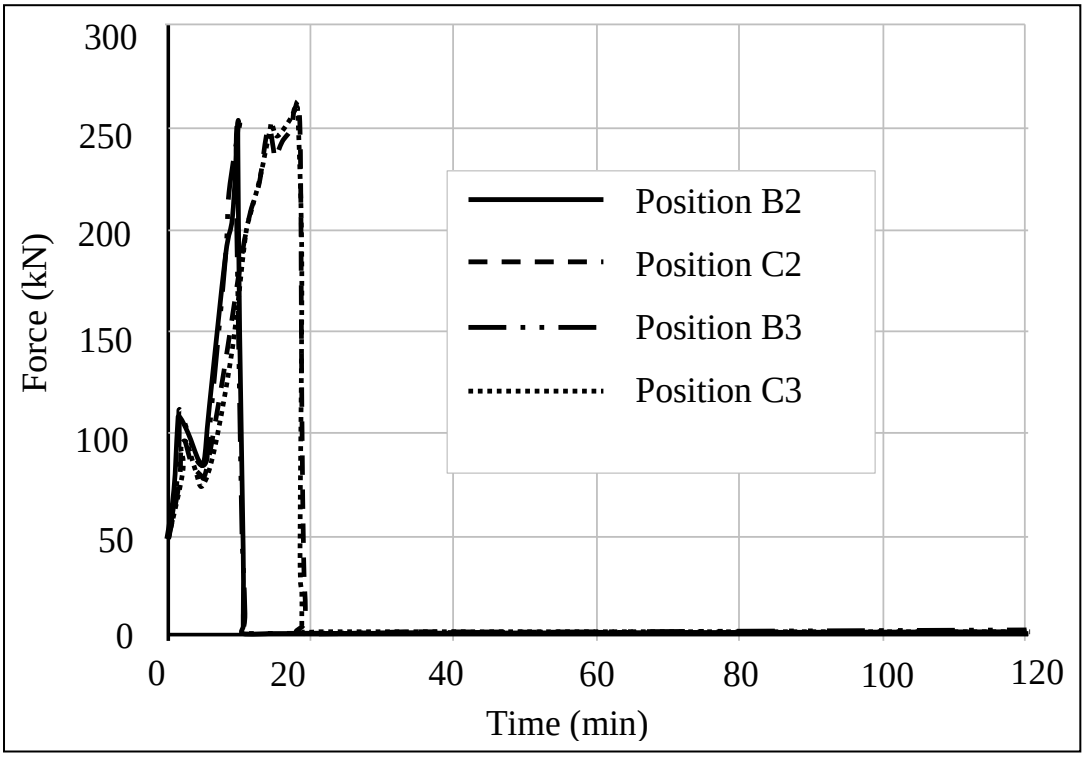

(b)

Figure 5.11 Predicted vertical shear forces of connections at different positions under Natural Fire: (a) connection shear force versus beam temperatures; (b) connection shear force versus time

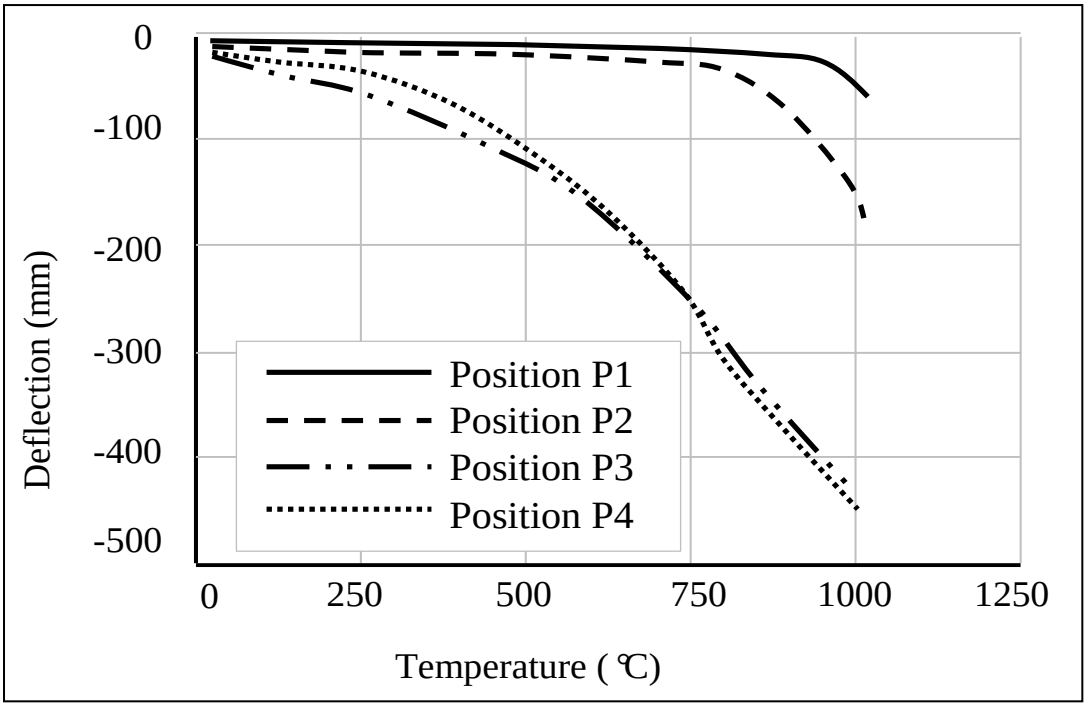

(a)

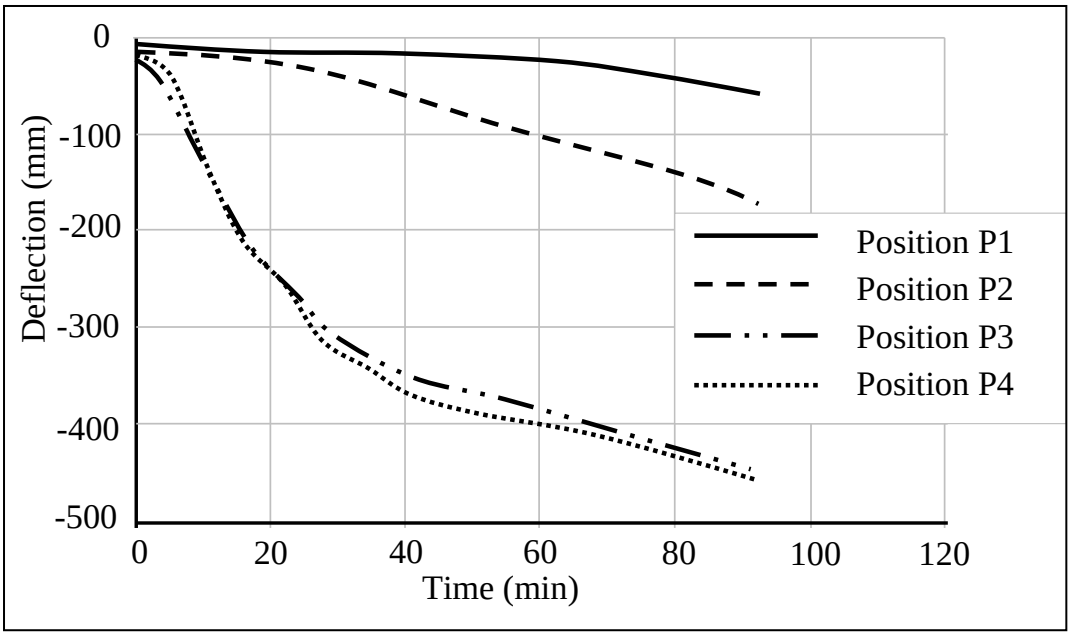

(b)

Figure 5.12 Predicted deflections at different positions under ISO Fire: (a) deflection versus beam temperatures; (b) deflection versus time

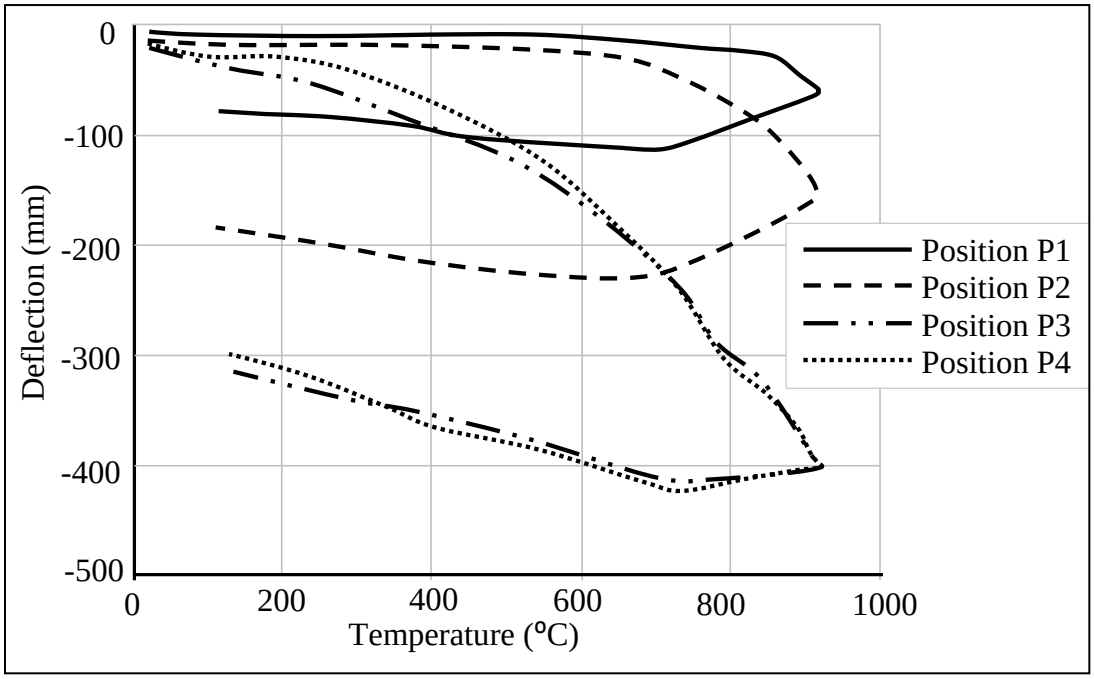

(a)

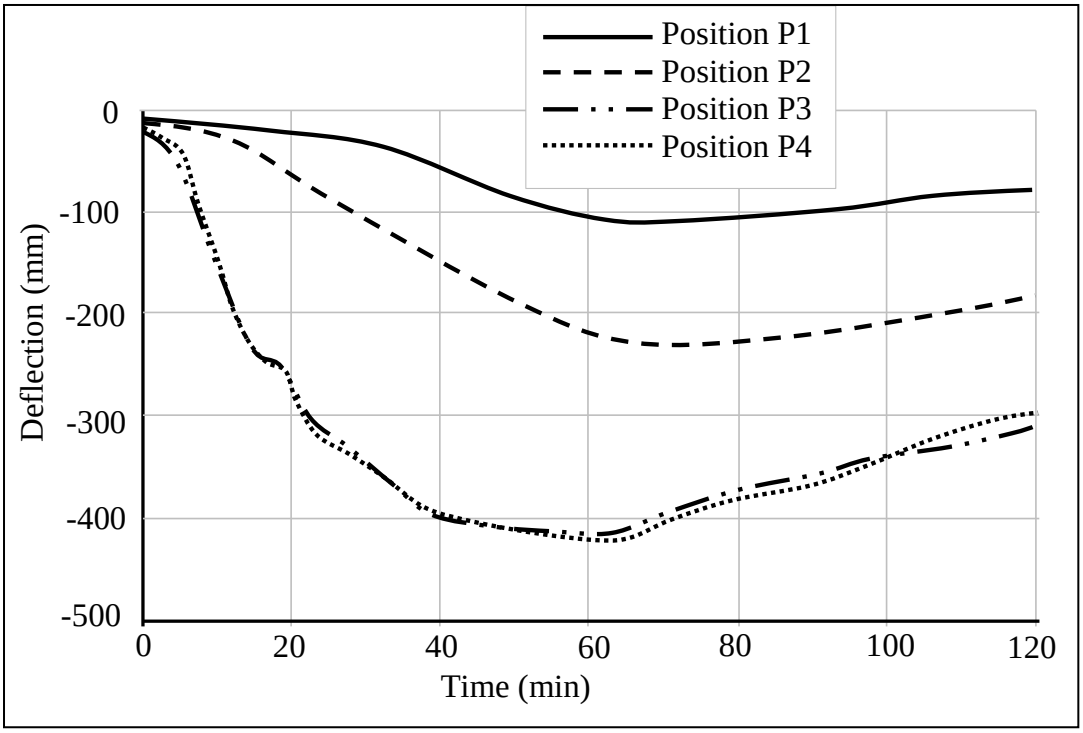

(b)

Figure 5.13 Predicted deflections at different positions under Natural Fire: (a) deflection versus beam temperatures; (b) deflection versus time

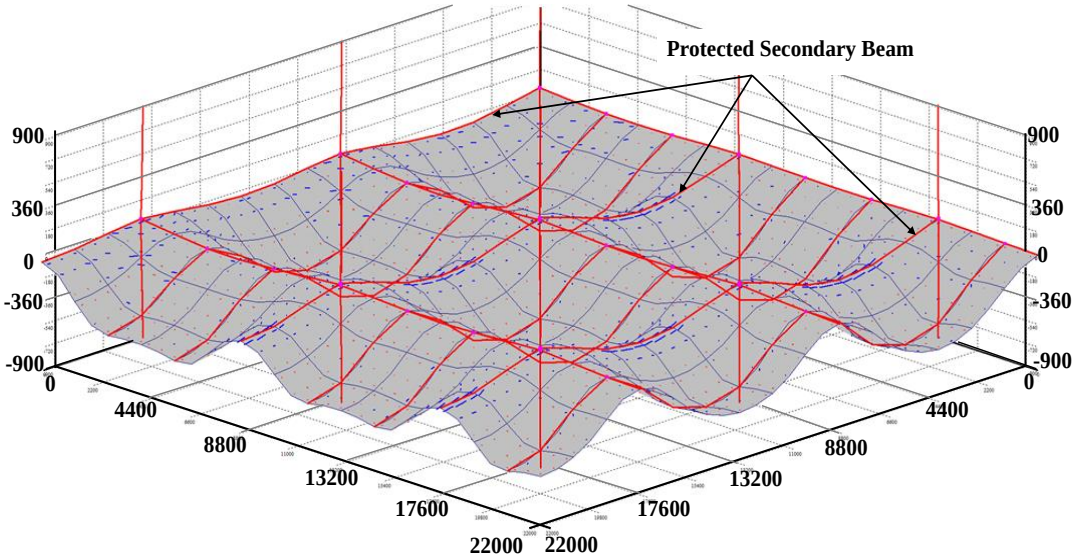

Figure 5.14 Deflection profiles of slab at 1008 ^{0}C

For the Natural Fire case, similar behaviours of protected secondary beams and floor slabs were noticed (see Figure 5.13). When the temperatures of the protected secondary beams approached around 150 ℃, the related temperatures of unprotected secondary beams were nearly 700 ℃. At this point, the strength and stiffness of unprotected secondary beams began to reduce. Within the fire compartment, alternative load paths were adopted to transfer the load. Therefore, with the increasing of temperatures, the deflections at position P2 is higher than that of position P1.

It is clear from the above analysis that the behaviour of connections positioned at the perimeter of slab panels has a significant influence on the formation of tensile membrane action. In this research, the load factor of the vertical shear of connections between protected secondary beams and columns is 0.3. However, in this case the connections still failed, due to loads transferred from unprotected beams to the protected beams as the fire developed. The failure of connections connected to the protected beams reduced the vertical support to the slab panels. Hence, the positive influences of tensile membrane action within the floor slab panel were significant reduced. Therefore, for the structural fire engineering design, if the designers want to leverage the benefits of tensile membrane action on the performance of composite floors in fire, the vertical shear capacity of the connections between protected secondary beams and columns needs to be significant increased compared to normal design. This ensures that the connections have

sufficient resistance to the larger loads, due to the load transfer from unprotected beams to the protected beams under fire conditions.

5.3.2 Influence of different slab reinforcement

Three different steel meshes (A142, A252 and A393) were taken into account in this research, to demonstrate the effect of slab reinforcement on the structural behaviour under fire conditions. The predicted deflections at position P3 and P4 under ISO834 Fire condition are illustrated in Figures 5.15 and 5.16. It can be observed that the impact of different slab reinforcement is negligible, up to 500 ℃. But beyond 500 ℃, the differences between the three steel meshes become more obvious. When the steel beams lose strength and stiffness at high temperatures, the concrete slab plays a more important role in supporting the loads. The ultimate load-carrying capacity of concrete slabs largely depends on the reinforcement area and strength. Therefore, at high temperatures, the impact of steel reinforcement becomes more significant.

Figures 5.17 and 5.18 show the predicted deflections at the centre of the panels P3 and P4, when modelling using the Natural Fire condition. The temperatures of the horizontal axis refer to the temperatures of the unprotected secondary beam. The behaviour of cooling phases was also taken into consideration. As can be seen from Figures 5.17 and 5.18, it is obvious that the deflection of slab panel would reduce, if using a higher steel mesh under fire conditions. As explained above, this is because the concrete slab plays a more important role in supporting the loads, when the strength and stiffness of steel beams decrease rapidly at high temperatures.

Figure 5.19 gives the distribution of principal membrane tractions (forces per unit width) at the Gauss points of the slab elements under ISO Fire condition. This vector plot was obtained when the temperature was 1008 ℃, with A142 slab reinforcement. The length of the vector is proportional to its magnitude. The thick (blue) line refers to compression, while the thin (red) line relates to tension. It can be clearly seen that the tensile membrane action occur within the centre of each slab panel, while a compressive ring forms around the perimeter of each slab panel. Figure 5.20 shows the distribution of principal membrane tractions, with A393 slab reinforcement at 1008 ℃. Compared to the A142 steel mesh, the tensile membrane action of slab panel with the A393 steel mesh is more significant.

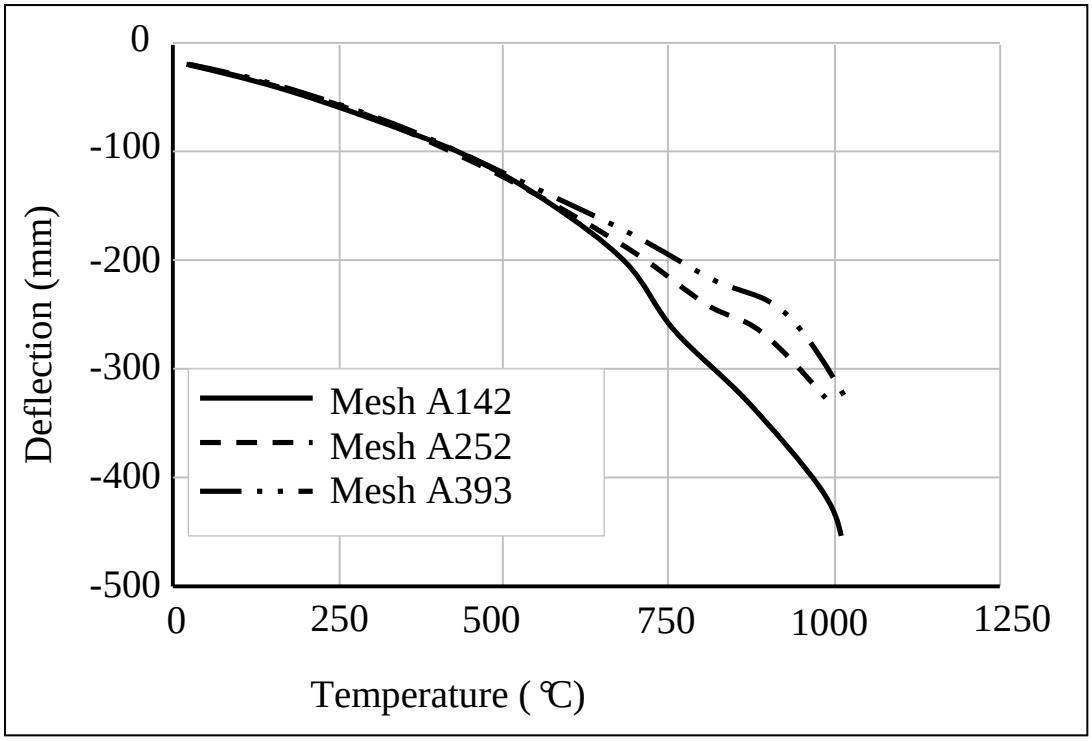

Figure 5.15 Predicted deflections at position P3 under ISO Fire using different steel meshes

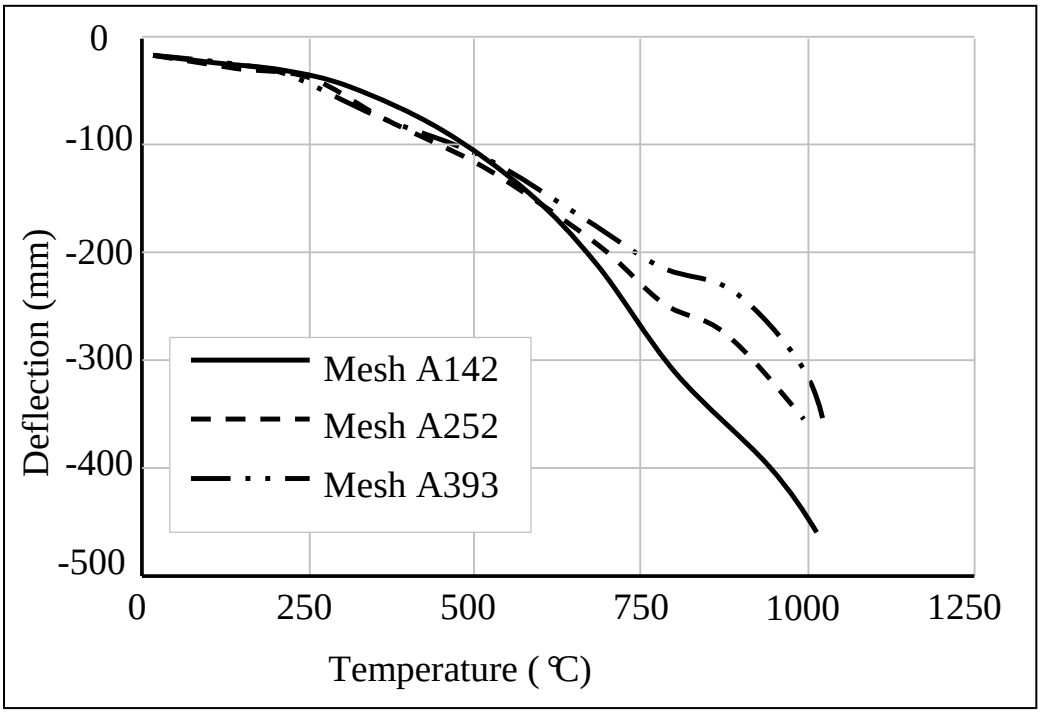

Figure 5.16 Predicted deflections at position P4 under ISO Fire using different steel meshes

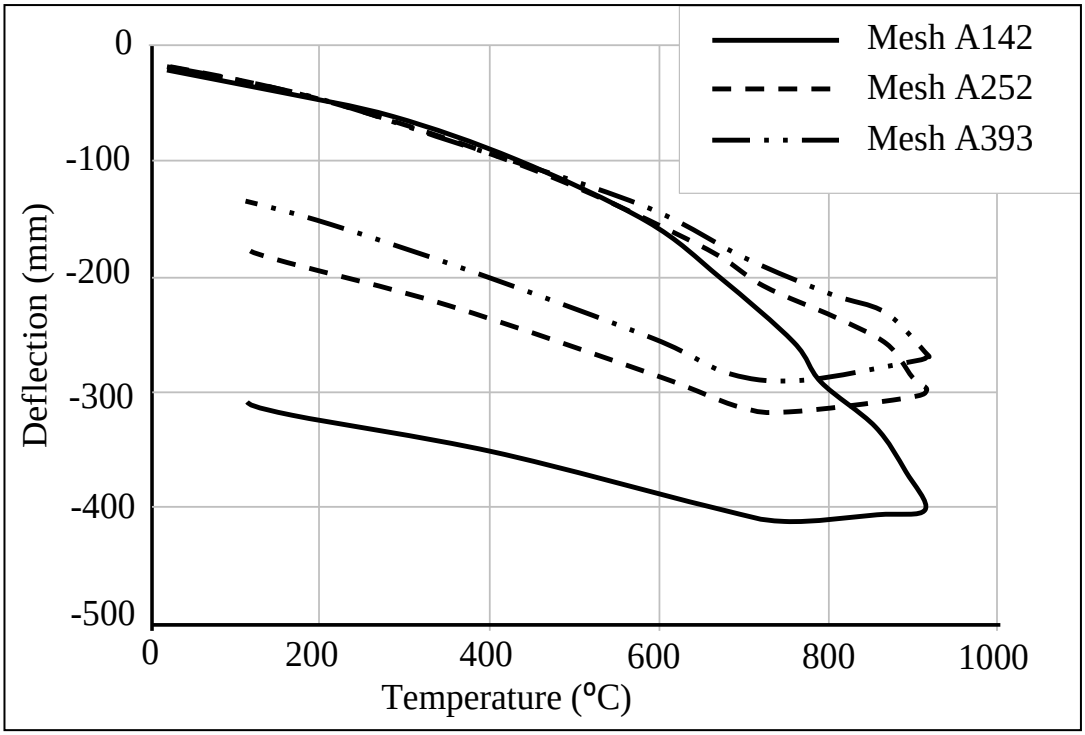

(a)

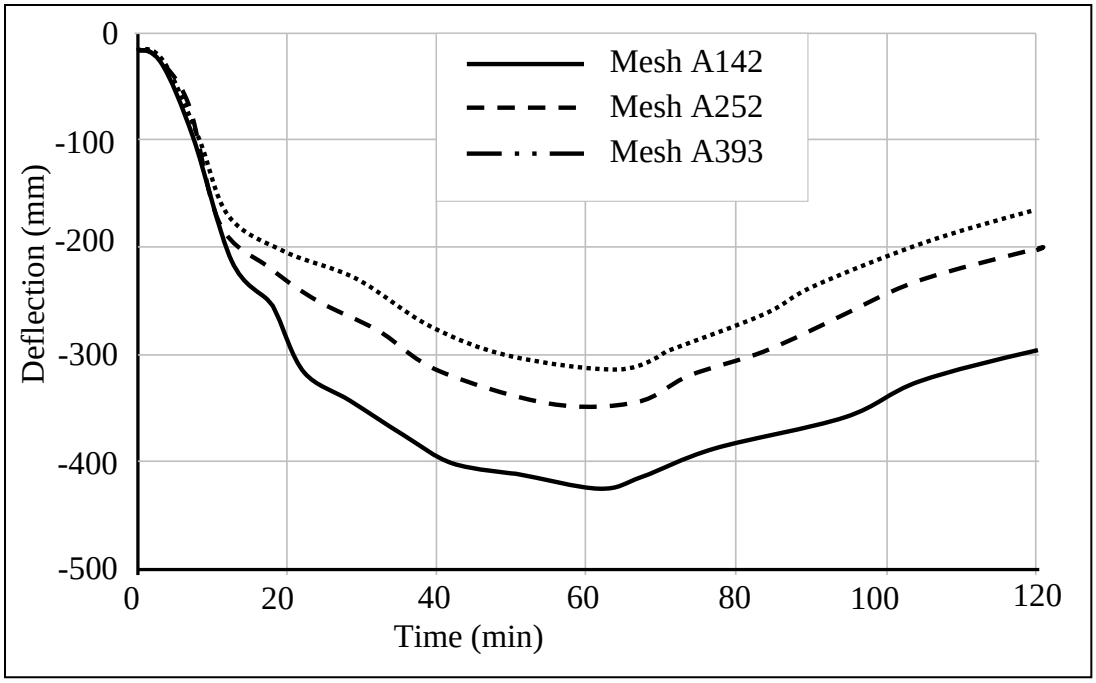

(b)

Figure 5.17 Predicted deflections at position P3 under Natural Fire using different steel meshes: (a) deflection versus beam temperatures; (b) deflection versus time

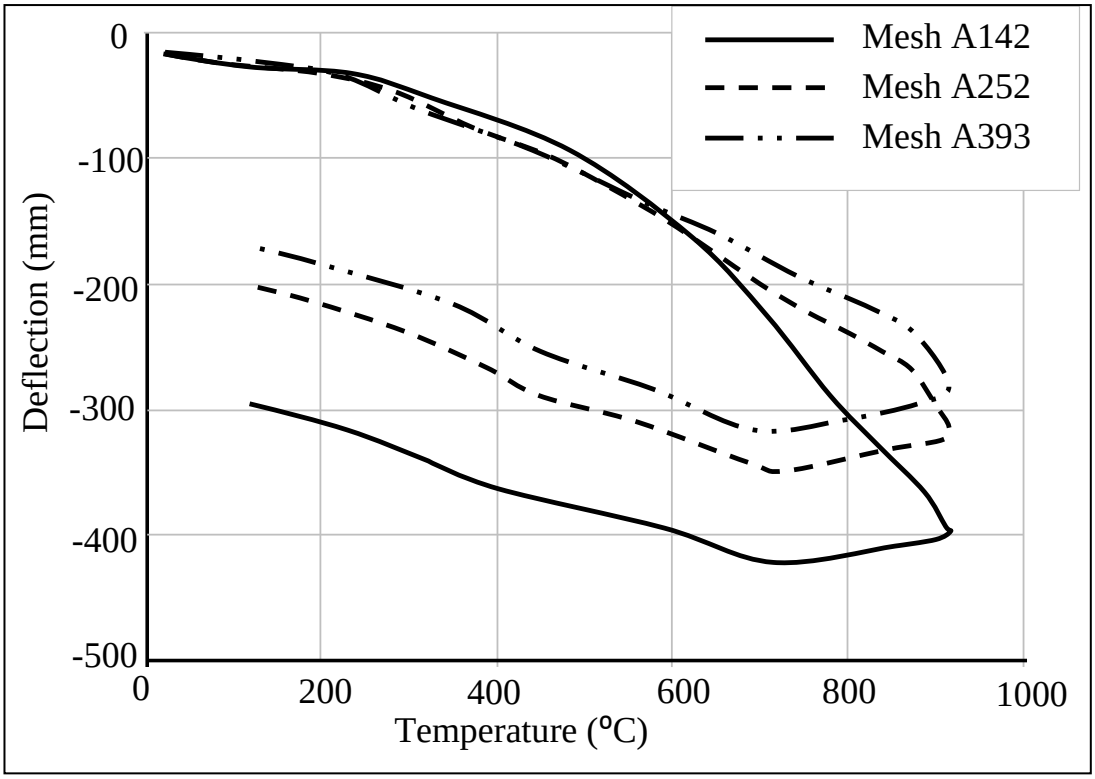

(a)

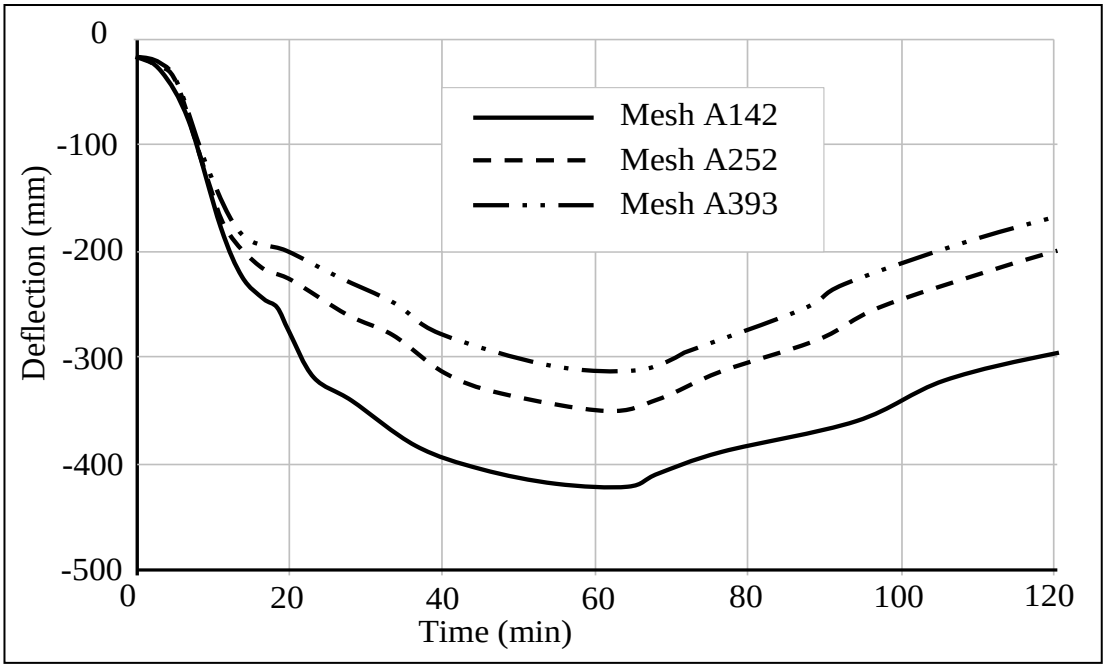

(b)

Figure 5.18 Predicted deflections at position P4 under Natural Fire using different steel meshes: (a) deflection versus beam temperatures; (b) deflection versus time

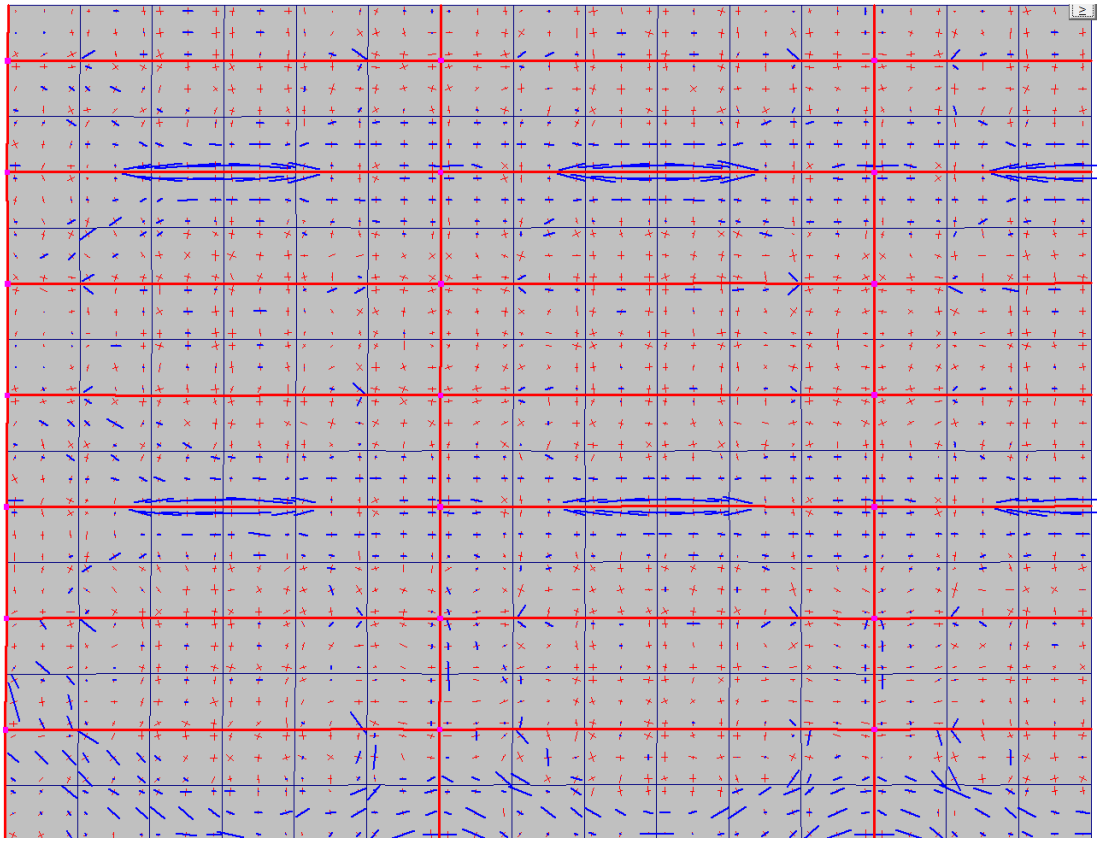

Figure 5.19 Distribution of principal membrane tractions with A142 mesh at 1008 ℃

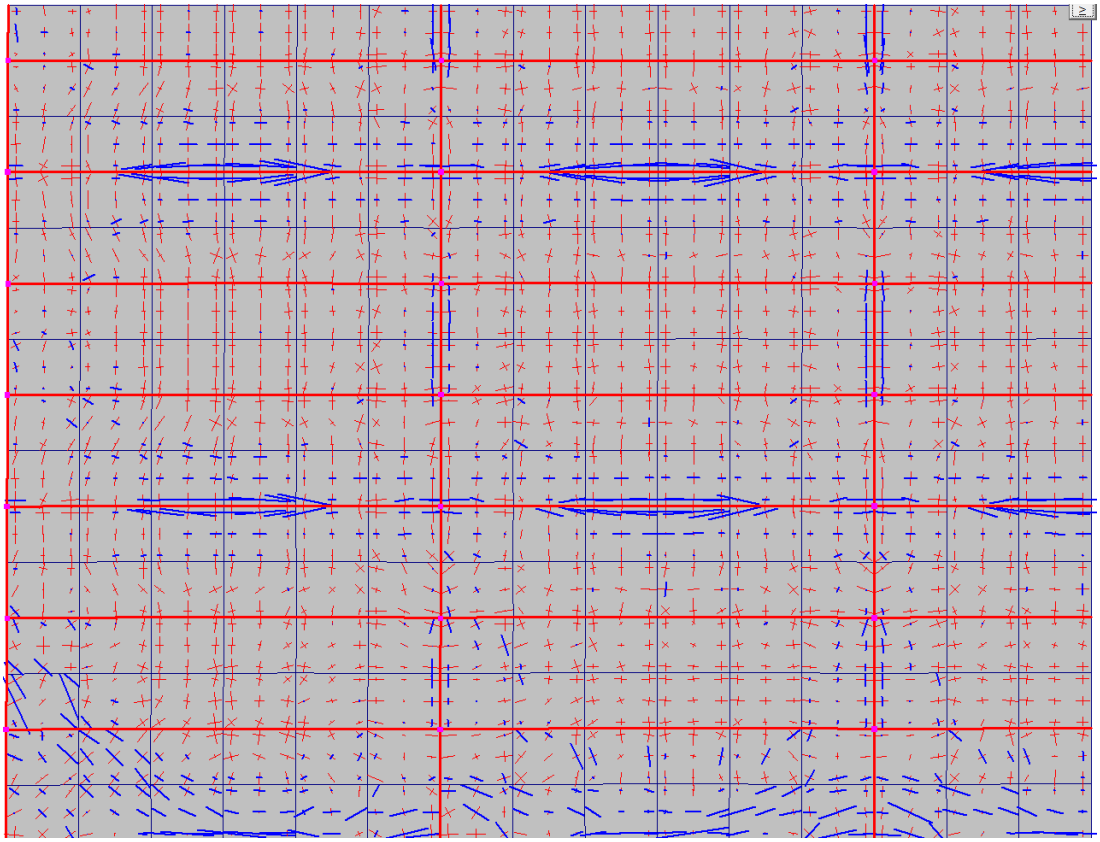

Figure 5.20 Distribution of principal membrane tractions with A393 mesh at 1008 ℃

5.3.3 Influence of vertical support of protected beams

In order to illustrate the effect of membrane action of the concrete floor slabs, both geometrically linear and nonlinear slab elements with A393 steel mesh were used to model the proposed composite frame under ISO Fire condition. When using the geometrically linear slab element to represent the concrete floor slabs for analysing the performance of fire compartment, only the normal bending of slab elements were taken into consideration. The effect of membrane actions within the floor slabs were totally ignored. For the modelling using the geometrically nonlinear slab elements, the membrane actions within the floor slabs were fully considered. Figures 5.21 and 5.22 give the comparison results of the floor slabs' deflections at position P3 and P4, for using geometrically linear and nonlinear procedures. It can also be clearly seen that in this case the influence of membrane action is very significant. When the temperature of the unprotected secondary beam reached about 1000 ^{0}C, the deflection at the centre of the slab panel which considered the effect of tensile membrane action was only half of that without considering membrane action. When the temperature of the unprotected secondary beam is less than 750 ℃, the deflection of the floor slabs is below 250 mm; hence, there was very little influence of tensile membrane action within the floor slabs. When the temperature increased further, the unprotected secondary steel beams lose its strength and stiffness significantly. Then, the loads within the floor slabs are mainly carried by the floor slabs, and the tensile membrane action within the floor slabs will play an important role in enhancing the load capacity of the floor slabs.

In order to quantitatively assess the influence of the vertical support provided by the protected beams along the edges of slab panel on the membrane actions of the floor slabs, the case with A142 mesh under ISO fire condition was reanalysed with all protected beams fixed vertically. This means that all protected beams along the column grid lines have no vertical deformation, and the slab panels were fully vertically supported along the edges.

Figures 5.23 to 5.25 demonstrate the comparisons of the displacements at position P3, P4, and P5, with fixed and non-fixed vertical support on protected steel beams. For the non-fixed case the protected steel beams were free to deflect vertically as the normal situation. From the comparison results, it can be noticed that the discrepancy between these two cases increases after the temperature of unprotected beams

reaches 700^0C. Beyond this temperature, the unprotected secondary beam loses strength progressively, leading to the loads above the slab panel being redistributed to the protected edge beams along the slab panel. For the normal case (with non-fixed support) the protected secondary beams were vertically deflected significantly due to the increased loads, especially when the temperature of unprotected beams was higher. Therefore, the slab panels of the fire compartment deformed less double curvature (see Figure 5.14). Hence, the tensile membrane action of the slab panel was considerably reduced. In comparison for the case with fixed support on the protected beams, the slab panel was fully vertically supported along the edges of the slab panel. Therefore, the slab panel was forced to deform double curvature hence the tensile membrane action within the slab panel was fully maximized. In this situation, the load capacity of the slab panel considered was significantly enhanced due to the tensile membrane action.

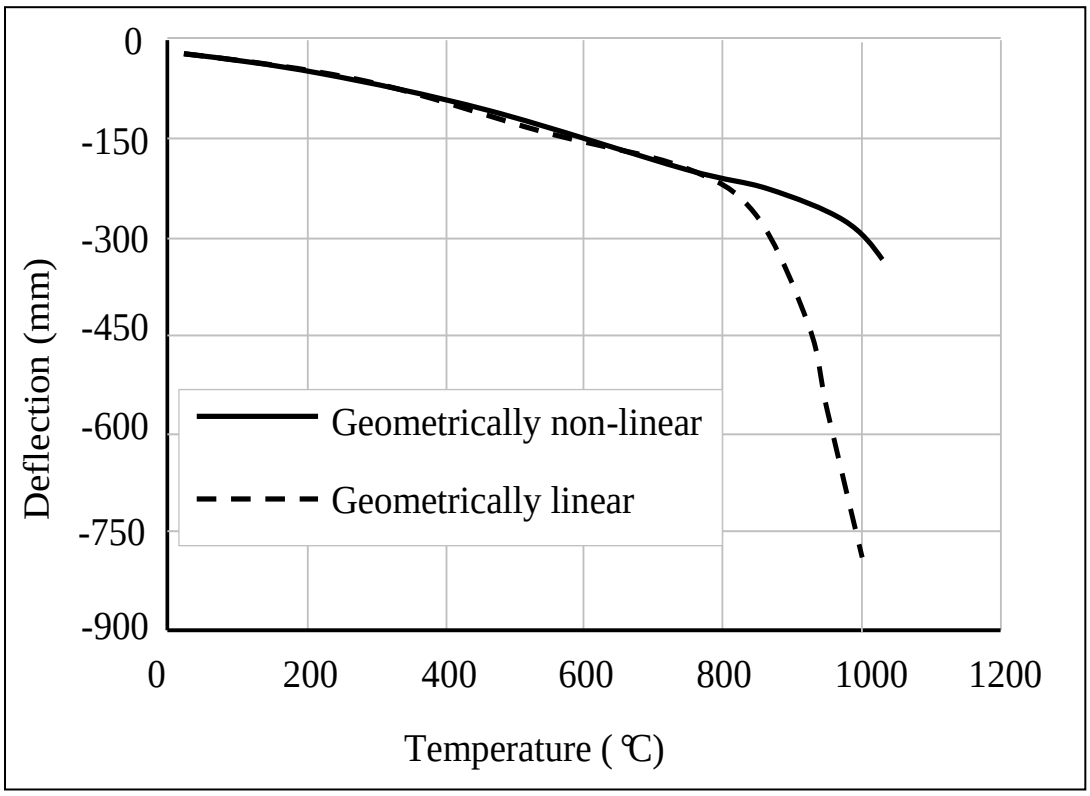

Figure 5.21 Predicted deflections at position P3 using geometrically linear and non-linear procedure with A393 mesh under ISO Fire condition

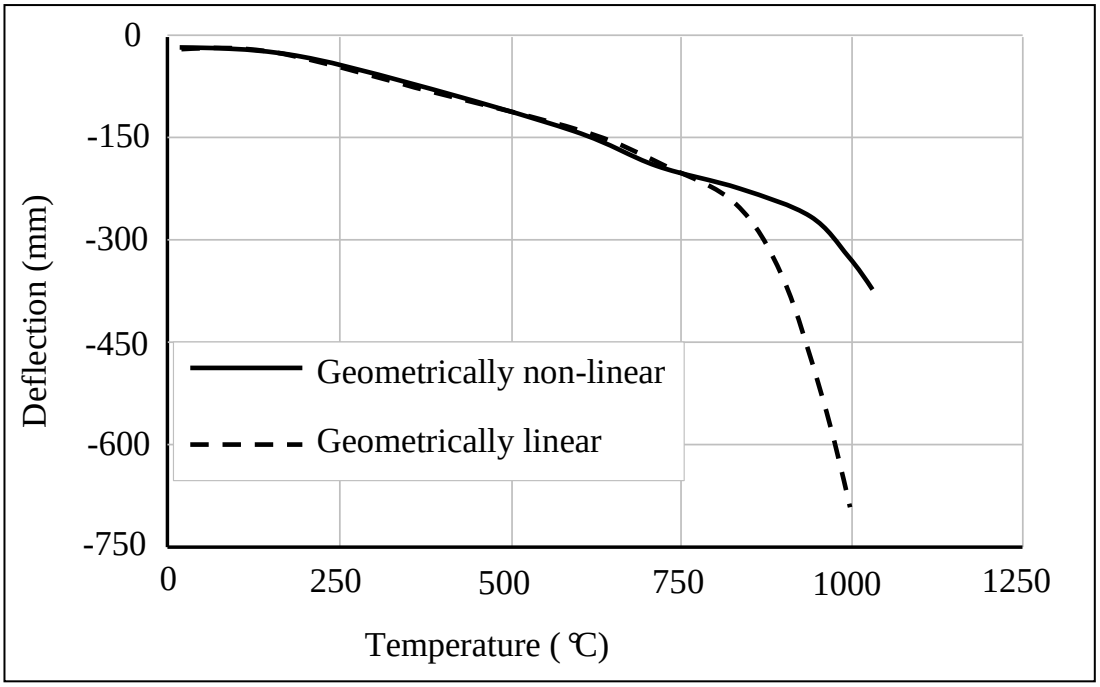

Figure 5.22 Predicted deflections at position P4 using geometrically linear and non-linear procedure with A393 mesh under ISO Fire condition

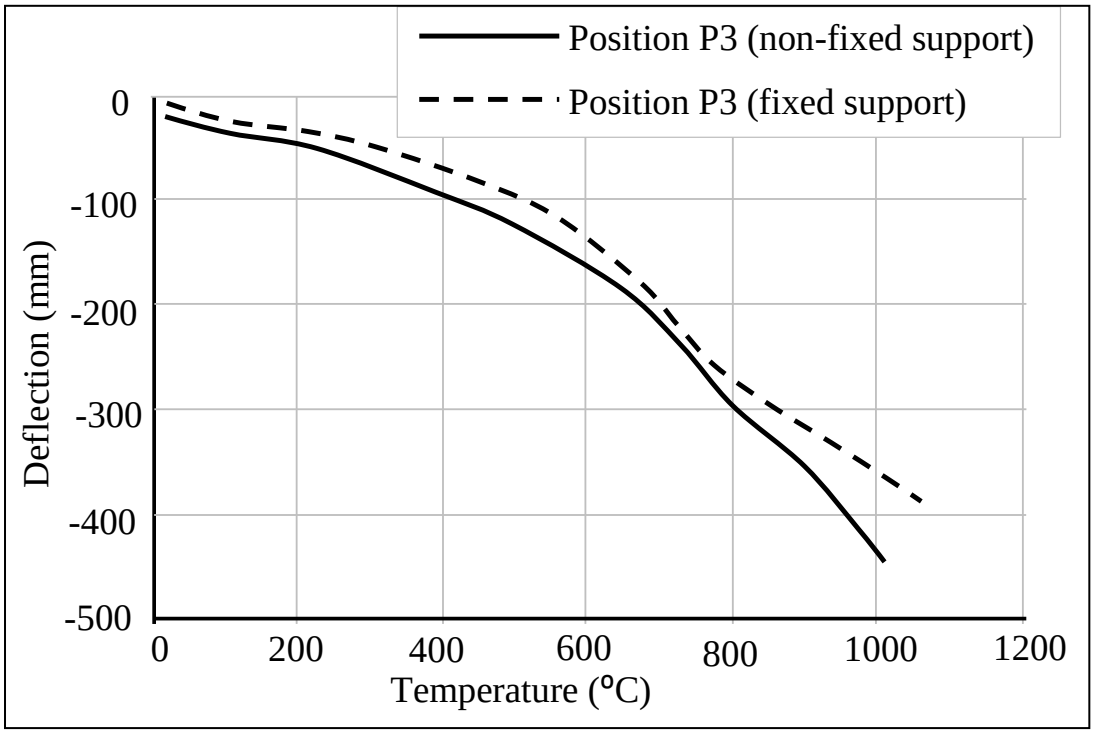

Figure 5.23 Comparison of predicted deflections at positions P3 subjected to ISO Fire with non-fixed and fixed vertical support on protected steel beams (A142 mesh)

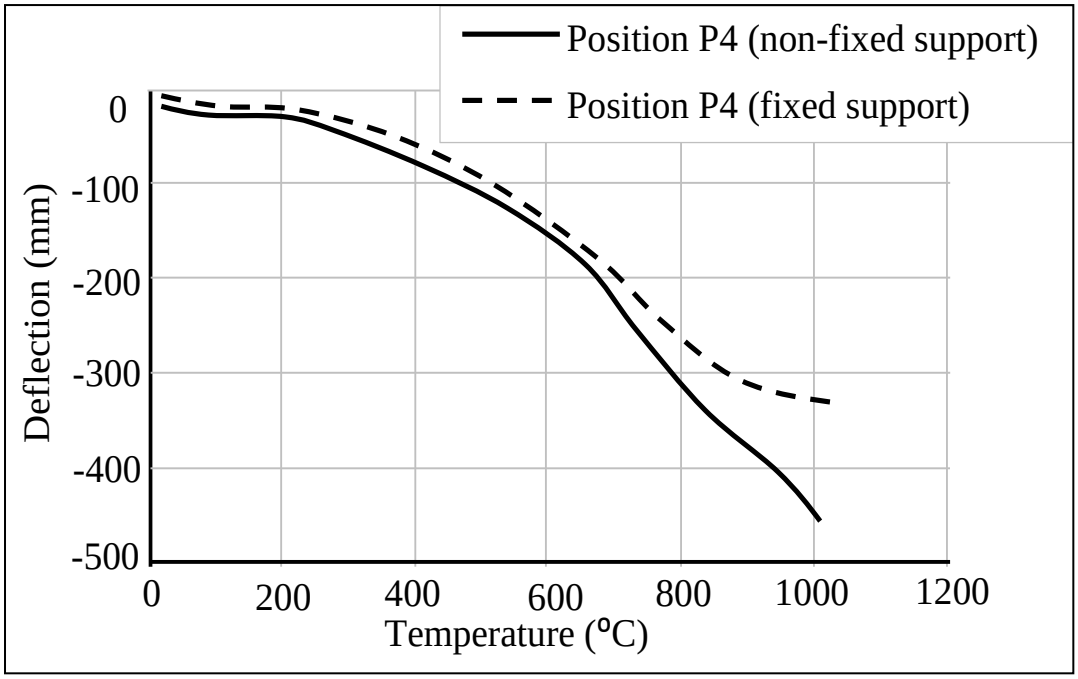

Figure 5.24 Comparison of predicted deflections at positions P4 subjected to ISO Fire with non-fixed and fixed vertical support on protected steel beams (A142 mesh)

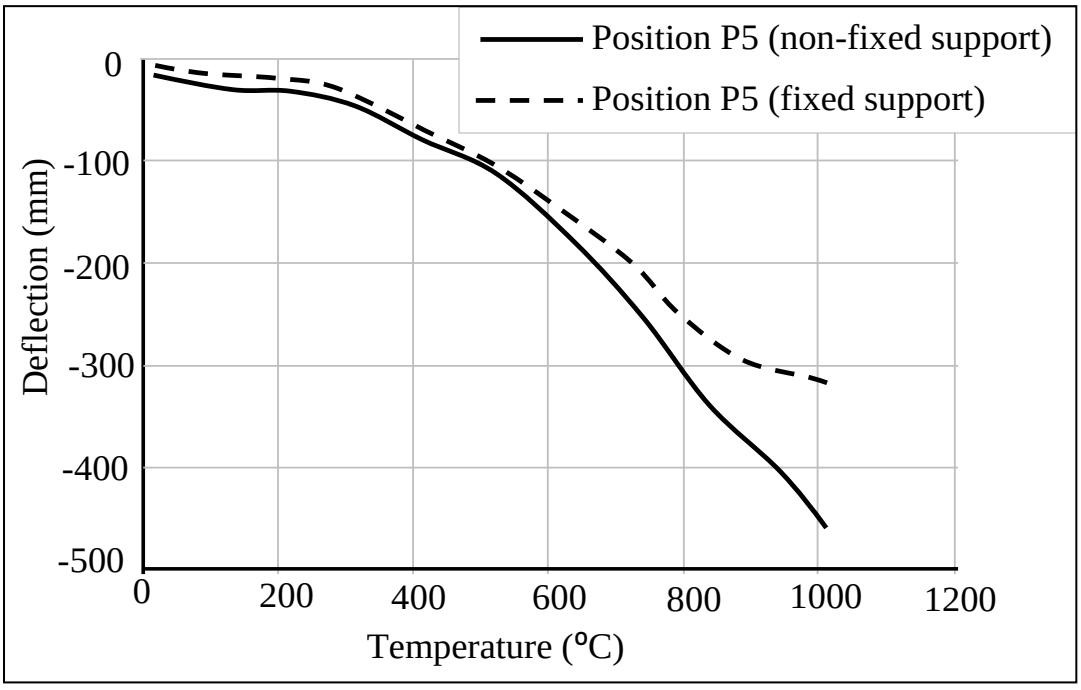

Figure 5.25 Comparison of predicted deflections at positions P5 subjected to ISO Fire with non-fixed and fixed vertical support on protected steel beams (A142 mesh)

The investigation reported above demonstrated that the influence of the vertical support condition on the tensile membrane action of floor slabs is significant. It is important for fire structural engineering designers account for this issue, when they attempt to utilise the tensile membrane action of floor slabs for as part of simpler design methods.

5.4 Design recommendations

The numerical studies described above show that the provision of vertical support along the slab panel has a significant impact in the formation of tensile membrane action within the floor slabs under fire conditions. At a higher temperature, the loads within the floor slabs of fire compartment (initially supported by unprotected secondary beams in the fire compartment) will be redistributed into protected beams along the column grid lines. This large load will cause the protected secondary beams to deform significantly. Also, the high load will result in vertical shear failure of the connections which connect protected secondary beams to the columns. All of this will significantly undermine the vertical support conditions on floor slab panels within the fire compartment. In return, the benefit of tensile membrane action for enhancing the load carry capacity of the floor slab panels, as initial assumed in the performance-based design, could be considerable reduced.

The primary requirements for effective use of the tensile membrane action of the floor slabs is to make sure that the strong vertical supports along the edges of floor slab panels are maintained during the required fire resistance period. Floor slab panels are forced to deform, as the double curvature takes shape. If the protected edge beams undergo excessive deformation, the floor slab panels may convert into a single-curvature deformation, which will reduce the benefit of tensile membrane action significantly. Therefore, some design recommendations are proposed as following:

- The protected beams along the perimeter of the slab panels should be designed carefully, to provide sufficient vertical support during fire. Larger cross-section sizes of protected secondary beams are needed compared to normal design.

- The load-carrying capacities of connections between protected beams and columns need to be adequately designed to resist larger vertical shear forces compared to normal design.
- A higher reinforcement ratio for floor slabs may also be used to enhance the positive influence of the tensile membrane action to improve the fire resistance of the composite floor system.

5.5 Conclusions

In this chapter, the performance of a generic three dimensional 45m x 45m composite floor subjected to ISO 834 Fire and a typical Natural Fire have been analysed. In this research, two robust 2-node connection element models have been utilised to assess the behaviour of end-plate and partial end-plate connections under fire conditions. A series of numerical studies has been conducted, in order to quantitatively assess the impacts of vertical supports on tensile membrane action in composite slabs. Different vertical support conditions and three steel meshes are adopted. The results show that at high temperatures, the strength and stiffness of steel beams reduce rapidly. The loads above the fire compartment are largely carried by the concrete slabs. Therefore, the impact of steel reinforcement becomes more significant. In the current study, the influence of steel connections on the 3D behaviour of real scale composite buildings in fire is also taken into consideration. The load-transfer mechanisms of the composite floor when the connections fail due to axial tension, vertical shear, and bending are described in detail. Based on these analyses, the partial end-plate connections, which connect protected secondary beams to the columns, would fail due to the transferred load from the intermediate unprotected secondary beams. Once the connections of protected beams fail, the vertical support for the slab panel would reduce. The floor slab would deform with less double curvature, causing significant reduction of the tensile membrane action within the floor slabs. Therefore, in real performance-based fire resistance design of steel framed composite buildings, the influence of connections need to be considered carefully in order to maximise the benefit of tensile membrane action. The designers should design adequate strength and stiffness into protected secondary beams and connections.

Chapter 6

Conclusions and Recommendations for Future Studies

The last two decades has seen significant progress on our understanding of steel-framed composite buildings under fire conditions. Investigations on the performance of various steel members at elevated temperatures have been conducted by different researchers, either in isolation or as part of a sub-frame assembly. Current research indicates that connections play an important role in maintaining the integrity of the structure, and preventing progressive collapse. The robustness of steel connections is therefore vitally important to the fire resistance of composite buildings. The development of effective connection models is a key issue in this research field. The PhD research reported here focused specifically on the development of robust connection elements for modelling steel connections at elevated temperatures.

6.1 Summary of the thesis contributions

6.1.1 Development of the flush and extended end-plate connection element

Flush and extended end-plate connections are the commonly-used connections for steel frames composite structures in the UK. In this thesis, a robust 2-node connection element has been developed for modelling the bolted end-plate connection between steel beam and column at elevated temperatures. The developed connection model was mainly based on the framework of two-node connection element proposed by Huang (2011). In this new model the end-plate connection has been represented as a two-node nonlinear spring element. However, the characteristic of the nonlinear spring connection element, such as rotational stiffness, bending, tension and compression, vertical shear resistances were calculated based on the component-based approach. The model developed therefore has the advantages of the simple connection model, whilst retaining the advantages of component-based models.

In this model the end-plate connection was considered to be an assembly of the column flange T-stub, and the end-plate T-stub; three failure mechanisms for a T-

stub assembly were taken into account. The steel material deterioration with temperatures was taken into consideration based on the degradation factors provided in EN 1993-1-2 (CEN, 2005b). The proposed model has also incorporated the works of Spyrou et al. (2004a) and Block et al. (2007). However, the tension resistance calculated from the Spyrou's model is too high compared to the experimental test results on the practical end-plate connections. In the research reported in this thesis, three displacement criteria were proposed based on the numerical parametric study conducted on the tested data of 45 T-stub specimens – with different geometrical and material properties, and temperatures. The proposed displacement criteria were incorporated into the current connection element model. Therefore, the proposed model can more precisely determine the tension, compression, and bending capacities of end-plate connections under fire conditions. In the model here, the connection failure due to bending, axial tension and compression were also considered. The influence of axial tensile force of the connected beam on the bending moment resistance of the connection was also taken into account.

In order to examine the accuracy of the proposed non-linear connection element, a total of 22 experimental tests were used to validate the model, including tests with and without applying axial force at both ambient and elevated temperatures, and two tests on a beam-to-column sub-frame subjected to natural fire.

6.1.2 Development of the partial end-plate connection element

Partial end-plate connections are also widely used in the construction of steel-framed composite buildings in the UK, because they are easy to fabricate and can be assembled and erected on site. Compared to flush and extended end-plate connections, a partial endplate connection has higher flexibility. The rotational response of partial end-plate connection is comprised of two stages, which contains the shift of compression centre from the bottom end of the end-plate to the middle of the beam bottom flange after sufficient rotation.

In this thesis, a simplified robust two-node connection element has been developed to model the behaviour of partial end-plate connections, between steel beams and columns under fire conditions. In the proposed partial end-plate connection element model, the degradation factors provided in EN 1993-1-2 (CEN, 2005b) were adopted to consider the steel material deterioration with temperatures. The two stage rotational responses of partial end-plate connections were taken into account, and

component-based approaches were employed to precisely determine the stiffness, tension, compression, and bending capacities of the partial end-plate connection under fire conditions. The connection failures, due to bending, axial tension or compression, and vertical shear, were also modelled. The current model was based on the two-node end-plate connection element framework mentioned above, with further developments for modelling partial end-plate connections at elevated temperatures.

Similar to for the flushed and extended end-plate connection, the capacities of tension and compression of the partial end-plate connection were derived using the component-based method. For the tension zone, the partial end-plate connection was regarded as the combination of three basic active components: the bolts, the weld, and the T-stub assembly. Experimental test data indicated that the failure mode of the partial end-plate connection can be classed mainly as failure Mode II of T-stub assembly – in which the T-stub flange suffers completed yielding. The whole tension resistance of the connection was considered to be the resistance of the weakest component within the tension zone. As for the compression zone, the main active component is the column web in compression. The force redistribution was also taken into account in the current model. The partial end-plate connection model presented in this thesis therefore retains the advantages of both the simple and component-based models.

The proposed model was validated against a total of fourteen partial end-plate connections, tested at both ambient and elevated temperatures by other researchers. In order to investigate the influences of the connections on the behaviour of steel structures, a series of numerical studies were also conducted on a 2D steel frame subjected to ISO834 Fire and a typical Natural Fire.

6.1.3 Analysis of a 3D composite floor under fire conditions

Observations from a series of full-scale Cardington fire tests have shown that steel framed composite structures can provide a significantly greater fire resistance than is suggested by standard fire tests on isolated structural members. This is due to an interaction between the heated members within the fire compartment, the concrete floor slabs, and the connected steel frame structure. If steel members within the structures loss strength and stiffness rapidly due to high temperatures, alternative

load paths would be adopted to transfer load for the remaining part of the structures. Experimental and analytical investigations involving full-scale fire tests indicated that tensile membrane action within the composite floor slabs plays an important role in enhancing the fire resistance of composite buildings.

In this thesis, a comprehensive study was conducted on a generic three dimensional 45m x 45m composite building, with realistic loading conditions and structural layout, under different fire conditions. A series of analyses has been carried out using different support conditions, on slab panels and slab reinforcement details. In this research, the end-plate connections were used to connect primary beams to columns. The partial end-plate connections were adopted to connect secondary beams to columns, and primary beams to secondary beams, respectively. These two types of connections were modelled using the simplified connection models developed in this thesis. The research conducted here systematically investigated the impact of the connections for protected beams on the tensile membrane actions of supported floor slabs, in which the failure of the connections due to axial tension, vertical shear, or bending was considered. The influence of the vertical deflections of protected beams on the tensile membrane action of the floor slabs has been analysed in detail. The effects of different reinforcement details of the floor slabs, on the performance of a composite floor under different fire conditions, were also evaluated.

6.1.4 Conclusions

Based on the numerical studies, the validations of the developed connection models and the results of the investigation on the three dimensional composite floor under fire conditions, the following conclusions can be drawn:

(1) The validation results of flush and extended end-plate connections show good agreement between the model predictions and the experimental data. This shows that the new connection element has the ability to accurately predict the behaviour of the end-plate connections at elevated temperatures.

(2) The validation results of partial end-plate connections show that the proposed connection model can predict the two stage rotational characteristics of partial end-plate connections with reasonable accuracy.

(3) Both the proposed connection models are very computationally efficient, with excellent numerical stability under a static solver condition. Hence, the models developed in this thesis can be used to represent flush end-plate connections, extended end-plate connections and partial end-plate connections for large scale 3D global modelling of steel-framed composite buildings in fire.

(4) It is evident that the influence of temperature on the behaviour of the connections is significant.

(5) Based on the comprehensive validations conducted in this thesis, it can be concluded that the developed models can be used to represent the flush end-plate connections, extended end-plate connections and partial end-plate connections for performance-based fire resistance design of steel-framed composite buildings.

(6) The results of numerical studies on partial end-plate connections indicate that the tensile failure of the connection is more likely to happen within the buildings during the cooling stage of a real fire.

(7) From these results, one can conclude that modelling a connection as pinned, without considering the failures of axial tension, is *unconservative* for structural fire engineering design, especially in the cooling stages of a fire.

(8) At high temperatures, the strength and stiffness of unprotected steel beams reduce rapidly. The loads above the fire compartment are largely carried by the concrete slabs. Hence, the impact of steel reinforcement on the behaviour of floor slabs becomes more significant.

(9) At higher temperatures, the loads within the floor slabs of fire compartment, initially supported by unprotected secondary beams, are redistributed into protected beams along the column grid lines. This large load causes the protected secondary beams to deform significantly.

(10) The high loads result in vertical shear failure of the connections, which connect protected secondary beams to the columns. All of this will significantly undermine the vertical support conditions on floor slab panels within the fire compartment.

(11) Once the connections of protected beams fail, the vertical support for the slab panel would reduce. The floor slabs within the fire compartments would deform less double curvature, causing significant reduction of tensile membrane action within the floor slabs.

(12) Therefore, in real performance-based fire resistance design of steel framed composite buildings, the influence of connections needs to be considered carefully. This is in order to maximise the benefit of tensile membrane action.

(13) The designers should design adequate strength and stiffness into protected secondary beams and connections. The primary requirements for tensile membrane action of the floor slabs to be effective used, is to make sure that the strong vertical supports along the edges of floor slab panes are maintained during the required fire resistance period.

6.2 Recommendations for future studies

It is clear from this study that there are questions to be addressed, regarding the behaviour of connections at elevated temperatures. In summary, it is recommended that the following areas should be considered for further work:

(1) More experimental data on the second stage of the rotational behaviour of partial end-plate connection (after the beam bottom flange contacts with the column) under fire conditions are needed. The experimental data can be used to further evaluate the accuracy and reliability of the proposed two-node partial end-plate connection element.

(2) Numerical study of how the axial tensile force of the connected beam influences the performance of the partial end-plate connections at elevated temperatures need to be carried out. A proper model for this needs to be developed and incorporated into the current two-node partial end-plate connection element model.

(3) Experimental data on the performance of minor-axis beam-to-column partial end-plate connections at elevated temperatures is as yet very limited. An extension of research on this connection configuration is necessary to

produce more test data for the validations and improvements of proposed models.

(4) Extensive studies of the effects of axial compressive force, on the behaviour of connections at elevated temperatures are needed.

(5) The frame works of the current proposed simplified connection model can be further extended and developed, for modelling other types of connections at both ambient and elevated temperatures, such as for the fin-plate, web angles, top and seat angles connections.

References

Abolmaali, A., Matthys, J. H., Farooqi, M. and Choi, Y. (2005) 'Development of moment–rotation model equations for flush end-plate connections', *Journal of Constructional Steel Research,* 61, pp.1595-1612.

Abu, A. K. (2009) *Behaviour of composite floor systems in fire*. PhD Thesis, University of Sheffield.

Abu, A.K., Burgess, I.W. and Plank, R.J. (2013) 'Tensile membrane action of thin slabs exposed to thermal gradients', *Journal of Engineering Mechanics*, 139(11), pp.1497-1507.

Al-Jabri, K.S. (1999) *The behaviour of steel and composite beam-to-column connections in fire*. PhD Thesis, University of Sheffield.

Al-Jabri, K.S., Burgess, I.W., Lennon, T. and Plank, R.J., (2005) 'Spring stiffness model for flexible end-plate bare-steel joints in fire', *Journal of Constructional Steel Research*. 61 (12), pp.1672-1691.

Al-Jabri, K.S., Seibi, A., Karrech, A. (2006) 'Modelling of unstiffened flush end-plate bolted connections in fire', *Journal of Constructional Steel Research,* 62, pp.151-159.

Aribert, J.M., Younes, I. and Lachal, A. (2002) 'Low-cycle fatigue of steel sections subjected to a transverse concentrated load: experimental investigation and practical formulation', *Proccedings of The European Conference on Steel Structures*, 2, pp.1067 - 1078.

Armer, G.S.T. and Moore, D.B. (1994) 'Full-scale testing on complete multi-storey structures', *The Structural Engineer*, 72(2), pp.30-31.

Association for Specialist Fire Protection, Steel Construction Institute and Fire Test Study Group (2004) *Fire protection for structural steel in buildings*. Berkshire: The Steel Construction Institute.

Bailey, C.G. (1995) *Simulation of the structural behaviour of steel-framed buildings in fire*. PhD Thesis, University of Sheffield.

Bailey, C.G., Lennon, T. and Moore, D.B. (1999) 'The behaviour of full-scale steel-framed buildings subjected to compartment fires', *The Structural Engineer*, 77, pp. 15-21.

Bailey, C.G. (2004) 'Membrane action of slab/beam composite floor systems in fire', *Engineering Structures*, 26, pp.1691-1703.

Bailey, C.G. (2007) *Structural fire engineering of steel framed buildings*. Proceedings of the 3rd International Conference on Steel and Composite Structures, Manchester, UK, pp.57-65.

Bailey, C.G. (2009) 'Science and Technology Developments in Structural Fire Engineering', *Structural Engineering International*, 19 (2), pp.155-164.

Beck, V. (1997) *Performance-based fire engineering design and its application in Australia*. Fire Safety Science-Proceedings of the Fifth International Symposium, pp. 23-40.

Block, F.M., Burgess, I. W., Davison, J.B. and Plank, R.J. (2004) *A Component approach to modelling steelwork connections in fire: behaviour of column webs in compression.* Proceedings of ASCE Structures Congress 2004, Nashville, Tennessee.

Block, F.M. (2006) *Development of a component-based finite element for steel beam-to-column connections at elevated temperatures*. PhD Thesis, University of Sheffield.

Block, F.M., Burgess, I. W., Davison, J.B. and Plank, R.J. (2007) 'The development of a component-based connection element for end-plate connections in fire', *Fire Safety Journal*, 42, pp. 498-506.

British Standards Institution (2003). *BS 5950: Part 8: 1990 Structural use of steelwork in building Part 8. Code of practise for fire resistant design*. London: British Standards Institution.

Buchanan, A.H. (2001) *Structural design for fire safety*. Chrichester: John Wiley & Sons, Ltd.

Buchanan, A. (2008) 'The Challenges of Predicting Structural Performance in Fires', *Fire Safety Science*, 9, pp.79-90.

Bukowski, R.W. and Babrauskas, V. (1994) 'Developing rational, performance-based fire safety requirements in model building codes', *Fire and Materials*, 18, pp.173-191.

Burgess, I.W. (2002) 'Fire resistance of framed buildings', *Physics Education*, 37(5), pp. 390-399.

Burgess, I.W., Davison, J.B., Dong, G. and Huang, S.S. (2012a) 'The role of connections in the response of steel frames to fire', *Structural Engineering International*, 22 (4), pp.449-461.

Burgess, I.W. (2012b) *The Robustness of Steel Connections in Fire.* Workshop of the Italian Group of Fracture, Forni di Sopra, Italy.

CEN (2002) *BS EN 1991-1-2:2002 Eurocode 1: Actions on structures-Part 1-2: General actions – Actions on structures exposed to fire.* Brussels: European Committee for Standardization.

CEN (2005a) *BS EN 1993-1-1:2005 Eurocode 3: design of steel structures-Part 1-1: General rules and rules for buildings.* Brussels: European Committee for Standardisation.

CEN (2005b) *BS EN 1993-1-2:2005 Eurocode 3: design of steel structures –Part 1-2: General rules- structural fire design.* Brussels: European Committee for Standardisation.

CEN (2005c) *BS EN 1993-1-8:2005 Eurocode 3: Design of steel structures – Part 1-8: Design of joints*. Brussels: European Committee for Standardisation.

CEN (2005d) *BS EN 1994-1-2: Eurocode 4-Design of composite steel and concrete structures, Part 1-2: General rules-Structural fire design.* Brussels: European Committee for Standardisation.

CEN (2006) *BS EN 1993-1-5: Eurocode 3- design of steel structures-Part 1-5: Plated structural elements.* Brussels: European Committee for Standardisation.

Chen, L. (2012) *Robustness in fire of steel framed structures with realistic connections*. PhD Thesis, University of Manchester.

Dai, X.H., Wang ,Y.C. and Bailey, C.G. (2010) 'Numerical modelling of structural fire behaviour of restrained steel beam-column assemblies using typical joint types', *Engineering Structures*, 32, pp.2337-2351.

Daryan, A.S. and Yahyai, M. (2009) 'Behaviour of bolted top-seat angle connections in fire', *Journal of Constructional Steel Research*, 65, pp.531-541.

Dat, P. X. and Tan, K. H. (2013) 'Membrane actions of RC slabs in mitigating progressive collapse of building structures', *Engineering Structures*, 55, pp.107-115.

Elghazouli, A.Y., Izzuddin, B.A. and Richardson, A.J. (2000) 'Numerical modelling of the structural fire behaviour of composite buildings', *Fire Safety Journal*, 35, pp.279-297.

El-Rimawi, J. A., Burgess, I. W. and Plank, R. J. (1997) 'The influence of connection stiffness on the behaviour of steel beams in fire', *Journal of Constructional Steel Research*, 43, pp.1-15.

El-Zanaty, M.H. and Murray, D.W. (1983) 'Nonlinear Finite Element Analysis of Steel Frames', *Journal of Structural Engineering*, 109(2), pp.353-368.

Faella, C., Piluso, V., and Rizzano, G. (1998) 'Experimental Analysis of Bolted Connections: Snug versus Preloaded Bolts', *Journal of Structural Engineering*, 124(7), pp.765-774.

FEMA (2002a) *World Trade Centre Building Performance Study*. Federal Emergency Management Agency, USA

FEMA (2002b) *World Trade Centre Building Performance Study: Data Collection, Preliminary Observations, and Recommendations*. Federal Emergency Management Agency, USA

Foster, S.J., Chladna, M., Hsieh, Y.C., Burgess, I.W. and Plank, R.J. (2007) 'Thermal and structural behaviour of a full-scale composite building subject to a severe compartment fire'. *Fire Safety Journal*, 42, pp.183-199.

Franssen, J. M., Cooke, G. M. E. and Latham, D. J. (1995) 'Numerical Simulation of a Full Scale Fire Test on a Loaded Steel Framework', *Journal of Constructional Steel Research*, 35, pp.377-408.

Franssen, J. M. (2005) 'SAFIR: A thermal/structural program for modelling structures under fire', *Engineering Journal-American Institute of Steel Construction Inc*, 42(3), pp.143-158.

Franssen, J. M., Kodur, V. and Zaharia, R. (2009) *Designing steel structures for fire safety*. London: Taylor&Francis Group.

Gao, Y., Yu, H. and Shi, G. (2013) 'Resistance of flush endplate connections under tension and shear in fire', *Journal of Constructional Steel Research*, 86, pp.195-205.

Gillie, M., Usmani A.S. and Rotter, J.M. (2001) 'A structural analysis of the first Cardington test', *Journal of Constructional Steel Research*, 57, pp.581-601.

Guo, T. N. (2005) *Fire situation and development of fire safety science and technology in China*. Fire Safety Science–Proceedings of The Eighth International Symposium, pp. 111-124.

Hertz, K. (2005) Assessment of performance-based requirements for structural design, *Fire Safety Science–Proceedings of The Eighth International Symposium*, pp. 315-325.

Hu, Y., Davison, J.B., Burgess, I.W. and Plank, R.J. (2008) *Experimental Study on Flexible End Plate Connections in Fire*. Proceedings of 5th European Conference on Steel Structures, Graz, Austria, pp.1007-1012.

Hu, Y. (2009a) *Robustness of flexible endplate connections under fire conditions*. PhD Thesis, University of Sheffield.

Hu, Y., Davison, J.B., Burgess, I.W. and Plank, R.J. (2009b) 'Component Modelling of Flexible End-plate Connections in Fire', *International Journal of Steel Structures*, 9, pp.29-38.

Huang, Z., Platten, A. and Roberts, J. (1996) 'Non-linear finite element model to predict temperature histories within reinforced concrete in fires', Building and Environment, 31(2), pp.109-118.

Huang, Z., Burgess, I. W. and Plank R. J. (1999a) 'Nonlinear analysis of reinforced concrete slabs subjected to fire', *ACI Structural Journal*, 96(1), pp. 127-135

Huang, Z., Burgess, I. W. and Plank R. J. (1999b) 'Influence of shear connectors on the behaviour of composite steel-framed buildings in fire', *Journal of Constructional Steel Research,* 51(3), pp. 219-237.

Huang, Z., Burgess, I. W. and Plank R. J. (2000) 'Effective stiffness modelling of composite concrete slabs in fire', *Engineering Structures,* 22(9), pp. 1133-1144.

Huang, Z., Burgess, I. W. and Plank R. J. (2002) 'Modelling of six full-scale fire tests on a composite building', *The Structural Engineer*, 80(19), pp. 30-37.

Huang, Z., Burgess, I.W. and Plank, R.J. (2003a) 'Modelling Membrane Action of Concrete Slabs in Composite Buildings in Fire. Part I: Theoretical Development', *Journal of Structural Engineering*, 129 (8), pp.1093-1102.

Huang, Z., Burgess, I. W. and Plank R. J. (2003b) 'Modelling membrane action of concrete slabs in composite buildings in fire. Part II: Validations", *Journal of Structural Engineering*, 129(8), pp. 1103-1112.

Huang, Z., Burgess, I. W. and Plank R. J. (2004) 'Fire resistance of composite floors subject to compartment fires', *Journal of Constructional Steel Research*, 60, pp. 339-360.

Huang, Z., Burgess, I. W. and Plank R. J. (2009) 'Three-dimensional analysis of reinforced concrete beam-column structures in fire', *Journal of Structural Engineering*, 135(10), pp1201-1212.

Huang Z. (2011) 'A connection element for modelling end-plate connections in fire', *Journal of Constructional Steel Research,* 67(5), pp.841-853.

ISO 834 (1975) *Fire resistance test, elements of building constructions*. International Standard ISO 834.

Jahromi, H. Z., Vlassis, A.G. and Izzuddin, B.A. (2013) 'Modelling approaches for robustness assessment of multi-storey steel-composite buildings', *Engineering Structures*, 51, pp.278-294.

Jaspart, J.P. (2000) 'General report: session on connections', *Journal of Constructional Steel Research,* 55, pp.69-89.

Kanvinde, A.M., Gomez, I.R., Roberts, M., Fell, B.V. and Grondin, G.Y. (2009) 'Strength and ductility of fillet welds with transverse root notch', *Journal of Constructional Steel Research*, 65, pp.948-958.

Kirby, B.R. (1986) 'Recent developments and applications in structural fire engineering design- a review', *Fire Safety Journal*, 11, pp.141-179.

Kirby, B. R. and Preston, R. R. (1988) 'High temperature properties of hot-rolled, structural steels for use in fire engineering design studies', *Fire Safety Journal*, 13, pp. 27-37.

Kodur, V., Dwaikat, M. and Fike, R. (2010) 'High-temperature properties of steel for fire resistance modelling of structures', *Journal of Materials in Civil Engineering*, 22(5), pp.423-434.

Kodur, V.K.R., Naser, M., Pakala, P. and Varma, A. (2013) 'Modelling the response of composite beam-slab assemblies exposed to fire', *Journal of Constructional Steel Research*, 80, pp.163-173.

Lagerqvist, O. and Johansson, B. (1996) 'Resistance of I-girders to concentrated loads', *Journal of Constructional Steel Research*, 39(2), pp.87-119.

Lamont, S. (2001) *The behaviour of multi-storey composite steel framed structures in response to compartment fires*. PhD Thesis, University of Edinburgh.

Lamont, S., Gillie, M. and Usmani, A.S. (2007) 'Composite steel-framed structures in fire with protected and unprotected edge beams', *Journal of Constructional Steel Research*, 63, pp.1138-1150.

Lawson, R.M. (1990) 'Behaviour of steel beam-to-column connections in fire', *The Structural Engineer*, 68(14), pp.263-271.

Lawson, R.M. and Newman, G.M. (1996) *Structural Fire Design to EC3 and EC4, and Comparison with BS 5950*. Berkshire: Silwood Park.

Lawson, R. M. (2001) 'Fire engineering design of steel and composite buildings', *Journal of Constructional Steel Research*, 57, pp.1233-1247.

Lennon, T., Moore, D.B., Wang, Y.C. and Bailey, C.G. (2007) *Designers' guide to EN 1991-1-2, 1992-1-2, 1993-1-2 and 1994-1-2*. London: Thomas Telford.

Leston-Jones, L.C. (1997a) *The influence of semi-rigid connections on the performance of steel framed structures in fire*. PhD Thesis, University of Sheffield.

Leston-Jones, L.C., Burgess, I.W. and Plank, R.J. (1997b) 'Elevated-temperature moment-rotation tests on steelwork connections', *Proceedings of The Institution of Civil Engineers-structures and Buildings*, 122, pp.410-419.

Li, G.Q., Guo, S.X. and Zhou, H.S. (2007) 'Modelling of membrane action in floor slabs subjected to fire', *Engineering Structures*, 29, pp.880-887.

Li, G.Q. and Guo, S.X. (2008) 'Experiment on restrained steel beams subjected to heating and cooling', *Journal of Constructional Steel Research*, 64, pp.268-274.

Lim, L., Buchanan, A., Moss, P. and Franssen, J.M. (2004) 'Numerical modelling of two-way reinforced concrete slabs in fire', *Engineering Structures*, 26, pp.1081-1091.

Lima, L.R.O., Andrade, S.A.L., Vellasco, P.C.G.S. and Silva, L.S. (2002) 'Experimental and mechanical model for predicting the behaviour of minor axis beam-to-column semi-rigid joints', *International Journal of Mechanical Sciences*, 44 pp.1047-1065.

Liu, T. C. H. (1996) 'Finite element modelling of behaviours of steel beams and connections in fire', *Journal of Constructional Steel Research*, 36(3), pp.181-199.

Liu, T. C. H. (1999) 'Moment-rotation-temperature characteristics of steel /composite connections', *Journal of Structural Engineering*, 125(10), pp.1188-1197.

Liu, T. C. H., Fahad, M.K. and Davies, J.M. (2002) 'Experimental investigation of behaviour of axially restrained steel beams in fire', *Journal of Constructional Steel Research*, 58, pp.1211-1230.

Lo, S. M., Zhao, C.M., Liu, M. and Coping, A. (2008) 'A simulation model for studying the implementation of performance-based fire safety design in buildings', *Automation in Construction*, 17, pp.852-863.

Lou, G.B. and Li, G.Q. (2006) *Nonlinear finite element modelling of behaviour of extended end-plate bolted moment connections in fire*. Proceedings of the Fourth International Workshop Structures in Fire, Portugal, pp.327-343.

Moore, D.B. and Lennon, T. (1997) 'Fire engineering design of steel structures', *Progress in Structural Engineering and Materials*, 1(1), pp.4-9.

Moss, P.J., Dhakal, R.P., Wang, G. and Buchanana, A.H. (2008) 'The fire behaviour of multi-bay, two-way reinforced concrete slabs', *Engineering Structures*, 30, pp.3566-3573.

Nadjai, A., Bailey, C.G., Vassart, O., Han, S., Zhao, B., Hawes, M., Franssen, J. M., Simms, I. (2011) 'Full-scale fire test on a composite floor slab incorporating long span cellular steel beams', *The Structural Engineer*, 89(21), pp.18-25.

Najjar, S.R. (1994) *Three-dimensional analysis of steel frames and sub-frames in fire*. PhD Thesis, University of Sheffield.

Nethercot, D.A. (2000) 'Frame structures: global performance, static and stability behaviour—general report', *Journal of Constructional Steel Research*, 55(1-3), pp.109-124.

Neves, L.C. and Gomes, F. (1999) *Guidelines for a numerical modelling of beam-to-column minor-axis joints*, COST C1 Report of W.G. 6-Numerical Simulation, European Commission, Brussels, pp.48-60.

Newman, G. M., Robinson, J. T. and Bailey, C. G. (2006) *Fire safety design: a new approach to multi-storey steel framed building*. London: The Steel Construction Institute.

ODPM (2000) *The Building Regulations 2000, Approved Document B, Fire Safety*. TSO.

Owens, G. W. and Moore, D. B. (1992) 'The robustness of simple connections', *The Structural Engineer*, 70(3), pp.37-46.

Parkinson, D.L. and Kodur, V.K.R. (2007) 'Performance-based design of structural steel for fire conditions- A calculation methodology', *Steel Structures*, 7, pp.219-226.

Purkiss, J.A. and Li, L.Y. (2013) *Fire safety engineering design of structures*. London: CRC Press.

Qian, Z.H. (2007) *Shear behaviour of steel members and beam-to-column joints under elevated temperatures*. PhD Thesis, Nanyang Technology University.

Qian, Z. H., Tan, K. H. and Burgess, I.W. (2008) 'Behaviour of steel beam-to-column joints at elevated temperature: Experimental investigation', *Journal of Structural Engineering*, 134(5), pp.713-726.

Ramberg, W. and Osgood, W.R. (1943) *Description of stress – strain curves by three parameters*. National Advisory Committee for Aeronautics, Technical Report 902.

Ramli-Sulong, N.H. (2005) *Behaviour of steel connections under fire conditions*. PhD Thesis, Imperial College London.

Ramli-Sulong, N.H., Elghazouli, A.Y., Izzuddin, B.A. and Ajit, N. (2010) 'Modelling of beam-to-column connections at elevated temperature using the component method', *Steel and Composite Structures*, 10(1), 23-43.

Roberts, T. M. and Rockey, K. C. (1979) 'A mechanism solution for predicting the collapse loads of slender plate girders when subjected to in-plane patch loading', *Proceedings of the ICE*, 67(1), pp.155-175.

Saab, H.A. (1990) *Non-linear finite element analysis of steel frames in fire conditions*. PhD Thesis, University of Sheffield.

Santiago, A. (2008) *Behaviour of beam-to-column steel joints under natural fire*. PhD Thesis, University of Coimbra.

Sarraj, M., Burgess, I.W., Davison, J.B. and Plank, R.J. (2007a) 'Finite element modelling of steel fin plate connections in fire', *Fire Safety Journal*, 42, pp.408-415.

Sarraj, M. (2007b) *The behaviour of steel fin plate connections in fire*. PhD Thesis, University of Sheffield.

SCI (2011) *P358: Joints in steel construction: Simple joints to Eurocode 3*. Berkshire: The Steel Construction Institute.

Scullion, T., Ali, F. and Nadjai, A. (2012) 'Finite element numerical evaluation of elliptical hollow section steel columns in fire', *Thin-Walled Structures*, 55, pp.22-36.

Selamet, S. and Garlock, M. E. (2014) 'Fire resistance of steel shear connections', *Fire Safety Journal*, 68, pp.52-60.

Shi, Y.J., Chan, S.L. and Wong, Y.L. (1996) 'Modelling for moment-rotation characteristics for end-plate connections', *Journal of Structural Engineering*, 122(11), pp.1300-1306.

Simões da Silva, L., Santiago, A. and Real, P.V. (2001) 'A component model for the behaviour of steel joints at elevated temperatures', *Journal of Constructional Steel Research*, 57, pp.1169-1195.

Simões da Silva, L. and Santiago, A. (2005) 'Behaviour of steel joints under fire loading', *Steel and Composite Structures*, 5(6), pp.485-513.

Spyrou, S. (2002) *Development of a component-based model of steel beam-to-column joints at elevated temperatures*. PhD Thesis, University of Sheffield.

Spyrou, S., Davison J., Burgess I.W. and Plank RJ. (2004a) 'Experimental and analytical investigation of the 'tension zone' component within a steel joint at elevated temperatures', *Journal of Constructional Steel Research*, 60(6), pp.867-896.

Spyrou, S., Davison, J.B., Burgess, I.W. and Plank, R.J. (2004b) 'Experimental and analytical investigation of the 'compression zone' component within a steel joint at elevated temperatures', *Journal of Constructional Steel Research*, 60 (6), pp.841-865.

Sun, R.R., Huang, Z. and Burgess, I.W. (2012) 'Progressive collapse analysis of steel structures under fire conditions', *Engineering Structures*, 34, pp. 400-413.

Swinden Technology Centre (1999) *The Behaviour of Multi-Storey Steel-Framed Buildings in Fire: A European Joint Research Programme.* British Steel plc, Rotherham, UK.

Taib, M. (2012) *The performance of steel framed structures with fin-plate connections in fire*. PhD Thesis, University of Sheffield.

Tavares, R.M. (2009) 'An analysis of the fire safety codes in Brazil: Is the performance-based approach the best practice?', *Fire Safety Journal*, 44, pp.749–755.

Tschemmernegg, F. and Humer, C. (1988) 'The design of structural steel frames under consideration of the nonlinear behaviour of joints', *Journal of Constructional Steel Research*, 11(2), pp.73-103.

Vassart, O. and Zhao, B. (2011) *FRACOF: Fire resistance assessment of partially protected composite floors: Design guide*. Arcelor/Mittal & CTICM.

Wald. F., Sim ões da Silva, L., Moore, D.B., Lennon, T., Chladna ´, M., Santiago, A., Benes˘, M. and Borges, L. (2006) 'Experimental behaviour of a steel structure under natural fire', *Fire Safety Journal* , 41, pp.509-522.

Wales, M.W. and Rossow, E.C. (1983) 'Coupled moment-axial force behaviour in bolted joints', *Journal of Structural Engineering*, 109(5), pp.1250-1266.

Wang, Y.C. (2000) 'An analysis of the global structural behaviour of the Cardington steel-framed building during the two BRE fire tests', *Engineering Structure*, 22, pp.401-412.

Wang, Y.C. (2002) *Steel and composite structures: Behaviour and design for fire safety*. London: Spon Press.

Wang, Y.C. (2005) 'Performance of steel–concrete composite structures in fire', *Progress in Structural Engineering and Materials*, 7(2), pp.86-102.

Wang, W.Y., Li, G. Q. and Dong, Y.L. (2007) 'Experimental study and spring-component modelling of extended end-plate joints in fire', *Journal of Constructional Steel Research*, 63, pp.1127-1137.

Wang, Y.C., Dai, X.H. and Bailey, C.G. (2011) 'An experimental study of relative structural fire behaviour and robustness of different types of steel joint in restrained steel frames'. *Journal of Structural Engineering*, 67(7), pp.1149-1163.

Wellman, E., Varma, A., Fike, R. and Kodur, V. (2011) 'Experimental evaluation of thin composite floor assemblies under fire loading', *Journal of Structural Engineering*, 137, pp.1002-16.

Yang. B. and Tan, K.H. (2012) 'Numerical analysis of steel beam-to-column joints subjected to catenary actions', *Journal of Constructional Steel Research*, 70(3), pp.1-11.

Yu, C., Huang, Z., Burgess, I.W. and Plank, R.J. (2010) 'Development and validation of 3D composite structural elements at elevated temperatures', *Journal of Structural Engineering*, 136(3), pp.275-284.

Yu, H.X., Burgess, I.W. Davison, J.B., and Plank, R.J. (2008) 'Experimental Investigation of the Behaviour of Flush Endplate Connections in Fire', Proceedings of Structures in Fire Workshop, Singapore, pp.150-157.

Yu, H.X., Burgess, I.W., Davison, J.B. and Plank, R.J. (2009a) 'Experimental investigation of the behaviour of fin plate connections in fire', *Journal of Constructional Steel Research*, 65, pp.723-736.

Yu, H.X., Burgess, I.W., Davison, J.B. and Plank, R.J. (2009b) 'Tying capacity of web cleat connections in fire, Part 1: Test and finite element simulation', *Engineering Structures*, 31, pp.651-663.

Yu, H.X., Burgess, I.W., Davison, J.B. and Plank, R.J. (2009c) 'Tying capacity of web cleat connections in fire, Part 2: Development of component-based model', *Engineering Structures*, 31, pp.697-708.

Yu, H.X., Burgess, I.W., Davison, J.B. and Plank, R.J. (2009d) 'Development of a Yield-Line Model for Endplate Connections in Fire', *Journal of Constructional Steel Research*, 65 (6), pp.1279-1289.

Yu, H.X., Burgess, I. W., Davison, J. B. and Plank, R. J. (2011) 'Experimental and numerical investigations of the behaviour of flush end plate connections at elevated temperatures', *Journal of Structural Engineering*, 137(1), pp.80-87.

Yu, X.M., Huang, Z., Burgess, I.W. and Plank, R.J. (2008) 'Non-linear analysis of orthotropic composite slabs in fire', *Engineering Structures*, 30 (1), pp.67-80.

Zhang, N.S. and Li, G.Q. (2010) 'A New Method to analyse the membrane action of composite floor slabs in fire condition', *Fire Technology*, 46 (1), pp.3-18.